SPRINGER BRIEFS IN GEOGRAPHY

Wafi Al-Fares

Historical Land Use/Land Cover Classification Using Remote Sensing

A Case Study of the Euphrates River Basin in Syria

Springer

SpringerBriefs in Geography

For further volumes:
http://www.springer.com/series/10050

Wafi Al-Fares

Historical Land Use/Land Cover Classification Using Remote Sensing

A Case Study of the Euphrates River Basin in Syria

Springer

Wafi Al-Fares
Institute of Geography, Remote Sensing
University of Jena
Jena
Germany

ISSN 2211-4165 ISSN 2211-4173 (electronic)
ISBN 978-3-319-00623-9 ISBN 978-3-319-00624-6 (eBook)
DOI 10.1007/978-3-319-00624-6
Springer Cham Heidelberg New York Dordrecht London

Library of Congress Control Number: 2013939822

Printed on acid-free paper

Springer is part of Springer Science+Business Media (www.springer.com)

To my parents, my country, my brothers and sisters, my wife, my children and my friends

Preface

The work described in this dissertation was performed under the supervision of Prof. Dr. Christiane Schmullius and Dr. Sören Hese at the Institute of Geography, Department of Remote Sensing at the University of Jena in Germany (Friedrich-Schiller-Universität Jena) from 2007 to 2011.

This thesis deals spatially and regionally with the natural boundaries of the Euphrates River Basin (ERB) in Syria. Scientifically, the research covers the application of remote sensing science (optical remote sensing: LANDSAT-MSS, TM, and ETM+ ; and TERRA: ASTER); and methodologically, in Land Use/Land Cover (LULC) classification and mapping, automatically and/or semi-automatically; in LULC-change detection; and finally in the mapping of historical irrigation and agricultural projects for the extraction of differing crop types and the estimation of their areas. With regard to time, the work is based on the years 1975, 1987, 2005, and 2007.

The remote sensing-based available data used are: LANDSAT-MSS data (eight scenes) acquired in June 1975; LANDSAT-TM data (16 scenes) acquired in May 1987, and in August 1987 (eight scenes for the extraction of the winter crops and eight scenes for extraction of the summer crops); LANDSAT-TM data (16 scenes) acquired in May 2007 and in August 2007 (eight scenes for extraction of the winter crops and eight scenes for extraction of the summer crops); and finally TERRA-ASTER data acquired in May and August 2005 (for extraction of the winter and summer crops). These have been combined with LANDSAT-ETM+ data (14 scenes) for two reasons; first to obtain complete spatial coverage of the study area, and second, to increase the spectral resolution of the ASTER-data. The LANDSAT-data was received from NASA-GLCF, while the TERRA-ASTER-data was obtained from the General Organization of Remote Sensing (GORS) in Syria.

Initially, preprocessing of the satellite data (geometric- and radiometric-processing, image enhancement, best bands composite selection, transformation, mosaicing and finally subsetting) was carried out. Then, the Land Use/Land Cover Classification System (LCCS) of the Food and Agriculture Organization (FAO) was chosen. The following steps were followed in LULC-classification and change detection mapping: visual interpretation in addition to digital image processing techniques; pixel-based classification methods; unsupervised classification:

ISODATA-method; and supervised classification and multistage supervised approaches using the algorithms: Maximum Likelihood Classifier (MLC), Neural Network classifier (NN), and Support Vector Machines (SVM). These were trialed on a test area to determine the optimized classification approach/algorithm for application on the whole study area (ERB) based on the available imagery. Pre- and post-classification change detection methods (comparison approaches) were used to detect changes in land use/land cover-classes (for the years 1975, 1987, and 2007) in the study area.

Classification accuracy has been improved by adopting historical statistical and ancillary data for the year 1975. For the 1987 coverages, the ground truth points from the International Center for Agriculture Research in Dry Areas (ICARDA) in Aleppo were adopted. For the other coverage years, 2005 and 2007, ground truth points were used that had been collected through two campaigns in Syria and through the GORS project in the Euphrates River Basin in Syria, which was completed between 2005 and 2010. Therefore, the accuracy of the results presented in this study is only as true as the quality and accuracy of the data used.

The remote sensing methods show a high potential in mapping historical and present land use/land cover classes and its changes over time. Significant results are also possible for agricultural crop classification in relatively large regional areas (the ERB in Syria is almost 50,335 km^2).

LULC-maps have been obtained automatically depending upon the satellite remotely sensed imagery and digital image processing available. Interpretation for the years 1975, 1987, 2005 and 2007 has been achieved by using digital image interpretation software (ERDAS v. 9.1, ENVI v. 4.3 and later 4.6, and ArcGIS 9.3).

The results of the different applied classification methods and algorithms were obtained keeping in mind the accuracies dependent on historical, statistical, ancillary, and ground truth data using the *kappa coefficient and error matrix*. Based on these accuracy measurements, the most successful approaches were the multistage classification and algorithm (Maximum Likelihood-MLC).

Change trends in the study area and period was characterized by land-intensive agricultural expansion. The rapid, more labor- and capital-intensive growth in the agricultural sector was enabled by the introduction of fertilizer, improved access to rural roads and markets, and the expansion of the government irrigation projects. Results from land cover change analysis, carried out from the post-classification approach, show that the cultivated land increased from 1,123,268 ha in 1975 to 1,783,286 ha in 2007 on account of a decrease in the natural vegetation area and an increase in bare areas. This approach shows obvious and detailed results. Pre-classification approach results were generalized but very effective in relation to the estimation of the occurred change on the cultivated areas, especially when these areas were vegetated and not fallow. The total change in the whole study area (5,062,082 ha, 100 %) between 1975 and 2007 was about 600,967 ha (11.93 %), in which 238,646 ha (4.74 %) was changed from natural vegetated areas to bare areas and 362,321 ha (7.19 %) changed from bare areas to cultivated areas (especially to irrigated agriculture). Areas recording no change equaled about 4,461,115 ha (88.62 %).

Irrigated areas increased 148 % in the past 32 years from 249,681 ha in 1975 to 596,612 ha in 2007.

These statistics were taken from the maps of the general LULC- classes based on LANDSAT-MSS-data acquired in June 1975, LANDSAT-TM-data in May 1987 and 2007, and ASTER-data, May 2005. The products of the post-classification change detection method were also used. The data mentioned above were also used to map the historical development of the irrigation projects in the ERB. Winter crops maps (especially wheat, barley, and sugar beet) were mapped based on LANDSAT-TM-data acquired in May 1987 and 2007, in addition to the ASTER data acquired in May 2005. The summer crops (especially cotton, maize, and watermelon) were mapped based on LANDSAT-TM-data from August 1987 and 2007, in addition to ASTER data from August 2005.

Acknowledgments

My great thanks go to my parents (Marwan and Wafaa), for mentoring me, and for providing me with the moral and financial support to obtain a university degree. In addition, my thanks also go to Syria, my country of origin, the Higher Education Ministry and the University of Teshreen in Lattakia for the financial support to pursue my education in Germany.

I cannot forget to thank my host country Germany, which has given me the opportunity to harness the advantages of its rich scientific environment, and to explore the possibilities awarded by my research area (Cartography and Remote Sensing).

I would also like to thank my supervisor Prof. Dr. Christiane Schmullius, and, of course, Dr. Sören Hese.

I would like to express my gratitude to numerous people who have played a part in the successful completion of this work.

I thank all my colleagues at the Institute of Geography and the Department of Remote Sensing at the Friedrich Schiller University in Jena.

Last but not least, I want to express my gratitude to my lovely wife, Nourah Al-Kasem, for her continuing support and perseverance during this period in my life. Particular recognition is needed of her encouragement and belief in me, which has helped me to keep pushing hard and continuing with my studies until the end. To my three beautiful children, Mohammad Marwan, Jawad, and Yaman, I want to express special thanks for their love.

Contents

Abbreviations

ACSAD	Arab Center for the Studies of Arid Zones and Dry Lands
AQUASTATE	FAO's global information system on water and agriculture
ASTER	Advanced Spaceborne Thermal Emission and Reflection Radiometer
ASZs	Agricultural Settlement Zones
AVHRR	Advanced Very High Resolution Radiometer
CBS	Central Bureau of Statistics
CWANA	Central and West Asia and North Africa (project)
EMS	Electro-Magnetic Spectrum
ERB	Euphrates River Basin
ETM+	Enhanced Thematic Mapper
FAO	Food and Agriculture Organization
GIS	Geographical Information System
GDP	Gross Domestic Product
GORS	General Organization of Remote Sensing
GPS	Global Positioning System
ICARDA	International Center for Agriculture Research in Dry Areas
IFAD	International Fund for Agricultural Development
LANDSAT	LAND SATellite
LULC	Land use/land cover
MAAR	Syrian Ministry of Agriculture and Agrarian Reform
MLC	Maximum Likelihood Classifier
MODIS	Moderate Resolution Imaging Spectroradiometer
MSS	Multispectral Scanner System
NDVI	Normalized Difference Vegetation Index
NNC	Neural Network Classifier
NOAA	National Oceanic and Atmospheric Administration
RMS	Root Mean Square
ROWA	Regional Office for West Asia
SAR	Synthetic Aperture Radar
SVMC	Support Vector Machine Classifier
SWIR	Short Wave Infra-Red
TIR	Thermal Infra-Red

TM	Thematic Mapper
UNEP	United Nations Environment Program
VIs	Vegetation Indices
VNIR	Visible Near Infra-Red

ck	Cubic kilometer
ha	Hectar
km	Kilo meter
km^2	Square kilometer
m	Meter
m^2	Square meter

Chapter 1
Introduction

1.1 Problem Statement and Research Questions

Syria, with a total area of 185,180,000 km^2, has arable land estimated at 6.22 million hectares, or 33 % of the total area of the country. The cultivated land is estimated at 5.66 million ha, which is 94.07 % of the cultivable area. Of this area, 4.27 million ha consists of annual crops and 0.67 million ha consists of permanent crops. About 62.41 % of the cultivated area is located in the three northern governorates (Aleppo, Arraqqa and Al-Hasakah), representing only 33 % of the total area of the country. The area of steppe and pastures is about 8.23 million ha, or 44 %; non arable land about 3.68 million ha, or 20 %; and forests quasi 0.57 million ha, or 3 % of the total area of Syria (Central Bureau of Statistics: CBS 2009). The total populations were 23.02 million in 2009 (as registered by the Department of Civil Status), while the number of permanent residents, excluding those who live outside Syria, were 19.88 million. Some 46.48 % of the population lives in rural areas. Actual population growth was 2.5 % for the period 2000–2005. Agriculture employs around 16.79 % of the total labor force, accounting for nearly 20 % of Gross Domestic Product (GDP), compared to 39 % in 1963. In 2004, the average population density was about 96 inhabitants/km^2 (CBS 2009). Almost 55 % of Syria is dry steppe or quasi-desert, suitable only for grazing sheep and goats. Rain-based farming of cereals, food and feed legumes is the backbone of agriculture in Syria. Irrigated land makes up about 23.91 % of cultivated land, which is about 7 % of the total area of the country (Kangarani 2006; CBS 2008).

Agriculture has traditionally been the foundation of the economy (46.48 % of the population was described as rural in 2009, with 16.79 % of the population employed in the agricultural sector and 20 % of Syria's GDP attributed to this industry). The agricultural sector has been influenced over the past 40 years by several factors. First, a growing population (4.565 million in 1960, compared to 19.88 million in 2009) with a slight increase in acreage. Secondly, the natural climactic conditions in Syria are not conducive to agricultural stability, due to heavy precipitation. Since the output of agriculture (both plant and animal) is heavily dependent on precipitation (only about 23.91 % of the cropped area is irrigated), the large variation in the

W. Al-Fares, *Historical Land Use/Land Cover Classification Using Remote Sensing*, SpringerBriefs in Geography,
DOI: 10.1007/978-3-319-00624-6_1, © The Author(s) 2013

quantities and timing of precipitation can be a reason for a large changes in areas planted, yields and production. Thirdly, over 90 % of the total Syrian territory (arable lands) needs sustainable irrigation, even in areas which receive large quantities of precipitation, since most of the rain falls during the winter rather than in the growing season. In addition, the discharge periods of Syria's rivers in March and May are late for winter crops and early for summer crops. The stream of the rivers varies significantly every year. Years of low stream make irrigation and agriculture difficult. These factors have led to a focus on large scale irrigation projects such as dam construction as a basis for economic and social development. The irrigable arable lands estimated in the ERB are 1,040,000 ha (ACSAD 2001). Syria has its own plans for irrigation development within the Euphrates basin. These involve using water from the Euphrates to irrigate six major regions: the Maskana-Aleppo-Basin (155,000 ha), the Arrasafa-Basin (25,000 ha), the Al-Balikh-Basin (185,000 ha), the Euphrates-Floodplain (170,000 ha), the Al-Mayadin-Plain (40,000 ha), and the lower Al-Khabour-Basin (70,000 ha) (see Fig. 3.2). This is a total of 645,000 ha (Beaumont 1996). Until now, only ca. 225,000 ha has been irrigated. Some 63 % of the irrigated areas in Syria are located in the Euphrates River Basin, according to the World Bank (CBS 2009).

Syria has limited water resources. There are 16 main rivers and tributaries in the country, of which six are main international rivers. The most important is the Euphrates, which is Syria's largest river, originating in Turkey and flowing to Iraq. Its total length is 2,880 km, of which 610 km are in Syria. The Euphrates River Basin has a surface area of 444,000 km^2 (17 %, or 75,480 km^2 in Syria) and its actual annual volume is 35.9 million cubic kilometers (ACSAD 2001; Kangarani 2006). Total actual renewable water resources in Syria are estimated at 16.797 million ck/year. The natural average surface runoff to the Syrian Arab Republic from international rivers is estimated at 28.515 million ck/year. The actual external renewable surface water resources are at 17.335 million ck/year, which includes 15.750 million ck of water entering the Euphrates, as unilaterally proposed by Turkey. The Euphrates River provides more than 80 % of the total Syrian water resource (Kangarani 2006; FAO 2009) and is the country's biggest source of irrigation water. Early in the 1960s, Syria, due to the need to expand the agricultural areas and to reduce the rain fed based agriculture areas, and the need for electricity, started utilizing the Euphrates water in irrigation and hydropower, with construction beginning on the Attabqa Dam in 1973 (it was completed in 1978) (FAO 2009).

Most regional crop estimate frameworks in Syria are based on knowledge from local experts (e.g., extension officers, farmers, grain traders etc.). These frameworks have developed depending heavily on the expertise of the various officials. Estimates were often based on historical regional, state and national level statistics, which were, and still are, collated by the Central Bureau of Statistics (CBS) via an agricultural census/survey at the province-/Muhafazah (statistical local area) scale. Lack of detailed province scale information further emphasizes the need for alternative accurate and objective crop area estimates to assist agro-industry decision-making at the regional scale.

Earth Remote Sensing can be defined as the detection, measurement and analysis of electromagnetic energy reflected, emitted or diffracted by an Earth surface feature without being in physical contact with it (Lillesand et al. 2008). This broad definition includes aerial imaging in the ultraviolet, visible and infrared (near, mid and far) reflective part of the spectrum, as well as thermal imaging and active technologies like radar, and moreover, geo-electric and geo-magnetic measurements. The use of remote sensing is essential in recording a variety of information about the Earth's surface and the atmosphere. This form of data gathering is an important tool in numerous sciences such as meteorology, environmental research and cartography. To make full use of the information potential of remote sensing, data must be processed, interpreted and evaluated systematically.

The used techniques for interpretation of remotely sensed data are based on many compatible disciplines including: remote sensing; pattern recognition; artificial intelligence; computer vision; image processing; and statistical analysis. The progress in automated analysis of remotely sensed data is optimistic by the growing volumes of data, the great developments in computer science (software and hardware) that processes these data, as well as the high cost and effort involved in ground surveying. The new generation of remote sensing sensors provides superior spatial and spectral resolution data, leading to the use of remotely sensed products and further underlining the need for more automated and simplified forms of processing, interpretation, and analysis. Earth Observation Remote Sensing has led to the development of human perspectives and increased greatly our understanding of the planet (Steffen and Tyson 2001). Beginning with data from the successful CORONA missions in 1960 and the start of the LANDSAT-program in the early 1970s, remotely sensed data are now globally available and deliver an exceptional amount of information about the Earth surface and the biosphere, thereby offering an enormous potential of information for monitoring (Campbell 2002; Jensen 2007).

A mainly central application of remote sensing is the production of LULC-maps from satellite imagery. Compared to more conventional mapping approaches such as terrestrial survey and basic aerial photo interpretation, LULC-mapping using remote sensing imagery has the competitive advantages of low cost, repetitive large area coverage. Earth Observation Systems (EOS) have the potential to offer spatially-distributed and multi-temporal information on LULC and its environmental state over extended areas. Furthermore, satellite systems offer near-real time information, which is particularly important for natural hazards and disaster management, as one example. Overall the conduction of LULC-information from remote sensing imagery is a significant application, concerning the support of multilateral environmental agreements, decision-making and monitoring systems. Its future use promises to be rewarding, judging by recent and rapid developments in sensor technology. Mainly remarkable in this view aspect is the superior spatial and spectral resolution of the imagery captured by new satellite sensors. As well as existing sensors such as LANDSAT-TM and SPOT-HRV, a number of new remote sensing sensors with up to 1 m spatial resolution are already in operation.

The quality of the agricultural information systems in Syria and the cropped areas estimate range from timely and reliable to virtually non-existent. Estimates are based on past trends (e.g., ground survey or census), and are sometimes adjusted by subjective judgment, rather than on objective information. There exists an established need for the nations of the world to better manage the planet's agricultural production, with improved seasonal information on crop prospects for important producing regions. This need, coupled with the state of technical development and the conceptual processing of remote sensing, has brought into focus the possibility of applying remote sensing and related technology, to the task of developing a technical concept for agricultural monitoring (Erb 1980). The reliance on remote sensing techniques and using its data in Earth Observing Studies has many important advantages for these studies in comparison to other old and classical approaches. These remotely sensed data are objective, well-timed, and recurrent and thus they could be able to present results (e.g., classification results) with a higher accuracy. During the last four decades, satellite-obtained information in the agriculture sector, using low spatial resolution images to high spatial resolution images, was helpful in the decision-making processes of governments. Agricultural production is highly dynamic and depends on complicated interactions of prices, weather, soils and technology all over the world. This production has an influence on the global food market. For the purposes of agricultural studies, there is the need for accurate data at a specific time. Here, because the meaningful forces (e.g., economic, food, policy and environmental impacts) of major strategic crops, it is significant to know the local distribution and the acreage of these types of crops. For these reasons, remote sensing, either alone or in combination with ground surveys (important for training samples gathering, classification use and ground truth points used for accuracing the classification results), has been used in crop acreage assessment (Erb 1980; Allen 1990; Wardlow and Stephen 2008).

The use of remote sensing data and its applications for distinguishing between types of agricultural crop and interior crop characteristics was widely researched during the last four decades (Cloutis et al. 1996; Blaes et al. 2005; Ozdogan 2010). The well improved tendencies involving particular types of crop, maturity, levels of the nutrient, and their reflectance values within the spectral bands and in correlation to the vegetation indices (VIs), are becoming more accurate and are helpful when the availability of ground truth data is limited (Senay et al. 2000).

Techniques of satellite remote sensing have a fundamental role in irrigation management. Some applications of satellite remote sensing techniques for irrigation management are: crop acreage; crop condition; crop yield; and performance of irrigation canal system. These techniques were applied effectively in monitoring irrigated lands in many areas around the world under a variety of climatic conditions. It offers a synoptic and a suitable temporal coverage of agricultural lands in several spectral regions. Its archived data offers comparison of imagery among dates, and yielding change over time. Up to now, there are many studies that have used remotely sensed imagery, mainly at high spatial resolutions such as LANDSAT, to observe and classify irrigated agriculture. The early studies focused

on determining the ability of remotely sensed data to classify, map and update irrigated land acreage. This was mainly used in the US and India (Draeger 1976; Rundquist et al. 1989). Some new studies have improved and tested new classification methods particularly appropriated for mapping irrigated lands (Eckhardt et al. 1990; Pax-Lenney et al. 1996; Abuzar et al. 2001; Dheeravath et al. 2010).

To monitor the changes in our surrounding Earth environment and to manage the natural resources of the Earth, researchers have presented many models and strategies, especially during the last few decades. The major element in structuring these models is how LULC-features change over the time dimension. Land use and land cover change has become a central component in current strategies for managing natural resources and monitoring environmental changes. Remote sensing satellite images have proven their ability in change detection studies. So-called *Change Detection Methods* have been applied to multi-temporal images, in order that variations and changes in the state (especially spectral) and spatial distribution of features and phenomena can be recognized, mapped and interpreted (Singh 1989; Coppin et al. 2004). This method includes procedures, which can identify and evaluate changes without past or present detailed knowledge of the land surface (Rogan et al. 2002). This information should offer land managers a better understanding of relations and interactions between the anthropogenic and natural phenomena. This should be able to offer an efficient distribution and management of available natural resources. The deep understanding and consideration of all other issues on the reflected EMR-signal, within and between multi temporal remotely sensed data, will offer the basis for successful change detection studies (Lu et al. 2004).

The research problem is that Syria, in general, and the Euphrates River Basin in particular, like other developing countries, rely very heavily on traditional statistical methods to monitor and study changes in the natural cover and land use over time. This is in order to obtain and compare statistical data and figures, and allows these data to act as a basis and reference to the decision makers in the development of national plans, including agricultural policy. Based on this collected data, with regard to the agriculture sector for example, decisions must be made on the abolition of creative projects, the development of new irrigation schemes, asset-sufficiency, and whether food should be imported or if local production covers the needs of the population. Many other procedures and policies rely on the accuracy of statistical information and data for their success. The statistical methods used in Syria give unreliable results, because of their complete dependence on the human element. There is a need for the application of other methods that produce more accurate data, and which may be less expensive and require less effort. The inability to represent the distribution and prevalence of various agricultural crops spatially increases the size of the problem and is a negative factor in statistical data collection in Syria.

One challenge for researchers lies in the need to find scientific tools and methods with a suitable methodology, which can be applied to the study area. Remote sensing can contribute a greater role to the understanding of this problem by providing accurate mapping data about land uses, including crop utilization

over multiple time periods. Remote sensing also results in a realistic depiction of land use, by providing a spatial dimension.

Many kinds of data supply, especially spatial data on the dynamics of LULC, are poor and thus insufficient. Nevertheless, extended knowledge on the state and changes of LULC is needed in order to support the implementation of sustainable strategies of regional development. Spatial information is the basis for various planning tasks. This information could be obtained by application of the remote sensing techniques.

This monograph discusses four basic themes in the study area: the mapping of land use and natural cover; development mapping of irrigated areas; the mapping of the distribution of irrigated agricultural crops, especially strategic crops; and mapping, monitoring and study of the changes in land use and natural landscape during the last 30 years. The questions this research poses and answers are:

Which automatic classification technique or approach is the best for the study area?

How can land use/land cover be mapped using different data from remote sensing instruments in arid and semi-arid regions?

How can remote sensing be applied to the mapping and monitoring of the spatial expand in the irrigated projects constructed in the Euphrates River Basin in Syria?

How can remote sensing be applied to the mapping of irrigated agricultural crops in arid and semi-arid regions?

Can mapping and monitoring aid understanding of land use/land cover changes over time by using the remote sensing concept in arid and semi-arid regions?

1.2 Significance of the Study

The importance of this research stems from the location of the study, the Euphrates River Basin. This basin is one of the most important areas and territories in Syria, containing the important elements of life: stability, food and water. The basin contains more than 80 % of the total water resources of the country. It is the food basket of Syria, and is made up of three provinces: Aleppo, Arraqqa and Deir Azzour. These agricultural provinces contain 34 % of the total population of Syria, 38.4 % of the total area of Syria and 37.4 % of the total arable land. Some 40.2 % of the country's total irrigated areas are found in these three provinces and almost half of the population that live there work in the agriculture sector. The equivalent of 37.67 % of the total acreage is planted with wheat, 51.27 % of the area in barley, 92.50 % in yellow corn (maize), 58.79 % cotton, 49.63 % sugar beet and 49.92 % watermelon.

1.3 Research Objectives

The major component in the development of LCLU-maps is satellite imagery. The objective of this work is the use of high resolution remote sensing data (LANDSAT: MSS, TM and ETM+; TERRA: ASTER) for the mapping of land use/land cover, land use/land cover change, and irrigated agricultural crops. The research objectives for this study are:

- Understanding the spatial and temporal distribution of the interested study area surface features;
- Determination of the major dominant LULC in the area using LANDSAT: MSS, TM and ETM+−, and TERRA: ASTER satellite imagery from 1975, 1987, 2005 and 2007;
- The temporal development mapping of irrigated areas;
- The creation of one classification method to provide a sufficiently accurate discrimination of the main irrigated crops types in the study area; and
- To determine and analyze the dynamics of change of LULC-classes (trend, nature, rate, location and magnitude of land use land cover change).

1.4 Research Hypotheses

The rural environments have unique spectral characteristics and the application of remote sensing provides a unique opportunity to study these requirements. The process of integration between remote sensing data (in the case studies: LANDSAT and ASTER), and developments in Computer Science (hardware and software) and mathematics (algorithms) allows for the mapping of the historical and current land use and natural land cover, thus ensuring access to the true spatial dimension of each type of land use. These technologies also allow the study and analysis of the changes in land use and natural cover over time, and the comparison of the current status of the region with how it was 30 years ago.

1.5 Organization of the Thesis

This study is organized into seven chapters including this *Introductory Chapter,* which provides a statement of intent and sets out research questions, study objectives and study hypotheses. Chapter 2 covers the necessary basics for understanding remote sensing in accordance to the current state of the art applications in use in Syria. Here, the classification process and various classification algorithms used, including unsupervised and supervised, parametric and non-parametric, pixel and object classification techniques, are discussed in detail

in addition to the application of remote sensing in land use/land cover classification. This Chap. 2 also reviews the literature on the current state of knowledge on regional scale crop area estimate approaches. This includes crop area estimates using remotely sensed data, the importance of temporal and spatial resolution, and the ability of satellite imagery to discriminate among crops.

The Chap. 3 describes the study area of the Euphrates River Basin, Syria. In this chapter the location, irrigation projects, climate, morphology, soil, hydrology, land use/land cover and human impacts are discussed. Chapter 4 describes the common resources that were available for this study, including satellite data, maps, field reference data, statistics and another ancillary data. Chapter 5 discusses the pre-processing techniques applied to the satellite images in order to obtain data with low calibration errors as a prerequisite for interpretation and comparison. Emphasis was placed on the geometric and radiometric accuracy of the processed data. In addition, research methodology, image processing, image classification and accuracy assessment are outlined in this chapter. In Chap. 6, results, analysis and thematic interpretations are discussed. The overall summary, general conclusions and recommendations of the research study are provided in Chap. 7.

References

Abuzar, M., McAllister, A., & Morris, M. (2001). Classification of seasonal images for monitoring irrigated crops in a salinity-affected area of Australia. *International Journal of Remote Sensing, 22*(5), 717–726.

ACSAD. (2001). *Surface water resources in the basins of the Euphrates and Tigris rivers* (p. 168). Damascus-Syria.

Allen, J. D. (1990). A look at the remote sensing applications program of the National Agricultural Statistics Service. *Journal of Official Statistics, 6*(4), 393–409.

Beaumont, P. (1996). Agricultural and environmental changes in the upper Euphrates catchment of Turkey and Syria and their political and economic implications. *Applied Geography, 16*(2), 137–157.

Blaes, X., Vanhalle, L., & Defourny, P. (2005). Efficiency of crop identification based on optical and SAR image time series. *Remote Sensing of Environment, 96*(3–4), 352–365.

Campbell, B. C. (2002). *Introduction to remote sensing*. London: Taylor & Francis.

Central Bureau of Statistics/CBS. (Several Years). *Statistical abstracts*. Damascus, Syria: Ministry of Planning.

Cloutis, E. A., Connery, D. R., Major, D. J., & Dover, F. J. (1996). Airborne multi-spectral monitoring of agricultural crop status: Effect of time of year, crop type and crop condition parameter. *International Journal of Remote Sensing, 17*(13), 2579–2601.

Coppin, P., Jonckheere, I., Nackaerts, K., Muys, B., & Lambin, E. (2004). Digital change detection methods in ecosystem monitoring: A review. *International Journal of Remote Sensing, 25*(9), 1565–1596.

Dheeravath, V., Thenkabail, P. S., Chandrakantha, G., Noojipady, P., Reddy, G. P. O., Biradar, C. M., et al. (2010). Irrigated areas of India derived using MODIS 500 m time series for the years 2001–2003. *ISPRS Journal of Photogrammetry and Remote Sensing, 65*(1), 42–59.

Draeger, W. (1976). *Monitoring irrigated land acreage using Landsat imagery: An application example*. USGS Open-file Report No. 76–630, (pp. 23). USGS, Sioux Falls, S.D.

Eckhardt, D. W., Verdin, J. P., & Lyford, G. R. (1990). Automated update of an irrigated lands GIS using SPOT HRV imagery. *Photogrammetric Engineering & Remote Sensing, 56*(11), 1515–1522.

Erb, R. B. (1980). The large area crop inventory experiment (LACIE); methodology for area, yield and production estimation; results and perspectives. In G. Fraysse (Ed.), *Remote sensing application in agriculture and hydrology* (p. 502). Rotterdam: Balkema.

FAO. (2009). Irrigation in the Middle East region in figures (AQUASTAT survey—2008). In K. Frenken (Ed.), *FAO water reports* (p. 423). Rome: Italy.

Jensen, J. R. (2007). *Remote sensing of the environment: An earth resource perspective* (2nd ed.). New Jersey: Pearson Prentice Hall.

Kangarani, H. M. (2006). *Euphrates and Tigris watershed: Economic, social and institutional aspects of forest in an integrated watershed management (working paper 81)*. Rome: FAO.

Lillesand, M. T., Kiefer, R. W., & Chipman, J. W. (2008). *Remote sensing and image interpretation* (6th ed.). Hoboken: Wiley.

Lu, D., Mausel, P., Batistella, M., & Moran, E. (2004). Comparison of land-cover classification methods in the Brazilian amazon basin. *Photogrammetric Engineering and Remote Sensing, 70*(6), 723–731.

Ozdogan, M. (2010). The spatial distribution of crop types from MODIS data: Temporal unmixing using independent component analysis. *Remote Sensing of Environment, 114*(6), 1190–1204.

Pax-Lenney, M., Woodcock, C. E., Collins, J. B., & Hamdi, H. (1996). The status of agricultural lands in Egypt: The use of multitemporal NDVI features derived from Landsat TM. *Remote Sensing of Environment*, *56*(1), 8–20.

Rogan, J., Franklin, J., & Roberts, D. A. (2002). A comparison of methods for monitoring multitemporal vegetation change using Thematic Mapper imagery. *Remote Sensing of Environment, 80*, 143–156.

Rundquist, D. C., Hoffman, R. O., Carlson, M. P., & Cook, A. E. (1989). The Nebraska center-pivot inventory: An example of operational satellite remote sensing on a long-term basis. *Photogrammetric Engineering and Remote Sensing, 55*(1), 587–590.

Senay, G. B., Lyon, J. G., Ward, A. D., & Nokes, S. E. (2000). Using high spatial resolution multispectral data to classify corn and soybean crops. *Photogrammetric Engineering & Remote Sensing, 66*(3), 319–327.

Singh, A. (1989). Review article: Digital change detection techniques using remotely-sensed data. *International Journal of Remote Sensing, 10*(6), 989–1003.

Steffen, W., & Tyson, P. (Eds.). (2001). *Global change and the earth system: A planet under pressure. The Global Environmental Change Programme* (Vol. 4, p. 32). IGBP Science. Elsevier, Stockholm, Sweden.

Wardlow, B. D., & Stephen, L. E. (2008). Large-area crop mapping using time-series MODIS 250 m NDVI data: An assessment for the U.S. Central Great Plains. *Remote Sensing of Environment, 112*(3), 1096–1116.

Chapter 2
Theoretical Background and State of the Art

This chapter provides a short overview of the principles of remote sensing outlines current studies focused on the Euphrates River Basin (ERB) and presents a survey of the literature available on the topics that the thesis covers. Within the confines of this study, remote sensing is defined as the measurement of emitted or reflected electromagnetic radiation, or spectral behaviors, from a target object by a multi-spectral satellite sensor. This thesis contains four main sections: land use/land cover classification, the mapping of irrigated areas, irrigated agriculture mapping (especially crops classification), and land use/land cover change detection mapping. A great number of papers have been published on the above four topics. In this section a small range is given, based on significance and likeness to this thesis, with the goal of providing no wide-ranging survey, but of giving an experience of the techniques, applications and performances found in the literature.

2.1 Remote Sensing Concept

For purposes of this text, discussion has been limited to Earth observation from space. "Remote sensing is the science and art of obtaining information about an object, area or phenomenon through the analysis of data acquired by a device that is not in contact with the object, area or phenomenon under investigation. Using various sensors, we remotely collect data that may be analyzed to obtain information about the objects, areas or phenomena being investigated. The remotely collected data can be of many forms, including variations in force distributions, or electromagnetic energy distributions" (Lillesand et al. 2008). Figure 2.1 illustrates the generalized processes and elements involved in the electromagnetic remote sensing of Earth resources.

Key to the consideration of remotely sensed imagery is the coverage, resolution and density of its spectral, spatial and temporal characteristics. *Spectral coverage* describes which part of the EMS (Fig. 2.2) is being used (e.g., visible, infra-red, thermal, etc.). *Spectral resolution* indicates to the spectral bandwidths in which the

W. Al-Fares, *Historical Land Use/Land Cover Classification Using Remote Sensing*, SpringerBriefs in Geography,
DOI: 10.1007/978-3-319-00624-6_2, © The Author(s) 2013

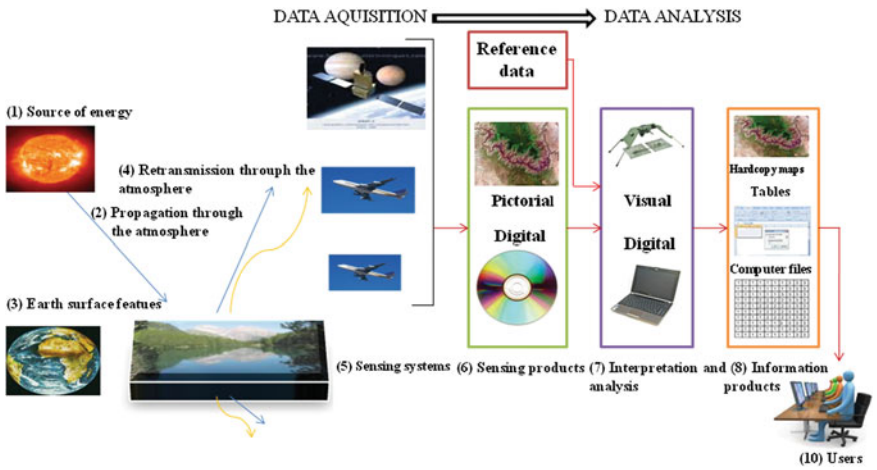

Fig. 2.1 Electromagnetic remote sensing of Earth resources (*Source* modified from Lillesand et al. 2008)

sensor collects information. *Spectral density* indicates to the number of spectral bands in an exacting part of the EMS (e.g., the LANDSAT-MSS has only four bands, while the TERRA-ASTER has 14 bands, etc.). *Spatial coverage* is the area enclosed by the image, while *spatial resolution* indicates to the smallest pixel or picture element recorded. *Temporal coverage* is the acquiring period over which the data is obtainable (e.g., LANDSAT-Sensors have a temporal coverage of 41 years). *Temporal resolution* relates to the time that the data is obtainable over. It is generally low by most remote sensing systems. *Temporal density* refers to the repeat properties of the satellite. A good repeating in gathering the data would, for some applications, offer more availability of cloud free data (McVicar and Jupp 1998). *Radiometric resolution* indicates to the active range or number of potential data file values in each spectral band (the number of bits into which the recorded energy/data is divided). For example, the total *intensity* of the energy for 8-bit data is measured from 0 to the maximum amount of 256 brightness values. Where 0 stands for no energy return, 255 is the maximum return of each pixel (ERDAS 1999).

A multispectral sensor (e.g., MSS) acquires multiple images of the same target Earth surface feature (e.g., water, soil, etc.) at different wavelengths (spectral bands). Each band measures single spectral characteristics about the target (e.g., the fourth near infra-red band of MSS is responsible for detection and recoding the spectral response of the natural vegetation). A spectral band is a data set recorded by the sensor with information from separate parts of the electromagnetic spectrum. One foundation of remote sensing is that LULC-features have different spectral properties and responses (McVicar and Jupp 1998). Analysts generate spectral signatures based upon the detected electromagnetic energy's measurement and place in the electromagnetic spectrum. A spectral signature contains statistics that define the spectral characteristic of a target feature or training samples. Image

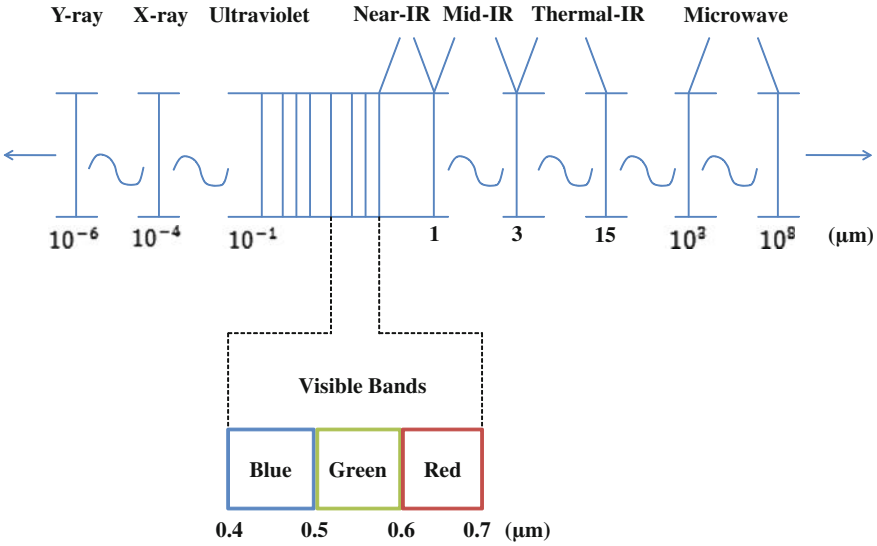

Fig. 2.2 The primary spectral regions of the electromagnetic spectrum that are of interest in Earth remote sensing applications (*Source* modified from Tso and Mather 2009)

interpreters detect the value of these statistics by quantitatively comparing the relation between studied class signatures and the used spectral bands. Spectral signatures are made more sophisticated by superior ground-truth points/measurements and accuracy assessment analysis. By utilizing the sophisticated spectral signatures in multispectral classification and thematic mapping, the interpreter generates new data for analysis (ERDAS 1999). Figure 2.3 shows idealized spectral reflectance plots for two types of vegetation, soils and water types, respectively.

2.2 Remote Sensing Application in Syria

The application of remote sensing in Syria is similar to the situation which exists in other developing countries. Remote sensing technology has been in place for more than two decades but has lacked the expected effectiveness of such technology as used in the countries of the developed world. The General Organization for Remote Sensing (GORS) was established by the Syrian Arab Republic (SAR) in 1986 and is today the most important and highest scientific body in the country competent to conduct remote sensing. It carries out many scientific projects and studies based on the application of remote sensing in Syria, and has utilized these skills even outside the country's borders (e.g., in Sudan). All of these studies have been addressed to the government's institutions and ministries, and thus the basics

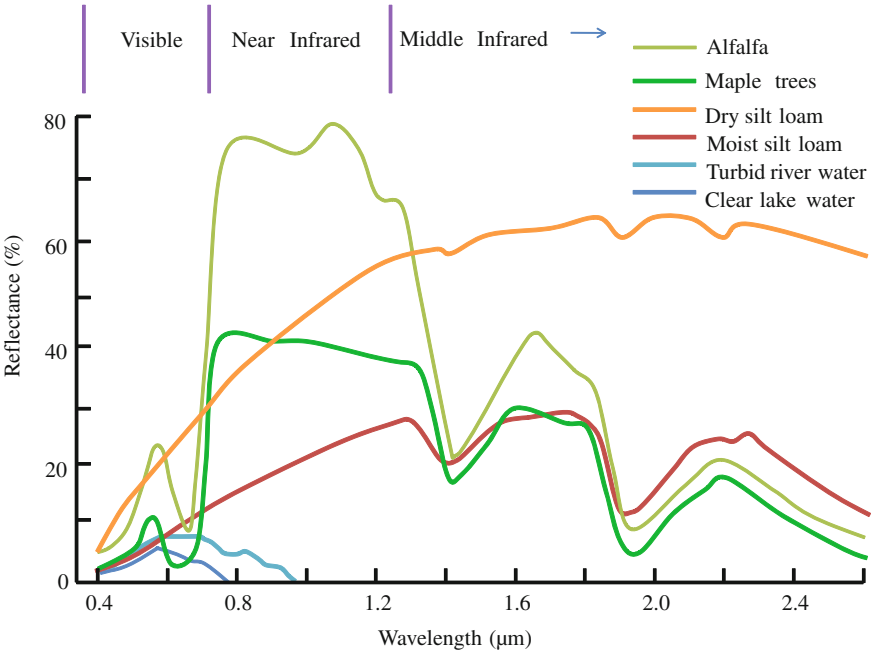

Fig. 2.3 Idealized reflectance plots for different land cover types (*Source* modified from Harrison and Jupp 1989)

and the details of remote sensing techniques has remained almost entirely within the confines of GORS and the researchers who work within this organization.

Plus GORS, there are two other scientific authorities who have published studies based on the use of remote sensing: the Arab Centre for the Studies of Arid Zones and Dry Lands (ACSAD) and the International Centre for Agriculture Research in Dry Areas (ICARDA). Unfortunately, these have refused to cooperate with university and graduate students, requiring several levels of approvals before any research is distributed for academic purposes. The other related international institutions in Syria are the Food and Agriculture Organization (FAO) and the United Nations Development Program (UNDP), which work in co-operation with national institutions mentioned above.

A vital component of the research required for this thesis was a project undertaken by GORS in the provinces of Arraqqa, Deir Azzour and Al-Hasakah. "The Survey of Natural Resources in the Eastern Regions of Syria in Cooperation with the Ministry of Agriculture and Agrarian Reform" was initiated in 2004 and was undertaken over a period of five years. Data was remotely collected from ASTER, IRES, SPOT and an Algerian satellite. The project included:

- A tour of the provinces in question to choose the appropriate areas from which to take spectrometry readings on a variety of crops for the purpose of spectral

profile/characterization, during which different stages of growth were to be distinguished spectrally using satellite images;
- Field testing of the devices to be used in the study (Spectrometer/FieldSpecPro and GPSs);
- The characterization of agricultural crops and land use during May 2005, consistent with the presence of winter crops, and during August 2005, consistent with the presence of summer crops. Some 1,050 sites were identified for the purposes of the study;
- Spectrometry readings on strategic crops (wheat, barley, lentils, sugar beet, cotton, watermelon and maize). These readings were conducted on average once every two weeks through the stages of crop growth;
- Input of field survey data and spectrometry readings to databases through electronic forms prepared for this purpose; and
- The creation of spectral signatures for each crop under study. Analysis of these spectral signatures led to the identification of the optimal time to request satellite images to be used in the estimation of the areas of winter and summer crops.

The project's objectives were: a study and cost estimate on crop area and yield for various strategic crops in Syria compared with traditional methods, and the production of maps of winter and summer crops, allowing the calculation of the level of agriculture in the regions. Many other studies focused on the ERB have proved essential during the development of this thesis.

Other studies were based on remotely sensed data, such (Beaumont 1996; Hirata et al. 2001; Zaitchik et al. 2002; De Pauw et al. 2004; De Pauw 2005; Celis et al. 2007a, b; Udelhoven and Hill 2009).

2.3 Land Use-Land Cover Mapping

2.3.1 The Classification Process

In general, classification of LULC-features using remote sensing data consists of numerous phases (Robinove 1981; Mather 2004; Schowengerdt 2007), as shown in Fig. 2.4:

- *Identifying*: the number and the name of classes that represents the real-world features which have defining priority;
- *Feature extraction*: data are frequently highly correlated between spectral bands. This high correlation might be inappropriate for classification of LULC-features and may reduce classification accuracy. Optionally, one can apply the spatial (e.g., smoothing filter) or spectral (e.g., bands subset) transformation of the multispectral data with the aim to: (1) differentiate between valuable information and noise or non-information; and (2) reducing the dimensionality

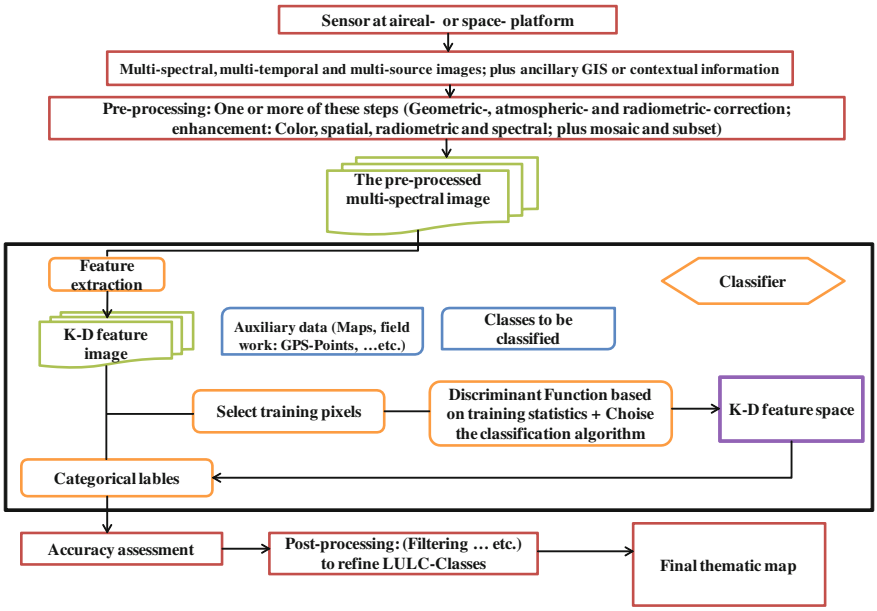

Fig. 2.4 The classification process (*Source* modified from Townshend and Justice 1986, Tutz 2000, Wilkinson 2005 and Schowengerdt 2007)

of the data to shorten the computing time needed by the classifier, and thus to raise the effectiveness of statistical estimators in a statistical classifier;

- *Training*: the term "training" is the choosing of the pixels to train the classifier to identify the preferred *themes*, or *classes*, and the selection of decision boundaries. Here, the drawing of boundaries around geographically located pixels has to be homogeneous, or suitably heterogeneous. This phase can be carried out either supervised or unsupervised; and
- *Labeling*: it is the process of allocating diverse pixels to their most likely class based on the use of the feature space decision boundaries. This process can be supervised or unsupervised. If a pixel is not spectrally alike to any of the available classes, then it can be assigned to an unknown class. There are two kinds of relationships between the object and the class label: one-to-one (producing a *hard classification*); or one-to-many (producing a *fuzzy classification*). The object may be a single pixel or a group of neighboring pixels forming a geographical unit. As a result, a thematic map is produced, presentating every pixel with a class label. The end result is a transformation of the digital image data into descriptive labels that classify unlike Earth surface objects or conditions.

2.3.2 The General Classification Techniques

Researchers have presented various approaches for image classification, which can be divided into three general groups (Fig. 2.5) (Pal and Pal 1993).

Statistical classifiers: these are ideally suitable for data that have information with an assumed theoretical model based distribution within each of the classes. The representative algorithms for this group are: MLC; PPC; k-NNC and MDC. Corresponding literature for these algorithms can be found in Swain and Davis (1978) and Hastie et al. (2001). *Fuzzy mathematical approaches*: Zadeh (1965) presented the concept of fuzzy sets in which unclear knowledge can be used to delineate a result. *Artificial intelligence* (*AI*): here, supervised classification approaches were developed from the starting of the 1970s, with the well-known "Arch Concept Learning" problem presented by Winston (1975). These methods based on the learning from descriptions of a constructive pattern, and therefore gave up the value-attribute based model that was used in other methods. AI-type models were constructed based on semantic networks and on predicate logic.

Liu and Mason (2009) summarized the classification approaches in seven categories: unsupervised classification; supervised classification; hybrid classification; single pass classification; iterative classification; image scanning classification; and feature space partition. In most cases, image classification approaches included: supervised and unsupervised; parametric and nonparametric; hard and soft (fuzzy) classification; per-pixel, sub-pixel, object-oriented and per-field; spectral classifiers, contextual classifiers and spectral-contextual classifiers; or combinative approaches of multiple classifiers (Lu and Weng 2007). This article presents: present practices; remotely sensed data classification troubles and scenarios. It highlighted the main advanced classification approaches, in addition to those techniques that can improve the at-end classification accuracy.

Unsupervised classification: when insufficient ground reference information is available (e.g., field work measurements) about the characteristics of specific classes for classification processes, an unsupervised classification is used to identify natural homogeneous groups (clusters) within the remotely sensed data. Unsupervised classification approaches are based on non-parametric statistical approaches, such as Iterative Self-Organizing Data Analysis Technique (ISODATA) (Tou and Gonzalez 1974), K-means-clustering (Johnson and Wichern 1988) algorithms, and the advanced unsupervised neural classification method Self-Organizing feature Mapping (SOM) (Kohonen 1989). In this approach, the

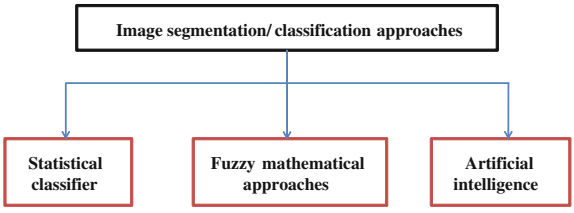

Fig. 2.5 Major approaches for image segmentation/ classification (*Source* modified after Pal and Pal 1993)

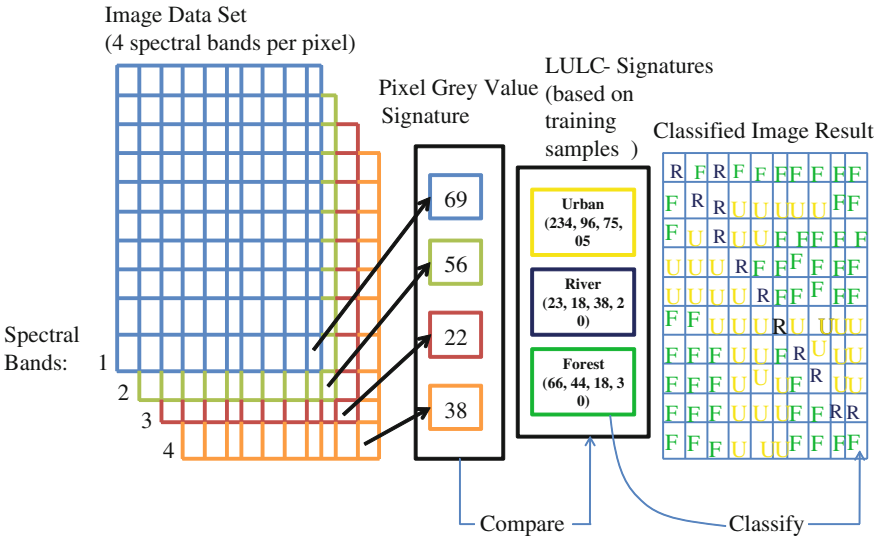

Fig. 2.6 The principal idea of the supervised classification approach for multi-spectral remote sensing (*Source* modified from Eastman 2006)

image processing software groups pixels that have similar properties (in feature space and in adequate representative spectrally-separable clusters for the ground surface features), based on the statistics of the radiometric value/digital number of each pixel. Then the analyst evaluates the classified map with field survey data, aerial photographs and other reference data, and labels these clusters (spectral classes) with its equivalent in the real world to information classes, without having a prior knowledge of the classes. Generally, some clusters must be subdivided or combined to make this equivalence. Results of an unsupervised classification can be used to define the training samples, which are a main input in the supervised classification, or the labeled cluster map can be just accepted as the final map (Schowengerdt 2007).

Supervised classification: supervised approaches, as seen in Fig. 2.6, are based upon training sites, and can assure the former but not the latter; unsupervised approaches can assure the latter but not the former (Tso and Mather 2009). Each image is characterized by *n*-observations (the values in *n*-data bands). Supervised image classification is an approach in which the analyst delineates the training samples (vectors in an *n*-dimensional feature space) on the image which are representative of each interested LULC-class (Mather 2004). A basic step in supervised classification and mapping is the design of a realistic classification scheme, which satisfies a clear definition of separable discrete informational LULC-categories within the available data (Cingolani et al. 2004). Training sites/samples can be created from fieldwork, aerial photography and other existing maps based on analyst knowledge (e.g., Google Earth), and are then used as reference information (Lillesand et al. 2008). Visual interpretation is used to locate the

training samples position on the image (Mather 2004). These training samples have to be homogeneous spectrally to represent specific LULC-classes. A supervised algorithm, after the training samples stage, uses the distribution of the training samples for each class to assess density functions in the feature space statistically and to divide the space into class regions (Fukunaga 1990). In other words, the used image's processing software recognizes the spectral signature of each training site based on its statistics, and then classifies the images in different LULC-classes according to the applied classification algorithm (Jensen 2005). Here, the information required from the training data differs from one algorithm to another. The most general and used supervised approaches are: The Maximum Likelihood Classifier (MLC) and the Minimum Distance Classifier (MDC). The advanced supervised classification algorithms are: The Artificial Neural Network (ANN), the Decision Tree Classifier (DTC), the Nearest Neighbor Classifier (NNC) and the Support Vector Machines classifier (SVM).

The supervised approach is more popular but requires more detailed a priori knowledge of the study area and analyst expertise, to identify suitable training sites and the resultant spectra for classification (ERDAS 1999). The characteristics of the training sites selected by the analyst have a great impact on the dependability and the functioning of a supervised classification process. This approach has a more subjective impact on the analyst during the defining of the LULC-categories characteristics and its representative training samples. Supervised classification approaches need more user-data-software interaction, especially in the collection of training data.

A general introduction to pattern recognition and classification is given in the textbooks by Duda et al. (2000) and Bishop (1995, 2006), and in the review paper by Jain et al. (2000). A detailed introduction in the context of remote sensing is given by Richards and Jia (2003).

2.3.3 Remote Sensing Applications in Land Use/Land Cover Mapping

The broad utilization of remote sensing is to extract and represent LULC-information from multispectral imagery as thematic maps, data and GIS-layers (Donnay et al. 2001). Research proves that remote sensing can be considered as a useful tool for studying arid and semi-arid ecosystems (Tucker et al. 1983; Justice and Hiernaux 1986; Townshend and Justice 1986; Maselli et al. 1993; Bastin et al. 1995; Hobbs 1995; Schmidt and Karnieli 2000; Kheiry 2003; Suliman 2003).

In comparison to the more classical classification methodologies such as basic aerial photo interpretation, LULC-mapping using satellite imagery has four distinct advantages: (1) LULC-classes can be mapped faster and often with lower costs; (2) fast and inexpensive updating of LULC-map products is possible, where the satellite imagery are captured for the same geographic area at a high repeat

ratio; (3) remotely sensed data are captured in digital forms and can thus be easily jointed with other types of ground feature information through such techniques as GIS; and (4) the large economies of scale offered by digital satellite image processing make it fairly low-cost to map large areas, meaning it is easier and more cost effective to produce large amounts of map products.

Although the optical remote sensing systems such as LANDSAT-MSS/TM/ETM+, ASTER, and SPOT have limitations in obtaining cloud-free imagery and the resulted difficulties in performing spectral classification for specific categories of LULC (Ulaby et al. 1982), they have proven an efficient device for LULC-mapping (Ji 2000). Kanellopoulos et al. 1992 conducted a 20 class classification test on SPOT High-Resolution Visible (HRV) images, and the end-result was proven to be satisfactory. De Colstoun et al. (2003) applied a decision tree on multi-temporal images from the ETM+ to distinguish between 11 features of land cover. The overall accuracy was clearly enhanced by using classifier ensemble techniques, as boosting. The paper from Berberoglu et al. (2007) aimed to evaluate the usefulness of integrating texture measures into MLC and ANN classifications in a Mediterranean environment, using LANDSAT-TM-imagery. The best classification accuracies were reached by using the ANN classifier. The dealing with the measures of texture characteristics were most effectively with the ANN rather than the MLC classifier. Yuan et al. (2009) explained and applying an automated two-module ANN classification system, i.e. an unsupervised SOM network module and a supervised MLP neural network module, using LANDSAT-TM. After an evaluation of the performance of MLC, DA, and ANN in image classification, ANN classifications have the advantages in image accuracy overall and for single land cover classes.

LULC-Classification using the three VNIR- and six SWIR- bands of ASTER-data has been discussed in the past 10 years. The most commonly used approach is separating the ASTER into two sets of images, i.e. 15 and 30 m resolution, where each have three and six spectral bands, respectively. For each set, support vector machine (SVM)-based algorithms (Zhu and Blumberg 2002) or segmentation algorithms (Marcal et al. 2005) were applied for processing of classification. An approach based on *wavelet fusion* was proposed by Bagan et al. (2004). Other studies based on the Principal Component Analysis (PCA) were used to the nine VNIR and SWIR. From the earlier obtained principal components, a supervised MLC was implemented (Gomez et al. 2005). But, most of the approaches referred to have not adopted thermal band data (TIR) in classification processing. Jianwen and Bagan (2005) used ASTER and the Kohonen's Self-Organized neural network feature Map (KSOM) to LULC-classification. It classified 7 % more accurately than MLC. Also, the study showed that the quality of ASTER was good for LULC classification. Yüksel et al. (2008) used ASTER and converted it into Top Of Atmosphere reflectance data (TOA) to generate LULC-maps according to the CORINE-Land cover project, using supervised and the knowledge-based expert classification systems to get a superior accuracy of the classified image.

These optical remotely sensed data can be integrated with recordings from remote sensing active systems such as the microwave sensors (e.g., Synthetic

Aperture Radar SAR), which has the ability to acquire remotely sensed imagery under various weather condition during both day and night. Studies (Solberg et al. 1994; Huang et al. 2007) using SAR and optical sensor data have confirmed clear enhancement in classification accuracies contrary to an optical sensor alone.

Xu and Gong (2007) evaluated the potential of the Earth Observing-1 (EO-1) Hyperion hyper-spectral (HS) data with that of the EO-1 Advanced Land Imager (ALI) multispectral (MS) data for distinguishing various LULC-classes in Fremont, California.

In addition to the progress achieved by the referenced studies, the use of object- or segment-based classification techniques is another new development in the environment of remote sensing image classification. This approach has achieved generally better success with the narrow bands and high spatial resolution data such as IKONOS, SPOT-5, or QUICKBIRD (Willhauck 2000). In several of the followed studies (e.g., Fuller et al. 2002; Marcal et al. 2005; Platt and Rapoza 2008) segment-based classifications were more accurate than conventional pixel-based classifications.

2.4 Land Use/Land Cover Change Detection Mapping

Change detection analysis is important in monitoring and managing the natural resources of the Earth. It gives statistical analysis of the occurred spatial distribution of the LULC-changes of interest (Singh 1989). Some of its applications are: Monitoring shifting agriculture, estimation of deforestation, estimation of desertification, and other environmental changes (Jingan et al. 2005). Natural change can have a wide impact on natural resources. So, in relation to LULC and natural resource and ecosystem management, there is an important need for timely, permanent, and truthful monitoring of changes occurring. But, the problems challenging the change detection process are: where is the change?, how much?, when did it occur?, and how great is its impact on the ecosystem? (Lambin and Linderman 2006). Changes can occur either suddenly or gradually (Bontemps et al. 2008). Here, the remote sensing techniques take on an increasing importance in natural resource monitoring programs and in answering the above questions (Wiens et al. 2009). In the case of LULC-changes, two kinds of change can be classified from previously published literature: conversion and modification (Lambin et al. 2003). LULC-conversion is the change from one cover category to another (e.g., the complete replacement of an agricultural parcel by man-made buildings), while LULC-modification is the modifications of structure or function without a complete change from one category to another (e.g., changes in productivity, biomass, or phenology).

2.4.1 Change Detection Techniques

There are numerous change detection approaches applied on remotely sensed data, as a result of increasing versatility in processing digital data and increasing computing power (Pacifici et al. 2007). Generally applied approaches are: image differencing; and image rationing (Singh 1989). Some of the proposed supervised and unsupervised approaches in the literature are: write function memory insertion; image algebra; multiple-date composite; post-classification comparison; image differencing; image rationing; change vector analysis; etc. (Nelson 1983; Singh 1989; Sohl et al. 2004). Expert systems and neural networks were too used in change detection (Seto and Liu 2003). These approaches use multi-date imagery from multi- and hyper-spectral sensors, so that alterations, in feature or phenomena, be accurately recognized, measured and if needed observed (Jensen 2007), each of which could be spatially, spectrally, or temporally controlled (Lu et al. 2003a). Figure 2.7 illustrates how the various frequently used techniques are located in this framework.

Returning to Fig. 2.7, change detection techniques can be separated into two general groups, depending on whether the technique needs classification before or after change detection process.

1. Techniques which first detect change and then assign classes (e.g., image differencing or PCA)-Unsupervised Approach- Pre-classification method.

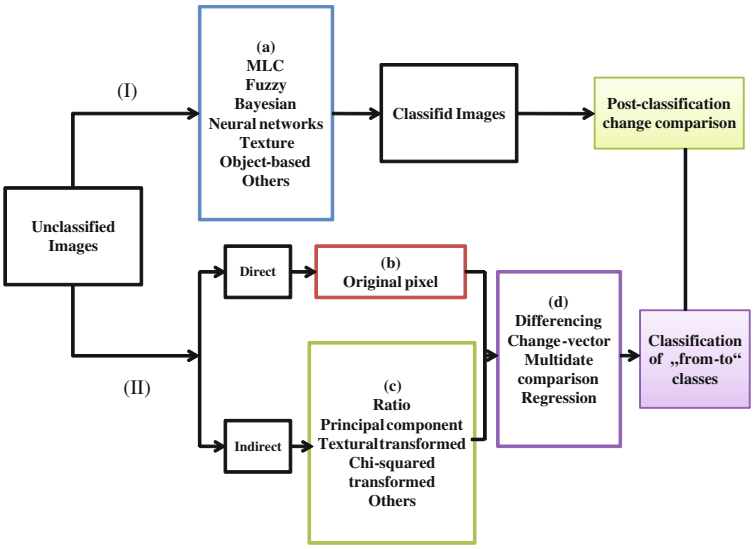

Fig. 2.7 A framework for classifying change detection methods (*Source* modified from Lam 2008)

Many unsupervised change detection approaches deal with the multispectral images to produce an additional image. The most essential basis for these algorithms is the determining of the finest global threshold in the histogram of the so-called generated difference image, where the classifying of change and unchange classes is made on the importance of the resulting spectral change vectors by applying of empirical or theoretical well-founded global threshold strategies. The best global threshold depends on the statistical irregularity of the two images, which are often unknown. Pacifici et al. (2007) reviewed the published techniques in the past decade: the *Image Differencing* (ID), *Normalized Difference Vegetation Index* (NDVI), *Change Vector Analysis* (CVA), *Principal Component Analysis* (PCA), *Image Rationing* (IR), *Expectation Maximization* (EM) (Bruzzone and Fernàndez-Prieto 2000), *Markov Random Field* (MRF) (Bruzzone and Fernàndez-Prieto 2000), Object-Level Change Detection (OLCD) (Hazel 2001), *Reduced Parzen Estimation* (RPE) (Bruzzone and Fernàndez-Prieto 2002), *Maximum a Posteriori Probability* (MPP) decision criterion (Kasetkasem and Varshney 2002), *Multivariate Alteration Detection* (MAD also called *Iteratively Reweighted* MAD (IR-MAD)) (Nielsen 2007), MAD and the combined MAF/MAD (*Maximum Autocorrelation Factor*) transformations, and *Genetic Algorithm* (GA) (Celik 2010).

The above techniques generally do not aim to identify clearly what types of LULC-changes have taken place in an area (e.g., which vegetated areas have been urbanized). They are suitable for applications such as detection of burned areas, or detection of deforestation. However, they are not useful when it is necessary to define the types of changes that have occurred in the studied area, for example, in: observing the shifting in cultivation; urban growth; or where it is required to know all the types of changes that occurred in investigated area.

Advantages: (1) pre-classification is not necessary, so, avoiding the tiring in classification process at the starting; (2) it is regarded as simple and rapid, and can be applied on a great number of images; and (3) the ease in fine-tuning to detect the specific interested changes, and they are, in general, likely to have a higher ability to find slight changes (Yuan et al. 2005). Disadvantages: (1) the detection of image changes, especially if focused on agricultural areas, may be affected by troubles with phenology and cropping. Such troubles could be worsened by inadequate image accessibility and poor quality in moderate zones, and the problems in adjusting poor images (Blaschke 2005); (2) also, these techniques are corrupted by: changes in illumination at two times, changes in atmospheric conditions, and in technical sensor calibration. These make complex a direct evaluation between raw imagery obtained at different times where additional processing steps are required (e.g., radiometric calibration) (Pacifici et al. 2007); and (3) there remains the problem of defining the threshold value at which the change between the two images is measured. Also, it is clear that using unsupervised methods is obligatory in many remote-sensing applications, when appropriate ground truth information is not always available (Bruzzone and Fernàndez-Prieto 2002).

2. Techniques which first assign classes and then detect change (post-classification comparison) Supervised Approach Post classification methods.

In order to overcome the limitations of the first technique, one can use techniques based on a supervised classification of multi-temporal images: *Direct Multi-data Classification* (DMC), *Neural networks* (NNs) (Bishop 1995), *Knowledge-Based Systems* (KBS), *Support Vector Machines* (SVMs) (Vapnik 1998), *Post-Classification Comparison* (PCC) (Del Frate et al. 2005).

The fame of the above techniques may be because they can be freely applied on available created single date classifications, where they are based on separate single-date classifications whose results are later compared with the result of the second independently classified image (Weismiller et al. 1977). This simple technique includes: (1) producing the classified image based on the classification process; and (2) assessment the occurred changes based on the principle of identifying the areas of change as pixel per pixel differences in class membership (Castelli et al. 1999).

Advantages: (1) the ability to clearly identify the kinds of occurred LULC-conversions; (2) the robustness to the various atmospheric and light conditions at the two recording times (Bruzzone and Fernàndez-Prieto 2000); (3) where the two datasets/imagery are separately classified, so it is not needed to normalize these data (Singh 1989); (4) it is more flexible than those used the comparison of multi-temporal raw data; (5) it allows one to make change detection also by using different sensors and/or multi-source data at two times; and (6) the possibility in entering several modifications on the used classifier in classification process (e.g., contextual information as using the texture of an image) would increase the change detection mapping accuracy (Pacifici et al. 2007). Also, the new image classification algorithms, other than the traditional MLC, can be used to increase both accuracy and effectiveness. Disadvantages: (1) requires more human supervision for classifying the images; (2) despite its potential, this category is not relevant to quick change detection, because user supervision is required to pre-classify the images; (3) limitations also include cost in terms of money and implementation time, and generated errors from classification of imagery, where the generation of a suitable training set has the two drawbacks, i.e. the difficulty and the high cost (Bruzzone and Fernàndez-Prieto 2000); and (4) finally, the accuracy of the change thematic map will be equal to the accuracies of each individual classification for each date.

2.4.2 *Change Detection in Arid- and Semi-Arid-Environments*

Approximately 50 % of the total surface areas of the world are arid and/or semi-arid regions (Meadows and Hoffman 2002). Arid and semi-arid areas feature irregular, low precipitation, dry ecosystems, and have a limited sustained economical potential (Adam et al. 1978). Because of the sensitive nature of these areas, it may only require a small amount of turbulence to cause clear changes within the environment (Okin et al. 2001). As a result, remote sensing is quickly becoming an essential tool to use in the study of these areas (Zhou et al. 1998).

There is a variety of problems that confuse the detection of variations in the reflected EMR: (1) low irregular precipitation and high potential ETP allows only spatially-limited low vegetation cover by the available moisture. As a result, the greater part of the area-averaged reflectance of a pixel is for the soil substrate (Smith et al. 1990a). Associated problems in these regions include the low organic components of the soils, which therefore tend to be bright. These issues join to negate, or reduce, the vegetation signal present within an individual pixel (Huete et al. 1985); (2) the variability of soils (light, dark, etc.), and their spectral responses, over the ecosystem of the study area and over the resulting image also cause problems to the detection of vegetation.

Existing remote sensing algorithms allow the application of LULC-change detection in moderate areas of the world (Berberoglu and Akin 2009). However these algorithms are less able to be applied in the Mediterranean environment because: (1) the high temporal variability of the spectral responses of major LC causes large inter-class spectral variability; (2) the complex mixed spatial frequency of the landscape; and (3) the similar reflectance responses of major LC makes spectral separation hard (e.g., the bright toned, often calcareous soil can have alike reflectance responses to urban areas and alike near-infrared reflectance to a crop canopy) (Berberoglu et al. 2000). Therefore, the observation of land cover change is complicated in Mediterranean environments.

Before mapping LULC-change detection using optical sensors data in arid and/or semi-arid areas, we have to answer this question: at which scale is green vegetation detectable and how can we best distinguish it? Siegel and Goetz (1977) demonstrated that major changes in the reflectance characteristics need a vegetation cover of more than 10 %, and that a vegetation signal has a tendency to be more significant than the soil signal when vegetation coverage is more than 30 %. Hill (2000) argued that this does not mean that vegetation coverage of less than 30 % is not detectable by remote sensing, but affirms that ratio based vegetation indices do not offer the best approximation. Vegetation approximation under the spectral un-mixing concept offers better approximation of the true vegetation coverage (Hurcom and Harrison 1998).

A number of change detection studies, such as (Ray 1995; Kwarteng and Chavez 1998; Ram and Chauhan 2009) rely on the clear difference between agricultural fields or urban areas, and the neighboring arid environment, in order to detect LULC-change. However, for example, the detection of vegetative change (within the same LULC-category) within arid areas is significantly more difficult. Image differencing, especially the vegetation index differencing, is one of the most familiar vegetation change detection approaches, because of its simplicity (Singh 1989; Lu et al. 2003a). Pilon et al. (1988) favored the use of the visible red spectral band information to detect changes for their semi-arid study area. Chavez and Mackinnon (1994) established that the red band differencing process presented improved information about vegetation change rather than NDVI in an arid environment. Lyon et al. (1998) accomplished that the NDVI-vegetation index differencing technique achieved the best when comparing several vegetation indices for change detection.

Serrano et al. (2000) compared different techniques developed to create a homogeneous time series of LANDSAT images from 1984 to 2007 for the Middle Ebro Valley in Spain. Mahmood and Easson (2006) explored the capability of using ASTER imagery integrated with LANDSAT-7-ETM+ imagery of south-western Bangladesh to detect equivalent measurements for change detection studies. The used methods were regression with Discrete Fourier Transform (DFT) and the cross-calibration method using digital number ratios. French et al. (2008) demonstrated and confirmed a method using ASTER-imagery obtained between 2001 and 2003 over the Jornada Experimental Range, to map the LULC-changes in a semi-arid area in southern New Mexico, USA. The results emphasize the importance of multispectral thermal infrared data that contains observations at wavelengths within 8–9.5 μm. Alberga (2009) proposed a technique for probable change detectors in multi-sensor configurations, based on similarity measures that did not rely totally on radiometric values. A chain of such measures was used for automatic change detection of optical and SAR-images and an evaluation of their functioning were carried out to detect the limits of their applicability and their understanding to the occurred changes.

2.5 Remote Sensing for Irrigated Agriculture

Exact information on irrigation spatial coverage is the foundation of many sides of the knowledge of the Earth's systems and global change research. Ozdogan and Gutman (2008) defined irrigation as "agricultural area that receives full or partial application of water to the soil to offset periods of precipitation shortfalls under dry land conditions". The remote sensing techniques offer a unique approach to the gathering of various data across place and time, facilitating the application of various methods to obtain irrigated area statistics. In addition, time-series remotely sensed data allow the dynamics of irrigated agriculture to be clearly researched, as differing from other land uses (mapping). To date, a number of researchers have used remote sensing to observe irrigated agriculture (Ozdogan 2010). Initial efforts focused on applying remote sensing in mapping and to update irrigated land areas mostly in the US and India (Draeger 1976; Rundquist et al. 1989). More recently, studies on classification irrigated areas were carried out based on advanced classification algorithms (Abuzar et al. 2001). These researchers concluded that irrigation monitoring and mapping using remote sensing were at an advanced phase of improvement (Ozdogan et al. 2006) and that multi-temporal data were more effective rather than single-date data in determining individual irrigated crop classes (Thiruvengadachari 1981). Spatial resolution of used remotely sensed data for irrigation mapping was seen as vital to obtaining sufficient spatial details about the irrigated fields (Pax-Lenney and Woodcock 1997), as was the potential of vegetation indices in classification irrigated fields, if suitable time-series are obtainable. This latter fact was proved in several studies (Martinez-Beltran and Calera-Belmonte 2001).

2.5.1 Remote Sensing Approaches for Vegetation Studies

The optical characteristics of vegetation and different leaves were explained in detail by (Kumar et al. 2001). In general the reflectance of vegetation in the visible wavelengths (0.43–0.66 μm) is small and reflection in near infrared (0.7–1.1 μm) is large (Fig. 2.2). The life cycle in crop plants includes the three major phases: a vegetative stage, reproductive phase and a grain-filling stage. Three features of leaves have an important impact on their reflectance characteristics: pigmentation (e.g., chlorophyll a and b), physiological structure and water content. *Pigments* absorb the energy of the visible wavelengths, where the highest level of absorption from chlorophyll a is located at 430 and 480 nm, while for chlorophyll b it is at 450 and 650 nm. As, the bandwidth of the TM is too wide to detect these thin absorption bands (Bidwell 1974). The reflectance response of *vegetation canopy* is affected by: the vegetated and non-vegetated areas spatial distribution, vegetation classes, leaf area index, distribution of the leaf angle, and bio-chemical and physical vegetation conditions. The *water content* of the leaves and water in the atmosphere decrease overall leaf reflectance and causes some thin absorption features (Irons et al. 1989).

The spectral response of vegetation changes permanently during the growing season and with alterations in moisture content. Appropriate information about these changes assists in the determining of the best time period for field work and in determining biophysical features to be measured. Figure 2.8 illustrates a simplified spectral reaction curve for vegetation from 400 to 2.500 nm. The relationship between the irradiation absorption and the irradiation reflection illustrated in this figure changes with wavelength. The biophysical controls (pigment, cell structure and water) of the irradiation to plant interaction are also affected by differing wavelengths (McCoy 2005).

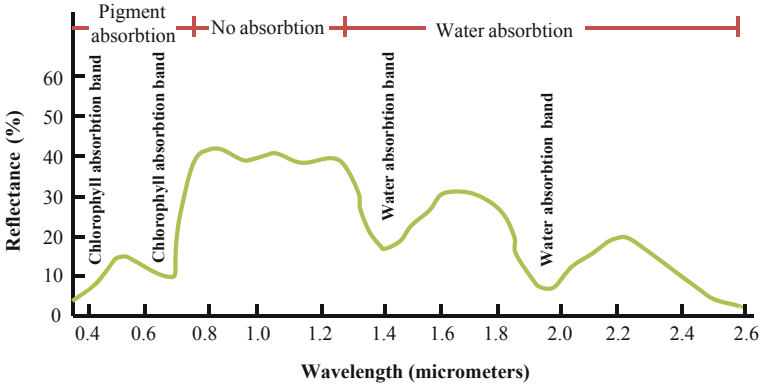

Fig. 2.8 The typical spectral response curve for vegetation showing the characteristic bands that differentiate vegetation spectrally (*Source* modified from Hoffer and Johannsen 1969)

Factors controlling the spectral responses of the vegetation and its reflectance measurements include many natural and technical parameters, such as: atmosphere conditions (e.g., the quantity of occurring sunrays and the proportion of water vapor, change reflectance from plant canopies) (Gao and Goetz 1992); soil background (Mickelson et al. 1998); wind (Lord et al. 1985); viewing angle (Galvao et al. 2004); the altitude of the sensor from plant canopies; and the amount of light.

There is an important relationship between the available images for an individual study area and the plant growth stages, where the growth stage determines which images are suitable for separation between the crops spectrally. So, learning the phenological details about the crops of interest to an individual study area may be required. These phenological details refer to the natural vegetation calendar or a crop calendar. Data for these calendars can be obtained from: literature of previous ecological studies; meeting with qualified field-oriented ecologists; in state or regional bureaus engaged with natural resource management in the region; or from field-work based observation and measurements (e.g., Spectrometer measurements).

Single-date captured remotely sensed data would be inadequate for primarily vegetated areas described by large temporal changeability and typical spatial patterns of highly frequent land cover changes between vegetation canopies. Multi-date remote sensing would be able to cover this problem: when specific data might not be suitable to separate individual LULC-classes, the use of another acquisition date might prove more appropriate for classification. Therefore, the use of the total multi-temporal information gives us a better separation between several classes, and consequently, more classification accuracy (see Fig. 5.23). Crop phenology understanding is very important in crop monitoring and classification (Chen et al. 2008).

2.5.2 Crop Discrimination from Satellite-Based Images

The most frequently practiced utilization of remote sensing for agriculture is the identification of crop types and then classification (Van Niel and McVicar 2000), where crop discrimination is a critical and difficult first step for most agricultural observing activities. The capability of remotely sensed data to identify crop class makes it promising to classify and estimate each crop area, and so calculate the relevant statistics automatically that can used as inputs to crop production forecasting models (Blaes et al. 2005). The application of remote sensing for discrimination between agricultural crop classes and internal crop characteristics has been widely studied throughout the past decade (Senay et al. 2000; Blaes et al. 2005; Satalino et al. 2009). Most of these researchers have focused on increasing classification accuracy through the development of several techniques and methods. In contrast, only small studies have been presented on determining the best time(s) to obtain images in order to distinguish different crops (Van Niel and McVicar 2004).

The temporal information dimension in used remotely sensed data is the most useful factor in natural vegetation and agricultural applications for identifying crop types (Wardlow et al. 2007). This is because agricultural features have great (within-class and within-season) spectral flexibility, that is based on several complex natural and biophysical factors (e.g., crop type/s, soil, water and geographical location). The observation and understanding of these various spectral responses of crops, and comparison with the physical characteristics of remotely sensed data recorded in various dates in the year (building a crop-specific temporal record), would give us the appropriate date(s) during the growing stages in which the crops of interest are spectrally separable. Also, by observing the physical derived spectral indices from remotely sensed data that are sensitive to natural vegetation cover over time, it is possible to discriminate crops (Ozdogan 2010).

Discrimination of crops using remote sensing imagery is generally achieved with supervised or unsupervised classification algorithms (Jensen 2007). Recently, nonparametric algorithms, expert knowledge and ancillary data have been used in the process of cropland classification, improving the overall classification accuracy. One example of this is the establishment of neural networks for crop type identification, which is the most important development in information extraction from remotely sensed data in the last 15 years (Del Frate et al. 2003). Multi-sensor data fusion and classification of time series data are being applied in cropland classification more and more (Chen et al. 2008). The most simple method of distinguishing crops is the classification of images into large-scale classification categories including all agricultural features (Level 1 in LULC-classification) (Campbell 2002). From this level of classification, agricultural features can be classified into cropping and non-cropping regions.

The interaction between crop field scale and pixel size is a significant factor, especially in heterogeneous cropping areas. For instance, large pixel dimensions allow an increasing chance of recording mixed reflectance values. This resulted mixed spectral response is confused by traditional local agricultural management practices, such as found in most areas of the Euphrates River Basin, where crops are sometimes planted in almost 30 m strips (see Fig. 5.29). This is alternated with un-cropped areas (bare soil, stubble, dirt roads, etc.) of similar size to the cropped strips. So, pixels that are not entirely homogeneous (e.g., solely forest, vegetation, wheat crop, etc.), have mean reflectance values (composite spectral response that might match neither feature's spectral response) as a result of more than one feature within the pixel area. Such pixels are known as mixels and are an ever-present problem in cropland classification, reducing their discriminating power (Chen et al. 2008). Spectral Mixture Analysis techniques (SMA) have been developed and used to solve the mixel-problem in remotely sensed data (Fitzgerald et al. 2005). Confusion between natural vegetation and cropland is also another major source of error in crop classification using low spatial and/or spectral resolution remotely sensed data. Sometimes this is also true of high-resolution imagery. This type of confusion is especially common in areas with very complicated traditional local agricultural management practices, which are controlled by natural topography or from land ownership (Loveland et al. 1999). An

additional factor to the quantity of this confusion type is the seasonal variation in the NDVI signals caused by seasonal difference in illumination geometry, which imitates a phenological cycle (McIver and Friedl 2002).

In order to support the capability of remotely sensed data to discriminate between the various crops, researchers have investigated many alternatives which have to do with: The sensor-type (e.g., optical or microwave); number of images (e.g., single-date or multi-date); timing of the imagery; digital processing techniques; or ancillary and spatial data integrating in the classification process (Van Niel and McVicar 2000).

2.5.3 Crop Area Estimation from Satellite-Based Images

Crop area measurement and survey are very common practices in agriculture. Photo-interpretation of images can give better information than statistical analysis to evaluate an amount, or area, for a thematic category (Ozdogan and Woodcock 2006). Usually, crop area estimation has been achieved with very costly and hard statistically-based ground surveys that do not determine either the area or the geographical distribution of individual crops. To overcome or decrease these drawbacks, remote sensing, either alone or in combination with ground surveys, were used in crop area estimation (Wardlow and Stephen 2008). Obtaining full efficiency of remote sensing for crop area estimation depends on the landscape characteristics, especially field size compared with the image resolution, where a suitable resolution for a specific landscape is realized when the most image pixels are pure. But, when this relationship is not realized, for example when using MODIS- or MERIS images especially for landscapes with small fields, then sub-pixel classification techniques (e.g., pixel un-mixing) can be used (GEO 2010). Remote sensing has not been widely used for crop area estimation, due to the tradeoff between spatial detail (the scale of the remote sensing data) and area coverage for each image. In addition, there is the relationship between the spatial resolution of the remotely sensed data and the agricultural field sizes. Agricultural fields in most countries in the world are rather small, requiring medium to high spatial resolution data. However, increases in spatial resolution provide a decrease in the temporal availability which in turn lowers the chance of clouds-free coverage. Even if the clouds-free suitable spatial resolution data were obtainable, the increased number of datasets makes the cost high, and the high spatial resolution sensor covers only small geographical areas at a time. This leads to an additional problem, the need for atmospheric corrections in automated image digital processing and classification, as the required images are often gained at diverse times during the growing cycle of a crop. Medium spatial resolution data (e.g., LANDSAT) may be too coarse in countries with very small cultivated fields (e.g., China), but high spatial resolution is more appropriate for use in countries with large cultivated fields, such as the U.S. (Ozdogan and Woodcock 2006). In contrast, lower spatial resolution data (e.g., MODIS) offer wide temporal and

geographical coverage at continental and global scales, but need detailed spatial information. The fact that not each pixel in an image represents only single crop type can introduce uncertainty into area estimates because of the mixture (Ozdogan and Woodcock 2006). Where cultivated areas are smaller than the spatial resolution of the image, here, both cultivated and uncultivated areas (e.g., roads, houses, irrigation channels) are integrated in a pixel classified as agriculture or cropland. In agricultural situations, the amount of uncultivated area has been reported to vary from 10 to 40 % (Crapper 1980; Frolking et al. 1999). To relatively solve this mixed pixel problem which occurs especially in high temporal resolution data at low spatial resolution, some contributors have developed techniques that use the concept of *temporal un-mixing* (Adams et al. 1986). It is similar to the traditional *spectral un-mixing* technique, where pure end-members are distinguished by their spectral response. Temporal un-mixing uses end-members defined by their single temporal response to improve the fractional area of each end-member based on its part to the mixed temporal reaction observed by the sensor (Ozdogan 2010).

There are two generally used area estimation methods with remote sensing (Ozdogan and Woodcock 2006). The first method calculates portions/fractions of a thematic category of interest for each pixel (Hansen et al. 2002). The essential drawback here is the accuracy assessment of fractions of the thematic field. However, area estimation by this method is becoming more common (Liu and Wu 2005). A second method is based on generating the thematic map through image classification and then multiplying the area of the pixels with their number in a specific class. The drawback here is the classification accuracy of the thematic map (Ozdogan and Woodcock 2006).

References

Abuzar, M., McAllister, A., & Morris, M. (2001). Classification of seasonal images for monitoring irrigated crops in a salinity-affected area of Australia. *International Journal of Remote Sensing, 22*(5), 717–726.

Adams, J. B., Smith, M. O., & Johnson, P. E. (1986). Spectral mixture modeling: A new analysis of rock and soil types at Viking Lander I site. *Journal of Geophysical Research*, *91* (B8), 8098–8112.

Adam, R., Adams, M., & Willens, A. (1978). *Dry lands: Man and plants* (1st ed.). London: The Architectural Press Ltd.

Alberga, V. (2009). Similarity measures of remotely sensed multi-sensor images for change detection applications. *Remote Sensing, 1*(3), 122–143.

Bagan, H., Jianwen, M., Qiqing, L., Xiuzhen, H., & Zhili, L. (2004). Land-use classification from ASTER data using wavelet fusion and self-organized neural networks. *Science in China Series D-Earth Sciences, 47*(7), 651–658.

Bastin, G. N., Pickup, G., & Pearce, G. (1995). Utility of AVHRR data for land degradation assessment: A case study. *International Journal of Remote Sensing, 16*(4), 651–672.

Beaumont, P. (1996). Agricultural and environmental changes in the upper Euphrates catchment of Turkey and Syria and their political and economic implications. *Applied Geography, 16*(2), 137–157.

Berberoglu, S., & Akin, A. (2009). Assessing different remote sensing techniques to detect land use/cover changes in the eastern Mediterranean. *International Journal of Applied Earth Observation and Geoinformation, 11*(1), 46–53.

Berberoglu, S., Curran, P. J., Lloyd, C. D., & Atkinson, P. M. (2007). Texture classification of Mediterranean land cover. *International Journal of Applied Earth Observation and Geoinformation, 9*(3), 322–334.

Berberoglu, S., Lloyd, C. D., Atkinson, P. M., & Curran, P. J. (2000). The integration of spectral and texture information using neural networks for land cover mapping in the Mediterranean. *Computers & Geosciences, 26*(4), 385–396.

Bidwell, R. G. S. (1974). *Plant physiology*. New York: MacMillan Publishing Company Inc.

Bishop, C. M. (1995). *Neural networks for pattern recognition*. Oxford: Oxford University Press.

Bishop, C. M. (2006). *Pattern recognition and machine learning* (1st ed.). New York: Springer.

Blaes, X., Vanhalle, L., & Defourny, P. (2005). Efficiency of crop identification based on optical and SAR image time series. *Remote Sensing of Environment, 96*(3–4), 352–365.

Blaschke, T. (2005). Towards a framework for change detection based on image objects. In S. Erasmi B. Cyffca & M. Kappas (Eds.), *Remote Sensing & GIS for Environmental Studies, (Göttinger Geographische Abhandlungen)* (Vol. 113). Göttingen: Verlag Erich Goltze.

Bontemps, S., Bogaert, P., Titeux, N., & Defourny, P. (2008). An object-based change detection method accounting for temporal dependences in time series with medium to coarse spatial resolution. *Remote Sensing of Environment, 112*(6), 3181–3191.

Bruzzone, L., & Fernàndez-Prieto, D. (2000). Automatic analysis of the difference image for unsupervised change detection. *IEEE Transactions on Image Processing, 38*(3), 1171–1182.

Bruzzone, L., & Fernàndez-Prieto, D. (2002). An adaptive semi-parametric and context-based approach to unsupervised change detection in multitemporal remote sensing images (Technical Report). Also: Appeared on *IEEE Transactions on Image Processing, 11*(4), 452–466.

Campbell, B. C. (2002). *Introduction to remote sensing*. London: Taylor and Francis.

Castelli, V., Elvidge, D. C., Li, C. S., & Turek, J. J. (1999). Classification-based change detection: Theory and applications to the NALC data set. In R. S. Lunetta & C. D. Elvidge (Eds.), *Remote sensing change detection environmental monitoring methods and applications* (Chapter 4: pp. 53–73). London: Taylor and Francis.

Celik, T. (2010). change detection in satellite images using a genetic algorithm approach. *IEEE Geoscience and Remote Sensing Letters, 7*(2), 386–390.

Celis, D., De Pauw, E., & Geerken, R. (2007a). *Assessment of land cover and land use in Central and West Asia and North Africa (CWANA) using AVHRR and agroclimatic data* (part 1.: land cover/land use—base year 1993, p. 54). Aleppo, Syria: ICARDA.

Celis, D., De Pauw, E., & Geerken, R. (2007b). *Assessment of land cover and land use in Central and West Asia and North Africa (CWANA) using AVHRR and agroclimatic data* (part 2: hot spots of land cover change and drought vulnerability, p. 69). Aleppo, Syria: ICARDA.

Chavez, P. S., & Mackinnon, D. J. (1994). Automatic detection of vegetation changes in the southwestern United States using remotely sensed images. *Photogrammetric Engineering & Remote Sensing, 60*(5), 571–583.

Chen, Z., Li, S., Ren, J., Gong, P., Zhang, M., Wang, L., et al. (2008). Monitoring and management of agriculture with remote sensing. In S. Liang (Ed.), *Advances in land remote sensing—system, modelling, inversion and adaptation* (pp. 397–421). University of Maryland, USA: Springer.

Cingolani, A. M., Renison, D., Zak, M. R., & Cabido, M. R. (2004). Mapping vegetation in a heterogeneous mountain rangeland: An alternative method to define and classify land-cover units. *Remote Sensing of Environment, 92*(1), 84–97.

Crapper, P. F. (1980). Errors incurred in estimating an area of uniform land cover using Landsat. *Photogrammetric Engineering and Remote Sensing, 46*(10), 1295–1301.

De Colstoun, E. C. B., Story, M. H., Thompson, C., Commisso, K., Smith, T. G., & Irons, J. R. (2003). National park vegetation mapping using multitemporal Landsat 7 data and a decision tree classifier. *Remote Sensing of Environment, 85*(3), 316–327.

De Pauw, E. (2005). Mapping the agricultural regions of Syria. In Annual Report (2004) (Ed.), *Natural resource management program*. Aleppo, Syria: ICARDA.

De Pauw, E., Oberle, A., & Zöbisch, M. (2004). *Land cover and land use in Syria: An overview*. Jointly published by Asian Institute of Technology (AIT), International Center for Agricultural Research in the Dry Areas (ICARDA) and the World Association of Soil and Water Conservation (WASWC).

Del Frate, F., Ferrazzoli, P., & Schiavon, G. (2003). Retrieving soil moisture and agricultural variables by microwave radiometry using neural networks. *Remote Sensing of Environment, 84*(2), 174–183.

Del Frate, F., Schiavon, G., Solimini, C. (2005). Use of high resolution satellite data for change detection in urban areas. In *Proceedings of ESA EUSC 2005 Conference: Image Information Mining—Theory and Application to Earth Observation, October, 2005, ESA/ESRIN, Frascati, Italy*.

Donnay, J., Barnsley, M. J., & Longley, P. A. (2001). *Remote Sensing and Urban Analysis*. New York: Taylor and Francis.

Draeger, W. (1976). *Monitoring irrigated land acreage using Landsat imagery: An application example*. USGS Open-file Report No. 76–630, (pp. 23). USGS, Sioux Falls, S.D.

Duda, R. O., Hart, P. E., & Stork, D. G. (2000). *Pattern classification* (2nd ed.). Chichester, New York: Wiley.

Eastman, J. R. (2006). *IDRISI Andes tutorial*. Worcester, USA: Clark Labs.

ERDAS. (1999). *Field guide: Earth resources data analysis system*. Atlanta, Georgia: ERDAS Inc.

Fitzgerald, G. J., Pinter, J., Hunsaker, D. J., & Clarke, T. R. (2005). Multiple shadow fractions in spectral mixture analysis of a cotton canopy. *Remote Sensing of Environment, 97*(4), 526–539.

French, A. N., Schmugge, T. J., Ritchie, J. C., Hsu, A., Jacob, F., & Ogawa, K. (2008). Detecting land cover change at the Jornada Experiment Range, New Mexico, with aster emissivities. *Remote Sensing of Environment, 112*, 1730–1748.

Frolking, S., Xiao, X., Zhuang, Y., Salas, W., & Li, C. (1999). Agricultural landuse in China: A comparison of area estimates from ground-based census and satellite-borne remote sensing. *Global Ecology and Biogeography, 8*(5), 407–416.

Fukunaga, K. (1990). *Introduction to statistical pattern recognition* (2nd ed.). Boston: Academic Press.

Fuller, R., Smith, G., Sanderson, J., Hill, R., & Thomson, A. (2002). The UK land cover map 2000: Construction of a parcel-based vector map from satellite images. *Cartographic Journal, 39*(1), 15–25.

Galvao, L. S., Ponzoni, F. J., Epiphanio, J. C. N., Rundorff, B. F. T., & Formaggio, A. R. (2004). Sun and view angle effects on NDVI determination of land cover types in the Brazilian Amazon region with hyperspectral data. *International Journal of Remote Sensing, 25*(10), 1861–1879.

Gao, B. C., & Goetz, A. F. H. (1992). A linear spectral matching technique for retrieving equivalent water thickness and biochemical constituents of green vegetation, pp. 35–37. In *Proceedings of the Third Airborn Annual JPL Geosciences Workshop (AVIRIS, TIMS and AIRSAR), Jet Propulsion Laboratory, Pasadena, CA*.

Gomez, C., Delacourt, C., Allemand, P., Ledru, P., & Wackerle, R. (2005). Using ASTER remote sensing data set for geological mapping, in Namibia. *Physics and Chemistry of the Earth, 30*(1–3), 97–108.

Group on Earth Observation/GEO. (2010). *Best practices for crop area estimation with remote sensing*. Retrieved September 14, 2010, from http://www.earthobservations.org/documents/cop/ag_gams/GEOSS%20best%20practices%20area%20estimation%20final.pdf.

Harrison, B. A., & Jupp, D. L. B. (1989). *Introduction to remotely sensed data*. Melbourne: CSIRO Publications.

Hastie, T., Tibshirani, R., & Friedman, J. (2001). *The elements of statistical learning*. New York: Springer.

Hazel, G. G. (2001). Object-level change detection in spectral imagery. *IEEE Transactions on Geoscience and Remote Sensing, 39*(3), 553–561.

Hansen, M. C., DeFries, R. S., Townshend, J. R. G., Sohlberg, R., Dimiceli, C., & Caroll, M. (2002). Towards an operational MODIS continuous field of percent tree cover algorithm: Examples using AVHRR and MODIS data. *Remote Sensing of Environment, 83*(1–2), 303–319.

Hill, J. D. (2000). Assessment of semiarid lands: Monitoring dryland ecosystems through remote sensing. In R. Meyers (Ed.), *Encyclopedia of analytical chemistry: Instrumentation and applications* (pp. 8769–8794). Wiley, Chichester.

Hirata, M. K., Shinjo, N., Fujita, H., Gintzburger, H., Miyazaki, G., & Akira, (2001). Vegetation classification by satellite image processing in a dry area of north-eastern Syria. *International Journal of Remote Sensing, 22*(4), 507–516.

Hobbs, T. J. (1995). The use of NOAA-AVHRR NDVI data to assess herbage production in the arid rangelands of central Australia. *International Journal of Remote Sensing, 16*(7), 1289–1302.

Hoffer, R. M., & Johannsen, C. J. (1969). Ecological potential in spectral signature analysis. In P. L. Johnson (Ed.), *Remote sensing in ecology* (pp. 1–16). Athens: University of Georgia Press.

Huang, H., Legarsky, J., & Othman, M. (2007). Land-cover classification using radarsat and Landsat imagery for St. Louis, Missouri. *Photogrammetric Engineering & Remote Sensing, 73*(1), 037–043.

Huete, A. R., Jackson, R. D., & Post, D. F. (1985). Spectral response of a plant canopy with different soil backgrounds. *Remote Sensing of Environment*, *17*(1), 37–53.

Hurcom, S. J., & Harrison, A. R. (1998). The NDVI and spectral decomposition for semi-arid vegetation abundance estimation. *International Journal of Remote Sensing, 19*(16), 3109–3125.

Irons, J. R., Weismiller, R. A., & Petersen, G. W. (1989). Soil reflectance. In G. Asrar (Ed.), *Theory and applications of optical remote sensing* (pp. 66–106). New York: Wiley.

Jain, A. K., Duin, R. P. W., & Mao, J. C. (2000). Statistical pattern recognition: A review. *IEEE Transactions on Pattern Analysis and Machine Intelligence, 22*(1), 4–37.

Jensen, J. R. (2005). *Introductory digital image processing: A remote sensing perspective* (3rd ed.). New Jersey: Prentice Hall Series in Geographic Information Science.

Jensen, J. R. (2007). *Remote sensing of the environment: An earth resource perspective* (2nd ed.). New Jersey: Pearson Prentice Hall.

Ji, C. Y. (2000). Land-use classification of remotely sensed data using Kohonen self-organizing feature map neural networks. *Photogrammetric Engineering & Remote Sensing, 66*(12), 1451–1460.

Jianwen, M., & Bagan, H. (2005). Land-use classification using ASTER data and self-organized neutral networks. *International Journal of Applied Earth Observation and Geoinformation, 7*(3), 183–188.

Jingan, S., Jiupai, N., Chaofu, W., & Deti, X. (2005). Land use change and its corresponding ecological responses: A review. *Journal of Geographical Sciences, 15*(3), 305–328.

Johnson, R. A., & Wichern, D. W. (1988). *Applied multivariate statistical analysis* (2nd ed.). New Jersey: Prentice-Hall, Inc.

Justice, C. O., & Hiernaux, P. H. Y. (1986). Monitoring the grasslands of the Sahel using NOAA AVHRR data: Niger 1983. *International Journal of Remote Sensing, 7*(11), 1475–1497.

Kanellopoulos, I., Varfis, A., Wilkinson, G. G., & Mégier, J. (1992). Land-cover discrimination in SPOT HRV imagery using an artificial neural network: A 20-class experiment. *International Journal of Remote Sensing, 13*(5), 917–924.

Kasetkasem, T., & Varshney, P. K. (2002). Image change detection algorithm based on Markov random field moedels. *IEEE Transactions on Geoscience and Remote Sensing*, *40*(8), 1815–1823.

Kheiry, M. A. (2003). *Monitoring and evaluation of vegetation cover changes in semi-arid areas: A case study of khartoum forest sub-sector, Sudan*. Master thesis, TUD, Germany.

Kohonen, T. (1989). *Self-organisation and associative memory*. New York: Springer.

Kumar, L., Schmidt, K., Dury, S., & Skidmore, A. (2001). Imaging spectrometry and vegetation science. In F. D. Van der Meer & S. M. De Jong (Eds.), *Imaging spectrometry* (pp. 111–155). Dordrecht: Kluwer Academic Publishers.

Kwarteng, A. Y., & Chavez, P. S, Jr. (1998). Change detection study of Kuwait city and environs using multitemporal Landsat Thematic Mapper data. *International Journal of Remote Sensing, 19*(9), 1651–1661.

Lam, N. S.-N. (2008). Methodologies for mapping land cover/land use and its change. In S. Liang (Ed.), *Advances in land remote sensing* (pp. 341–367). New York: Springer.

Lambin, E. F., Geist, H. J., & Lepers, E. (2003). Dynamics of land-use and land-cover change in tropical regions. *Annual Review of Environment Resources, 28*, 205–241.

Lambin, E. F., & Linderman, M. (2006). Time series of remote sensing data for land change science. *IEEE Transactions on Geoscience and Remote Sensing, 44*(7), 1926–1928.

Liu, W., & Wu, E. Y. (2005). Comparison of non-linear mixture models: Subpixel classification. *Remote Sensing of Environment, 94*(2), 145–154.

Lillesand, M. T., Kiefer, R. W., & Chipman, J. W. (2008). *Remote sensing and image interpretation* (6th ed.). Hoboken, NJ: Wiley.

Liu, J. G., & Mason, P. J. (2009). *Essential image processing and GIS for remote sensing*. London, UK: Wiley.

Lord, D., Desjardins, R. L., Dube, P. A., & Brach, E. J. (1985). Variations of crop canopy spectral reflectance measurements under changing sky conditions. *Photogrammetric Engineering and Remote Sensing, 51*(6), 689–695.

Loveland, T. R., Zhu, Z., Ohlen, D. O., Brown, J. F., Reed, B. C., & Yang, L. (1999). An analysis of the IGBP global land-cover characterization process. *Photogrammetric Engineering and Remote Sensing, 65*(9), 1021–1032.

Lu, D., Mausel, P., Brondizio, E., & Moran, E. (2003a). Change detection techniques. *International Journal of Remote Sensing, 25*(12), 2365–2407.

Lu, D., & Weng, Q. (2007). A survey of image classification methods and techniques for improving classification performance. *International Journal of Remote Sensing, 28*(5), 823–870.

Lyon, J. G., Yuan, D., Lunetta, R. S., & Elvidge, C. D. (1998). A change detection experiment using vegetation indices. *Photogrammetric Engineering and Remote Sensing, 64*(2), 143–150.

Mahmood, T., & Easson, G. (2006). Comparing aster and Landsat-7 ETM+ for change detection. In *Proceedings of ASPRS Annual Conference, May 1–5, 2006, Reno, Nevada*.

Marcal, A. R. S., Borges, J. S., Gomes, J. A., & Da Costa, J. F. P. (2005). Land cover update by supervised classification of segmented ASTER images. *International Journal of Remote Sensing, 26*(7), 1347–1362.

Martinez-Beltran, C., & Calera-Belmonte, A. (2001). Irrigated crop estimation using Landsat TM imagery in La Mancha, Spain. *Photogrammetric Engineering & Remote Sensing, 67*(10), 1177–1184.

Maselli, F., Conese, C., Petkov, L., & Gilabert, M. A. (1993). Environmental monitoring and crop forecasting in the Sahel through the use of NOAA NDVI data. A case study: Niger 1986–89. *International Journal of Remote Sensing, 14*(18), 3471–3487.

Mather, P. M. (2004). *Computer processing of remotely-sensed images: An introduction* (3rd ed.). Chichester: Wiley.

McCoy, R. M. (2005). *Field methods in remote sensing*. New York, NY: Guilford Press.

McIver, D. K., & Friedl, M. A. (2002). Using prior probabilities in decision-tree classification of remotely sensed data. *Remote Sensing of Environment, 81*(2–3), 253–261.

McVicar, T. R., & Jupp, D. L. B. (1998). The current and potential operational uses of remote sensing to aid decisions on drought exceptional circumstances in Australia: A review. *Agricultural Systems, 57*(3), 399–468.

Meadows, M. E., & Hoffman, M. T. (2002). The nature, extent and causes of land degradation in South Africa: Legacy of the past, lessons for the future? *Area, 34*(4), 428–437.

Mickelson, Jr, John, G., Civco, D. L., Silander, Jr, & John, A. (1998). Responses of spectral indices to variations in vegetation cover and soil background. *Photogrammetric Engineering and Remote Sensing, 64*(9), 915–921.

Nelson, R. F. (1983). Detecting forest canopy change due to insect activity using Landsat MSS. *Photogrammetric Engineering & Remote Sensing, 49*, 1303–1314.

Nielsen, A. A. (2007). The regularized iteratively reweighted MAD method for change detection in multi- and hyperspectral data. *IEEE Transactions on Image Processing, 16*(2), 463–478.

Okin, G. S., Murray, B., & Schlesinger, W. H. (2001). Degradation of sandy arid shrubland environments: Observation, process modelling, and management implications. *Journal of Arid Environments, 47*(2), 123–144.

Ozdogan, M. (2010). The spatial distribution of crop types from MODIS data: Temporal unmixing using independent component analysis. *Remote Sensing of Environment, 114*(6), 1190–1204.

Ozdogan, M., & Gutman, G. (2008). A new methodology to map irrigated areas using multi-temporal MODIS and ancillary data: An application example in the continental US. *Remote Sensing of Environment, 112*(9), 3520–3537.

Ozdogan, M., Salvucci, G. D., & Anderson, B. C. (2006). Examination of the Bouchet–Morton complementary relationship using a mesoscale climate model and observations under a progressive irrigation scenario. *Journal of Hydrometeorology, 7*(2), 235–251.

Ozdogan, M., & Woodcock, C. E. (2006). Resolution dependent errors in remote sensing of cultivated areas. *Remote Sensing of Environment, 103*(2), 203–217.

Pacifici, F., Del Frate, F., Solimini, C., & Emery, W. J. (2007). An innovative neural-net method to detect temporal changes in high-resolution optical satellite imagery. *IEEE Transactions on Geoscience and Remote Sensing, 45*(9), 2940–2952.

Pal, N. R., & Pal, S. K. (1993). A review on image segmentation techniques. *Pattern Recognition, 26*(9), 1277–1294.

Pax-Lenney, M., & Woodcock, C. E. (1997). The effect of spatial resolution on the ability to monitor the status of agricultural lands. *Remote Sensing of Environment, 61*(2), 210–220.

Pilon, P. G., Howath, P. J., & Bullock, R. A. (1988). An enhanced classification approach to change detection in semi-arid environments. *Photogrammetric Engineering & Remote Sensing, 54*(12), 1709–1716.

Platt, R. V., & Rapoza, L. (2008). An evaluation of an object-oriented paradigm for land use/land cover classification. *Professional Geographer, 60*(1), 87–100.

Ram, K., & Chauhan, J. S. (2009). Application of remote sensing and GIS to assess land use changes in Jhunjhunu district of arid Rajasthan. *Journal of the Indian Society of Remote Sensing, 37*(4), 671–680.

Ray, T. W. (1995). *Remote monitoring of land degradation in arid/semiarid regions*. Doctoral dissertation, California Institute of Technology.

Richards, J. A., & Jia, X. (2003). *Remote sensing digital image analysis: An introduction* (3rd ed.). New York: Springer.

Robinove, C. J. (1981). The logic of multispectral classification and mapping of land. *Remote Sensing of Environment, 11*, 231–244.

Rundquist, D. C., Hoffman, R. O., Carlson, M. P., & Cook, A. E. (1989). The Nebraska center-pivot inventory: An example of operational satellite remote sensing on a long-term basis. *Photogrammetric Engineering and Remote Sensing, 55*(1), 587–590.

Satalino, G., Mattia, F., Le Toan, T., & Rinaldi, M. (2009). Wheat crop mapping by using ASAR AP data. *IEEE Transactions on Geoscience and Remote Sensing, 47*(2), 527–530.

Schmidt, H., & Karnieli, A. (2000). Remote sensing of the seasonal variability of vegetation in a semi-arid environment. *Journal of Arid Environments, 45*(1), 43–59.

Schowengerdt, R. A. (2007). *Remote sensing models and methods for image processing*. New York: Academic Press.

Senay, G. B., Lyon, J. G., Ward, A. D., & Nokes, S. E. (2000). Using high spatial resolution multispectral data to classify corn and soybean crops. *Photogrammetric Engineering & Remote Sensing, 66*(3), 319–327.

Serrano, L., Filella, I., & Peuelas, J. (2000). Remote sensing of biomass and yield of winter wheat under different nitrogen supplies. *Crop Science, 40*(3), 723–731.

Seto, K. C., & Liu, W. (2003). Comparing ARTMAP neural network with the maximum-likelihood classifier for detecting urban change. *Photogrammetric Engineering and Remote Sensing, 69*(9), 981–990.

Siegel, B. S., & Goetz, A. F. H. (1977). Effect of vegetation on rock and soil type discrimination. *Photogrammetric Engineering and Remote Sensing, 43*(2), 191–196.

Singh, A. (1989). Review article: Digital change detection techniques using remotely-sensed data. *International Journal of Remote Sensing, 10*(6), 989–1003.

Smith, M. O., Ustin, S. L., Adams, J. B., & Gillespie, A. R. (1990a). Vegetation in deserts: I. A regional measure of abundance from multispectral images. *Remote Sensing of Environment, 31*(1), 1–26.

Sohl, T. L., Gallant, A. L., & Loveland, T. R. (2004). The characteristics and interpretability of land surface change and implications for project design. *Photogrammetric Engineering and Remote Sensing, 70*(4), 439–448.

Solberg, A., Schistad, H., Jain, A. K., & Taxt, T. (1994). Fusion of multitemporal satellite images and GIS data for land-use classification. *IEEE Transactions in Geoscience and Remote Sensing, 32*(4), 768–778.

Suliman, M. M. (2003). *Assessing and mapping land use/land cover change using remote sensing and GIS: A case study of El-Amud Al-Akhdar Settlement, southern Darfur-Sudan*. Master thesis, TUD, Germany.

Swain, P. H., & Davis, S. M. (Eds.). (1978). *Remote sensing: The quantitative approach*. New York: McGraw-Hill.

Thiruvengadachari, S. (1981). Satellite sensing of irrigation patterns in semiarid areas: An Indian study. *Photogrammetric Engineering and Remote Sensing, 47*, 1493–1499.

Tou, J., & Gonzalez, R. (1974). *Pattern recognition principles*. Reading, Massachusetts: Addison-Wesley.

Townshend, J. R. G., & Justice, C. O. (1986). Analysis of dynamic of African vegetation using the NDVI. *International Journal of Remote Sensing, 7*(11), 1124–1242.

Tso, B., & Mather, P. M. (2009). *Classification methods for remotely sensed data* (2nd ed.). Boca Raton: CRC Press.

Tucker, C. J., Vanpraet, C., Boerwinkel, E., & Gaston, A. (1983). Satellite remote sensing of total dry matter production in the Senegalese Sahel. *Remote Sensing of Environment, 13*(6), 461–474.

Tutz, G. (2000). *Die Analyse kategorialer Daten: Anwendungsorientierte Einführung in Logit-Modellierung und kategoriale Regression*. München: Oldenbourg Wissenschaftsverlag.

Udelhoven, Th., & Hill, J. (2009). Change detection in Syria's rangelands using long-term AVHRR data (1982–2004). In P. Aplin (Ed.) *Recent advances in remote sensing and geoinformation processing for land degradation assessment* (pp. 117–132). ISPRS Series, Boca Raton: Taylor and Francis Group.

Ulaby, F. T., Moore, R. K., & Fung, A. K. (1982). *Microwave remote sensing: Active and passive, from theory to applications* (vol. III). Massachusetts: Artech House.

Van Niel, T. G., & McVicar, T. R. (2000). *Assessing and improving positional accuracy and its effects on areal estimation at coleambally irrigation area* (Technical Report 101/00, p. 101). Cooperative Research Centre for Sustainable Rice Production.

Van Niel, T. G., & McVicar, T. R. (2004). Determining temporal windows for crop discrimination with remote sensing: A case study in south-eastern Australia. *Computers and Electronics in Agriculture, 45*(1–3), 91–108.

Vapnik, V. N. (1998). *Statistical learning theory*. Chichester, New York: Wiley.

Wardlow, B. D., Egbert, S. L., & Kastens, J. H. (2007). Analysis of time-series MODIS 250 m vegetation index data for crop classification in the U.S. Central Great Plains. *Remote Sensing of Environment, 108*(3), 290–310.

Wardlow, B. D., & Stephen, L. E. (2008). Large-area crop mapping using time-series MODIS 250 m NDVI data: An assessment for the U.S. Central Great Plains. *Remote Sensing of Environment, 112*(3), 1096–1116.

Weismiller, R. A., Kristoof, S. J., Scholz, D. K., Anuta, P. E., & Momen, S. A. (1977). Change detection in coastal zone environments. *Photogrammetric Engineering and Remote Sensing, 43*(12), 1533–1539.

Wiens, J. A., Sutter, R. D., Anderson, M., & Blanchard, J. (2009). Selecting and conserving lands for biodiversity: The role of remote sensing. *Remote Sensing of Environment, 113*(7), 1370–1381.

Wilkinson, G. G. (2005). Results and implications of a study of fifteen years of satellite image classification experiments. *IEEE Transactions on Geoscience and Remote Sensing, 43*(3), 433–440.

Willhauck, G. (2000). Comparison of object oriented classification techniques and standard image analysis for the use of change detection between SPOT multispectral satellite images and aerial photos. *Analysis, XXXIII*, 214–222.

Winston, P. (1975). Learning structural descriptions from examples. In P. Winston (Ed.), *The psychology of computer vision* (pp. 157–209). New York: Mc Graw Hill.

Xu, B., & Gong, P. (2007). Land-use/land-cover classification with multispectral and hyperspectral EO-1 data. *Photogrammetric Engineering & Remote Sensing, 73*(8), 955–965.

Yuan, F., Sawaya, K. E., Loeffelholz, B. C., & Bauer, M. E. (2005). Land cover classification and change analysis of the Twin Cities (Minnesota) metropolitan area by multitemporal Landsat remote sensing. *Remote Sensing of Environment, 98*(2–3), 317–328.

Yuan, H., Van der Wiele, C. F., & Khorram, S. (2009). An automated artificial neural network system for land use/land cover classification from Landsat TM imagery. *Remote Sensing, 1*(3), 243–265.

Yüksel, A., Abdullah, E. A., & Gundogan, R. (2008). Using ASTER imagery in land use/cover classification of Eastern Mediterranean landscapes according to CORINE land cover project. *Sensors, 8*(2), 1237–1251.

Zadeh, L. A. (1965). Fuzzy sets. *Information Control, 8*, 338–353.

Zaitchik, B., Smith, R., & Hole, F. (2002). Spatial analysis of agricultural land use changes in the Khabour river basin of northeaster Syria. In *Proceedings of ISPRS Symposium Land Satellite Information, Denver, Colorado*.

Zhou, Q., Robson, M., & Horn, G. (1998). Comparisons between the results from different ground vegetation cover estimation methods in a rangeland environment. In *Proceedings of the 9th Australasian Remote Sensing and Photogrammetry Conference, Sydney, Australia*.

Zhu, G., & Blumberg, D. G. (2002). Classification using ASTER data and SVM algorithms: The case study of Beer Sheva, Palestina. *Remote Sensing of Environment, 80*, 233–240.

Chapter 3
Overview of Study Area

3.1 Syria

Present-day Syria (Fig. 3.1) forms only a small part of antique geographical Syria. Until the twentieth century, when western forces started to form the irregular outlines of the modern countries of Syria, Lebanon, Jordan, and Palestine, the entire settled land at the eastern ending part of the Mediterranean Sea was named Syria, a name came from the ancient Greeks to the land connection that links the three continents of Asia, Africa, and Europe. Historians and political scientists mostly use the expression "Greater Syria" to indicate this region in the pro-state time. Historically, Greater Syria rarely ruled itself, mainly because of its susceptible location between the Mediterranean Sea and the desert. As a district between commonly powerful empires on the north, east, and south, Syria was frequently an arena for the political fates of dynasties and empires (Kangarani 2006).

3.2 The Euphrates River Basin

The name of this river comes from Old Persian and means "good to cross over". The geographical coordinates of the ERB are 36°49′N, 38°02′E at the Turkish border and 34°29′N, 40°56′E at the Iraqi border. The ERB (Fig. 3.1) includes the majority of the three governorates of Aleppo, Arraqqa and Deir Azzour. The variation in altitude is from ca. 520 m at the Turkish border to ca. 185 m at the Iraqi border. The Euphrates goes up in the mountains of eastern Turkey, and the sink has high mountains to the north and west and wide plains to the south and east. Two-thirds of river's course flows throughout the highlands of eastern Anatolia in Turkey and the valleys of the Syrian and Iraqi flat terrain before downwarding into the arid plain of Mesopotamia. The Euphrates has its sources in the eastern highlands of eastern Turkey, between Lake Van and the Black Sea, and is created by two major tributaries, the Murat and the Karasu. It enters the Syrian territory at Karkamish, down-tributary from the Turkish town of Birecik. It is then

W. Al-Fares, *Historical Land Use/Land Cover Classification Using Remote Sensing*, SpringerBriefs in Geography,
DOI: 10.1007/978-3-319-00624-6_3, © The Author(s) 2013

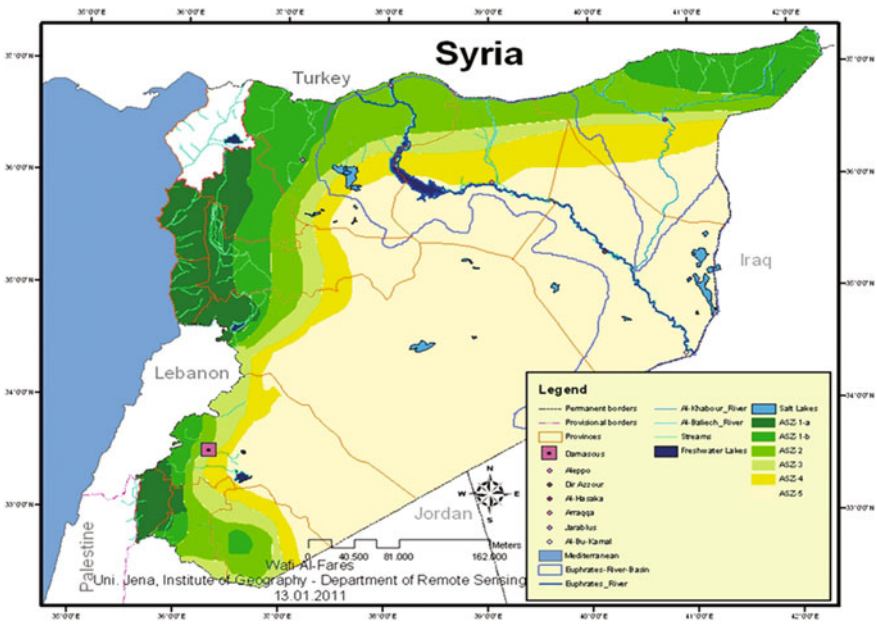

Fig. 3.1 Present-day Syrian borders, the 14-governorates administrative divisions, Agro-climatic Zones, and the Euphrates River Basin study area

joined by its major tributaries, the Al-Balikh and Al-Khabour, which too begin in Turkey, and streams southeast across the Syrian flat terrain before inflowing Iraqi terrain near Qusaybah. The Euphrates watershed includes five counties (Table 3.1): Turkey, Iraq, Syria, Saudi Arabia and Jordan. Its real annual volume is 35.9 billion cubic meters (Kibaroglu 2002; FAO 2009). For almost its total length, the river streams in a valley changeable in width from 2 to 12 km, and with the valley base some 80–250 m less than the neighboring plains. In several places, the river splits into two or more canals, constructing several atolls/islands, several of which support dense thickets. There are also meanders, oxbow lakes, gravel pits and silted old water courses covered in reed-beds. Much of the river bank contains low alluvial cliffs. The water level was previously some 3–4 m higher in spring than in autumn due to the snow-melt in the Turkish highlands, but with the production of several large dams in Turkey during the previous decade, this yearly flood is now greatly decreased.

The Euphrates River has a number of main tributaries where the Syrian government has carried out numerous projects. These flows are: (1) The Al-Khabour River (460 km), which rises in the Raas Al-ain region in Syria and flows into the Euphrates; (2) The Assajour River, which originates in Turkey and flows through Syria for a length of 48 km; its annual runoff is 100 million m^3; and (3) The Al-Balikh River, which rises near the Syrian villages of Aain Al-Arous and Tal-Abiad and flows through 105 km within Syria before joining the Euphrates. Its annual runoff is 150 million m^3.

Table 3.1 General statistical information on the ERB

Country-name	Basin-area (km^2)	Length (km)	Catchment-area (%)
Turkey	98,000	1,230	62
Syria	59,500	710	38
Iraq	140,000	1,060	0
Saudi Arabia	52,500	0	0
Jordan	105	0	0
Total	350,000	3,000	100

Source modified from Kattan 2008 and FAO 2009

3.3 Irrigation Projects in the ERB

Table 3.2 explains the water requirements in the three major ERB countries. The available level of irrigated agricultural projects in Syria on the Euphrates is 194,000 ha (although according to other sources, it is about 250,000 ha). Over the coming decade, some further 542,275 ha will be irrigated, thus in the future, some 636, 275 ha will be irrigated in Syria with water from the Euphrates. The future water demand, including steam water, equals 13.263 billion m^3. If we deduct from the returning water 2,463 billion m^3, one obtains net 10.8 billion m^3, representing the water needs of Syria from the Euphrates. This amount represents 34 % of current flow. In 1987, Syria and Turkey signed a water agreement over the Euphrates River, determining the water flows on the Syrian-Turkish border at 500 m^3/s. In 1990 a similar deal was agreed to between Syria and Iraq, dividing the Euphrates into the proportions of 42 % for Syria and 58 % for Iraq, thus allowing the current water situation for Syria of not more than $15.7 \times 0.42 = 6.627$ billion m^3/pa Euphrates water. The 15.7 billion m^3/pa corresponds to the amount of water that flows from Turkey towards Syria, as a result of the temporary agreement of 1987. Research sources expect that the 6.627 billion m^3/pa Euphrates water are sufficient only for the irrigation of 308,000 ha instead of the planned 640,000 ha. According to others, a deficit of one billion m^3 in Syria will give a proportion of withering from 26,000 ha of agricultural land and transform it into unusable land. This would lead to at least a total of 110,000 ha from 640,000 ha, that could be converted to unusable lands (Al-Fares 2007).

Syria too has its individual strategies for irrigation expansion within the Euphrates Basin (Table 3.3, Fig. 3.2). The water need for such land, assuming a water application rate of about 10,000 m^3 ha^{-1} yr^{-1}), would be $6{,}450 \times 10{,}000 = 64{,}500{,}000$ m^3, or about 16 % of the unregulated stream of the Euphrates where it enters Syria from Turkey (Beaumont 1996).

Table 3.2 The water needs in the countries located on the Euphrates River

	Turkey	Syria	Iraq	Total
The executed agricultural facilities (ha)	300,000	194,000	1,200,000	1,694,000
The futuristic facilities (ha)	1,146,300	542,275	752,400	2,840,975
The total agricultural land (ha)	1,446,300	636,275	1,952,400	4,024,975
The total amount of the waters' needs in future (irrigation + evaporation) (billion m^3/pa)	17.40	13.26	25.10	55.76
The returning water (billion m^3/pa)	1.70	2.47	5.10	9.26
Net consumption (average) (billion m^3/pa)	15.70	10.80	20.00	46.50
Ratio of the net consumption to amount of the river flow (%)	50	34	64	148

Source Al-Samman 1991

Table 3.3 Reclamation and irrigation projects on the Euphrates River

Project name	The area, which have to irrigated/ 1000 ha	The current investment status
The Al-Balikh Basin	141	
The pioneering project (Arraed)	19.9	Under investment
Beer Al-Hishm project	10	Under investment
Reclamation project of the part (1-B)	10	Under investment
Remaining sections of the Al-Balikh Basin	101.1	Under construction
The Euphrates Basin	152	
The Middle Euphrates project	27	Under investment
The Lower Euphrates project	125	Under construction
The Lower Al-Balikh Basin	70	Under construction
The Arrusafa Basin	25	Under construction
The Al-Mayadin Basin	40	Under construction
The Maskana Basin	166	
The 17,000 ha project and the state farm	21	Under investment
The Maskana-west project	20	Under investment
The Maskana-east project	17.8	Under investment
The rest of the Maskana Basin	107.2	Under construction
The total	594	–

Source The Syrian Ministry of Irrigation 2005

3.4 Climate

The yearly precipitation in the Mesopotamian plain is seldom above 200 mm, while it attains 1,045 mm in other parts in the basin. The summer season is very hot and dry with midday temperatures reach 50 °C and daytime relative humidity about 15 %. These climatic conditions demonstrate that the Euphrates streams within arid and semi-arid areas inside Syria with increasing aridity downstream

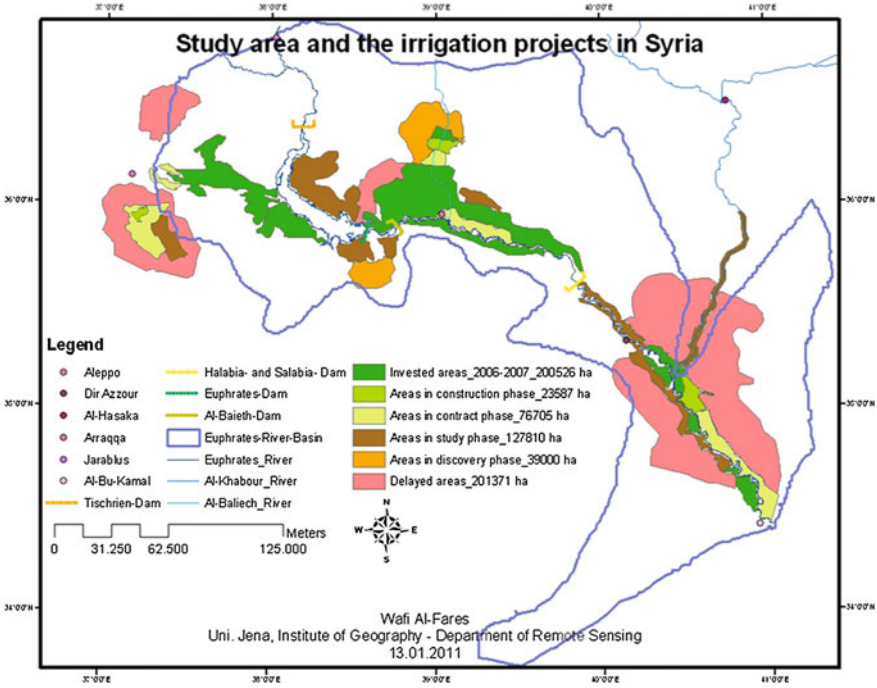

Fig. 3.2 Study area and the irrigation projects in Syria (*Source* MAAR 2008)

(Hillel 1994 cited in Kibaroglu 2002). The yearly standard temperature of the whole ERB is 18 °C. It is about 5 °C in January, although it can decline to −11 °C in the coldest areas in the basin. This yearly standard temperature in July reaches 31 °C, although it can raise to 37 °C in the hottest areas (Hillel 1994 cited in Kibaroglu 2002 and FAO 2009). In the Syrian part of ERB, the winter season is usually cool (5–10 °C) and rainy, and the summer is warm (30–45 °C) and almost totally devoid of precipitation. The average annual air temperature increases from north to south, and differs between 18 °C in Jarablous and 20 °C in Al-Bou-Kamal, where the dryness becomes more emphasized. The average monthly precipitation increases—from October to May—from south at Al-Bou-Kamal with 5–30 mm to north at Jarablous with 20–60 mm. The average annual precipitation increases over the year from south at Al-Bou-Kamal with about 130 mm, over Dir Azzour with about 160 mm, to the north at Jarablous with about 350 mm. The average yearly precipitation value over the whole ERB in Syria is around 240 mm. The average yearly value of the relative air humidity differs between 56 % (Jarablous) and 47 % (Dir Azzour), and declines to less than 44 % (Al-Bou-Kamal), the lowest recorded value in Syria. The highest values of average monthly relative humidity (60–70) % are commonly observed during the coolest time period (i.e., December to January), while the lowest 25–30 % happen in the

warmest months (i.e., July and August). The potential evapo-transpiration value commonly goes above the precipitation and varies from 1,300 to 2,600 mm, with an average yearly value about 2,100 mm (Kattan 2008).

3.5 Morphological Structure

The major topographical characteristic of ERB territories is the simplicity. There are some of little height hills, essentially areas surrounds the Lake Al-Asad. The average height of ERB territories is 350 m in the north at Jarablous and 180 m in the south at Al-Bou-Kamal. Euphrates's ''base valley'' located downstream below 200 m. Its path-slope is about (0.25 m/km^{-1}) (Kattan 2008).

Euphrates has a length of about 675 km in Syria. It across Syria within a low geological formation. The major geological components return to the three geological times: Paleogene (argillaceous limestone); Neogene (gypsum, silty clays, sandstone, siltstone, clays, and pebbles); and Quaternary (pebbles, gravels, loams, and sandy loams) (Ponikarov 1967). The alluvial aquifer, composed mainly of gravels and boulders at the base and bigger alluvial sediments (i.e., loams and sandy loams) at the top, is the mainly significant water bearing system in the basin (Kattan 2008).

3.6 Soils

Soil is found on either side of the Euphrates in Syria which despite having copious irrigation, offers bad growing conditions, and thus reduce crop yield. The humus is low in the arid east, where mostly raw soils are found on soft, low resistive source rock. The soil debris, the plaster floors, and dust and loose soils of the Syrian desert steppe and desert are heavily climate conditioned. This may represent an almost insurmountable obstacle for agricultural use in the northeast of Aleppo, especially for trees and vines. Soils with a high salt or gypsum content are not suitable for agricultural use. Fortunately, the Miocene gypsum and anhydrite of the lower Fars in Syria is found only in a large area in the desert steppe. The salt or salt surfaces of Sabchat Al-Jabboul, which today is the dry-end lake Syria, are also not so significant (Wirth 1971). Gypsiferous crust soils covers a wide parts of ERB territories. The breakdown of irrigation water canals because flowing of the water within canals material due to soil salinization. The second major reason for salinization is over-pumping. After salinization due to the aforementioned reasons, the soil will be exposed. As a result, ERB soils have to be carefully irrigated.

3.7 Hydrology

The Euphrates River has a relatively regular watery regime/system, described by two months of very high rate stream in April and May, and a phase of eight dry months from July to February (Fig. 3.3). The yearly stream differs significantly from year to year (Fig. 3.4), as well as very low stream records between July 1957 and January 1963, during which time the average flow decreased to only 83 % of the long-term average. Euphrates's discharge rate is from 200 to 300 m^3/s. It begins to increase during early spring, i.e. in February. Then, becomes it more abundant in March during the melting of snow in the high mountains in Turkey. The peak of discharge is in April and May with 2,000 m^3/s and sometimes more. Because snow melts on peaks of mountains and because the high rates of rain in April and May, the most flooding will be happening from mid-April to early May. Starting from July, the discharge begins to decrease. The bottom of discharge is either in September or in October. In April and May, discharge during the two months records for 42 % of the yearly full amount. Minimum streams happen from August through October and add only 8.5 % of the whole discharge (Beaumont et al. 1988; Shahin 1989) (Figs. 3.3 and 3.4).

3.8 Vegetation and Land Use—Land Cover

Figure 3.5 provide general information about the LULC-activities in the ERB and Syria.

The natural vegetation of the Euphrates River Basin includes riverine thickets of *Populus euphratica*, *Tamarix articulata*, *Salix* sp., *Glyzyriza glabra*, *Lycium barbarum*, and reed-beds of *Phragmites* sp. and *Typha* sp. The river banks are intensively cultivated: There are vast areas of irrigated cotton and cereals, as well as orchards and plantations of *Populus* and *Pinus halepensis*. The heavily cultivated steppe of the Al-Jazirah region lies to the east and the Syrian Desert to the southwest (Murdoch et al. 2005). For instance, an old and random *Pistacia*

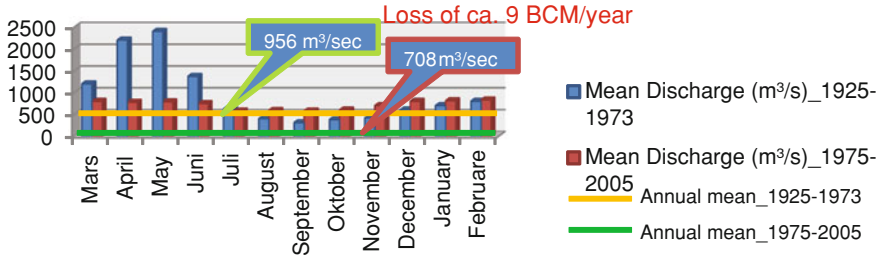

Fig. 3.3 Euphrates River monthly mean discharges (m^3/s) for the period 1925–2005 (*Source* adapted from DIWU 2009)

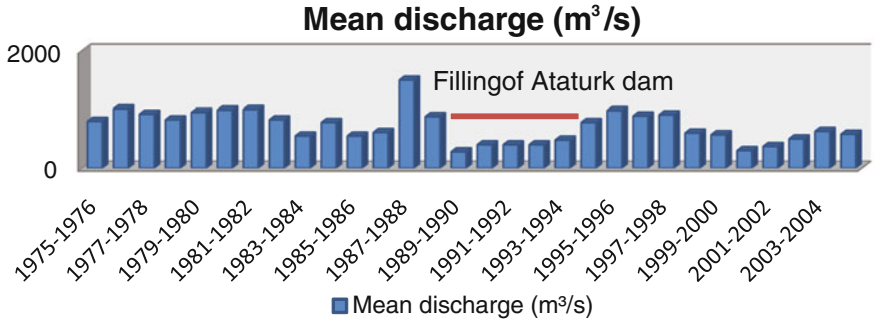

Fig. 3.4 Mean annual discharge of the Euphrates River (m^3/s) for the period 1975–2005 (*Source* adapted from DIWU 2009)

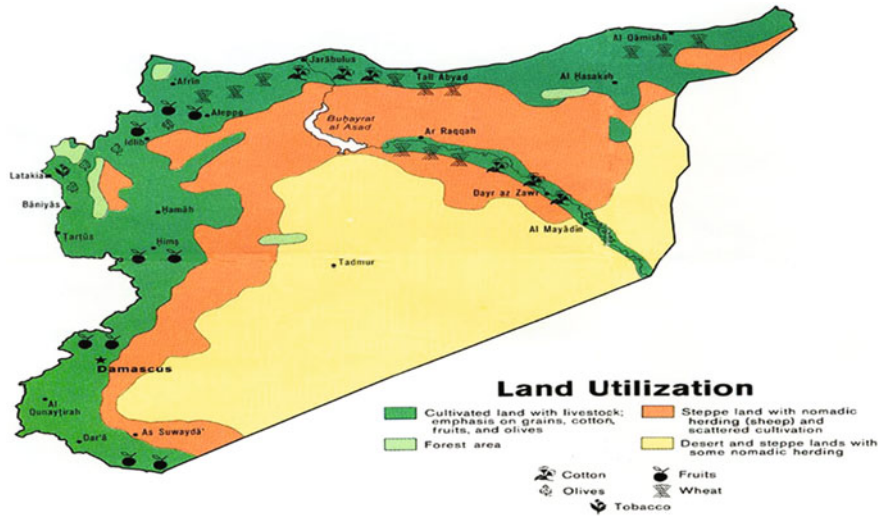

Fig. 3.5 Approximate spatial LULC-distribution in the ERB and Syria (*Source* http://images.nationmaster.com/images/motw/middle_east_and_asia/syria_land_1979.jpg)

atlantica trees found in Jabal Abd Al-Aziz region. For decades, no young growth has been recorded because the destruction of the undergrowth has significantly deteriorated the micro-climate and the soil surface is now largely eroded. It is predicted that it will take only a few more decades in many parts of Syria before all of the few remaining tree ruins die and the last remnants of former high forests will disappear. This is due in the main because of thousands of years of human cultural activity. The desert steppe in the ERB was originally densely vegetated featuring tall grasses over 50 cm in height, with species such as Stipa, Agropyrum, and Festucaspecies dominating. This grassland likely contained sparse groves or woods of pistachios. In addition, it is thought the steppe was home to junipers such

as Juniperus excelsa, Kreuzdorn Rhamnus Palaestinae, Prunus, Pirus, Crataegus and Amygdalus. Occasional old pistachio trees of up to 5 m in height can still be found on many desert heights (e.g., Jabal Al-Bilaas, 500 m above sea level, near Deir Azzour). They have been however, decimated at alarming rates by the firewood needs of the camping nomads in winter. This wood steppe is traditionally the habitat of sheep and camel nomads. The nomads have largely destroyed the original vegetation over the centuries. The establishment of additional water supplies from deep wells and the transport of water by truck have also had disastrous consequences on this fragile ecosystem. The steppe is also home to a variation of groundwater and riparian natural vegetation, on the floodplains and low terraces of the rivers which are not in use for agricultural purposes. In this region, this vegetation consists mainly of Euphratpappeln (*Populus euphratica*) and pastures (*Salix acmophyll*), with an understory of tamarisk (*Tamarix tigrensis*) (after German to English translation and modification from Wirth 1971).

For the human activities of land use in the ERB, we different between two geographical-historical regions: (1) the Young-settled (Arraqqa- and Deir Azzour-provinces) dominant winter cereals (wheat and barley) on dryland and cotton on irrigated ground almost to the level of monoculture. These represent the major growing crops in Syria. Much of the harvesting of these relative sparsely populated areas goes to market or is readied for export. Tillage and harvest are increasingly mechanized; and (2) the Old-settled (Aleppo Province) shows, in contrast a much larger variety of crops. Wheat and cotton are also cultivated in large parts of the fields in this region but not to the point of monoculture, as there are competitors with many other crops. Less demanding summer plants can grow well here, even without extra irrigation. Permanent crops, such as tree groves, as well as intensive, irrigated vegetable crops are found almost solely in these old-settled areas. Only a relatively small portion of the harvest is exported. Here, too, is find a juxtaposition of rain- and irrigated- crops; both are cultivated at a much greater extent with more traditional tools than in the Young-settled areas (after German to English translation and modification from Wirth 1971).

Cultivation of olive trees, which has a long tradition in Syria (oil presses such as Ugarit were already in use around 2000 BC), is located almost exclusively in the Old-settlement. Vineyards are located throughout this region, either on pure dry land or at the edge of the irrigation areas. All other fruit trees are found only small areas. The cultivation of pistachios is focused primarily on the perimeter of Aleppo (after German to English translation and modification from Wirth 1971).

Field-irrigation is used in almost all of the agricultural areas of the ERB. In the areas with more than 400–500 mm, only intensive crops which need a high water demand are irrigated, e.g. vegetables, sugar beets, and peanuts. The irrigated land here is embedded with little natural contrast to a rain-floor, and both winter and summer crops flourish. In the areas with about 200–400 mm average annual precipitation only winter crops can be grown without additional irrigation. During the summer months, the irrigation fields are lush green islands, raised above the dry yellow and brown rain-fed land. Between the two there is a clear division of function: in analogy, the drying fields of wheat and barley were appointed/ordered,

while the irrigated areas in the old-settled areas had intensive cultivation of vegetables, a variety of summer fruits and fruit trees. The focus of irrigation in the dry steppe areas of northern Syria has been the use of groundwater pump wells (after German to English translation and modification from Wirth 1971).

References

Al-Fares, W. (2007). *Wasserkonflikt zwischen Syrien und Türkei über das Wasser des Euphratesbecken und die Rolle, die das Südostanatolienprojekt auf diesem Konflikt spielt (Diplomarbeit)*. Göttingen: Geographisches Institut zur George August Universität.

Al-Samman, N. (1991). War of the water from the Nile to the Euphrates: Transmission over the Syrian ministry of irrigation. *Al-Wahda Al-Arabiea-Studien, 74*(6), 124–140.

Beaumont, P., Blake, G. H., Wagstaff, J. M. (1988). *The middle east: a geographical study*. 2nd ed., London: David Fulton Publishers.

Beaumont, P. (1996). Agricultural and environmental changes in the upper Euphrates catchment of Turkey and Syria and their political and economic implications. *Applied Geography, 16*(2), 137–157.

Directorate of Irrigation and Water Use (DIWU). (2009). *Water requirements for the agricultural plan 2007/08*. Damascus, Syria.

FAO. (2009). Irrigation in the Middle East region in figures (AQUASTAT survey—2008). In K. Frenken (Ed.), *FAO water reports* (p. 423). Rome: Italy.

Hillel, D. (1994). *Rivers of Eden: The struggle for water and the quest for peace in the Middle East* (pp. 74–110). New York: Oxford University Press.

Kangarani, H. M. (2006). *Euphrates and Tigris watershed: Economic, social and institutional aspects of forest in an integrated watershed management* (working paper 81). Rome: FAO.

Kattan, Z. (2008). Estimation of evaporation and irrigation return flow in arid zones using stable isotope ratios and chloride mass-balance analysis: Case of the Euphrates River, Syria. *Journal of Arid Environments, 72*(5), 730–747.

Kibaroglu, A. (2002). *Building a regime for the waters of the Euphrates-Tigris River Basin*. London: Kluwer Law International, New York: The Hague.

Ministry of Agriculture and Agrarian Reform (MAAR). (2008). *The distribution of irrigation projects in Euphrates River Basin*. Damascus, Syria.

Murdoch, D. A., Vos, R., Abdallah, A., Abdallah, M., Andrews, I., Al-Asaad, A., Van Beusekum, R., Hofland, R., Roth, T., Saveyn, B., Serra, G., & Wells, C. (2005). *A winter survey of Syrian wetlands* (final report of the Syrian wetland expedition, January–February 2004). Privately published, London, UK.

Ponikarov, V. O. (1967). *The geology of Syria. Explanatory notes on the map of Syria, Scale: 1/500.000, part II, mineral deposits and underground water resources* (p. 120). Moscow: Technoexport.

Shahin, M. (1989). Review and assessment of water resources in the arab region. *Water International, Journal of the International Water Resources Association, 14*, 206–219.

The Syrian Ministry of Irrigation. (2005). *Reclamation and irrigation projects on the Euphrates river*. Damascus, Syria: Report.

Wirth, D. (1971). *Syrien: Eine geographische Landeskunde*. Darmstadt: Wissenschaftliche Buchgesellschaft.

Chapter 4
Data

One decides what information and data is needed to achieve the purpose of a study. The data collection is, however, often controlled by what is obtainable or what the financial map will allow, rather than what is actually needed. During the searching process, one may find other undecided data sources or types that are useful to the achievement of the research. Data and information for the LULC-component is available from administrative divisions, libraries, universities and private companies can offer data. Processing time and resources require attention, depending on the amount of data collected and organized. Enough data is essential to guarantee accuracy and answerability. At sensor type choosing stage, in relation to rapid sensor development and various sensor configuration, one has to consider the broad range of application sectors in an attempt to give potentials that meet actual obligations, as it is impossible to find a specific sensor type to satisfy the all specific needs of all cases. Here, to optimize the choice of the remotely sensed data, we have to determine the purpose of the research and which dataset can realize the two criterions of being cost effective and providing the relevant information in relation to the research purpose. Finally, at these basic stages of choosing and preparing the dataset, it is also significant to consider the relationship between the used dataset and the required mapping scale (Liu and Mason 2009). The purpose of the current study is to set maps of land uses and the natural coverage of the ERB. The satellite images suggest basic inputs for a comprehensive study of this area, which is also reliant on other data and information to achieve targets, such as topographic maps and statistical records. Lastly, the study cannot be fulfilled without reliance on field observations.

4.1 Satellite Data

LANDSAT and ASTER general characteristics (Fig. 4.1, Tables 4.1, 4.2) are: medium spatial resolution, medium area coverage, moderate revisit capability and multispectral bands characteristic. The scale of the area coverage of the LANDSAT

W. Al-Fares, *Historical Land Use/Land Cover Classification Using Remote Sensing*, SpringerBriefs in Geography,
DOI: 10.1007/978-3-319-00624-6_4, © The Author(s) 2013

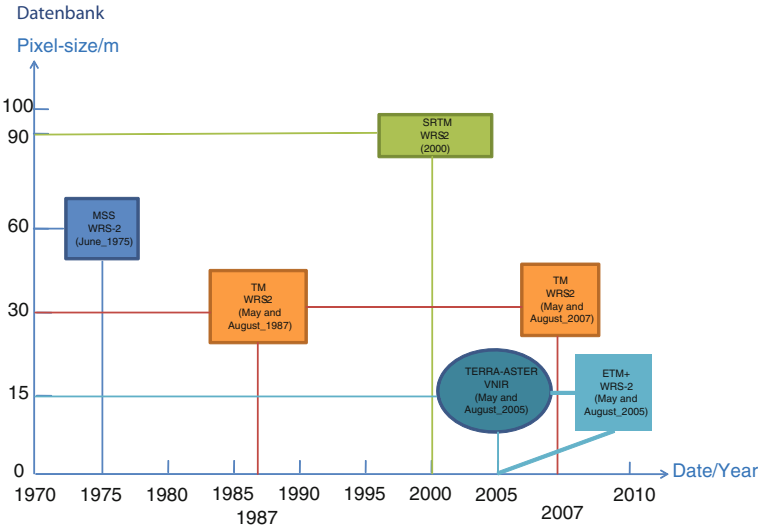

Fig. 4.1 An overview on the general characteristics of the used satellite dataset in the study

and ASTER makes them mainly suitable for LULC-studies for extended areas, such as countries and continents. The largest part of Earth observation satellites that have a medium resolution are in a sun-synchronous orbit. The LANDSAT data archive at the USGS/EROS Center-holds an unequaled 36-year record of the Earth's surface and is available at no cost to users via the Internet (Woodcock et al. 2008). The Earth Science Data Interface (ESDI) has a data archive with a global coverage, free for download or for very low managing and delivery costs to large numbers of countries around the world. The data-archive includes: ortho-rectified LANDSAT-imagery from the three Sensors (MSS, TM, and ETM+); composite MODIS-imagery; and remotely sensed data based derived products (e.g., NDVI). The owner of this archive is NASA and it hosted at the University of Maryland in the USA. The Earth Observing System Data Gateway (EOS) provides a big archive of land, water and atmosphere data products. Also, the source of these data comes from NASA in USA. There are also a valuable and gratis remotely sensed data or with an inexpensive shipping costs.

4.1.1 LANDSAT (MSS, TM and ETM+) Sensors

Lauer et al. (1997) provides a short history of the LANDSAT-program and its noted successes. The development of the LANDSAT-program originated from global efforts to improve our knowledge of Earth, and it is perhaps the most successful satellite remote sensing program devoted to land monitoring. The first Earth Resources Technology Satellite (ERTS-1) was launched to space on 23 July

Table 4.1 General information about the two satellites LANDSAT and TERRA-ASTER

Satellite	Launch dates	Decommission	Altitude (km)	Indination (degrees °)	Period (min)	Temporal resolution (days)	Crossing time (a.m.)
LANDSAT-1	23.07.1972	07.01.1978	920	99.20	103.34	18	9:30
LANDSAT-2	22.01.1975	25.02.1982	920	99.20	103.34	18	9:30
LANDSAT-3	05.03.1978	31.03.1983	920	99.20	103.34	18	9:30
LANDSAT-4	16.07.1982	30.06.2001	705	98.20	98.20	16	9:45
LANDSAT-5	01.03.1984	Operational	705	98.20	98.20	16	9:45
LANDSAT-6	05.10.1993	Did not achieve orbit					
LANDSAT-7	15.04.1999	Operational	705	98.20	98.20	16	10:00
TERRA-ASTER	18.12.1999	Operational	705			16	10:30

Source Adapted from Schowengerdt (2007), Chander et al. (2009)

1972 in cooperation between the National Aeronautics and Space Administration (NASA) and other USA-federal agencies. It was later renamed LANDSAT-1. This launch is seen as the birth of the present age of Earthly satellite remote sensing. LANDSAT-1 was a Nimbus-type platform which held a sensor box and data-relay tools. ERTS-2 was launched to the space on 22 January 1975. It was too renamed to LANDSAT-2. Other four LANDSATs (3, 4, 5 and 7) were launched in 1978, 1982, 1984 and 1999 respectively. Each successive launch has included improved sensor and communication capabilities. This has had a huge influence in several application fields (Lauer et al. 1997). In comparison to the military satellite systems, the civilian LANDSAT-family of satellites has supplied civilization with over 34 years of consistent, medium spatial resolution, multispectral images of the world. Due to the long historical record of the LANDSAT-program, no other remotely sensed data sets allow us to study the nature of the Earth and the human activities and impacts so effectively (Williams et al. 2006). This continuous record was realized because of good luck and superb engineering rather than careful management oversight (Williams et al. 2006). The LANDSAT World Wide Reference (WWR) system catalogs the Earth's landmasses into 57,784 scenes, each 185 km wide and 170 km long (USGS 2009).

The famous family of LANDSAT-satellites (LANDSAT-1, 2, 3, 4, 5, 6 and 7) and sensors (MSS, TM, ETM and ETM+) can be divided to three common types based on the characteristics of their sensors and platforms: (1) LANDSAT (1, 2 and 3), that have the sensor type of MSS and the camera type of Return Beam Vidicon (RBV). The platform was like a Nimbus (cloud). MSS has the spatial

Table 4.2 General information about the sensors-data used in the study

Platform	Sensor	Spatial resolution (m)	Spectral bands	Spectral range (μm)	Swath width (km)	Pointing capability (degrees °)	Mapping scales (m)
LANDSAT (1–5)	MSS-multispectral	60	1–4	0.5–1.1	185 × 185	No	1/160,000
LANDSAT (1–3)	RBV—return beam vidicon	25	1	0.505–0.750	185 × 185	No	1/50,000
LANDSAT (4–5)	TM-multispectral	30	1–5, and 7	0.45–2.35	185 × 185	No	1/60,000
	TM-thermal	120	6	10.40–12.50	185 × 185	No	
LANDSAT (7)	ETM+/multispectral	30	1–5, and 7	0.450–2.35	185 × 185	No	1/60,000
	ETM+/thermal	60	6-1, 6-2	10.40–12.50	185 × 185	No	1/120,000
	ETM+/panchromatic	15	8	0.52–0.90	185 × 185	No	1/30,000
TERRA-ASTER	VNIR	15	1–3 N	0.52–0.86	60 × 60	±24	1/30,000
	Stereoscopic	15	3B	0.76–0.86	60 × 60	±24	1/30,000
	SWIR	30	4–9	1.600–2.430	60 × 60	±8.55	1/60,000
	TIR	90	10–14	8.125–11.65	60 × 60	±8.55	1/180,000
SRTM	C- and X-bands	90			1 degree latitude × 1 degree longitude		1/180,000

Source Adapted from Van der Meer et al. (2002), Schowengerdt (2007), Liu & Mason (2009)

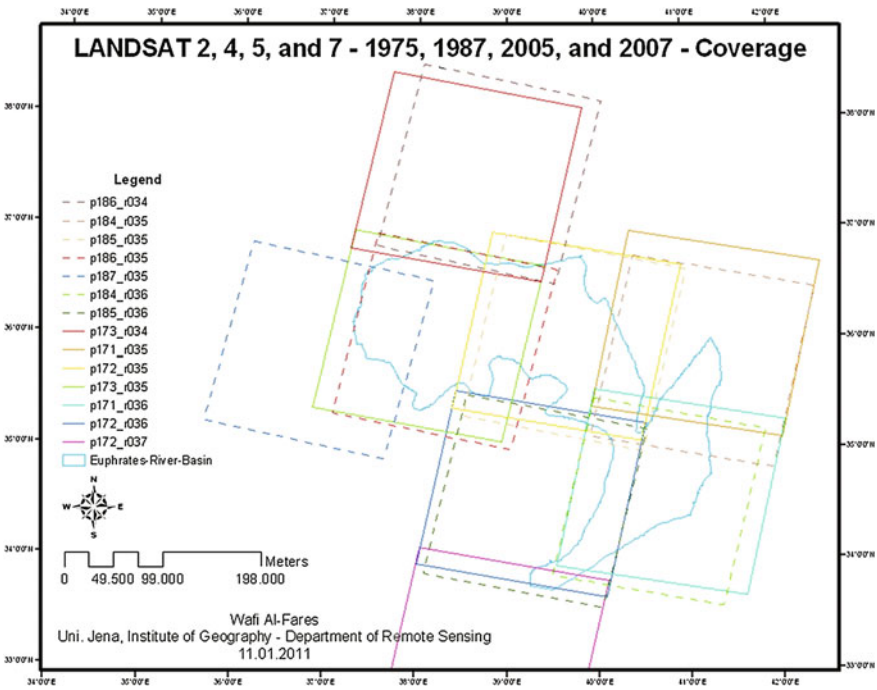

Fig. 4.2 The used imagery spatial coverage of the sensors: MSS (June, 1975), TM (May and August, 1987 and 2007), and ETM+/SLC-Off/corrected (May and August, 2005)

resolution of 79 m (frequently, prepared to be 60 m as pixel size). Its spectral resolution is not large enough for some studies (e.g., crops classification), where it has four spectral bands only. These bands located within the four spectral portions (wavelengths) with a four typical band-naming: blue (MSS-4), green (MSS-5), red (MSS-6) (the visible spectral portion); and the Near-Infra-Red (NIR) (MSS-7). Only the third LANDSAT hold a MSS sensor that has five spectral bands, were the fifth one was a thermal infrared (10.4–12.6) μm. This standard is no longer used; instead the MSS-bands are referred to the bands 1, 2, 3 and 4 respectively, consistent with the TM and ETM+ sensors; (2) LANDSAT (4 and 5), which carried the TM sensor, in addition to the MSS. This second generation offered a clear enhancement in remote sensing through the supplement of a more advanced sensor, enhanced gaining and transmission of data, and more rapid data processing at a highly automated processing capability. The MSS-sensor was kept to provide continuity with the previous LANDSAT-missions, but TM-data rapidly became the main source of information used from these satellites because of its enhanced spatial, spectral, radiometric and geometric characteristics in comparison to MSS-data. Finally, the gaining was limited to real-time download only, since there were no onboard recorders on these sensors (Chander et al. 2009); and (3) LANDSAT (6 and 7), consisting of LANDSAT-6 which carried the Enhanced Thematic Mapper

(ETM) sensor and failed on launch, and LANDSAT-7, with its Enhanced Thematic Mapper Plus (ETM+) sensor. LANDSAT-7 also had a 378 gigabit Solid State Recorder (SSR) that could store 42 min (about 100 scenes) of sensor data and 29 h of housekeeping telemetry concurrently (L-7 Science Data User's Handbook). No MSS-sensors were included on either satellite (Fig. 4.2).

4.1.2 TERRA-ASTER

In 1999, after the cooperation between NASA and the Japan's Ministry of Economy Trade and Industry (METI), the Advanced Space-borne Thermal Emission and reflection Radiometer (ASTER) was launched into the space. It was held on board the NASA-TERRA satellite. The ASTER-sensor represents the next generation in remote sensing, following the older LANDSAT-TM. It acquires high spatial resolution data in 14 spectral bands, ranging from visible to thermal infrared portions. This sensor contains three separate instrument subsystems that operate in different spectral portions and have their own telescope(s). The subsystems are: (1) the Visible and Near Infra-Red (VNIR): operates within three spectral bands at visible and NIR wavelengths of 0.52–0.86 μm, with a spatial resolution of 15 m. It is especially useful for topographic interpretation because of its along-track stereo coverage with 15 m spatial resolution. Also, it is useful in assessing vegetation and iron-oxide minerals in surface soils and rocks; (2) the Short-Wave Infra-Red (SWIR): operates within six spectral bands in the NIR region of 1.600–2.430 μm, through a single-nadir pointing telescope that offers a spatial resolution of 30 m. These six bands were selected mainly for the purpose of surface soil and mineral mapping; and (3) the Thermal Infra-Red (TIR): operates within five bands inside the thermal infrared region of 8.125–11.65 μm, using a single, fixed-position, and nadir looking telescope with a spatial resolution of 90 m. This subsystem allows for a more accurate determination of the variable spectral emissivity of the land surface, and hence a more accurate determination of the land surface temperature. The spatial coverage of the ASTER-sensor is at 60 × 60 km (Fujisada 1995; Yamaguchi et al. 1998).

The relatively high spatial (Fig. 4.1) and spectral (Fig. 4.3) resolution of the ASTER-data in comparison to LANDSAT-data can increase the ability of separation between the various ground surface features and decrease the problems of mixed pixels (Yamaguchi et al. 1998). Therefore, ASTER-data are more suitable for LULC-classification (Bagan et al. 2008).

The ASTER-sensor, because it is the only high spatial resolution sensor, is the "zoom lens" for the other carried sensors onboard the TERRA-satellite. TERRA is in a sun-synchronous orbit, 30 min behind LANDSAT-ETM+, and it crosses the equator at about 10:30 am local solar time. ASTER can obtain data over the whole globe with an average obligation cycle of 8 % for each track. This offers a gaining of about 650 scenes per day (subject to on-board storage limitations), that are processed to the two products types (Level-1A; of these, about 150 are processed

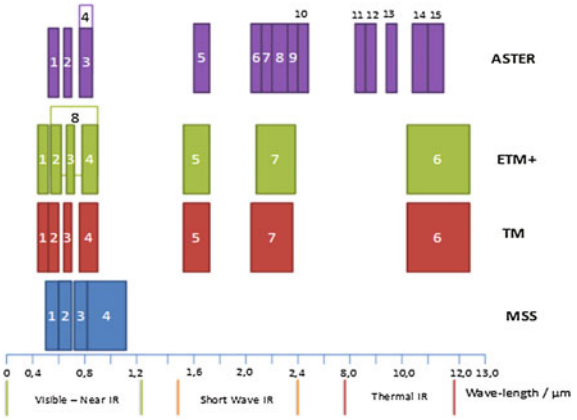

Fig. 4.3 Comparison of the spectral coverage between LANDSAT-sensors (MSS, TM, and ETM+) and the ASTER-sensor

to Level-1B). ASTER-L1A data are officially classified as reconstructed, unprocessed data at full resolution. They contain the image data, the radiometric coefficients, the geometric coefficients and other supplementary data without applying the coefficients to the image data, thus keeping the original data values. The L1B-data are produced by applying the coefficients for radiometric calibration and geometric resampling. All gained 1A and 1B scenes are transferred to the EOSDIS archive at the EROS Earth Data Center's EDC Land Processes Distributed Active Archive Center (LP-DAAC), for storage, distribution and processing to higher-level data products. All ASTER-data products are stored in a specific implementation of Hierarchical Data Format called HDF-EOS.

ASTER's geometric system correction mainly contains the rotation and the coordinate transformation of the line of sight vectors of the detectors to the coordinate system of the Earth. This is done as part of ASTER-Level-1 processing at GDS using extra engineering data from the sensor and similar auxiliary data from the spacecraft platform. The geometric correction of ASTER has developed in two complex processes of both pre-flight and post-launch calibration. Tests have proven that ASTER has superb radiometric, geometric and spectral functioning (Ono et al. 1996) (Fig. 4.4).

The main scientific purpose of the ASTER-mission is to gain better knowledge of the local and regional scale processes happening on or near the Earth's surface and lower atmosphere, as well as the relations between the Earth surface and the atmosphere. Special applications are: (1) earth surface climatology; (2) vegetation and ecosystem dynamics; (3) volcano observing; (4) hazard observing; (5) aerosols and clouds; (6) carbon cycling in the marine ecosystem; (7) hydrology; (8) geology and soil; and 9) LULC-change (Yamaguchi et al. 1999).

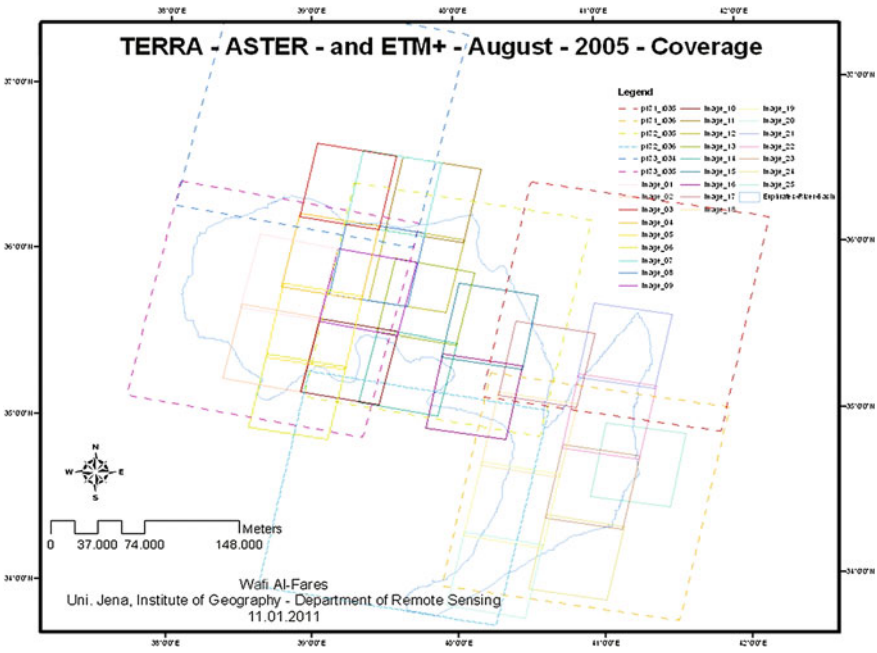

Fig. 4.4 The used imagery spatial coverage of the sensors ASTER (May and August, 2005), and ETM+/SLC-Off/corrected (May and August, 2005)

4.1.3 SRTM

The Shuttle Radar Topography Mission (SRTM) was started in February 2000. This mission took eleven days and named as STS-99-mission. The mission was ended successfully after an international cooperation. The goal of this mission was to offer a new source for deriving of topographical data digitally, especially the height element/z, where the traditional methods were based on digitizing the contours lines from the topographic maps. After achieving the goal of the mission, we had become the Digital Elevation Models (DEM). This product was until 2009 the most complete archive of digital topographical data, which covers a near-global scale from 56° S to 60° N with a high spatial resolution. To realize the above mentioned goal, the mission included a specially modified RADAR-system, which was based basically on the model used in the 1994 Shuttle, the older Space-borne Imaging Radar (C and X) bands Synthetic Aperture Radar (SIR-C/X-SAR). The system was carried on board of the Endeavour Space Shuttle. The technique used to generate topographic data digitally from the space with representation of the elevation element (z), is the Interferometric Synthetic Aperture Radar (ISAR). The SRTM mission was supplied with two radar antennas. “One antenna was placed in the Shuttle’s payload bay, the other, a critical change from the SIR-C/X-SAR allowing single-pass interferometry, on the end of a 60 m mast that extended

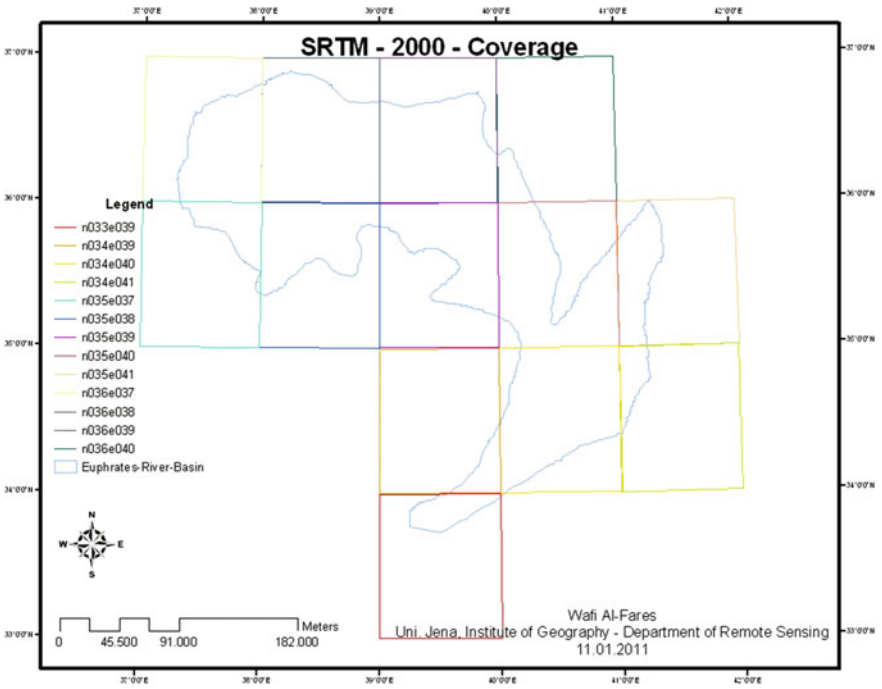

Fig. 4.5 The used imagery spatial coverage of the sensor SRTM

from the payload bay as soon as the Shuttle was in space" (Farr et al. 2007). "The elevation models were set into tiles, each covering one degree of latitude and one degree of longitude, named according to their south western corners. It follows that "n45e006" stretches from 45° N 6° E to 46° N 7° E and "s45w006" from 45° S 6° W to 44° S 5° W. The resolution of the cells of the source data is one arc second. The one arc second 30 m data have only been released over United States territory; for the rest of the world, only three arc second 90 m data are available" (Farr et al. 2007). The second realized DEM-product was presented from ASTER-sensor in 2009. Thus, it can charge the digital topographic database with new and different source. It named as Global Digital Elevation Model (GDEM) (Fig. 4.5).

4.2 Reference- and Complementary-Data

Reference and complementary data can be obtained from information sources other than the imagery data itself, such as field observations and measurements, aerial photograph interpretation, thematic maps and other archival materials. The expression "ground truth" can be substituted by the more appropriate expression "reference information", which is seen to be "more inclusive than "ground" and

less absolute than "truth"". Generally, no study should be carried out without study area visits, but it is often possible to select training and testing samples for accuracy assessment from high resolution aerial photographs or from a suitable thematic maps showing LULC-categories, in addition to topographic maps and Google Earth data. On the other hand, social science can help to confirm and analyze remotely sensed observations (e.g., validating remote observations versus data gathered on the ground). As, it is possible to determine a number of land use activities (classes) during classification remote sensing imagery based on a few social behaviors (McCoy 2005). One of the interesting example presented by Lesschen et al. (2005) presents other data sources such as questionnaires. It is particularly helpful to obtain management-related data (e.g., agricultural crop cycles) and can also give insight into the main factors of LULC-change.

4.2.1 Field Reference Data

One of the mainly steps in any remotely sensed based study is gathering the thematic data (attribute data, such as qualitative breaks by vegetation cover density: low, medium, high), and measurements (e.g., a quantitative differentiation of vegetation cover density by break points: <10, 11–40, >40 %), or observations (e.g., determination which category of the legend is more suitable to a surface feature) of the phenomenon of interest in the field. This is also the most difficult step, because it is a very time-consuming, often boring task which entails difficulties such as what want the researcher measuring and observing, where it is important to determine that before the field work, and then it is important to choose the method to be applied in the field to gather the required data. Ground truthing is important for remote sensing to properly identify objects, provide precise image registration and verify results. Before beginning to gather reference data in the field, two steps must have been completed: (1) study goals must be obviously determined; and (2) a classification scheme for all LULC-classes must have been selected (McCoy 2005).

Spectro-radiometry is a frequently used ground-based reference data source in remote sensing techniques. It can measuring the values of radiance, irradiance, reflectance or transmission of individual targets or objects, by locating the radiometer above the targets of interest, and records these values as digital spectral quantitative records. It used mostly as hand-held cameras (or mounted on a tripod, tower, tractor etc.). After finishing the measuring process, the user compares them to the biological, chemical and physical characteristics of the object. For agriculture, red and NIR portions of the EMS profile utilized particularly to calculate and generate the Vegetation Indices (VI) that are correlated with parameters of canopy structure (e.g., LAI). Spectro-radiometers named also radiometers or InfraRed Thermometers (IRT) (Schowengerdt 2007).

For this study, the major related field-work/s was: the 1987-GPS points (ICARDA); the 2005-GPS points (GORS); the 2007 and 2009 GPS-points obtained from two excursions; Spectrometer-measurements (GORS); and the NDVI-measurements (GORS). (see Chap. 5.4).

4.2.2 Maps

Thematic maps of LULC-types should be a part (especially in the visual interpretation) of the selection of training samples and the gathering of testing sites for accuracy assessment when there is no alternative. They are generalized information with two drawbacks, in that they are probably based on unlike designations for classes, plus an unlike minimum unit (cell or pixel) size than that which is being used in a specific study. So, most maps are considered unreliable and unacceptable for use as reference data, other than for a general understanding of the area (McCoy 2005).

Soils and thematic maps are reproduced from previous studies (from ICARDA-Aleppo), as well as topographic maps with various scales from 1/25,000 to 1/100,000, which cover the whole study area. These were purchased from the General Organization for Military Survey in Damascus. Some aerial photos for small areas in the Aleppo were also obtained from the military survey.

4.2.3 Statistics

The analysis of spatial distribution of agricultural features were based on: statistical data taken at both village and the administrative district level for the years of 1975, 1987, 2005, and 2007; on previously achieved studies relating to the study area; and on the field observations. They were checked and proven. They are the basic foundation of Syrian agricultural statistics. These data are collected by agrarian engineers working in counselling units centred in the administrative sectors.

Also, there are general information and agricultural statistical records for the period 1970–2010. These are useful to understand the geographical history of the study area in relation to nature and human activities, and especially the historical development of the irrigation projects in the ERB. Each of these information and statistical records has a periodical annual publication, issued by the CBC in Damascus. The agricultural statistical records are collected on various levels, including village, administrative region, governorate, agricultural stable zones and the whole area of Syria.

Detailed information and statistics for the period 1970–2010 about the agricultural irrigation projects were obtained from IGDEP in the city of Arraqqa.

4.2.4 Ancillary Data

Ancillary data is used to facilitate a better understanding of LULC-dynamics and the reasons behind them. There are a various obtainable types of ancillary data: digital elevation models; soil map; housing and population density; road network; temperature; and precipitation. These can be integrated, as external inputs to remotely sensed data into a classification process in various concepts (Lu and Weng 2007). This integration has the benefit of improving the overall accuracy of produced thematic maps based on classification of remote sensing imagery. The percentage of this improvement based essentially on the used classifier (Heinl et al. 2009).

Climatic data (e.g., precipitation) was gathered for the climatic stations that existed in the major governorates within the ERB: Aleppo, Arraqqa, and Deir Azzour, during the temporal period of the study. These were obtained from the General Organization for Meteorology in Damascus. These data were useful for radiometric normalization using (iMAD) (see Chap. 5.2.3). Ancillary data for the entire water basin of the Euphrates is also included, as well as the agricultural calendar.

References

Bagan, H., Qinxue, W., Masataka, W., Satoshi, K., & Yuhai, B. (2008). Land-cover classification using ASTER multi-band combinations based on wavelet fusion and SOM neural network. *Photogrammetric Engineering & Remote Sensing, 74*(3), 333–342.

Chander, G., Markham, B. L., & Helder, D. L. (2009). Summary of current radiometric calibration coefficients for Landsat MSS, TM, ETM+, and EO-1 ALI sensors. *Remote Sensing of Environment, 113*(5), 893–903.

Farr, T. G., Rosen, P. A., Caro, E., Crippen, R., Duren, R., Hensley, S., Alsdorf, D. (2007). The shuttle radar topography mission. *Reviews of Geophysics, 45* (RG2004), 33.

Fujisada, H. (1995). Design and performance of ASTER instrument. *Proc. SPIE (The International Sociery for Optical Engineering)*, *2583*, 16.

Heinl, M., Walde, J., Tappeiner, G., & Tappeiner, U. (2009). Classifiers vs. input variables: The drivers in image classification for land cover mapping. *International Journal of Applied Earth Observation and Geoinformation, 11*(6), 423–430.

Lauer, D. T., Morain, S. A., & Salomonson, V. V. (1997). The Landsat program: It's origins, evolutions, and impacts. *Photogrammetric Engineering and Remote Sensing, 63*(7), 831–838.

Lesschen, J. P., Verburg, P. H., & Staal, S. J. (2005). *Statistical methods for analysing the spatial dimension of changes in land-use and farming systems* (p. 80). Nairobi: International Livestock Research Institute, LUCC Report Series, N. 7.

Liu, J. G., & Mason, P. J. (2009). *Essential image processing and GIS for remote sensing*. London: Wiley.

Lu, D., & Weng, Q. (2007). A survey of image classification methods and techniques for improving classification performance. *International Journal of Remote Sensing, 28*(5), 823–870.

McCoy, R. M. (2005). *Field methods in remote sensing*. New York, NY: Guilford Press.

Ono, A., Sakuma, F., Arai, K., Yamaguchi, Y., Fujisada, H., Slater, P. N., et al. (1996). Pre-flight and in-flight calibration plan for ASTER. *Journal of Atmospheric and Oceanic Technology, 13*(2), 321.

Schowengerdt, R. A. (2007). *Remote sensing models and methods for image processing*. New York: Academic Press.

USGS. (2009). *USGS announcement: Opening the Landsat archive*. Retrieved January 5, from http://landsat.usgs.gov/mission_headlines2009.php.

Van der Meer, F. D., Schmidt, K. S., Bakker, W., & Bijker, W. (2002). New environmental remote sensing systems. In A. Skidmore (Ed.), Environmental modelling with GIS and remote sensing. New York: Taylor and Francis.

Williams, D. L., Goward, S., & Arvidson, T. (2006). Landsat: Yesterday, today, and tomorrow. *Photogrammetric Engineering & Remote Sensing, 72*(10), 1171–1178.

Woodcock, C. E., Allen, A. A., Anderson, M., Belward, A. S., Bindschadler, R., Cohen, et al. (2008). Free access to Landsat imagery. *Science, 320*, 1011.

Yamaguchi, Y., Fujisada, H., Kudoh, M., Kawakami, T., Tsu, H., Kahle, A. B., et al. (1999). ASTER instrument characterization and operation scenario. *Advances in Space Research, 23*(8), 1415–1424.

Yamaguchi, Y., Kahle, A. B., Tsu, H., Kawakami, T., & Pniel, M. (1998). Overview of advanced spaceborne thermal emission and reflection radiometer (ASTER). *IEEE Transactions on Geoscience and Remote Sensing, 36*(4), 1062–1071.

Chapter 5
Research Methodology

This chapter gives a review about techniques and methodologies that were applied to answer the presented research questions and to confirm the hypothesis of this thesis. The conceptual workflow chart of the thesis is illustrated with an overview provided in Fig. 5.1.

Tone or color is the basis factor for most methods of digital image analysis. It is represented as a digital number in each cell of the recorded remote sensing image. The first step is applying a various procedures of preprocessing on the raw digital image. To carry out image classification, many steps have to be considered: choosing of a fit classification system; choosing of training samples; preprocessing of image(s); drawing out the feature; choosing of fit classification approaches; processing the resulted products of classification; and accuracy assessment.

Utilization of several variables during the classification process can make the classification accuracy worse because of unlike capabilities in separation between classes of interest (Price 2003). Therefore, many potential variables were used in image classification for the study case of this thesis, including spectral signatures, vegetation indices and transformed images (NDVI), multi-temporal images (1975, 1987, 2005 and 2007; April, May, July and August), multi-sensor images and ancillary data (GPS measurements, spectral information, statistical records, Google Earth etc.).

In this thesis, I will try to propose the methodological means which contribute to analysis of various data and information, and to integrate some of these data between each other, if necessary, to extract the information/results from the satellite images, to be presented in the final thematic maps.

Setting three local levels with multi-temporal levels to process sensory data available for obtaining thematic maps.

The first local-level: this level was embodied in the four administrative areas' borders (Menbij, Al-Jurnia, Ain Eisa and Athawra), and was accredited to test and compare several algorithms and automated classification methods in order to best determine the optimized algorithm and method of classification. Algorithms such as MLC, NN and SVM were tested in two ways. The first approach relied on a hierarchical shape and involved the extraction of classification outcomes through

W. Al-Fares, *Historical Land Use/Land Cover Classification Using Remote Sensing*, SpringerBriefs in Geography,
DOI: 10.1007/978-3-319-00624-6_5, © The Author(s) 2013

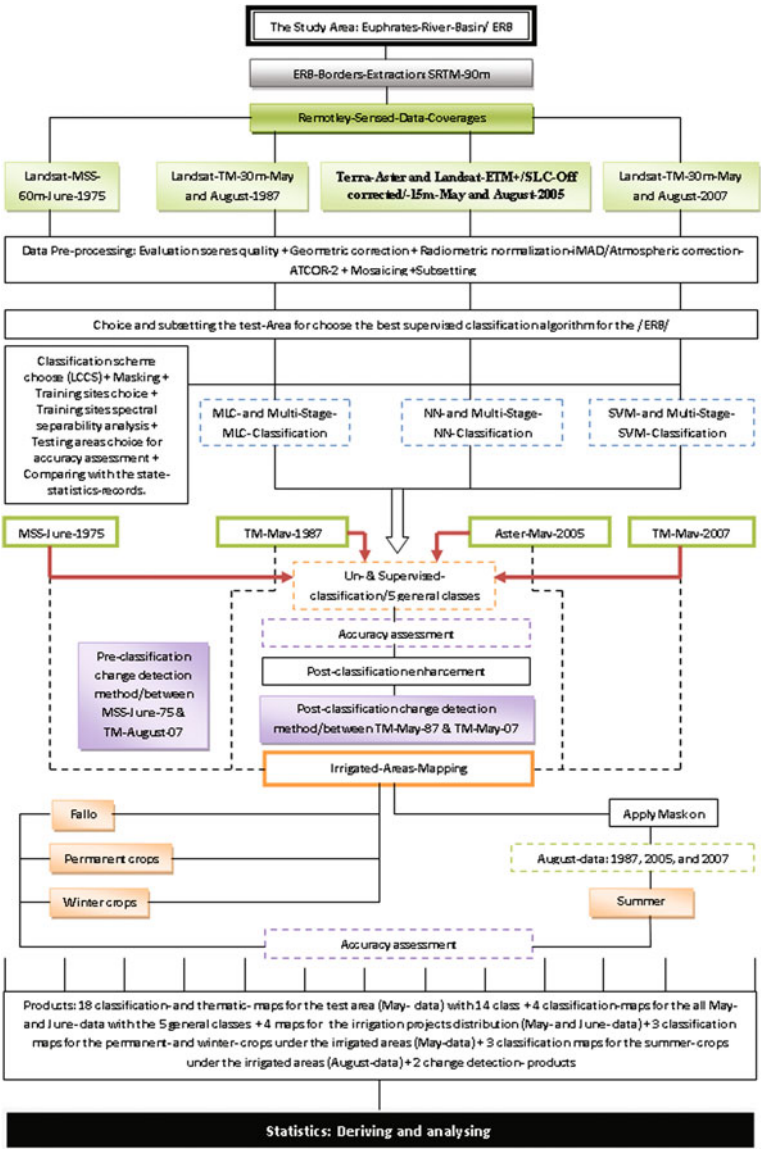

Fig. 5.1 The general conceptual workflow chart of the thesis

multiple stages, starting from the wide general level with little details and ending up at low levels subdivided from the previous general one, yet, advantaged with more detailed classes. The second approach classified sensory data through one stage. The used data were: LANDSAT-MSS-June-1975-60 m; LANDSAT-ETM+/SLC-Off/corrected and fused with ASTER-May-2005-15 m; and LANDSAT-TM-May-2007-30 m.

The second local-level: represented in the entire natural borders of the ERB. This level's outcomes were represented in three products. The first product involved setting thematic maps to represent the natural coverage and the wide general land uses distribution (LULC). Five classes counting on classification system were accredited in this study. The used data and dates were: LANDSAT-MSS-June-1975-60 m; LANDSAT-TM-April-1987-30 m; LANDSAT-ETM+/SLC-Off/corrected-April-2005-15 m; and LANDSAT-TM-April-2007-30 m). Here, for the automated classification process, one product (map) was obtained for each year (coverage), which represented and illustrated the quality and quantity of the spatial and temporal distribution of the natural coverage and uses of the lands. A quantitative analysis of produced maps was set (statistical data and tables) to compare, explain and analyze these numbers. Comparison was made between recordings extracted from various sensory data, regarding spatial and spectral resolution) positives, negatives, advantages and disadvantages).

The third product involved setting map/s representing the temporal and spatial change of the natural coverage distribution as well as land uses, utilizing the pre-classification change detection approach. For this, the LANDSAT-MSS-June-1975 and the LANDSAT-TM-August-2007 coverages were used.

Regarding the last two products, temporal and spatial changes were studied and analyzed.

The third local-level: represented in distribution of the irrigated agricultural projects within the natural limits of the ERB. The first product involved setting maps of distribution and change of agrarian irrigated areas, temporally and spatially, for the following data and years: LANDSAT-MSS-June-1975-60 m; LANDSAT-TM-May-1987-30 m; LANDSAT-ETM+/SLC-Off/corrected and fused with ASTER-May-2005-15 m; and LANDSAT-TM-May-2007-30 m.

As for the second product, this was manifested by setting thematic maps to represent the distribution of winter and summer basic crops in irrigated plantation projects, the types of cultivations and their area. The used data for this purpose was as follows: For the winter crops: LANDSAT-TM-May-1987-30 m; LANDSAT-ETM+/SLC-Off/corrected and fused with ASTER-May-2005-15 m; and LANDSAT-TM-May-2007-30 m. For the summer crops: LANDSAT-TM-August-1987-30 m; LANDSAT-ETM+/SLC-Off/corrected and fused with ASTER-August-2005-15 m; and LANDSAT-TM-August-2007-30 m).

The development of irrigated agricultural areas was calculated for the past 40 years.

5.1 Extraction of the Study Area

Extraction of the natural aquatic borders of the ERB in Syrian lands through the use of the digital elevation model DEM available from the sensor data SRTM in 90 m spatial resolution, in addition to the DEM-data from ASTER in 30 m. Data was imported to the ArcGIS 9.3 program using the following steps: Export raster

data (raw-data) to GRID-format; ArcToolBox/Spatial Analyst Tools/Hydrology: (Fill/Flow direction/Flow accumulation/Conditional-Con/Stream to feature/Add one point—.shp file-/Watershed); Conversation Tools: (from raster—Watershed-/Raster to polygon); and Analysis Tools: (Extract/Clip). Throughout the proposed results, the spatial distribution layer of the natural borders of river-basin was obtained from the SRTM-data. Concerning ASTER-data, there has been an unwillingness to depict the river basin edges because of their higher spatial resolution rather than the SRTM-data. Unfortunately, dealing with this data proved to be exhausting and full of errors. Therefore, a return to the SRTM-data ensued. There has been no accredited map issued by the Ministry of Irrigation that draws the borders of the ERB. The majority of Syria's irrigation projects lie within the natural boundaries of the ERB, except for some projects in the north and the south of the city of Aleppo, where waters have been extracted from the Euphrates River for the past five years. This means that many of these projects are not introduced in this study, as they occurred after the date of the last remote sensing data used (i.e., 2007).

5.2 Pre-Processing of the Satellite Data

"A good player never makes more effort than he needs to win"—old Arabic wisdom.

Remote sensing data may have two common types of distortions (systematic and non-systematic). This is because the method act of the Earth observation system and the characteristics of Earth's surface (Richards and Jia 2003). There are a variety of preprocessing procedures that could be applied on satellite data: finding and replacement of damaging lines of pixels; geographical registration of image and geometric rectification; radiometric calibration and atmospheric correction; and correction the topographical effects. According to Mather (2004), preprocessing procedures used to correct the generated deficiencies of geometric and radiometric formation of a remotely sensed image, and then it used to remove the errors of data. These deficiencies and errors have to be removed or at least manipulated, if it is achievable, before the starting with imagery classification. Which method would be applied, is dependent upon the goal of study. The most availability of preprocessing procedures or programs—automatic, is for coarse and medium spatial resolution data (e.g., LANDSAT-TM) and for high temporal resolution data (e.g., NOAA-AVHRR).

A good optimization in presentation of an individual object in the dataset of remote sensing data, is a result of a suitable selection of digital image preprocessing procedures. This goodness can be confirmed using a visual interpretation (Liu and Mason 2009). There are many digital methods to better enhancement of an image. These methods have the benefit of increasing the visual interpretability of used data and thus the thematic information of interest could be easily derived. The common three methods of image-enhancement are: (1) enhancement of

contrast ("more of the available range of digital values is used, and the contrast between targets and their backgrounds is increased" (Jensen 2005)); (2) spatial enhancement (spatial filtering, edge enhancement, and Fourier analysis etc.); and (3) spectral transformation (generating more valuable data or products—e.g., NDVI—based on manipulation—e.g., division of several spectral bands of data).

Despite the LANDSAT-images being level 1G corrected (Level-1G was corrected from USGS, and this modification consists of the basic corrections of radiometric and geometric distortions. But these corrections are not suitable for each application and thus user have to make additional corrections if the from USGS corrections are not sufficient), they are not good enough accurately registered in form pixel-to-pixel. USGS had pointed to a possible error of up to 250 m, and had not atmospherically corrected the data, thus all findings were subsequently re-corrected geometrically for this work (see Sect. 5.2.1). Atmospheric effects on the spectral signal were also minimized with a correction method (see Sect. 5.2.2). In addition to radiometric normalization (see Sect. 5.2.3), the ASTER data were delivered in Level 1A without any corrections.

ETM+-bands 6 and 8, plus TM-band 6, were eliminated from the entire processing and classification. The panchromatic information of band 8 was only used for pan sharpening. The sixth thermal spectral band—with its thermal information—was not used because the two reasons: it has a coarse spatial resolution; and it can recording only the transmitted radiation from objects in contrast to other spectral bands that measure the reflected radiation.

All image processing, classification and preparing the final results were carried out using two programs: ENVI, Version 4.6 and ArcGIS, Version 9.3.

5.2.1 Geometric Data Processing

"The more time steps involved for a change analysis, the more effort should be spent on image registration and radiometric adjustment" (Wulder and Franklin 2003 cited in Schultz 2011). So, the goodness or badness of method used in the registration of remote sensing data (image/s) will determine the quality/accuracy of the resulting change detection product (Schultz 2011). Townshend et al. (1992) assumes that the "problems created by misregistration are likely to be greater in the sensing of land surfaces compared with the atmosphere or many ocean properties".

There are several common expressions used to explain geometric correction process (registration, rectification, geo-coding and ortho-rectification) (Schowengerdt 2007). This process corrects the two different errors types (systemic and nonsystematic) resulting from the two different sources (within the remote sensing system itself, and during the recording of images) (Lo and Yeung 2002). The various applications of geometric correction on remotely sensed data are: co-registration of images that cover the same area on the Earth but they were obtained from two or more different sensors, or they were obtained at two or more different

periods of times, or they were obtained from two or more different sites; and rectifying an image to be accurate to an individual coordinate system (geo-coding) (Liu and Mason 2009). "Spatial distortion arises from scanner characteristics and their interaction with the airborne platform or satellite orbital geometry and figure of the Earth" (Schowengerdt 2007). Geometric correction can maximize the usefulness of the remotely sensed data for information extraction (e.g., thematic maps).

The geometric correction is the first image processing step (pre-classification approach) carried out when the remotely sensed data are not geo-rectified (Liu and Mason 2009). However, geo-rectification can be carried out as a post-classification approach to reduce the errors and distortions resulting from the geometric correction process. Generally, it is more competent to begin with geo-rectifying the still unprocessed data. Therefore, all products that will result from the raw data will be automatically geo-rectified (Liu and Mason 2009).

The problems that can occur in pixels of an image that will be rectified to other one (source image) are: the pixels have a different position; different orientation; and different size (Fig. 5.2). With this in mind, resampling methods have been developed to cope with these problems. The methods are based on choosing well-known and matching sites in both images of the selected cartographic projection. Based on these sites, a resampling technique will calculate the relation between their positions in the two images. These positions can be located exactly on an image using the so-called *Ground Control Points* (*GCPs*). These points are potential to define a suitable transfer function to be applied between the both images, i.e. rectify and master scenes (McCloy 1995). There are three components to the process: (1) selection of suitable mathematical distortion model(s); (2) coordinate transformation; and (3) resampling (interpolation). These are also known as *warping* (Wolberg 1990).

"*Resampling* is the process of calculating the data file values for the pixels in the rectified image by the use of data file values in the source image data" (McCloy 1995). There are three resampling schemes: nearest neighbor (sometimes called *zero-order interpolation*); bilinear interpolation; and cubic convolution. In the nearest neighbor approach, "the data file value of the nearest pixel to the retransformed pixel in the source image is adopted as the data file value for the output rectified pixel" (Liu and Mason 2009). By comparison with the other two schemes, it has the advantages: that it does not change the digital number value in

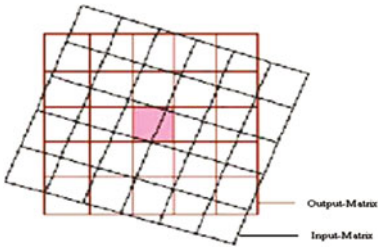

Fig. 5.2 Reposition pixels from their original locations (input matrix) in the data array into a specified reference grid (output matrix) (*Source* modified from Lillesand et al. 2008)

the data file; it is simple and rapid; and the main drawback is the stair stepped effect (Liu and Mason 2009).

Ground control points (GCPs) are pixels with well-defined positions in an image for which the output map coordinates are previously definite. They must have the following conditions and characteristics: (1) they have to be recognizable with a site both on the image and the real world surface; (2) they are accessible in the field; (3) they are consistently located within the study area of interest; (4) there are sufficient of them; (5) they have a small feature size; and (6) they have to be fixed over time. The most frequently used method to select these GCPs is the visual method (Liu and Mason 2009). If the point features to be GCPs are difficult to be exactly located on an image, it is better to select the ground object features to be a GCP (e.g., intersections of linear features). In an image-to-image registration model, intersections of highways or main roads are frequently used as GCPs. The next mathematical statement determines the minimum number of GCPs to be used:

Minimum number of GCPs = ((*n*1)(*n*2))/2, where (n) is the order of polynomial.

To obtain superior classification results, additional GCPs to the minimum number are commonly used. There is an error measurement technique that can compute the correctness of selected GCPs. It named the *Root Mean Square* (*RMS*) error, which is the distance between the input (source) position of a GCP in the input-matrix and the re-transformed position for the same GCP in the output-matrix. RMS-error is computed using the next mathematical statement:

$$RMS{-}Error = \sqrt{(x_r - x_i)^2 + (y_r - y_i)^2}$$

where: x_i, y_i : The input source coordinates; x_r, y_r: The retransformed coordinates.

The RMS error will be determined for each GCP. Then, the total RMS error will be computed by calculation the all RMS error of all GCPs. In the third step, the RMS error will then be tested for accuracy. If the overall RMS error is not good enough, then those GCPs with high RMS errors must be removed. This previous step will be repeated until the RMS error is good enough.

For comparison and combination based studies that use diverse sources of data and information, like remote sensing imagers obtained from diverse sensors (e.g., MSS, TM, etc.), field reference points (e.g., GPS-points), topographical data (e.g., DEM) and other available data for a study area, it is important to transfer all these data into a reference cartographic projection system; the result of which is a generally suitable data basis. The ERB projection parameters are: (Projection: UTM, Ellipsoid/spheroid: WGS84, Datum: WGS84, Units: Meters, Zone: 37 North). The study area is in one UTM-zone (37 N), which was an advantage for this work, since no geometric problems occurred due to changes between two UTM-zones.

All LANDSAT-data with their different sensors have no spatial deformations among them. However, during the connection and use of mosaic scenes, which result from gathering individual sensor images together, it was necessary to register the mosaic scenes to each other by accrediting one scene as the master-scene

and linking the other scene/s. Regarding the ASTER-data, the majority of images were not geometrically corrected, particularly between close paths. Therefore, a geometric correction was needed, in addition to a spatial registration with ETM+-data which was considered to be the geographical reference. Here, the problem was that ASTER-data had a geographical reference different from the geographical projection system of the ETM+-data, and with a 16 × 16 m pixel dimensions. For the purposes of this study, they were re-projected from: Geographic Lat/Lon, Datum: WGS-84, 16 × 16 m Pixel Dimensions to UTM, Datum: WGS-84, Zone: 37 North, Units: Meters, 15 × 15 m pixel dimensions using Rigorous Transformation.

Although the program ENVI can automatically correct the ASTER-data geometrically, these data were geo-referenced using the "Image to Image" concept, and then analyzed on the basis of LANDSAT-data, prior to fusing the two sensors-data. Figure 5.3 illustrates the results of the geometric correction for two ASTER-images.

The registration of the multispectral images was carried out using ENVI 4.6 software. The three general steps were: (1) locate GCPs in the two image to be corrected using the GCP-editor. The GCPs were interactively selected manually;

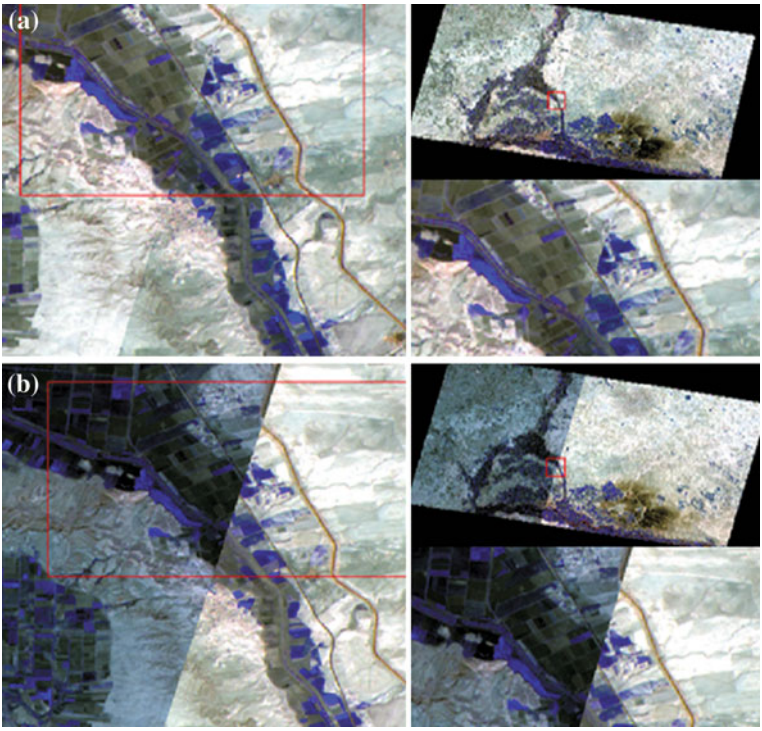

Fig. 5.3 The geometric correction (including the radiometric corrections) results of two ASTER-scenes **a** Before corrections **b** After corrections

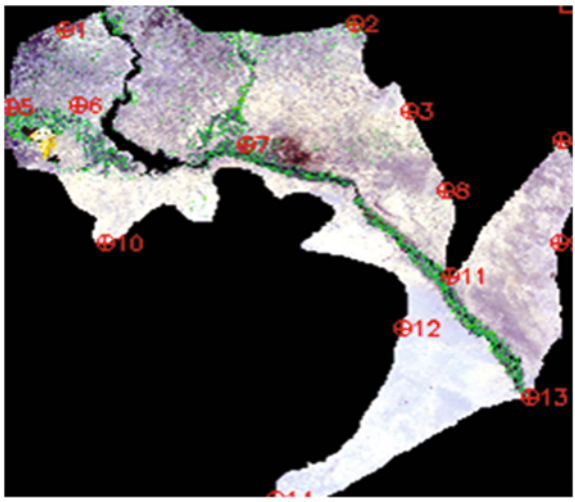

Fig. 5.4 The distribution of the 14-GCPs, used for registration of the tow data set (MSS-June-1975 and TM-August-2007), image-to-image concept

(2) compute the transformation matrix using the GCP editor and the transformation editor until the RMS error is small enough. A first-order polynomial was sufficient for the transformation; and (3) resample the image data. The nearest neighbor resampling technique was applied for rectifying the multispectral imagery.

For example, the geo-registration for the two remotely sensed data coverages LANDSAT-MSS-June-1975 and LANDSAT-TM-August-2007, was carried out using 14 GCPs (Fig. 5.4) which distributed across the image, especially on the margins (the number was dependent on the size and image spatial resolution of the used remote sensing data set). Table 5.1 lists the GCPs coordinates. It was simple to gather and present good results. The nearest neighbor 1st order polynomial correction was also used. According to the criteria presented in the literature of remote sensing, the RMS error per image must be always less than the half of spatial resolution of the image pixels, namely, <15 m (0.36) (Townshend et al. 1992; Mather 2004; Jensen 2007).

5.2.2 Atmospheric Correction

Electromagnetic energy detected and recorded above the atmosphere by remote sensing sensors (here, those that work in the optical section of the EM spectrum/ especially in the visible and near-infrared regions) includes two sources of energy: reflected and/or emitted from the ground surface; and energy scattered within and/ or emitted from the atmosphere. The quantity of this electromagnetic energy is dependent on the quantity of exhaustive solar energy (irradiance), which is reduced due to many factors: atmospheric absorption; the reflectance characteristics of the various ground surface features; the differences in path length; the

Table 5.1 The selected GCPs coordinates, used for registration the tow data set (MSS-June-1975 and TM-August-2007), image-to-image concept

GCPs	Base (x)	Base (y)	Warp (x)	Warp (y)	Predict (x)	Predict (y)	Error (x)	Error (y)	RMS-error
1	74,730,000	63,920,000	14,390,000	74,400,000	14,370,695	74,499,013	−19,305,143	0.99013222	0.50213654
2	13,666,000	62,370,000	76,300,000	59,400,000	76,309,792	59,333,543	0.97916066	−0.66456802	0.10258974
3	14,781,000	82,830,000	87,465,000	26,392,500	87,461,775	26,395,139	−0.32248964	0.26385880	0.41667857
4	18,051,000	89,730,000	12,016,000	33,310,000	12,016,498	33,305,137	0.49801720	−0.48629317	0.69606191
5	63,010,000	81,650,000	26,400,000	25,190,000	26,523,039	25,180,724	12,303,943	−0.92761745	0.23569874
6	77,410,000	81,380,000	17,030,000	24,930,000	17,053,866	24,916,530	23,866,399	−13,470,035	0.15429854
7	11,331,000	90,470,000	52,975,000	33,990,000	52,958,665	34,021,619	−16,335,435	31,618,867	0.15214582
8	15,591,000	10,136,000	95,570,000	44,930,000	95,562,622	44,923,377	−0.73775910	−0.66228433	0.99141768
9	18,008,000	11,303,000	11,973,000	56,590,000	11,973,374	56,594,625	0.37395907	0.46254371	0.59480422
10	83,510,000	11,310,000	23,170,000	56,650,000	23,159,195	56,647,066	−10,804,704	−0.29344471	0.20245697
11	15,686,000	12,107,000	96,510,000	64,630,000	96,512,613	64,628,173	0.26131315	−0.18272012	0.31885922
12	14,659,000	13,287,000	86,250,000	76,430,000	86,242,500	76,424,509	−0.74995666	−0.54913877	0.92950975
13	17,364,000	14,886,000	11,329,000	92,410,000	11,329,206	92,409,188	0.20638698	−0.081211834	0.22179032
14	11,962,000	17,240,000	59,270,000	11,595,000	59,275,189	11,595,316	0.51886214	0.31586047	0.60744198
									Total RMS error: 0.367236

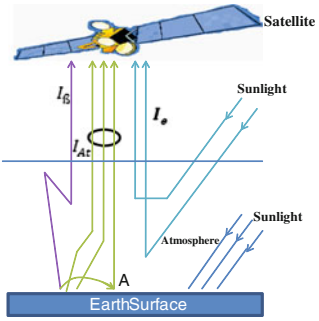

Fig. 5.5 A simplified model of the atmospheric effects on the reflection on a target object (*Source* modified from Kaufman 1985)

Schematic of the atmospheric influence on the recorded radiation at the sensor. The Sunlight is broken into three compenents:

$I_{\uparrow}$: Air light.

$I_{ß}$: Diffuse lighting. Distracted Radiation and Reflection/Emission.

I_{At} : Direct Reflection/Emission + Reflection/Emission by neighborhood effects.

A: Target

atmospheric conditions; and the wavelengths. Hence, energy recorded by the sensor is a constructed process of: (1) incident energy (irradiance); (2) target reflectance; (3) atmospherically scattered energy (path radiance); and (4) atmospheric absorption (ERDAS 1999; Liang 2004). Figure 5.5 illustrates this process.

A large amount of optical remote sensing data is affected by the impact of the atmosphere. This impact is called atmosphere effects (Liang 2004). It includes "molecular and aerosol scattering and absorption by gases, such as water vapor, ozone, oxygen and aerosols" (Liang 2004). These effects are note measured as "error", because they are a component of the entire recorded signal by a receiver or sensor (Bernstein 1983). To deal with these effects in optical remote sensing, there is a procedure known as *Atmospheric Correction.* It corrects for surface reflectance from remotely sensed images. However, it is not always simple to remove or enhance these effects. The procedure of atmospheric correction includes: assessment of the parameter of the atmosphere; and regain of the surface reflectance. To correctly regain the surface reflectance based on converting of sensor measurements to actual reflectance values on the ground using radio transfer codes, may be need a well knowledge about the atmospheric conditions at the time of image acquisition by a remote sensing sensor (e.g., humidity and temperature).

The assumptions that the reflectance values recorded on the remotely sensed data (optical remote sensing) are equal to the real reflectance of the different features on the ground surface, and that there is representative relation between the recorded values on the images and between the three properties of the ground surface (physical, chemical and biological), is not acceptable unless atmospheric corrections are applied (Liang 2004). Smith and Milton (1999) had presented the next more radical principle: "to collect remotely sensed data of lasting quantitative value then data must be calibrated to physical units such as reflectance".

It is not always necessary to apply an atmospheric correction technique for each remotely sensed study, since the necessity for that depends on the goals of the analysis and the expected results or products. For clarification, it is very important to be applied when a remotely sensed data of a certain region are to be evaluated over a time period—e.g., over a period of a crop growing—(Liang 2004). Atmospheric correction is necessary for classifying a multi-sensor (especially when integrated for an image classification) or multi-date imagery. It is moreover, essential for mapping of change detection over a time, since it used to guarantee that gray values of pixels are comparable in both images in a temporal sequence (Liang 2004), since atmospheric effects are one of the error sources in change detection studies (e.g., Chavez and Mackinnon 1994; Coppin et al. 2004).

In general, if a single-date image is used in LULC-classification, it may not require atmospheric correction as long as the atmospheric effects are consistent over the whole scene, since their impacts are similarly on the spectral vectors of training and unknown pixel, and their relative positions in spectral space are unaffected. However, if the atmospheric conditions varies largely within the study area (e.g., due to haze, smoke or dust storm), then spatially-dependent correction is needed (Song et al. 2001; Schowengerdt 2007).

A lot of techniques were founded to normalize and, if possible, to correct the radiometric distortions of the data and the atmospheric effect related to atmosphere conditions. These include, for example: the simple relative calibration approaches (e.g., the dark-object subtraction); and the complex approaches (e.g., 6S) (Markham and Barker 1987; Canty et al. 2004). These methods include: (1) *Invariant-Object Methods* (Moran et al. 1992; Chavez 1996) (2) *Histogram Matching Methods* (Richter 1996a, b); (3) *Dark-Object Methods* (Chavez 1988; Kaufman et al. 2000), which is frequently used; (4) *Contrast Reduction Methods* (Tanre et al. 1988); (5) *Cluster Matching Method* (Liang et al. 2001); (6) *The MODTRAN-code* (Berk et al. 1998); and (7) *The Second Simulation of the Satellite Signal in the Solar Spectrum 6S-code* (Vermote et al. 1997).

In the study presented here, the simplified and fast correction approach using the software program *ATCOR-2* (Richter 2011) was used to atmospherically correct the images when needed.

The *ATCOR-2/ATmospheric CORrection* program was developed by the German Center for Aerospace (DLR/Deutschen Zentrum für Luft- und Raumfahrt) (see: Richter 1996b, 2011). It provides spatially adaptive and fast algorithm. It supports the remote sensing sensors LANDSAT-MSS/TM and SPOT from SPOT-4. It works with a set of functions for atmospheric correction. This set was developed based on MODTRAN-2 and SENSAT-5 code. ATCOR-2 assumes that the target objects have an isotropic reflection behavior, where the error effect is taken in account by the blooming effect. The program uses the comparative analysis of the measured reflectance of a target object on the sensor with the back-calculated reflection of the same target, which it derived from models. It is also implemented in ERDAS IMAGINE (http://www.geosystems.de; http://www.atcor.de). The software has been available since 1996/2002, and is a part

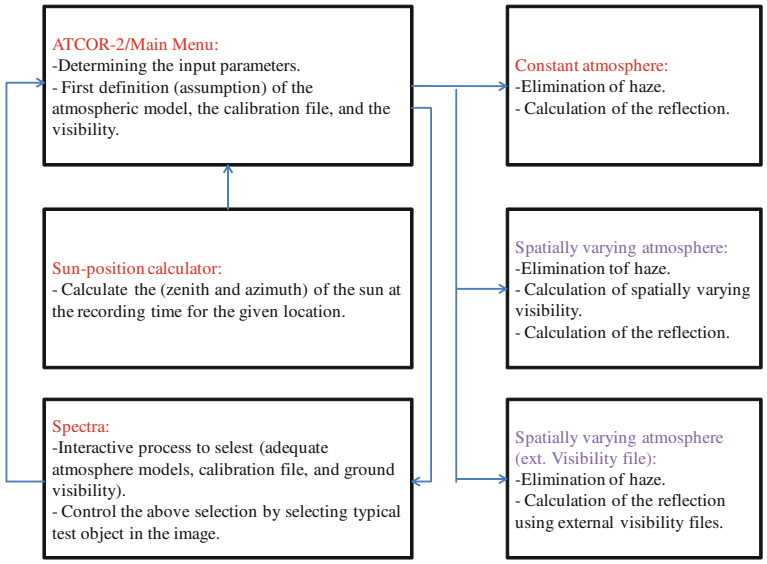

Fig. 5.6 ATCOR-2 and its central sub-modules (*Source* modified from Leica Geosystems 2005)

of other digital image processing software such as ENVI and PCI-Geomatica, or as an independent program.

Some of its advantages are: (1) short times required for computing process; (2) adequate results in comparison to other simple approaches or models; (3) it is easy to get the required parameters to be input to the program; and (4) it is uncomplicated to set and modify these parameters separately across the study area, especially if this area is large enough to have different radiation effects (Leica Geosystems 2005). Figure 5.6 subdivides the module ATCOR-2 into many sub-modules.

The parameters that have to be entered in the ATCOR-2/main menu are: (1) the image has to be corrected, the input-file source location, and the output-file destination after finishing the process of correction; (2) selection of spectral bands to be corrected; (3) determining the sensor specifications (calibration file); (4) determining the atmospheric model (based on meteorological information and the parameters of the applied model); (5) the size of the study area; (6) size of the used filter (to minimize the blooming effect), reflection- and emission- correction factors using the maximal dynamic range of the output-file by rescaling 8 bit; (7) some secondary information (e.g., location coordinates, recording date/time, mean elevation, air pressure, air temperature, absolute and relative humidity, and visibility); and (8) selection of the suitable atmospheric conditions from constant and spatially varying by comparison with secondary sources (Leica Geosystems 2005). The Spectra-module can be used optionally after point 7 as parameter number 8 in the module (main menu), checks whether the selected atmospheric model and the visibility are adequate (and if necessary adjusts the parameters iteratively).

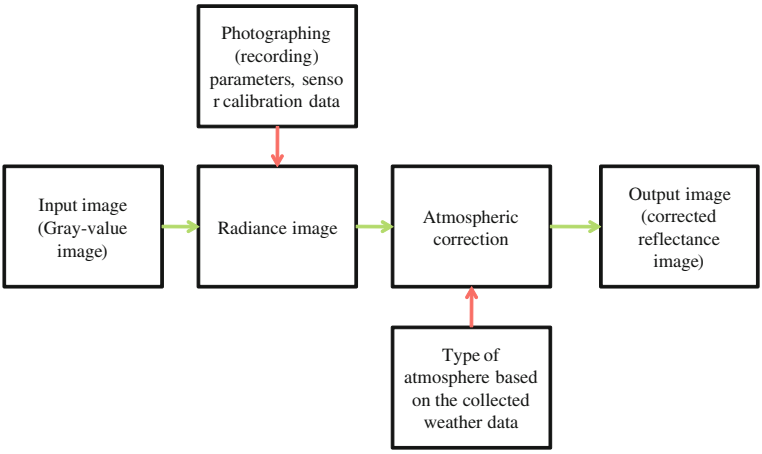

Fig. 5.7 The general concept of atmospheric correction using ATCOR-2

Figure 5.7 illustrates the major followed steps in atmospheric correction of the data set in this study. The solar zenith/sun elevation (61.07 °) and the solar azimuth/sun angle (126.22 °) were calculated using the sun position calculators based on the recoding date of the image (e.g., p172r035)/(07.8.2007), scene-center-scan-time (07:50:59 clock), and the Longitude (039 45 10 E) and Latitude (35 10 05 N) of the scene center. The necessary information can be found in the header file of the image data. The used atmospheric type was midlat-summer-rural, where: midlat = radiation region of the mid-latitudes, summer = season, and rural = aerosol type. Table 5.2 provides the used weather information. If the meteorological data are not always obtainable, then the standard atmosphere (dry desert) have to be used, which took into account the atmospheric effects in a good approximation (Richter, ATCOR-2/3 User Guide, 2011).

The sensor calibration file represents another important input. This file includes the calibration data (correction factors: Bias [c0] and Gain [c1]) of each channel. Bias: Describes the spectral radiation on the sensor for a gray value of zero. Gain: Represents the gradient calibration. The data takes place in the unit of electromagnetic radiation [mW cm^{-2} sr^{-1} μm^{-1}] (Lillesand et al. 2008). ATCOR-2 calculates the reflection on the sensor using these factors in the linear equation:

Table 5.2 Weather data from the Arraqah climatic station (Longitude: 039 59 00 E; Latitude: 35 54 00 N; Elevation: 250 m), 07.08.2007, 8.20 clock

Temperature	30.4 °C
Relative humidity	44 %
Visibility	35 km
Air pressure	870.3 hPa
Sun elevation	61.07

Source The General Authority for Meteorology, Damascus, 2008

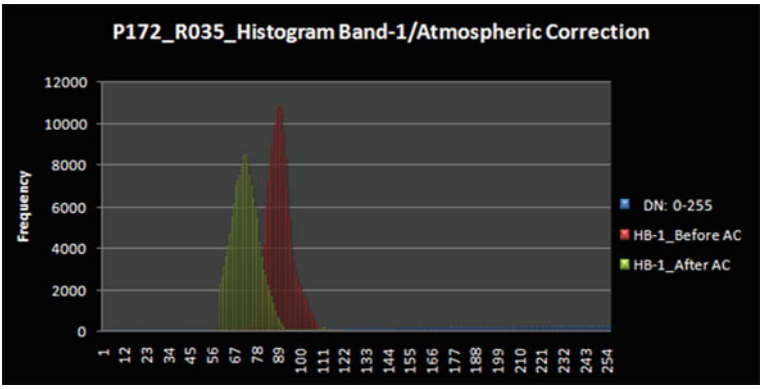

Fig. 5.8 Histogram comparison of the (LANDSAT-TM-Band-1) before and after the atmospheric correction

$\mathbf{L} = c0 + c1 \times \mathbf{DN}$, where: $\mathbf{L}$ = calculated radiance on the sensor; $\mathbf{DN}$ = digital numbers.

The new atmospheric corrected image (LANDSAT-TM-p172r035-070807) has new gray-values (e.g., DNs-before: 50, 65, 83; DNs-after: 41, 45, 65). The corrected histogram band 1 has, in comparison to the raw data, the same trends. It is darker, the individual object-groups are more evident through peak formation in the corrected data (DN-values), and they are, therefore, better to delimit than in the raw data (uncorrected) (Fig. 5.8).

5.2.3 Radiometric Processing/Calibration

The application of the information-extraction algorithms for LULC-classification, change detection and other remotely sensed Earth observation studies can be generally useful when the data are radio-metrically processed. On the other hand, if the user select an approach, that is based on products resulting after classification, for mapping the change detection, then radiometric correction is avoidable (Jensen 2007). It is true when only one image at each compared time (no mosaic) is used in classification, and when each image has the same irradiance conditions (e.g., no haze or dust). However, the using of some change detection approaches (image differencing), would requires a radiometric normalization. Also, radiometric correction is necessary for some applications (e.g., image mosaicing) (Yang and Lo 2000).

The radiometric correction set can correct radiometric distortion, which occurs because of sensor noises and atmospheric effects. Radiometric correction of remotely sensed data is a process of converting the recorded pixels' brightness values (where they are simply numbers, without physical units) to an absolute

independent scale of radiance that serves as a more direct link between image and biophysical phenomena, then addressing the errors in pixel values. It is then possible to manipulate these values to maximize their information for studies that are based on the digital processing of remote sensing data (Wulder and Franklin 2003; Liang 2004; Lillesand et al. 2008).

Schowengerdt (2007) has listed three levels of radiometric calibration. The first converts the sensor DNs to at-sensor radiances. The second transforms the at-sensor radiances to radiances at the Earth's surface. The third transforms it to surface reflectance.

The radiometric correction/adjustment set includes the three mechanisms: (1) calibration of the sensor: it is the process of converting the DNs to at-sensor radiance for inter-sensor data comparison. Gains and offsets are well-known for each remote sensing sensor, and these used to the recorded signals to generate the DNs. This first mechanism is frequently calculated at the satellite ground stations; (2) atmospheric correction (see Sect. 5.2.2); and (3) radiometric normalization (absolute and relative). (A) Absolute radiometric normalization: "for a linear sensor, is performed by ratioing the digital numbers (DNs) from the sensor, with the value of an accurately known, uniform radiance field at its entrance pupil" (Liang 2004). In this case, user has to carry out atmospheric corrections, which require atmospheric information at the time of the image acquisition (see Sect. 5.2.2). However, when it is difficult to obtain these atmospheric parameters and/or the absolute surface radiance is not necessary, one can change to (B) relative radiometric normalization: it is an in-image technique which uses the information contained within the image itself, and used when the full radiometric calibration for remote sensing data is complex. The concept is based on the supposition that it is possible, by application of linear functions, to estimate the at-sensor radiances recorded at two different times and for the same area but under different conditions (Yang and Lo 2000). This technique has the disadvantages of difficulty and time-consuming, where it has to determine the suitable time-invariant features upon which the normalization is based (Teillet and Fedosejevs 1995; Schowengerdt 2007). This method is applied especially in applications based on LULC-classification and post classification change detection (Song et al. 2001).

Several methods (Schott et al. 1988; Moran et al. 1992; Du et al. 2002) were developed and proposed to be applied as techniques for the relative radiometric normalization in remote sensing applications. Canty et al. (2004) proposed a method based on MAD, which use the advantage of the invariance properties of MADs. Canty and Nielsen (2008) further improved this approach by introducing an iteratively re-weighting method of the MADs, which executed superior in isolating no-change pixels fit to use for the relative radiometric normalization. The MAD method, after the modifications by Canty et al. (2004) and Schroeder et al. (2006) provides better radiometric normalization than those achieved with manual selected invariant features.

MAD can be used for bi-temporal change detection and for automatic relative radiometric normalization (Nielsen 2007; Canty and Nielsen 2008; Canty 2010). Canty (2010) explained the mathematical background of MADs.

To create a MAD-image, it is necessary to select two multi-spectral images that have alike spatial dimensions (size of the pixels). The two images will be modeled as a casual variable G1 and G2. When each image has, for example, 123 pixels, then these 123 pixels have a 123 times repetition of a mathematical random experiment, where,—here, the accurate value of pixels are not defined or described. If G1, G2 represent only a specific pixel or an entire image, then it will be illogical for them. What is important here is the properties of the causal variables G1, G2. Some suppositions about G1, G2 can be made by using the metrics of histogram (e.g., empirical variance, mean-based assessment of predictable value). Each image includes an N spectral bands, with G1 (also G2) as a random vector (Schultz 2011).

The X^2 image expresses the representative pixels which may be suitable for the radiometric normalization (Canty 2009). The X^2 distributions are only the pixels that satisfy the formula: /Pr (no change) > t, where (t) is a decision threshold that is typically 95 %/. The radiometric normalization based on these satisfying pixels will be used to perform an orthogonal regression.

The iMADs, X^2-values can only be calculated for overlapping areas, since the iMAD is designed for applying the automated radiometric normalization of multi-temporal remotely sensed data sets.

Adjacent scenes can be normalized by selecting their overlapping area (subsets) and followed by using the created transfer function of the orthogonal regression expressed on an entire image. It is important to cover all LULC-properties in the overlapping region of the two images (master and target), while pixels with an alike spectral behavior from overlapping and non-overlapping regions will be treated according to the regression function (Canty and Nielsen 2008).

Large water bodies affect the iMAD negatively (Canty 2009). Clouds and their shadows do not affect the normalization superiority, while they are detected as change (Canty and Nielsen 2008).

Summarized after Canty and Nielsen (2008) and Schultz (2011), the performed radiometric normalization was achieved in the five phases: (1) insert the dual-temporal data set; (2) compute CVs, build MADs and reweighing the spectral information accordingly; (3) repeating until no significantly improvement in correspondence of the CVs; (4) select pixels that have a no-change chance greater than a threshold value (t); and (5) determine the two radiometric normalization coefficients, i.e. slope and intercept, based on the orthogonal regression on selected pixels that have to be performed previously. The iMAD was applied to the imagery using ENVI 4.6 and IDL 7.06. The source code used was provided by Morton Canty and can be downloaded at "http://mcanty.homepage.t-online.de/software.html". In Canty (2009) the implementation and installation of the software to ENVI 4.6 is presented and explained.

To normalize the radiometry of all the used remote sensing sensor (e.g., LANDSAT-MSS-June-1975 and LANDSAT-TM-August-2007) data sets, a

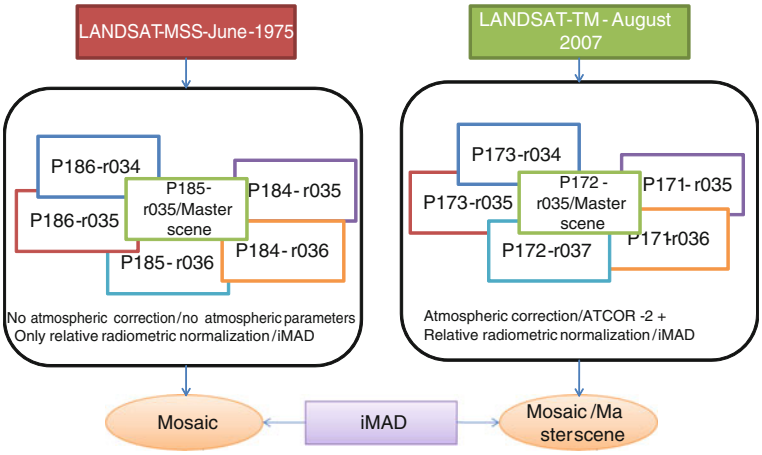

Fig. 5.9 Radiometric normalization between the two data-sets, which were used for change detection

master scene has been selected in each data set to which all other scenes have been adjusted. LANDSAT-MSS scene (p185r035) and LANDSAT-TM scene (p172r035) were selected as master scenes for each data set, as each was in the center of the study area and covered the greater part of it. Atmospheric conditions/ illumination were the same overall in each scene (e.g., no dust, no haze, etc.), and they had no cloud cover. All other scenes in each data set were radio-metrically adjusted based on the two master scenes. Regions in the image overlap areas of the bordering scenes were used to calculate regression coefficients, which were applied in a second phase to the complete sub-scene. The overlapping areas were selected to represent the variability of surface across the scenes. Finally, after mosaicking the images of each data set, the TM-Mosaic-Image was chosen as a master scene to normalize the MSS-Mosaic-Image radio-metrically (Fig. 5.9).

Figure 5.10 provides the results of the radiometric normalization using iMAD.

MSS-1975-Mosaic/before (iMAD) MSS-1975-Mosaic/after (iMAD) TM-2007-Mosaic/Master scene.

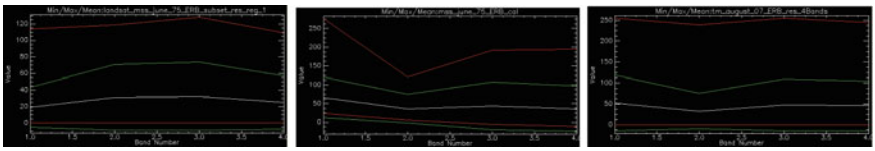

Basic Stats	Stdev	Stdev	Stdev
Band 1	24.345611	53.79413	66.910881
Band 2	39.756239	38.173823	42.59285
Band 3	41.205301	63.594957	62.193548
Band 4	31.961721	60.645272	59.189952

Fig. 5.10 iMAD results for the two data sets MSS-1975 and TM-2007. We can notice that the basic statistics (e.g., Stdev) of the radiometric normalized image are more similar to the master scene than the unnormalized image

A radiometric correction process was fulfilled on the mosaic scenes which carefully covered the study area. This was achieved by accrediting one of the scenes as a radiometric-reference (master-scene). Then, the other image/s were matched with it radio-metrically, i.e., a transformation process of the radiometric characteristics of the source-scene was conducted on the other images (targets). This resulted in obtaining close and similar radiometric characteristics for all scenes that covered the study area, because all had the same reference/source (i.e., the master-scene). Consequently, the Earth features (e.g., wheat fields) that existed in an individual scene, appeared spectrally (reflectance values/gray values) and radio-metrically, similar to those wheat fields located in each of the other scenes. This degree of similarity was based on the applied radiometric correction method/s and on the nature of the ground surface features that existed in the satellite image.

After finishing the atmospheric correction using ATCOR-2, a radiometric correction process was conducted of the scenes covering the study area (MSS-June-1975 and TM-August-2007) using iMAD. A radiometric correction was applied upon the two mosaic-scenes, since the TM-data was too basic for use with iMAD. As to the scenes that could not pass the radiometric correction process (for instance, TM-May-2007-data), it was enough to make atmospheric correction using ATCOR-2, followed by an automated classification applied for each image. Finally, the mosaicing-process was applied for the produced thematic maps that resulted from classifying each image. This mosaicing-process was helpful, in that it made it easier to find the final statistical results for the whole study area, and to compare the area with other results from separate data and dates.

5.2.4 Data Fusion

Image fusion is the process of fusing the lower multi-spectral spatial resolution with the higher panchromatic spatial resolution, to generate a higher multi-spectral resolution data set, which has the advantages of both: the high spatial resolution of the panchromatic image; and the higher spectral resolution of the multi-spectral image. It is one of the spatial enhancement techniques which are able to use the corresponding information that obtained from different imagery about the same terrain features in an effective way (Liu and Mason 2009).

Fusing panchromatic- and multispectral- data includes two general steps: (1) the geometrically registration the low-resolution multispectral imagery to the high-resolution panchromatic imagery (see Sect. 5.2.1); and (2) merging the information contents, spatial and spectral, to produce one data set that have the best characteristics of the two input data sets. Examples of image fusion techniques are: IHS (Intensity-Hue-Saturation); PCS (Principal Component Substitution); HPF (High-Pass Filter); RVS (Regression Variable Substitution); and SVR (Synthetic Variable Ratio). In this study, the Gram Schmidt Spectral Sharpening Algorithm was used.

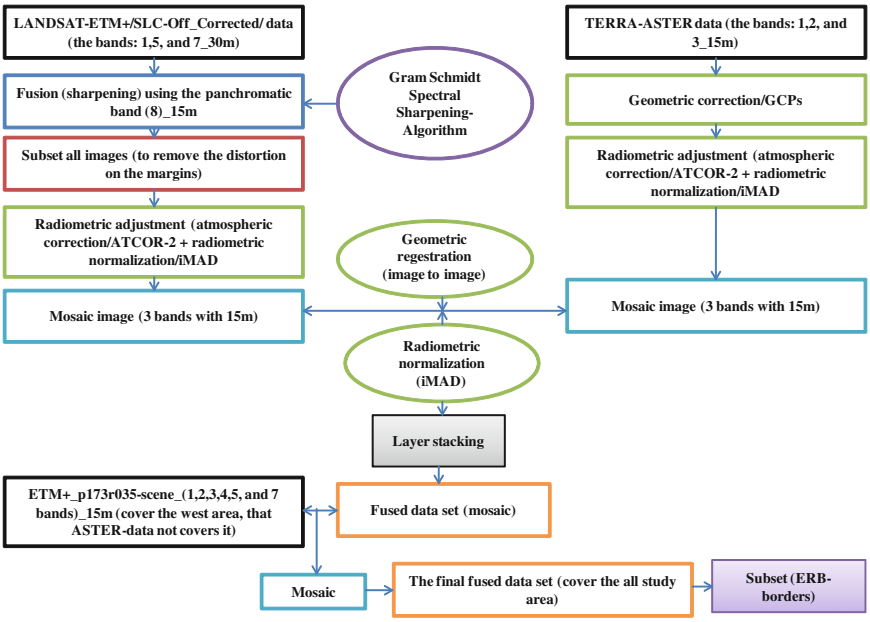

Fig. 5.11 Fusion- and mosaic-concept for LANDSAT-ETM+ and TERRA-ASTER data set, acquired in May and August 2005

The merged data were fit for further digital classifications, since the spectral separability for LULC- and crops- classes/six spectral bands of the merged data was better than the spectral separability of the original data. This was because there were only three spectral bands. Therefore, merged images were used for visual interpretation and for features extraction (classification).

Figure 5.11 explains the concepts followed to generate the final fused and mosaiced data set of the ERB-borders based on TERRA-ASTER & LANDSAT-ETM+ images.

The ASTER data did not cover the entire study area, only the first three bands with a resolution of 15 m. This data was before tested on the separability among the extracted classes of interest from the study area and compared to the same ASTER data after they were merged with the three spectral bands (1, 5 and 7) of LANDSAT-ETM+. However, these three bands were useless in the classification process due to their low separability when compared with the results of spectral separability that resulted after fusing with the other three bands of ETM+ (see Tables 5.4, 5.5). Therefore, ETM+-scenes which were corrected SLC-off data were used. This data had similar temporal coverage to the ASTER data. The idea was to increase the spectral resolution which in turn, increased the spectral separability between classes. These offered classification results with higher accuracy rather than using only the three spectral bands of ASTER data.

Because the ASTER data had a spatial resolution of 15 m, and in order to benefit from this to compare results with the results of MSS-60 m, and TM-30 m,

a spatial enhancement of the ETM+-scenes with the spatial resolution of 30 m was required. This was conducted by transforming the data into a 15 m spatial resolution using the ENVI-program and selecting the Schmidt Spectral Sharpening Algorithm. Figure 4.4 shows the spatial distribution of the two remotely sensed data which were used in the fusion and mosaicing process.

5.2.5 *Mosaicing, Subsetting and Masking*

The mosaic-process was applied to data which had similar atmospheric conditions and no radiometric distortion overall, or to those data whose atmospheric and/or radiometric distortions were corrected or normalized using ATCOR-2 and/or iMAD (see Sects. 5.2.2 and 5.2.3). For the data which were impossible to correct, a LULC-classification was carried out for each scene and then mosaiced to the results, to determine statistics. These results were in turn compared with those of the other data set (e.g., post-classification change detection) (see Sect. 5.12.2). The advantages of the mosaic process were found to be their ease and the speed in digital image processing.

Section 5.2.4 and the figures (Figs. 5.9 and 5.11) explain the followed process for two data sets. Figure 5.12 explains the difference between two generated mosaics and the importance of the pre-processing steps, mainly color balancing, radiometric normalization and atmospheric correction.

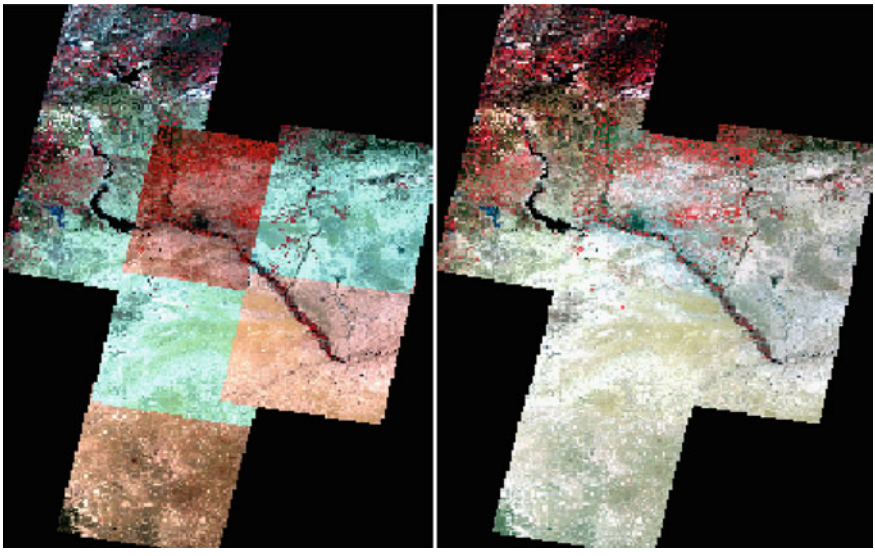

Fig. 5.12 Two mosaic-results of the data set (LANDSAT-TM-August-2007). *Left* without any digital pre-processing steps/techniques or corrections; r*ight* after applying corrections

The masking operation enables researchers to use an image file to choose (mask) definite areas and/or values from a matching raster file, and use those areas and/or values to generate one or more new files. The input mask file and input file must be the same as masking will be performed on the image area that both files have in general through the intersection process. This operation was used too often in the Multi Stage Classification Approach (see Sect. 5.7.1.2), especially in crops classification (see Sect. 5.11). The masking areas were selected by generated class values or were based on NDVI transformation (the masking operation was a processing and not a pre-processing step). All the class values of classes to be masked were set to zero or recoded to zero, then all unwanted zero signed features will be ignored when masking was executed.

The sub-setting operation was used broadly in this study to cut and remove the distorted margins of the LANDSAT-data; to subset only the study area (ERB borders) from each image or from the whole data set mosaic scene; to reduce processing time; and to reduce the geographical local extent that increased the spectral differences of the existing ground surface features. The final subset of the study area was about 50,335 km^2.

Mosaics for the ASTER-May and August-Data in 2005 were produced, eight paths from left to right (path-1: 4 rows, path-2: 4 rows, path-3: 3 rows, path-4: 3 rows, path-5: 3 rows, path-6: 4 rows, path-7: 5 rows, and path-8: 4 rows).

After the enhancement of the three bands of the ETM+-data (six bands for the scene (p173r035), i.e., the bands (1, 2, 3, 4, 5 and 7) which covered a part of the study area that the ASTER data did not cover), scenes were collected in one mosaic-scene. Here, before mosaicing, subsets were completed for each scene to remove margin deformations. After that, a geographic registration was applied for the ASTER-mosaic-scene with the ETM+-mosaic-scene as master-scene, using the image to image method. Before the last step, the three bands of ASTER data were composited with the three bands of ETM+-data (one layer-stack). The last step created a mosaic for the last scene which resulted from fusing ASTER-bands with ETM+-bands, and for the p173r035-scene of ETM+-data that covered the rest of the study area. The final result was the creation of one compound mosaic scene from both the ASTER- and ETM+-data that was homogeneous: Radiometrically (i.e., no or acceptable spectral appearance of the same features overall in the mosaic-scene); spatially (15 m); and spectrally (six bands).

In order to reduce temporal and effort processing series on the remote sensing scenes which covered more than the spatial distribution of the study area, these scenes were subsetted to include only the spatial distribution of the ERB borders.

5.3 Design of the LULC-Classification System

A LULC-classification starts with defining a classification system. A successful LULC-classification requires a suitable classification system and an adequate number of training sites. Its design is related to: the needs of the user; the spatial

resolution of used remote sensing data; the capability with the prior studies; the used algorithms for image-processing and classification; and the time limitations. A system of LULC classification categorizes the all definable LULC-features into classes in the system. A good system should have three characteristics (informatively, exhaustively and separability) (Jensen 2007). Also, a good system structure can be located at any point on the map/ground into one and only one LULC-category.

An a priori hierarchical structure system for the LULC-classification for the study area was build. This system was adopted to increase the flexibility of classification procedures and to take different conditions into account. Furthermore, the LULC-classification system used the "diagnostic criteria and their hierarchical arrangement to form a class (*map-ability function*), that had the ability to define a clear boundary between two classes. Hence, diagnostic criteria should be hierarchically arranged in order to assure a high degree of geographical accuracy at the highest levels of the classification. These prerequisites can only be accomplished if the classification has the possibility of generating a high number of classes with clear boundary definitions" (Di Gregorio 2005).

The *Land Cover Classification System* (*LCCS*) was designed with two main phases (see Fig. 5.13): (A) an initial *Dichotomous Phase*, in which eight major land cover types were defined: (1) Cultivated and Managed Terrestrial Areas; (2) Natural and Semi-Natural Terrestrial Vegetation; (3) Cultivated Aquatic or Regularly Flooded Areas; (4) Natural and Semi-Natural Aquatic or Regularly Flooded Vegetation; (5) Artificial Surfaces and Associated Areas; (6) Bare Areas; (7)

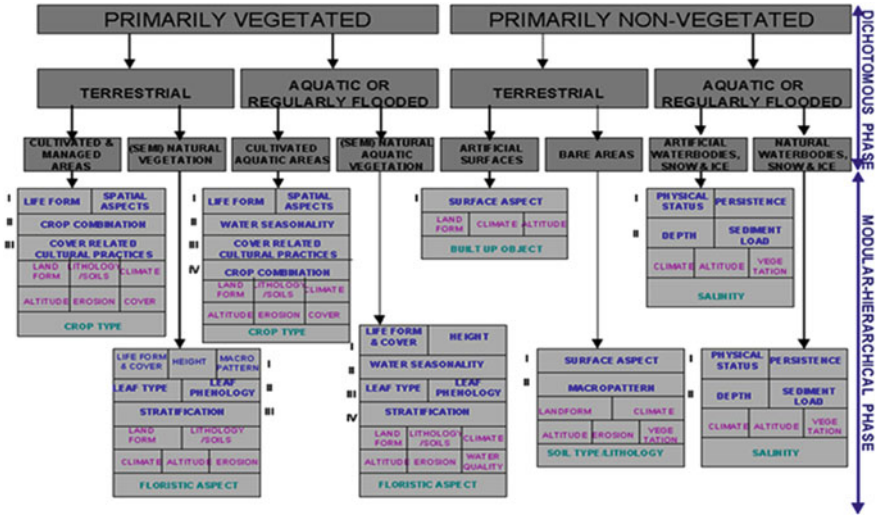

Fig. 5.13 Overview of the land cover classification system (LCCS), its two major phases and the classifiers (*Source* adapted from Di Gregorio 2005)

Artificial Water bodies, Snow and Ice; and (8) Natural Water-bodies, Snow and Ice (Di Gregorio 2005).

Five major classes were classified: 1, 2, 5, 6 and 8, since the classes 3, 4 and 7 did not exist in the study area ERB. A dichotomous key was applied at the major level of classification to identify the major land cover classes (see Fig. 5.13). Three classifiers were used in the dichotomous phase, i.e.: *Presence of Vegetation*; *Edaphic Condition;* and *Artificiality of Cover*. "These three classifiers were hierarchically arranged, although independent of this arrangement, the same eight major land cover types would be keyed out. The hierarchical arrangement is thus not important in this phase, but was a guiding principle in the subsequent Modular-Hierarchical Phase" (Di Gregorio 2005).

This was followed by a subsequent so-called: "(B) *Modular-Hierarchical Phase,* in which land cover classes were created by the combination of sets of pre-defined classifiers. These classifiers were tailored to each of the eight major land cover types. The tailoring of classifiers in the second phase allowed the use of the most appropriate classifiers to define land cover classes derived from the major land cover types and at the same time, reduced the likelihood of impractical combinations of classifiers" (Di Gregorio 2005).

The classifiers of the pure land cover can be jointed with so-called *attributes* for additional description. There are two kinds of these attributes, which form separate levels in the classification: (Di Gregorio 2005): "(1) *Environmental Attributes*: these attributes (e.g., climate, landform, altitude, soils, lithology and erosion) influence land cover but are not inherent features of it and should not be confused with "pure" land cover classifiers. These attributes can be combined in any user-defined order; and (2) *Specific Technical Attributes*: these attributes refer to the technical discipline. For Semi- Natural Vegetation, the *Floristic Aspect* can be added (the method on how this information was collected as well as a list of species); for Cultivated Areas, the *Crop Type* can be added either according to broad categories commonly used in statistics or by crop species; and for bare soil, the *Soil Type* according to the FAO/UNESCO Revised Soil Legend can be added. These attributes can be added freely to the pure land cover class without any conditions".

The LCCS is a wide-ranging, standardized a priori classification system, designed to meet specific user requirements, and formed for mapping exercises, free from scale factor or means used to map. Any LULC-feature well-known overall around the world can be readily contained. The classification uses a set of diagnostic standards that are independent and that able to allowing a correlation with presented classifications and legends. The advantages of the classifier or parametric approach are manifold. The system created is a highly flexible a priori land cover classification in which each land cover class is clearly and systematically defined, thus providing internal consistency. The system is truly hierarchical and applicable at a variety of scales. Re-arrangement of the classes based on re-grouping of the classifiers used facilitates extensive use of the outputs by a wide variety of end-users. Accuracy assessment of the end product can be generated by class or by the individual classifiers forming the class. All land covers can be

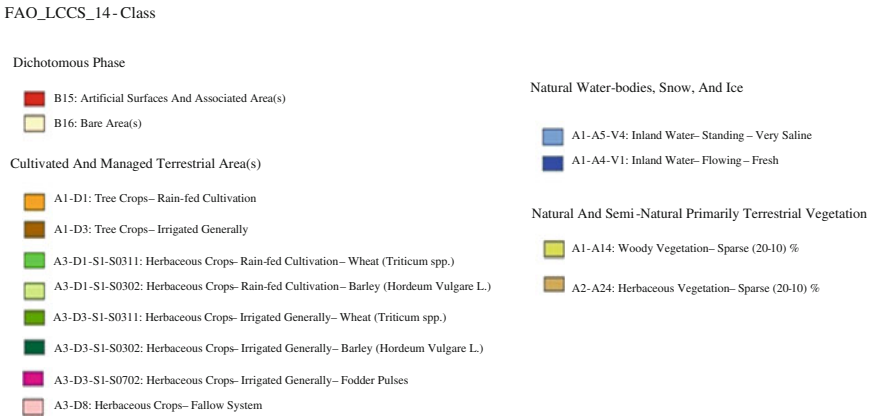

Fig. 5.14 Description of the resulting 14-class for the four 4-regions sub-study-area (*Source* adapted from LCCS-Software/Version 2.0)

accommodated in this highly flexible system; the classification could therefore serve as a universally applicable reference base for land cover, thus contributing towards data harmonization and standardization (Di Gregorio 2005).

Included here is the general legend which generated from the LCCS-Software, because it is difficult to read the description of the resulted classes once the legend is integrated with the resulting thematic maps (Fig. 5.14).

5.4 Field Work

The identification of the potential LULC-classes and the thematic content that a classification can or should be included is crucial, where a classification process is a thematic analysis of the landscape (Jensen 2007). Such interpretation to be founded, it is necessary to identify and understand factors that control and determine the form of features or phenomena. So, field work and observations are essential if a supervised based classification method will be used (Richards and Jia 2003).

Interviewing local farmers provides important understanding of the general characteristics of the LULC in the study area during the past decades. So, interviews were conducted with village leaders and farmers. The main reason for interviewing these people was to find the relationship between the satellite data and the qualitative LULC-history in the surroundings of the villages.

Field work was carried out in June, 2007 (Fig. 5.15), since measurements can be taken (GPS-points) for either winter and/or summer crops. Annually in June in Syria, the wheat and barley are harvested (N.B., most irrigated wheat in east Syria will not be harvested yet), the sugar beet will still be green, cotton and corn will

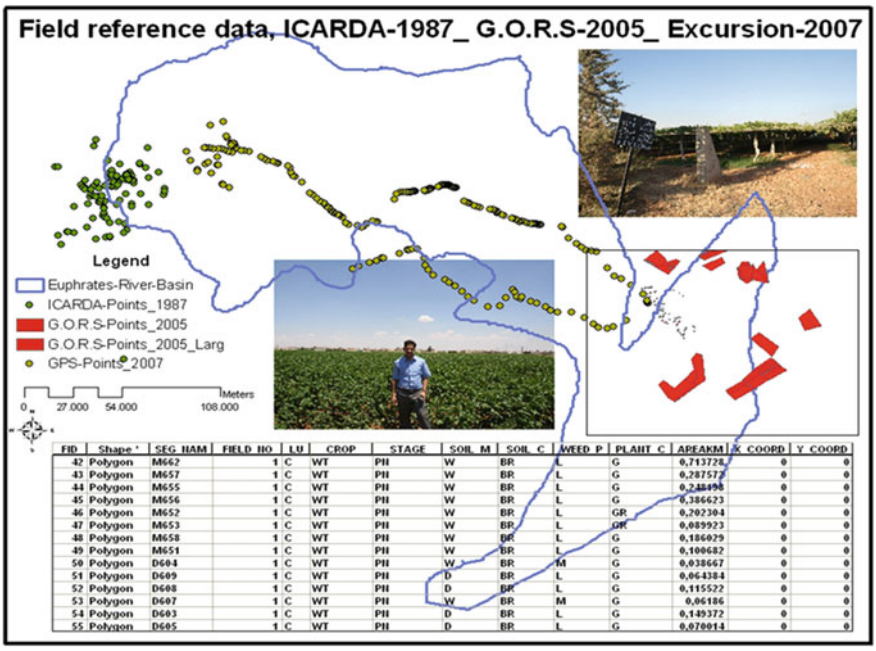

Fig. 5.15 Excursion-GPS-points-2007 and other GPS-measurements from ICARDA and GORS

grow without problems. A second campaign was conducted in July 2009 for complementary information and some GPS-measurements based on the knowledge of the farmers. These two field work periods were held to increase the understanding of the patterns of LULC in the study area. Preliminary image classification (unsupervised) and RGB-composite imagery of the study area were printed to show target areas to be surveyed depending on the accessibility of each site. The data were gathered from different sites depending on the differing soil types and irrigation systems in the study area. Random sampling methods were used. Each plot was registered by using GPS-technology (using a GARMIN-Colorado-300 global positioning receiver) to allow for further integration with the spatial data in a geographic information system (GIS) and image classification programs.

Information was gathered based on specific procedures such as: identification of the dominating species of trees, shrubs and herbs; detection of the physical aspects of the soil; conduction of interviews and group discussions with local farmers to extract historical information about the LULC in the study area; and gathering of information about prior LULC activities regarding to types, densities, distributions, and species.

Figure 5.16 illustrates one example from the study area as explanation of the steps followed during the excursion in 2007 to collect ground truth data (especially for agriculture). The outputs of this first experimental stage were the gathering of the training samples and the testing of sites for automated supervised classification

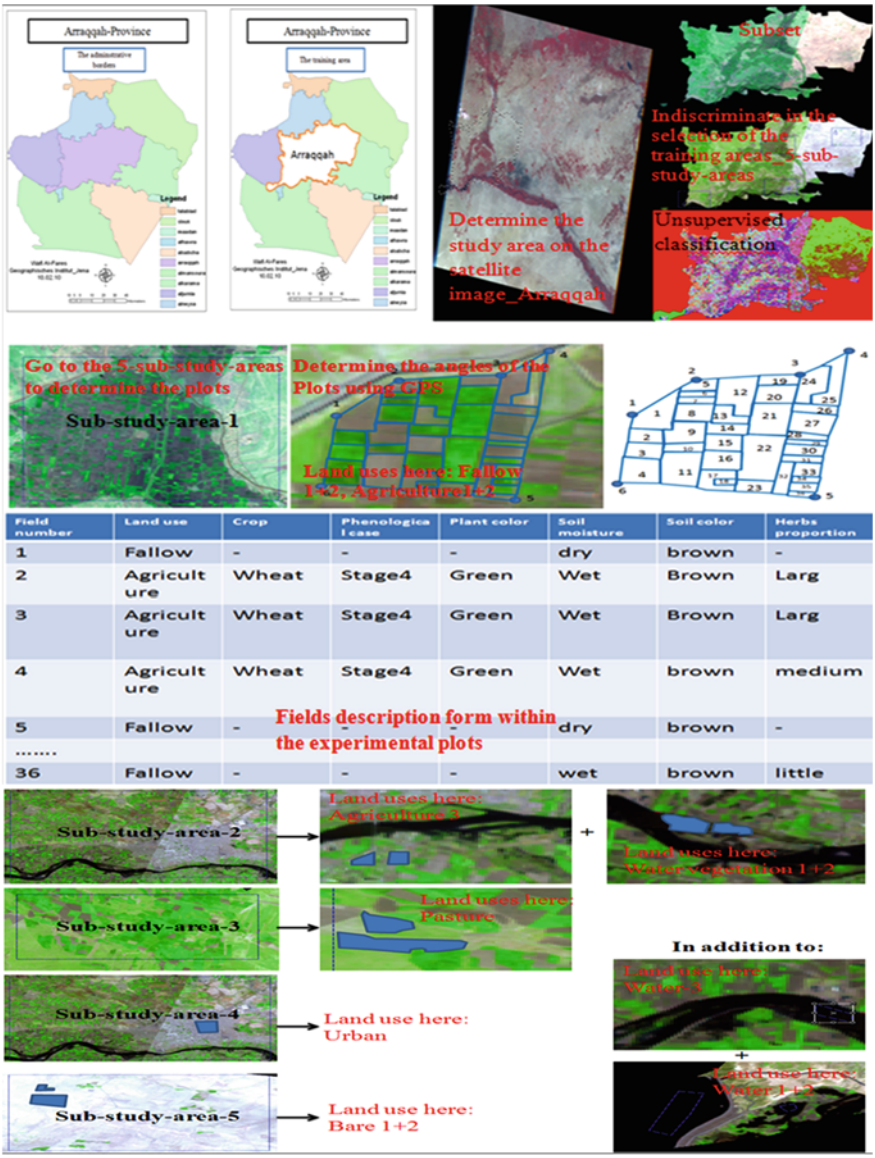

Field number	Land use	Crop	Phenological ease	Plant color	Soil moisture	Soil color	Herbs proportion
1	Fallow	-	-	-	dry	brown	-
2	Agriculture	Wheat	Stage4	Green	Wet	Brown	Larg
3	Agriculture	Wheat	Stage4	Green	Wet	Brown	Larg
4	Agriculture	Wheat	Stage4	Green	Wet	brown	medium
5	Fallow	-	-	-	dry	brown	-
.....							
36	Fallow	-	-	-	wet	brown	little

Fig. 5.16 The followed methodology for collecting the ground truth data during the field-work in 2007

algorithm/s and accuracy. Figure 5.17 presents the complementary stages of the field-work, which could perhaps be described as "office work". This was essentially based on the gained output-results of the previous stage and their use as inputs in the automated supervised classification processes chain. The classification process in this work included two types (see Sect. 5.13; Chap. 6.2); the first

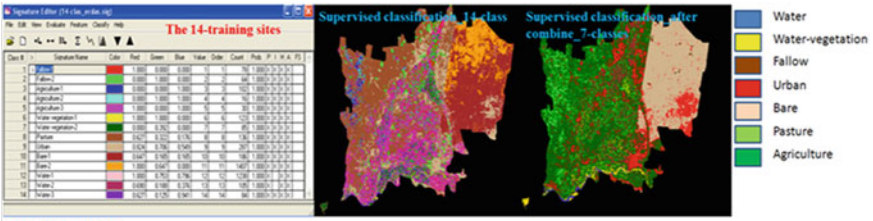

Validation

Class	Producers Accuracy %	Users Accuracy %	Overall Accuracy %
Water	100	100	
Water vegetation	90	89	
Fallow	95	92	85.57
Urban	70	67	
Bare	85	84	
Pasture	73	74	
Agriculture	86	79	

Callculation the classes-areas and comparisons

Class	Pixel Number	Pixel Size/m	Space_1000-Hectar	%	%/statistic of the Agriculture Ministry	The different/ %
Water	1090	30	00,327	1.86	2.45	-0.59
Water vegetation	4607	30	13,823	7.84	6.23	+1.61
Fallow	6812	30	20,436	11.59	15.86	-4.27
Urban	6141	30	18,425	10.45	7.45	+3
Bare	15716	30	47,149	26.74	24.48	+2.26
Pasture	7235	30	21,705	12.31	13.47	-1.16
Agriculture	17168	30	51,504	29.21	30.06	-0.85
Total	58775	30	176,325	100	100	

Fig. 5.17 The followed methodology for collecting the results during the "office-work"

using the automated accuracy assessment based on trusted data (e.g., aerial photographs, GPS-measurements, etc.); and the second manually comparing the resulted readings from remote sensing data with the state statistical records. One cannot separate between these two stages, especially when the desired classification result reaches a very detailed level of information about the LULC-features (e.g., crops mapping). Thus, these stages have been linked and described in the same place here.

5.5 The Possibility of Spectral Separation Between Crops/ Spectral Considerations

Satellite data was procured based on agricultural crop calendars and separability (dependant on crop cover, density, leaf area, crops growth stage, etc.) of the main crops cultivated in the region. By application of remote sensing data in agriculture, the observing of spectral of the crops at one exact stage is more common than those over the entire growing season. Thus, the spectral behavior of plants and the effects of the background surface (soil or water) should be well understood.

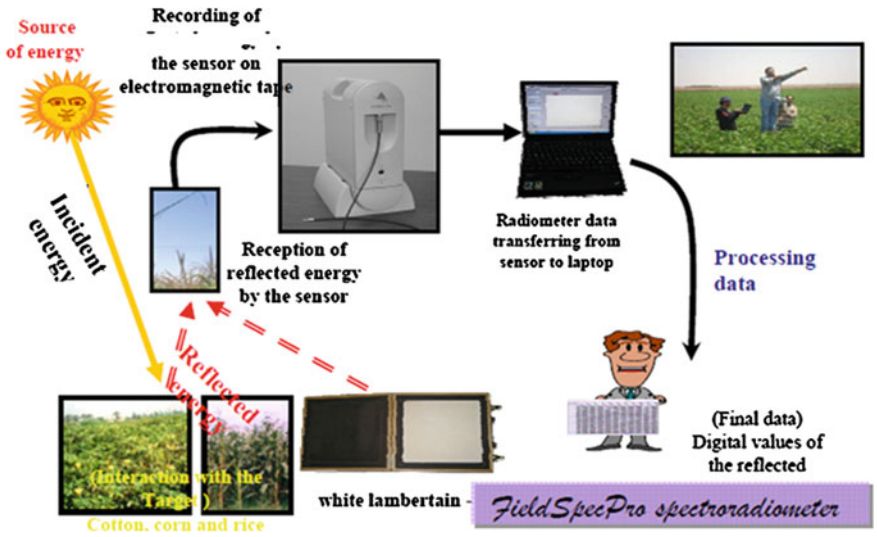

Fig. 5.18 The followed concept in spectral measurements using (FieldSpecPro) by (GORS)

The questions related to the spectral characteristics of the used data are: what are the agricultural features that have to be classified? Are they spectrally separated from the other associated agricultural features and land cover types (especially the natural plants)? Which EMS portion, wavelength, or spectral band are most helpful for spectrally distinguishing and classifying the agricultural features? and what time period of the year is more suitable, in which remote sensing data would be acquired? This based on the fact that the spectral behavior of these agricultural features is unique or more unique during certain times of the year (Hoffer 1980).

The conceptual method and the final results carried out from the GORS-project (see Chap. 2.2) using the spectrometer measurements were used to determine the appropriate date/s, in which is it was possible to separate between the agricultural crops spectrally and then to classify the individual winter and summer crops. This presentation was to confirm the temporal choice of the various remotely sensed data that are used in this study.

A FieldSpecPro spectrometer by GORS was used to collect the radiometric measurements of the major crops. It had a spectral range of 350–2,500 nm, with a spectral interval of 1 nm. It offered very sensitive and accurate measurements in the spectral ranges of visible, near infra-red, far infra-red, and thermal, and was equipped with two software-programs. The first, RS3, recorded target reflectance and saved the measurement records. The second, ViewSpecPro, processed the recorded data and transformed them to digital-format, for ease of analysis (Fig. 5.18).

Fig. 5.19 The distribution of the training fields used in the spectral measurements

The total radiometric readings numbered 2,669 measurements that represented 103 training-fields of different crops (Fig. 5.19).

These displayed the values of the spectral reflectance as spectral signature for each crop, within the wave-lengths from 35 to 2,500 nm and with a spectral interval of 1 nm for the crops in the study area through their growth stages, allowing for a temporal succession of 15 days between the various readings, from planting and germination until harvest. The spectral results that represented the winter crops included wheat, barley and sugar beet. For example, the training fields of wheat in Arraqqah Province were made up of 35 fields (Fig. 5.20).

Figure 5.21 illustrates the bond between the spectral responses of the irrigated wheat during 10 different growth stages and the characteristics of the eight bands of ASTER. It is clear that the reflectance potential is greatest at the third band among the whole growth stages, with the exception of the time period from 04.12 to 23.01 in the study year, where the reflectance of the soils prevailed.

Figure 5.22 illustrates the change in the spectral response of the irrigated wheat in relation to the eight spectral ASTER-bands among the 10 various growth stages.

After analyzing the various spectral responses of the different winter crops in the study area, the appropriate date for separation between the three irrigated major strategic crops (wheat, barley and sugar beet) was determined in the first days of May. In addition, sugar beet was found to have another separation date in mid-June, when the other two crops (wheat and barley) were harvested or had a dry and yellowish appearance (Fig. 5.23).

Secondly, the spectral results that represent the major summer crops included cotton, corn and watermelon. Figure 5.24 illustrate the spectral response of each crop. The third spectral band of the ASTER-sensor had the greatest sensitivity and

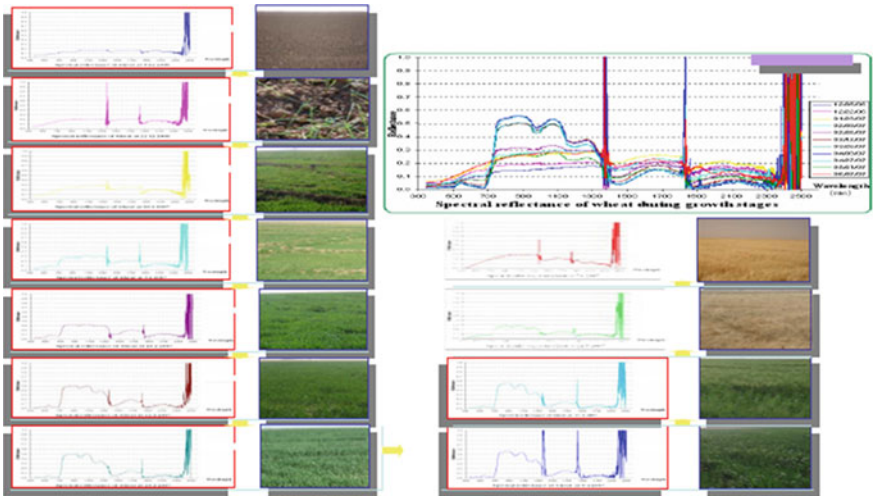

Fig. 5.20 Spectral reflectance measurements for wheat at different growth stages

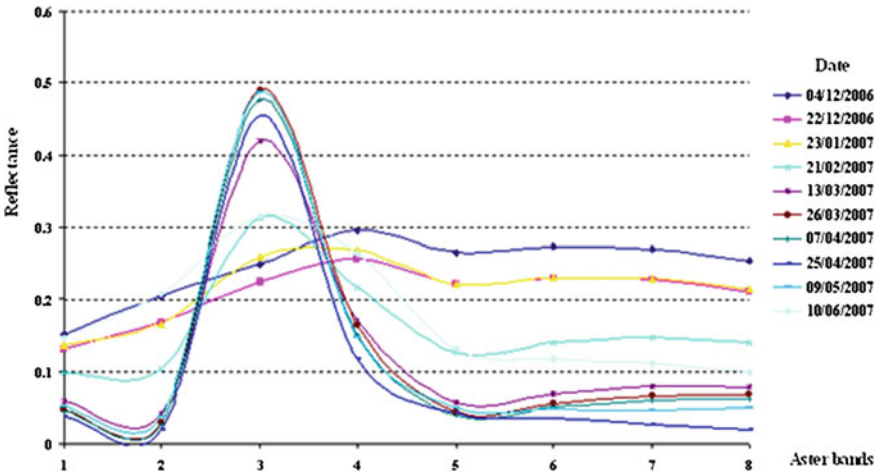

Fig. 5.21 Spectral reflectance values of irrigated wheat during its growth stages in Arraqqah using the ASTER-bands

potential to detect the spectral characteristics of the three crops of interest, among the various growth stages, using the first three ASTER-bands.

Figure 5.25 represents the effect of the vegetation growth stages on the spectral response of cotton at the third ASTER-band.

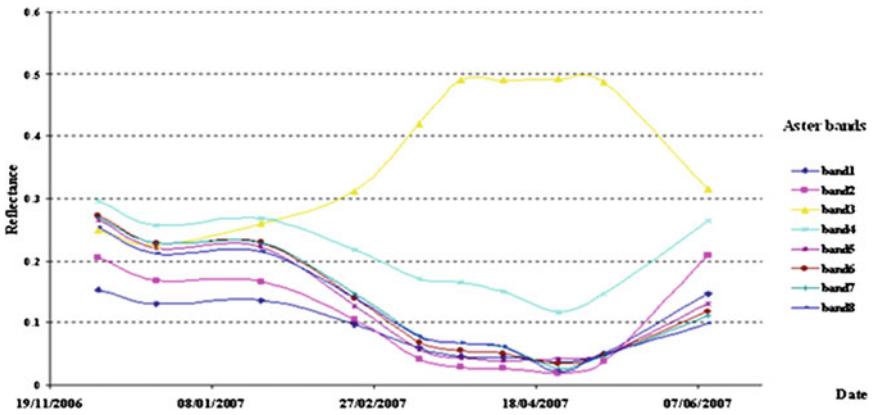

Fig. 5.22 Spectral reflectance values of ASTER-bands during the different growth stages of the irrigated wheat

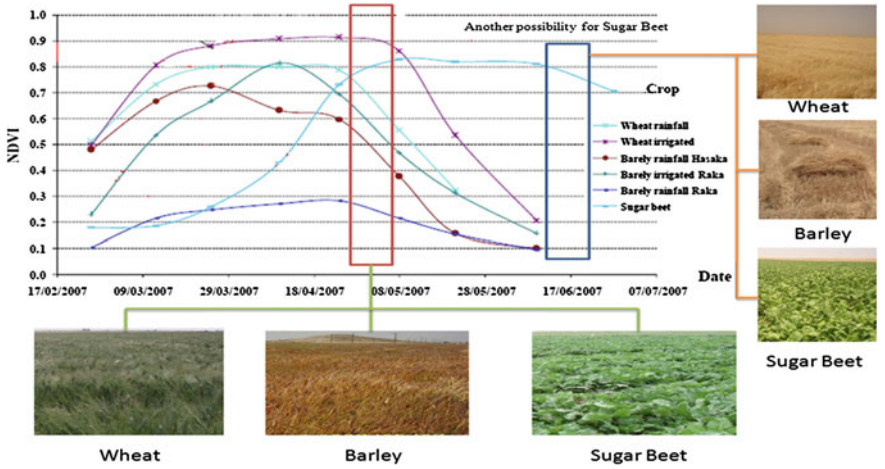

Fig. 5.23 NDVI-values of major winter crops during growth stages in Arraqqah Province in Syria

The suggested date of separation and classification of the three summer crops is between 20 July and 20 August (Fig. 5.26). Figure 5.27 illustrates the different spectral responses of these major crops.

These results are compatible with both ASTER-data and LANDSAT-data, and it is possible to generalize them with other remotely sensed data that operates especially in the visible and the near infra-red spectral ranges.

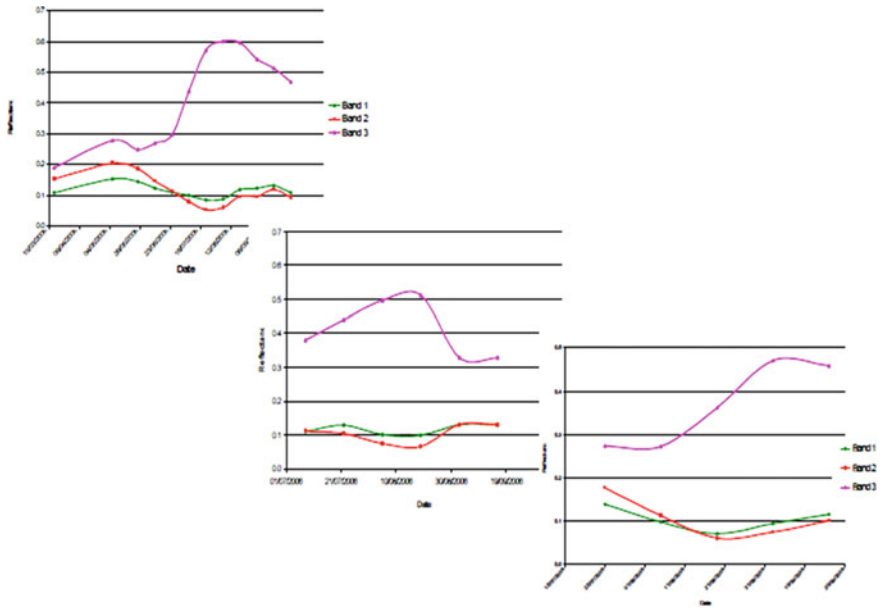

Fig. 5.24 The relationship between the spectral reflectance and the different growth stages of the three essential summer crops by the first three spectral bands of ASTER

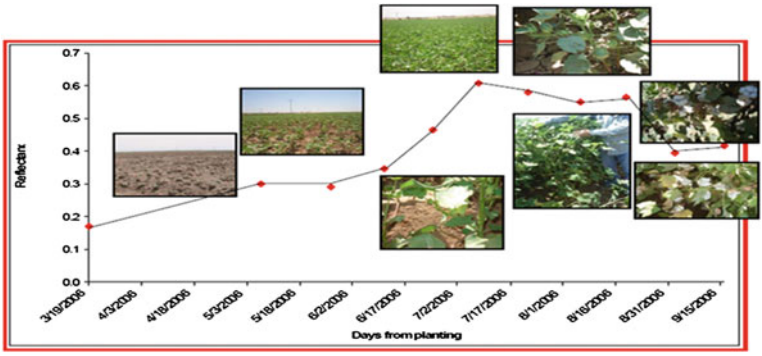

Fig. 5.25 The relationship between the spectral reflectance and the different growth stages of cotton by the third spectral band of ASTER

5.5.1 The Phenological Case of the Different Crops/the Agricultural Calendar

With the use of remote sensing to separate the crops, the spatial dimension of LU were obtained but the problem remained of identifying of the crops spectrally, particularly those whose spectral behavior was similar in the date of access to the

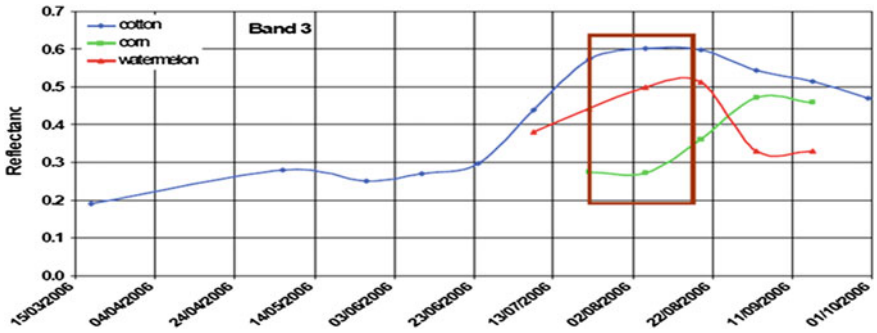

Fig. 5.26 Temporal- and spectral-separability of cotton, corn and watermelon by the third spectral band of ASTER

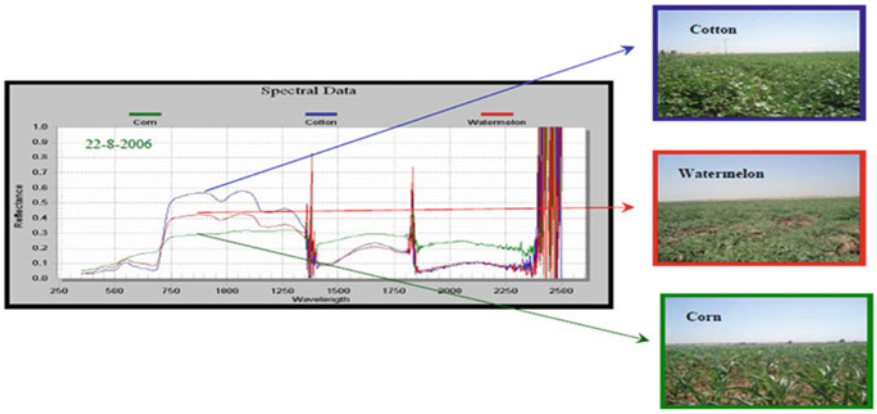

Fig. 5.27 The spectral response of cotton, corn and watermelon during the suggested dates to recognize these summer crops in the spectral range (350–2,500) nanometer

remotely sensed data (e.g., wheat and barley). To overcome this latter problem, good knowledge of the study area was required in terms of types of crops that were cultivated, growth stages, the dates of propagation and harvest (agricultural calendar), and the type of farming prevailing, whether irrigated crops/plantations, rain-fed, or mixed.

"Agricultural crops have rapid changes in spectral characteristics at various times in the growing season. As, at the beginning of May, wheat planted in the ERB presents a green canopy of vegetation to the remote sensor, but by late May, the same wheat will be golden brown and nearing maturity. Two weeks later between mid and late June, the crop will have been harvested and one will see only the highly reflective yellow straw. Sometimes, when there has been no tillage or another crop has been planted, many weeds and green vegetation will be mixed in with the straw, which could be observed as grazed pasture or perhaps hay. So, it is

important to understand the rapid seasonal changes of the crops or other Earth surface features of interest (mainly natural vegetation). To this end, crop calendars can be developed for any particular geographic area. Crop calendars describe the general characteristics of the different crops types as a function of the time of year and the geographic location. They can vary from one year to the next, depending on the various conditions such as extreme weather events of that particular year. Finally, crop calendars should be developed more well in areas of the world where seasonal changes are distinct" (Hoffer 1980).

Crop phenology (regular information on the growth cycle of crops) is important in the monitoring and classification of LU, where it can have a significant effect on the accuracies of crop yield and acreage change. It controls the temporal changes observed from remotely sensed data. The integration of space and time represent crop growth in remote sensing. So, crop phenology contributes to the understanding and monitoring (e.g., spectral measurements) of crop type reorganization and area measurement. Different crops (wheat, barley, cotton, corn, etc.) have a clear and unmistakable spectral response exhibit and period of maximum greenness. This information or phenology can be used in the classification process to accurately discriminate vegetation classes (Hoffer 1980).

Phenological knowledge (beside the spectral measurements) plays a critical role in determining optimal acquisition dates for the selection of the remotely sensed data for agricultural monitoring and classification. As, wheat can be easily recognized from other crops and vegetation because of its greater Greenup, that occurs earlier than for other crops. Crop phenology is generally divided into: "(1) vegetative stage: is largely defined by the part of the growth cycle where the crop develops and grows, starting emergence to tasseling; and (2) reproductive stage: starts at anthesis and ends after maturity. For dry-land crops, several transitions are important in terms of management: emergence, tasseling and initiation of senescence" (Chen et al. 2008).

5.5.2 *The Size of the Agriculture Holdings and Methods of Water Supply/Spatial Considerations/Spatial Aspects of Spectral Response Patterns*

The questions related to spatial characteristics of the used data are: how much is the size area concerned? Is it sufficient to classify only a sample of all the data, or is it necessary to classify the all data for the whole coverage of the study area? What format of results is needed (maps and/or tables)? If the needed format is a map as a final product, then what scale and level of accuracy is needed? What are the spatial characteristics of the agricultural features in comparison to the characteristics of the used remotely sensed data (Hoffer 1980)? And finally, what are the spatial aspects of the spectral response patterns?

Geographic variability of various categories or crop species of interest is another aspect of spatial variability of spectral signatures. I.e., the same crop species does not have the same spectral response in all geographic locations on any one date. As, barley may be harvested in east Syria at the beginning of May when it has reached maturity, but has not yet been harvested in west Syria, and perhaps is still immature and green in southern east Syria. Based on the spectral (signature) concept, it is impossible to define a single spectral response pattern that will be applicable for the same crop species in all geographic areas at any one time. Geographic variability of agricultural crops includes another related aspect, since not all crop species are found in all geographic locations. So, knowledge of the location from which remote sensor data was obtained can prove useful in attempting to identify a particular crop species, even if the spectral response of that crop may not be well known at that time of the year because of lack of ground truth data. As, when data from east Syria is analyzed, it could be concluded that the particular spectral response patterns would be essentially wheat, barley, cotton and corn, and not, as, tobacco, which does not grow in the area to a large extent. Instead, it is planted widely in the west near the Mediterranean Sea.

Three methods of water withdrawal at present dominated for irrigation the agriculture features in the Euphrates Basin: (A) floodplain irrigation (small holdings, not organized geometrically); (B) canal irrigation/farmers (small up to big holdings, semi-organized geometrically); and (C) canal irrigation/state (medium up to very big holdings, full organized geometrically) (Fig. 5.28).

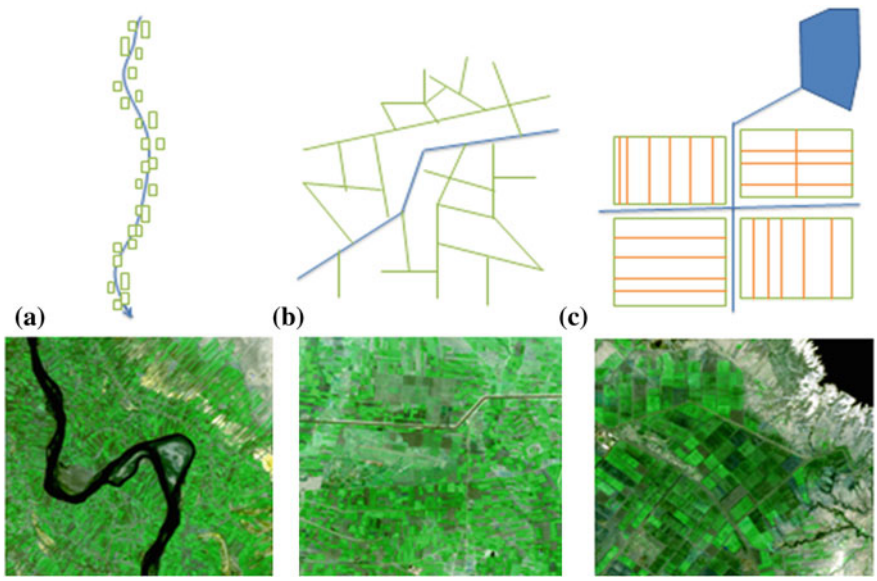

Fig. 5.28 Schematic diagrams of the spatial characteristics of the irrigated agricultural areas in the study area, ERB. *A*, floodplain; *B*, canal irrigation (farmers); and *C*, canal irrigation (state)

5.5.3 The Choice of the most Appropriate Time to Obtain Satellite Images/Temporal Considerations/Spatial Aspects of Spectral Response Patterns

The questions related to temporal characteristics of the used data are: how much of the remotely sensed data has to be obtained at a certain time? What time or times of the year are more suitable (or required) for obtaining these remotely sensed data? Are there particular daytime considerations that have to be involved during the obtaining of data (Hoffer 1980)? and, what are the spatial aspects of the spectral response patterns?

Image acquisition date selection is essential for successful classification of many vegetation covers, especially agricultural crops.

The study of LULC using remotely sensed data faces the problem of the selection of the date in which the image was captured, i.e., the year and the month. This selection is decisive with regard to the information which researchers receive. Most of the irrigation projects discussed in this study were located within the five agriculturally stable zones in Syria, which receive insufficient precipitation to establish a rain-fed agriculture. Therefore, the majority of cultivated areas are irrigated either in winter or in summer. The agricultural cycle of both winter and summer crops ends in May and August, respectively. This means the spectral differences reach their maximum point of clarity at this time, despite different patterns of land use. For remote sensing based studies, the time of year of the image capture is an important factor, because of the density of vegetation, both natural and cultivated. This depends on many factors, notably the amount of precipitation that changes from year to year; and human factors, such as the use of fertilizers, which lead to changes in the characteristics of spectral reflectance/response of a specific crop. For example, the spectral response of fertilized wheat will differ from a field of the same crop which is unfertilized. The use of fertilizers where insufficient water exists will lead to early yellowing of the crops.

World-wide, the best date range for identifying winter wheat is late March through to early May, when the crop is at peak greenness. To identify corn and other summer crops, the best date range is late July to mid-August. The most important and best way to choose a proper time for remotely sensed data is to study the growth stages of each type of vegetation and the spectral change in its behavior during the months of growth, through field work and the use of spectral reflectance measurement devices (Spectrometer) (see Sect. 5.5). As a result of these measurements, the growth periods of a variety of crops and the differences in their spectral reflections can be determined.

The results of the spectrometry readings taken for the purposes of this study are outlined in Sect. 5.5. When comparing the spectral reflectance curves of the studied summer crops (cotton, and corn), it was found that the best spectral region for the separation of crops was the near infrared domain. Under the conditions of the project area, the best period to distinguish these differences was found to be the period between July 20 and August 20. Based on previous results, it was

recommended that the satellite imagery for the study area was brought with the same referred date to use in estimating crop area of summer crops. The best spectral range for the separation of winter crops (wheat, barley and sugar beet) was also found to be the near infrared domain. The best period to distinguish these crops was found to be during the month of May.

"There are more short-term temporal variations in the spectral responses of crops and other ground surface features, such as differences in spectral behavior at different times of the day or night. Differences in the angle of the sun cause variations in atmospheric damping. Sometimes, vegetation that is not under moisture stress early in the morning will show severe symptoms of this later in the day" (Hoffer 1980). "Researchers have also found the problem of temporal definition of a particular cover type of interest, for example, the use of remotely sensed data to classify corn. At what stage of growth do you define a particular agricultural field as being corn?; do you call field (X) a field of corn after it has been planted or after emergence, or when the corn-stems are 15 cm high?; or is it not until the corn covers 25 % of the ground surface?; or indeed 50 %?" (Hoffer 1980).

5.5.4 Choice of the most Appropriate Bands Composite of the Satellite Images

The optimal selection of spectral bands for classification was broadly discussed in a variety of literature (Jensen 2007). There are two general kinds of techniques: (1) graphic analysis (e.g., bar graph spectral plots, two-dimensional feature space plot, and ellipse plots); and (2) statistical methods (e.g., average divergence, transformed divergence, Bhattacharyya distance, Jeffreys–Matusita distance). They were both applied to find an optimal subset of spectral bands (Jensen 2007).

Generally, it may appear that three spectral bands may be more suitable than two, as more information is offered. Also, data that have a broader radiometry field may provide improved results, since some of the problems related to parametric models are avoided, whose support significantly falls outside of the data domain. Yet, by using three spectral bands instead of two with broader data domain instead of the standard one, classification and estimation may in fact be much slower.

"Classification accuracy does not increase linearly, or even increase at all, as the number of spectral bands used is increased" (Hoffer 1980). However, this is not true for the spectral separability of crops or other Earth surface features, which increases steadily as the spectral bands increased.

5.6 Training Samples: Selection, Analysis and Evaluation

The main factor in selecting training sites for supervised classification is that all the variability within classes is representative. Only a few sites will be required in some homogeneous classes, and more sites in classes with high variability.

A general concept offered by Jensen (2007), is that in developing training statistics, it is necessary to select a number of pixels in each class that is at least 10 times greater than the number of bands used during the classification process. This is enough to allow good computations of variance–covariance matrices, which are usually carried out with classification software. Related to size of sample sites, it is noted that "as sites grow larger than 10 pixels, there may be no new information added. So, it would be better to have six sites of 10 pixels in each class rather than one training site of 60 pixels" (Schowengerdt 2007).

To classify the remotely sensed data, the classification algorithm needs to be trained to distinguish one class from another. Representative identical class sites are known as *prototypes*, *exemplars* or *training samples*. After the classifier is trained to statistically analyze to "distinguish" the unlike classes represented by the training sites, the "rules" that were developed during the phase of training are used to label all pixels in the image to their "in real world" classes (Schowengerdt 2007).

A large enough number of training samples and their ability of representativeness are significant for image classifications (Mather 2004). When the biophysical structure of the study area is complex and heterogeneous, selecting enough training samples will be difficult. This problem would be greater if medium or coarse spatial resolution data were used for classification, because a large number of mixed pixels may occur. So, the choice of training samples must consider the three standards: (1) the spatial resolution of the available remote sensing imagery; (2) availability of ground truth data; and (3) the complexity of the biophysical structure (Lu and Weng 2007).

Training samples are usually collected from fieldwork/in situ, fine spatial resolution aerial photographs and satellite images/in-image, recently from Google Earth, etc. Different gathering strategies, such as single pixel, seed and polygon, can be used (Chen and Stow 2002).

Care must be taken to collect representative and non-auto-correlated training samples. The problem in spatial autocorrelation occurring in remote sensing data is that pixels in the image should not be considered as fully discrete features independent of their juxtaposition, but rather a set of continuous features influenced by their neighbors (Campbell 1981). This exists among pixels that are neighboring (e.g., neighboring pixels have a high chance to have alike brightness values), which can cause a decrease in variance between neighboring pixels (Campbell 1981). This decrease in variance can make large masses of neighboring training pixels less representative of a particular LULC-class in the entire image; in contrast, the use of several single-pixel training samples that are situated spatially separately from each other can result in better classifications than large masses (polygons) of neighboring training pixels (Medhavy et al. 1993). Therefore, if such care is taken, classification results for LULC-types (especially for crop recognition, since they have, generally speaking, a relatively small spatial distributions/fields) can be more effective.

Google Earth (http://earth.google.com/) contains ever more wide-ranging coverage of the globe at very high spatial resolution 0.61–4 m, allowing the user to zoom into particular areas to get great detail. Google Earth data were used in this

study for: (1) identification and labeling the broadly general classes (e.g., water surfaces) and some sub-classes (e.g., trees, since they change slowly over the time); (2) help in drawing the out-borders of the irrigated projects; and (3) assistance in assessing the classification accuracy (especially for general classes). Ground-reference data were compiled from ICARDA for the remotely sensed data obtained in the year 1987, from GORS for the remotely sensed data coverage for 2005, and from the two excursions carried out in the years 2007 and 2009. Parts of these ground truth data were used in the generation of training samples and others were used for accuracy assessment at the end of the classification.

Several measures of class separability have been suggested as way to isolate optimal or near-optimal subsets of features for use with classification algorithms. Swain (1978) found three approaches: divergence; Jeffries–Matusita distance; and transformed divergence. The general concept is that the used approach can make a quality measure of the discrimination ratio of a group of spectral features, when achieved over all classes. By comparing between all the achievable combinations of subsets of the spectral features (e.g., which three out of nine available spectral bands), the one that presents the highest quality metric can be used. Only the reduced subset of spectral bands is then used in the overall image classification process. A potential problem is that if one combination of spectral bands creates classes with a large divergence values for some classes and small values for other classes, and a second creates a small divergence values for all classes, which represents a better overall pair-wise selection of features. This suggests that increasing the pair-wise divergence has a decreasing return (Schott 2007). Swain (1978) invented the Jeffries–Matusita distance to overcome this problem, but it had the disadvantage of time-consuming computing. A more commonly used heuristic approach is the transformed divergence that has the mathematical statement:

$$Div_{ij}^{T} = 2\left[1 - e(Div_{ij}/8)\right]$$

"This has the characteristic of exponential saturation of the divergence measure and scales the transformed divergence over the range 0–2″ (Schott 2007). Mausel et al. (1990), in assessing separability measures, used the scaling factor of 2000 rather than 2 that gave larger additions for differences between small divergence values (Schott 2007).

For example, when classifying crops, it is important to train not only the crop classes of interest but also the other classes of no interest such as urban, water, etc. if they occur in the region. Alike, when we focus on a few existing crops (e.g., wheat, barley, etc.), we also have to classify all other crops (e.g., lentil, cumin, etc.) and list them under "other crops", for example. Failure in the training phase generally results in cases of the untrained classes being commissioned. This means that the analyst must spend considerable time and effort in training the classes of no interest.

Training samples selection also depends on many factors which affect classification results and their accuracy. They are, according to Foody et al. (2006): (1)

number of training sites for each category; (2) method of sampling (random or systematic sampling); (3) source of the used data for labeling training sites (ground data, air photographs, etc.); and (4) timing of data collection.

Several authors have proven that good separability values between the LULC-features to be classified will improve classification accuracy, because there is no narrow relation between the average transformed divergence for a feature set and the accuracy reached during classification (Chen et al. 2004). The reason is because the separability measures are usually calculated only from the training sites. So, these measures cannot predict the exact classification accuracy for classified LULC-features in the whole image, if the training sites are not fully representative for all spectral ground surface feature variations in the remotely sensed image, including areas of potential edge effects. In general, a specified value of an obtained separability measure can estimate a certain range of possible classification accuracies for the examined training sites (Landgrebe 2003).

The training sites were chosen in a way to give the broadest possible range that can represent all, or almost all, existing LULC-categories (especially crops) spatially and spectrally. Crop fields with various planted and fallow areas (on light soil, on dark soil, etc.) were visited. The size of the training areas was chosen to be at least 50 × 50 m, since some studies have concluded that this is a suitable size for training sites in semi-arid areas (Olsson 1985). Larger training sites were selected, when it was possible, to reduce the effect of possible technical geometrical noise in satellite data and GPS-data. Homogeneous agricultural fields smaller than about 100 × 100 m were excluded, while they were too small in contrast to LANDSAT-pixels of 30 × 30 m. The training site plots were taken in the centre of the homogeneous area. The GPS-measurements were taken twice in the middle of the field to obtain a mean value and reduce possible noise related to the GPS-type (Fig. 5.29).

The size of samples also has a great importance, together with distribution, for providing representative training sites. Justice et al. (1981) recommended that the using of a model that takes advantage of using the characteristics of the spatial image to define the size of a training site. The suggested model can approximate the size of any sample quadrant as a function of the pixel size and the predicted geometric accuracy of the images.

$L = P(1 + 2\ G)$, Or: $A = P(1 + 2G)^2$; where: (L: length of any side, A: area to be sampled, P: pixel size, and G: geometric accuracy of the image). So, using TM images with 1-pixel geometric accuracy, the size of the training site will be 0.81 hectare, the equivalent to a 3 × 3 pixel kernel area.

Generally, two procedures were used: (1) ground truth data based approach: here, the crops to be classified were defined in addition to some of their attributes (e.g., statistical records, agricultural calendar, etc.). Of key interest were the strategic crops, such as the winter crops of wheat, barley, and sugar beet, and the summer crops of cotton and corn. Random GPS-measurements were then taken at the study area and other historical agricultural information was obtained from local farmers in Aleppo in the Upper-Euphrates and in Deir Azzour in the Lower Euphrates Basin. The training sites were analyzed statistically using the two

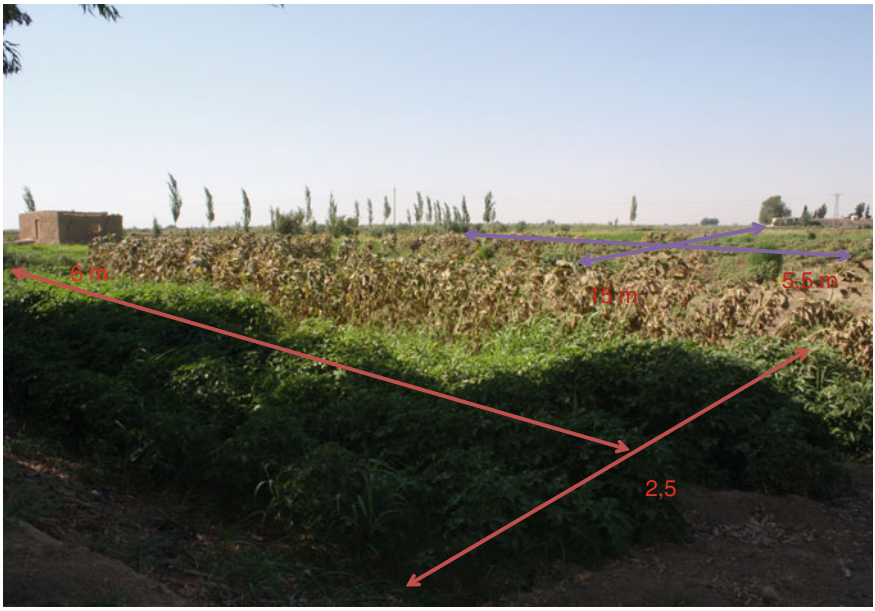

Fig. 5.29 The small and very small crops fields on the Euphrates River banks near Deir Azzour in July 2009

spectral separability measurements (*Jeffries–Matusita* and *Transformed Divergence)* to determine how the used remotely sensed data would be able to distinguish the interested classes (spectrally) on average. According to PCI (2001) and Richards and Jia, (2003), measurements <1,000 = very bad spectral separability; 1,000 < measurements < 1,900 = limited separability; and measurements >1,900 = very good spectral separability. The majority of the training sites satisfied the last consideration; and (2) satellite image based approach: this approach in gathering the training sites was based on visual interpretation, using the background of the interpreter about the study area. This approach was used only for gathering the representative training sites for the five general LULC-classes. It was also possible to select the training samples for the agricultural class (trees, especially Poplar) from Google Earth visually by shadows that appear clearly. This method was used to confirm the measurements/or choice based on the statistical records for the year 1987, (see Sect. 5.10) for the training sites of some crops. Other remotely sensed images were only used visually without processing. For this purpose, if some fields appear black/burned on an image recorded in August for example, this would indicate it was a wheat field. Sugar beet appeared on the July images as green in contrast to wheat, which once harvested, appeared as burned/black, straw/yellow, or tillaged/light- or dark- brown. Table 5.3 gives an overview about the used training samples in the supervised classification.

Table 5.3 Variations, source, and date used training samples in the supervised classification process

Classes	1975	1987	2005	2007
Cultivated and managed areas	Visual interpretation	Visual interpretation	Visual interpretation	Visual interpretation
Trees		Topographic maps	Google Earth	Google Earth
Herbaceous (permanent- and winter-crops/ irrigated):	N.C.	N.C.	N.C.	N.C.
Alfalfa	N.C.	ICARDA-points, statistical records, and detailed schemes	N.C.	N.C.
Vetch	N.C.	ICARDA-points, statistical records, and detailed schemes	N.C.	N.C.
Wheat	N.C.	ICARDA-points, statistical records, and detailed schemes	GORS-points, and visual interpretation for multi-temporal images in this year	Field work, and visual interpretation for multi-temporal images in this year
Barley	N.C.	ICARDA-points, statistical records, and detailed schemes	GORS-points, and visual interpretation for multi-temporal images in this year	Field work, and visual interpretation for multi-temporal images in this year
Sugar beet	N.C.	ICARDA-points, statistical records, and detailed schemes	GORS-points, and visual interpretation for multi-temporal images in this year	Field work, and visual interpretation for multi-temporal images in this year

(continued)

Table 5.3 (continued)

Classes	1975	1987	2005	2007
Other crops	N.C.	ICARDA-points, and visual interpretation	GORS-points, and visual interpretation for multi-temporal images in this year	Field work, and visual interpretation for multi-temporal images in this year
Rain-fed crops	N.C.	Visual interpretation	N.C.	N.C.
Fallow	N.C.	Visual interpretation	Visual interpretation	Visual interpretation
Herbaceous (summer crops/irrigated):	N.C.	N.C.	N.C.	N.C.
Cotton	N.C.	ICARDA-points, statistical records, and detailed schemes	GORS-points, and visual interpretation for multi-temporal images in this year	Field work, and visual interpretation for multi-temporal images in this year
Corn	N.C.	ICARDA-points, statistical records, and detailed schemes	GORS-points, and visual interpretation for multi-temporal images in this year	Field work, and visual interpretation for multi-temporal images in this year
Other crops	N.C.	ICARDA-points, and visual interpretation	GORS-points, and visual interpretation for multi-temporal images in this year	Field work, and visual interpretation for multi-temporal images in this year
Fallow	N.C.	Visual interpretation	Visual interpretation	Visual interpretation
Natural vegetation	Visual interpretation	Visual interpretation	Visual interpretation	Visual interpretation
Artificial surfaces	Visual interpretation	Visual interpretation	Visual interpretation	Visual interpretation
Bare areas	Visual interpretation	Visual interpretation	Visual interpretation	Visual interpretation
Natural water-bodies	Visual interpretation	Visual interpretation	Visual interpretation	Visual interpretation

N.C., not classified

It was impossible to get training samples for the study area based on accurate remotely sensed data for 1975 and partially for 1987, as no remote sensing based research had been carried out in this area. This is one drawback of using the historical data, where one cannot make any field-work and gather ground truth data. But, there is the essential advantage in the provision of initial information about the study area, with which to compare to the present. It was not necessary to obtain ground truth for the remotely sensed data of LANDSAT-MSS-1975, because classification can only be done in the broad general classes in the study area, as they have poor spectral and spatial resolution. Therefore, it was easy to collect the represented training samples and the accuracy data, from the remotely sensed data itself using visual interpretation. The ground truth data for LANDSAT-TM-1987 were found by ICARDA, but were scarce. Attempts were made to increase the potential of these truth data by taking advantage of integrating the remotely sensed data, the historical statistical records and the detailed spatial schemes of the various irrigation projects (see Sect. 5.10).

Twenty GPS points were collected for each class of LULC. These points were collected along the study area in fields with almost 300 × 300 m dimensions to ensure the survival of location points in case technology related errors occurred which would affect the accuracy of the measurements. Photographic images were taken for several GPS-points to provide extra descriptive information about LU, in which reference points exist, such as plants' density, length and phenological cases (when the LULC is agriculture or natural vegetation). As regards to some LULC such as airports, constructions areas, rivers and lakes, it was easy to find reference points using the satellite images themselves, topographic maps or Google Earth. Hence, the majority of reference points represent the more detailed crops types falling under the more general class of cultivated areas.

Spectral signature generation, analyses and evaluation were processed iteratively. As a result, many signature files were produced due to the two classification approaches (One- and Multi-stage classification), and multi-temporal remotely sensed data (over many months and years) used in the study. Some results of spectral separability based on transformed divergence were presented. The presented training sites here were those used mainly in the training study area (see Sect. 5.7), and for which the optimized classification algorithms MLC, NN, SVM were chosen. Tables 5.4, 5.5, Figs. 5.30, 5.31 illustrate the increase of spectral separability in relation to the bands used, and give an illustrated example of how spectral separability was calculated quantitatively.

The resulting training samples for all classes were checked for normal distribution of their digital numbers in the remotely sensed data multispectral bands. Where the training samples' statistical characteristics differed from normal distributions, various classification algorithms and approaches were experimented with to improve the relation of the classes and the characteristics of the study area (geographical, location and its related effects on other sub-characteristics such as climate).

The incapability of actual representation of the studied area regarding the accuracy ratio of automated classification and the ROIs-separability ratio among various classes of interest to be classified, can be put down to several reasons,

Table 5.4 The spectral separability of the training samples related to ASTER-data (3 spectral bands, 15 m)

Pair separation (least to most)	FW	SW	AS	BA	F	NW	NH	TR	TI	WR	WI	BR	BI	PI
Fresh water		2000	2000	2000	2000	2000	2000	2000	2000	2000	2000	2000	2000	2000
Saline water	2000		2000	2000	2000	2000	2000	2000	2000	2000	2000	2000	2000	2000
Artificial surfaces	2000	2000		2000	2000	1999	2000	2000	2000	2000	2000	2000	2000	2000
Bare areas	2000	2000	2000		2000	2000	2000	2000	2000	2000	2000	2000	2000	2000
Fallow	1999	2000	1991	1924		2000	1999	2000	1999	2000	2000	1968	2000	2000
Natural woody	2000	2000	1996	2000	1899		2000	2000	1999	2000	2000	1999	2000	2000
Natural herbaceous	1978	1999	1984	1963	1054	1847		2000	1999	2000	2000	2000	2000	2000
Trees-rainfed	1999	2000	1995	1926	0836	1834	0613		2000	2000	2000	2000	2000	2000
Trees-irrigated	2000	2000	1988	2000	1773	1483	1342	1399		2000	2000	2000	2000	2000
Wheat-rainfed	2000	2000	1989	2000	1992	1828	1524	1894	1675		2000	2000	1999	1998
Wheat-irrigated	2000	2000	1976	2000	1975	1793	1669	1848	1383	0718		2000	1999	1979
Barley-rainfed	2000	2000	1998	2000	2000	1999	1202	1652	1866	1986	1997		2000	2000
Barley-irrigated	2000	2000	1974	2000	1973	1902	1614	1831	1203	1532	1514	1962		2000
Pastoral-irrigated	2000	2000	1994	2000	1999	1969	1753	1977	1967	1000	0878	1999	1957	

Table 5.5 The spectral separability of the training samples related to fused ASTER-data with LANDSAT-ETM+-data (6 spectral bands, 15 m)

Pair separation (least to most)	FW	SW	AS	BA	F	NW	NH	TR	TI	WR	WI	BR	BI	PI
Fresh water		2000	2000	2000	2000	2000	2000	2000	2000	2000	2000	2000	2000	2000
Saline water	2000		2000	2000	2000	2000	2000	2000	2000	2000	2000	2000	2000	2000
Artificial surfaces	2000	2000		2000	2000	2000	2000	2000	2000	2000	2000	2000	2000	2000
Bare areas	2000	2000	2000		2000	2000	2000	2000	2000	2000	2000	2000	2000	2000
Fallow	2000	2000	2000	2000		2000	2000	2000	2000	2000	2000	2000	2000	2000
Natural woody	2000	2000	2000	2000	2000		2000	2000	2000	2000	2000	2000	2000	2000
Natural herbaceous	2000	2000	2000	2000	2000	2000		2000	2000	2000	2000	2000	2000	2000
Trees-rainfed	2000	2000	2000	2000	1934	2000	2000		2000	2000	2000	2000	2000	2000
Trees-irrigated	2000	2000	2000	2000	2000	1997	2000	2000		2000	2000	2000	2000	2000
Wheat-rainfed	2000	2000	2000	2000	2000	2000	1996	2000	2000		1974	2000	2000	2000
Wheat-irrigated	2000	2000	2000	2000	2000	2000	2000	1985	2000	1776		2000	2000	1989
Barley-rainfed	2000	2000	2000	2000	2000	2000	1994	2000	2000	2000	2000		2000	2000
Barley-irrigated	2000	2000	2000	2000	2000	2000	1992	1986	2000	2000	1915	2000		2000
Pastoral-irrigated	2000	2000	2000	2000	2000	2000	2000	2000	2000	1962	1835	2000	2000	

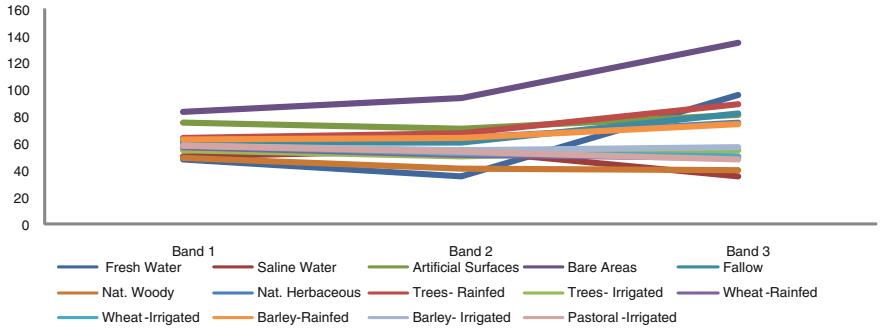

Fig. 5.30 Spectral class signatures (band means) related to ASTER data (3 spectral bands, 15 m)

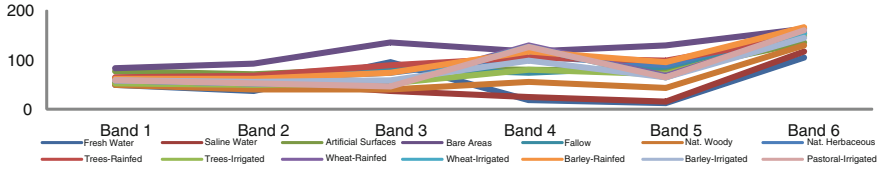

Fig. 5.31 Spectral class signatures (band means) related to fused ASTER data with LANDSAT-ETM+ data (6 spectral bands, 15 m)

including: the interaction among classes of land uses and the natural coverage distribution; and the lack of concrete borders to separate them. There were two factors affecting and complicating this: The geographical location of the study area; and nature and type of classes of LULC, which was affected generally by the geographical location.

Another main reason is that the selection of the training sites is not completely an objective process, affected by the person who selects and trains the sites. When a researcher selects the training samples, they do so because they consider them fit, appropriate and representative to the LULC in the study area. The training process may not include all areas and classes in a study area (especially within the same class); as, there are several kinds of wheat (hard and soft), some are rain-fed and some irrigated, some are located on dark humid soils, while others are on light and less moisture-rich soils, some have organic and chemical fertilizers added, while others grow in different quantities; some wheat-fields may be peppered with natural herbs and plants that grow within the wheat plants, while other fields have homogeneous growth of only wheat plants; and finally, some wheat-fields may be infected with disease. Where these differences are related to one class (i.e., wheat) this will make spectral and spatial bias between wheat and other crops hard. Each difference (or more collected differences) leads to diverse spectral appearances on the image. So, the analyst has to gather training samples that satisfy the entire different spectral responses of the crop especially if there are natural or agricultural crops in the area with a similar spectral response.

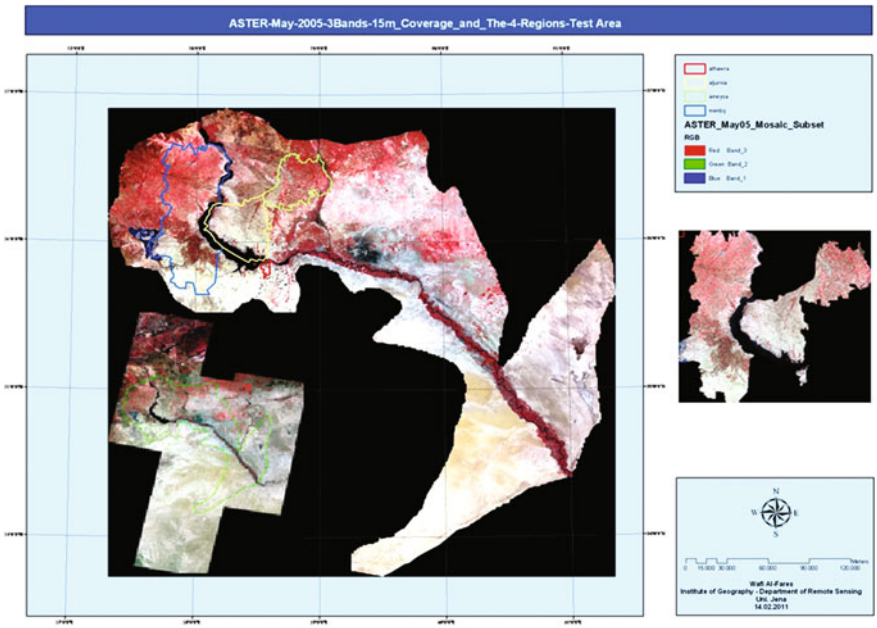

Fig. 5.32 The spatial extent of the four administrative regions (Athawra, Al-Jurnia, Ain Eysa and Menbij)

5.7 The Choice and Evaluation of the Optimized Method of Automated Classification

A comparative study of different remotely sensed data classification algorithms is often conducted to find the optimized classification result for a specific study (Lu and Weng 2007). Many considerations, such as: spatial resolution of the remotely sensed data (how many meters?); spectral resolution (how many bands?); different sources of data (which sensors?); a classification system (which scheme?); and training samples (which statistical distribution?), must be taken into account when selecting a classification algorithm for use. Each algorithm has its merits and deficits. So, the issue of which classification algorithm is more fit for a specific study in a specific area is not easy to answer. And, diverse classification results could be obtained depending on the classifier(s) chosen.

Experiments were conducted on the testing study area to determine the suitable algorithm to use on the entire ERB study area. The supervised classification algorithms tested were: MLC: Maximum Likelihood Classifier, NN: Neural Network, and SVM: Support Vector Machine (Fig. 5.32). Two classification procedures were also applied: (1) one stage classification approach; and (2) multi stage classification approach, to produce land cover maps.

To compare and judge the different classification algorithms results, we have to, as far as possible, exclude the influence of interfering factors. So, while this is a comparative study, a wider choice in the same training samples (size, number, location, etc.) in each studied year and for all remotely sensed data, and for all compared classification algorithms, would be useful. This would not be applicable when using the masking operation used in the multi stage classification approach.

5.7.1 The Test Area

The four administrative areas of Menbij, Ein Eisa, Al-Journia and Athawra were selected as testing areas (sub-study-area) for applying various automated supervised classification approaches and algorithms. These sites were adopted as they contained the majority of natural coverage forms and land uses which exist among the entire ERB area. These areas were also sited within range of the agricultural stabilization zones in the basin and contained a number of irrigated projects. Finally, the sites were distributed in only one scene of the LANDSAT-data, which satisfied the homogeneity in spectral and radiometric characteristics. The result: this testing area was considered as representative to the whole basin area from the perspective of natural and climatic characteristics, distribution of natural coverage and land uses. Therefore, any outcomes resulting from the sub-study-area could be adopted, generalized and applied to the whole Basin.

5.7.1.1 Unsupervised Classification

Methods of unsupervised classification have the ability to define the different classes that could be presented in the study area before the going to the field. Then, the natural objects that are presented in the remotely sensed data can be identified and linked to the resulting spectral classes of classes of interest (crops, land cover classes, etc.) (Hoffer 1980). For this research, the initial thematic map generated from this approach helped to identify the features and provide the feel of the study area, although the images could not be directly used for other analysis without field-work.

The migrating means (or ISODATA, or nearest mean) algorithm (Ball and Hall 1965), is the most commonly used algorithm in unsupervised classification approaches. It frequently executes a complete classification process; recalculates statistics; uses lowest spectral distance method (reducing the value of the function is the average Euclidean distance between each sample point and the matching cluster mean) repeatedly to classify the pixels; and re-specifies the rules of each LULC-class or candidate pixel (iterative processes). Naturally, the calculated minimized value of the average Euclidean distance is equal to creating sphere-shaped clusters with little difference or dispersity. There is no logical technique for creating clusters that minimize the value of the average Euclidean distance. So, the

data will be continuously classified until either a maximum number of iterations have been executed or a maximum percentage of unchanged pixels have been achieved between two iterations (Jensen 2005). The process starts with an identified number of random cluster means or the means of existing signatures, and then it processes iteratively, so that those means move to the means of the clusters in the data. "The ISODATA-classifier filters cluster by splitting (if the cluster standard deviation exceeds a predefined value and the number of pixels is twice the threshold for the minimum number of members) and merging (if either the number of members (pixel) in a cluster is less than a certain threshold or if the centers of two clusters are closer than a certain threshold)" (Jensen 2007). There are various forms of this technique, but in all of them at least two factors have to be defined by the analyst: clusters number; and the iterations maximum number (this ensures the method will stop if convergence is not achieved).

It has some drawbacks. A few of the generated clusters are not important in regard to reality as they represent a mix of unlike LULC-features or "on the ground" classes. It is also not unusual that some spectral classes build one functional class, and it has to be remerged. And, there is a causal bond between the functionality of this algorithm and the ability of the user to identify the number of present spectral classes (Hoffer 1980). Many of the data characteristics that a photo interpreter would use to identify an individual LULC-feature (such as: shape, size, texture, shadow, etc.) are not used in classification of the data that operated based on the computer digitally (Hoffer 1980).

The ISODATA-algorithm has proved useful as an indicator and guide as it provides an idea of the relative stability of each category (McCoy 2005). The individual data are processed using the unsupervised ISODATA-algorithm to generate a large number of class assortments. These so-called *clusters* are then supposed to represent classes in the image and are utilized to compute statistics of the class signatures. It is helpful to define relatively homogeneous features to be used as training sites in the potential supervised classification approach (Schowengerdt 2007), where pixels that always arise jointly in the same cluster are strong and are a very homogeneous category.

It was found that the hybrid-procedure integrating ISODATA-clustering with the supervised classification algorithms such as MLC seemed to be the most satisfactory and effective procedure to follow as it simplified the work and produced better results. This was the case mainly in land areas with wild habitat where the fields were small, or where the LULC-categories and spectral classes were complex (Hoffer 1980). The classification approach is illustrated in Fig. 5.33.

The parameters for the performance of ISODATA-algorithm were given as follows: Number of classes = 25; Maximum iterations = 20; Convergence threshold = 0.98. A thematic raster layer and a signature file (identifiable) were created from the ISODATA-clustering. As, it was found that water bodies, bare areas, artificial surfaces and fallow ground could be clearly identified using the ISODATA-clustering. It gave general information about the spectral mixture between the various LULC-features. Mixtures were between built-up areas and dark color-tones bare areas; dark color-tones bare areas and fallow on dark soils;

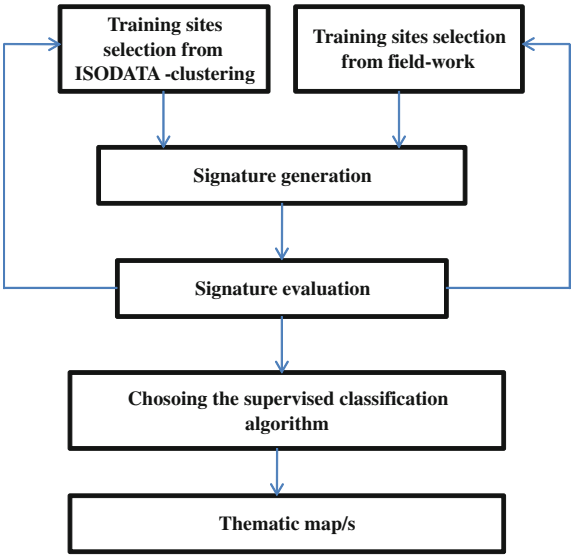

Fig. 5.33 Integrating the ISODATA-clustering with the supervised classification algorithms in a so-called hybrid-procedure

light color-tones bare areas and fallow on light soils; very dense irrigated trees (especially Poplar) and dark water; and between vine and sugar beet.

5.7.1.2 Supervised Classification

The Multi Stage Classification Approach

The decision tree classifier is a hierarchically based classification method which compares data with a variety of well-chosen features. The selection of these features is controlled by an estimation of the spectral distributions or separability of the classes. There is no commonly confirmed formula and each decision tree or set of rules must be constructed by a specialist. If a decision tree presents just two outputs at each stage, then it will be named a *Binary Decision Tree Classifier* (*BDTC*). This procedure was applied in many cases due to its flexible characteristics. In agriculture applications, the rules of a decision tree are acquired via analyzing the specific attributes (understanding the various spectral responses, the agricultural calendar, etc.) of different crop types (Chen et al. 2008). Figures 5.34, 5.35 illustrate the steps applied in the multi stage classification approach to generating the classification results of the four region study area.

Training sites and testing areas are fulfilled separately and compared to satellite images for each classification algorithm after applying the masking-process. This is done because, for example, the mask that represents the distribution of the irrigated agriculture (separation and classification of the irrigated agriculture areas and the rain-fed agriculture areas) using the MLC-algorithm covers areas differing

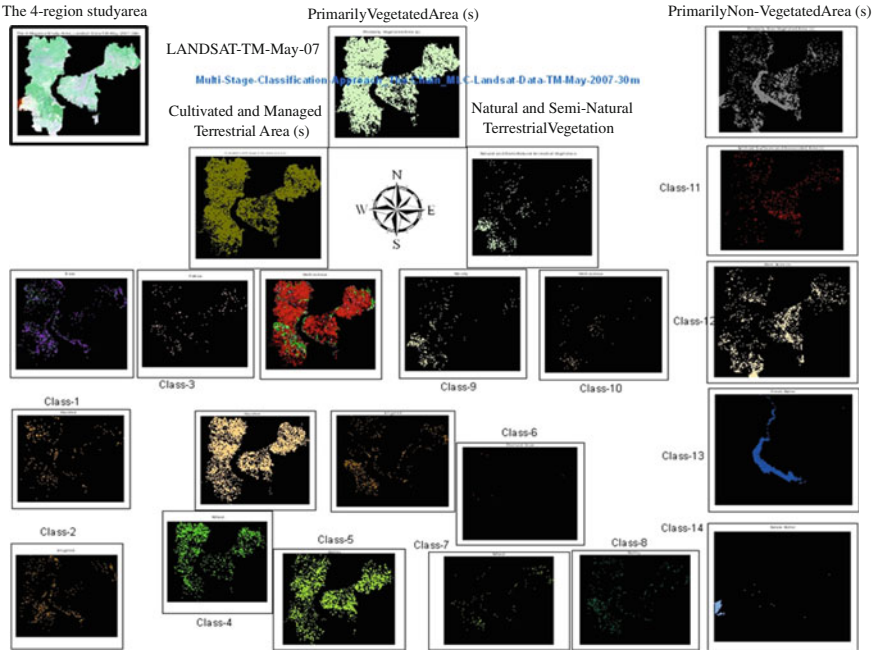

Fig. 5.34 Illustration the application of multi stage classification approach (chain-steps), using MLC-algorithm, on the LANDSAT-TM-data of May 2007 with spatial resolution of 30 m

from those areas covered by the same mask. This results from using the SVM-algorithm in the classification process. After finishing the multi stage hierarchal classification, various classes resulting from each stage are collected and fused in one scene that represents the LULC in the study area using ENVI-program (band-math), or the ArcGIS-software (Fig. 5.36).

Obtaining 100, 90 % or other percentages reflecting accuracy and quality of automated classification, does not necessarily mean that the percentage completely represents LU distribution or the prevalence of LC on real ground. The accuracy percentage of 100 % obtained from the classification of primarily vegetated areas and non-primarily vegetated areas does not mean that the total area contains the same percentage of classification. Of the primarily vegetated areas (e.g., 100,000 ha) perhaps 1,000 ha are primarily non-vegetated areas. This error/s in classification would then be repeated in each step or stage of the multi stage classification approach. This means that the primarily vegetated areas class might appear under classification of the components of the second level (i.e., the second terrestrial and aquatic level underlying under the first primarily non-vegetated areas level) within the used classification scheme (i.e., LCCS), although it should have been classified and separated into the first level. So, the LCCS-principle of classification should be strictly adhered to, that is separation between classes in every level and every stage in classification system. Here the primarily vegetated areas, (for example the 1,000 ha that had been classified incorrectly under the

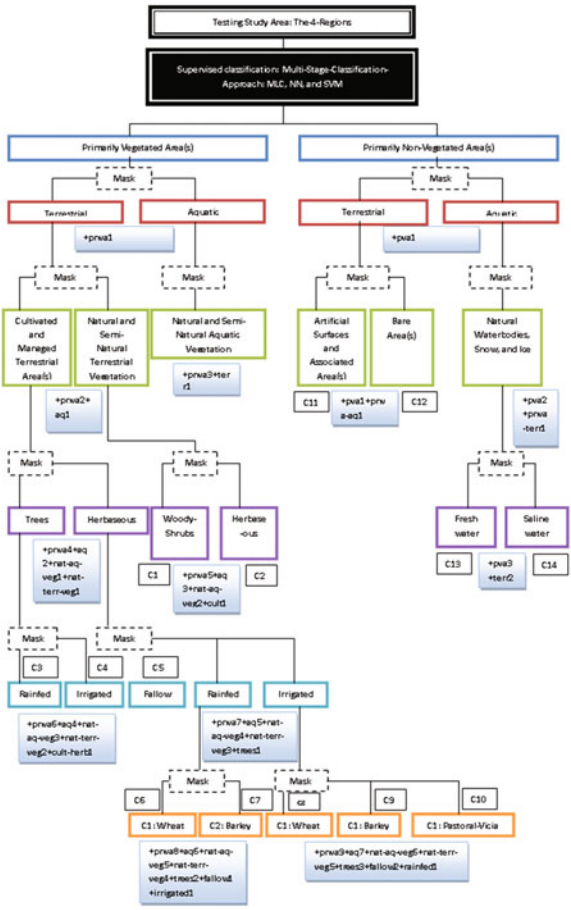

Fig. 5.35 The flow-chart of the applied multi stage classification approach in this study

primarily non-vegetated areas class) will during the automated classification process, be automatically fused with classes within the second general level (i.e., primarily non-vegetated areas), thus creating accumulated error/s in the classification process. Part of the resolution of this problem is to re-classify the wrongly-classified areas when moving to the next stage or level of classification, as long as there are lands representing the wrong classified class within the various levels of the multi stage hierarchical classification approach. When we return to the example of the 1,000 ha, which were classified as non-vegetated areas and consider this at the second level of classification, instead of training sites that represent only the two classes of this level (i.e., terrestrial and aquatic), extra training sites will be selected that represent the 1,000 ha area/s. If this 1,000 ha were completely separated and classified within the second level, it will be appropriate. Otherwise, if a further part of this area, such as 100 ha would appear within the next level, again extra training sites would be trained to represent this class in the classification process.

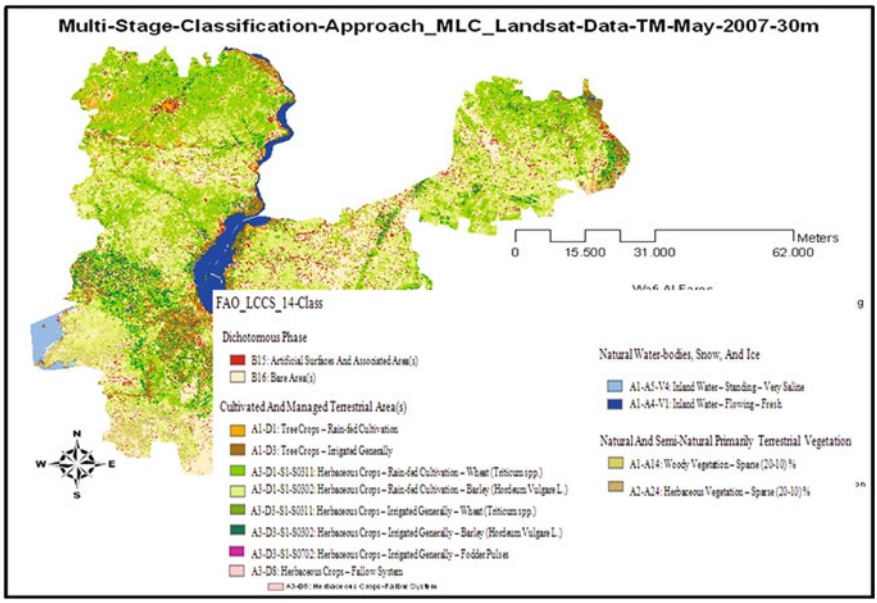

Fig. 5.36 Combine the 14-class illustrated in the previous figure in one thematic map, using ArcGIS-software to sum the individual thematic results, and LCCS-software to prepare the legend

MLC

The *Maximum Likelihood Classifier* (*MLC*) has been employed since the late 1940 s. It found increasing investment in the two fields of: pattern recognition; and remote sensing techniques (Nilsson 1965). It is offered in about all remote sensing and image processing software packages, and it is usually applied as the typical supervised classification approach. It is a widely robust supervised algorithm, and it is the primary approach for most multi-spectral remote sensing interpretations at present (Lillesand et al. 2008). Its general concept defines the maximum likelihood decision rule, which is the probability that a pixel belongs to an individual class. This classifier is derived from the *Bayes-rule* in which classes have equivalent priorities. It uses the training data gathered during field-work or on image itself to calculate the mean vector and variance–covariance matrix for each required class. Both means and variances are then employed to assess the probabilities (Jensen 2005). This algorithm is based on the supposition that the likelihood degree function for each class is multivariate, and often a *Gaussian distribution* is assumed. A pixel is lastly classified to that class, for which it has the highest probability (Lillesand et al. 2008).

MLC operates (see Fig. 5.37) by using the training-samples-based means and standard deviations of individual spectral bands in order to scheme LULC classes as *centroids* in feature space. These *centroids* are circumscribed by likelihood

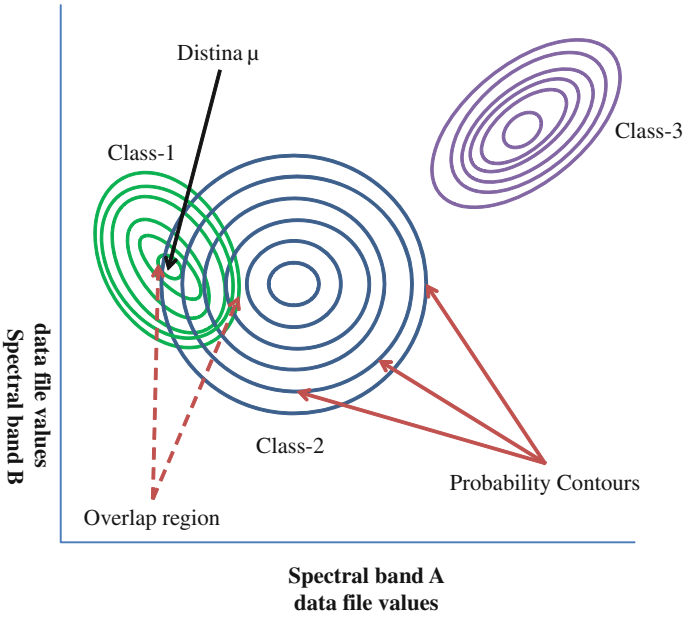

Fig. 5.37 Maximum likelihood classifier (MLC) concept (*Source* modified from ERDAS IMAGINE®, 1999)

curves. The likelihood degree function supposes that the representative sample values for each presented class are normally distributed (Bastin 1997). The so called *Gaussian threshold* can border the class space in feature space, which is the radius (in standard deviation units) of a hyper-ellipsoid around the mean of the class in feature space. Here, observations which do not locate inside the hyper-ellipsoid of any class are allocated to a *null class* (Strahler 1980). The necessary number of training samples needed to calculate the statistics of a class for a Gaussian (quadratic) classifier is in addition linked to the square of features number (Fukunaga 1990). This presents increase in the *Hughes effect*: for a limited number of training samples, the classification accuracy increases in the beginning with the number of features (or difficulty in measurement), but then it attains a maximum and begins to decrease when more features are added. It is generally agreed that the class spectral separability is constantly higher for data with a superior dimensionality, but this superior or higher dimensionality impacts and decreases the accuracy of the statistics estimation when the dimensionality becomes too high, and in some cases, this has the result of producing a lower classification accuracy despite the presented and improved theoretical class separability (Landgrebe 2003). Enough training samples for each spectral class of interest must be presented to offer logical approximations of the elements of the mean vector and the covariance matrix to be determined. For an (N) dimensional multi-spectral space, at least (N + 1) samples are needed, to avoid the covariance matrix being singular.

The strong benefit of the MLC algorithm is its applying for well-developed probability theory. If it is true that the class likelihood degree functions are Gaussian, then MLC is the best classifier which reduces the overall chance of error (Liu et al. 2002). Benediktsson et al. (1990) noticed that even for data which have not got a normal distribution, the MLC produced a better classification result, although it has also serious known faults under specific situations. Firstly, if the histogram/frequency distribution of the image data does not ensure the normal distribution, the essential idea of this classifier is violated and presents poor or confusing results. Secondly, the computational cost needed to classify each pixel (data with a large number of spectral bands, or data containing many spectral classes to be distinguished) is at issue. The computing cost increases in conjunction to the square of the applied features channels (Benediktsson et al. 1990). Thirdly, the algorithm works acceptably for relatively low spatial resolution data with a limited number of bands, but it may not be acceptable for the high resolution and/or high dimensionality data sets, which tend to increase the within-class variability. This means that the volume of feature space occupied by each class is extended and increases the risk of class overlap in feature space (Qiu and Jensen 2004). Fourthly, the relationship between sample size and the number of features impacts the assessments of mean vector and variance–covariance matrix. Also, inadequate ground truth data may present a false assessment of the mean vector and the variance–covariance matrix of population (poor classification results). Fifthly, in case of high correlation between two spectral bands (LANDSAT-data), or when the training samples used for signature generation are not adequately homogeneous, the covariance matrix becomes unstable. This can be overcome through the use of other robust statistical method (e.g., PCA) before proceeding to classification (Albertz 2009). Sixthly, an inherent weakness of MLC is that the subset of features applied in classification is not necessarily to be the optimal selection for all classes (Swain and Hauska 1977). Finally, when auxiliary data is integrated into a classification process, the assumptions of MLC cannot be confirmed.

There have been a number of researchers who have MLC, such as (Brisco and Brown 1995; Huang et al. 2007). MLC can be used with multi-source data with separate scales of measurement (Arora and Mathur 2001), while a parametric MLC, which is commonly used for pixel-based hard classifications, can be used to segment imagery (e.g., Geneletti and Gorte 2003) or expand to a fuzzy classification idea (e.g., Schowengerdt 1996).

ANN

Humans are good pattern recognizers. This tenet has given researchers in the field of pattern recognition the basic concept to examine whether computer systems based on a simplified model of the human mind can simulate the real world, and whether better overall accuracies can be given compared to traditional statistical approaches. The *Artificial Neural Networks* (ANN) algorithm is an example of

these recently advanced methods. It is designed to simulate human learning processes through organization and strengthening of passage ways between input data and output data. Because of the nonparametric structure of the NN-classifiers and while networks are general-purpose calculating tools that can overcome the complex non-linear problems, the use of NNs for classifying remotely sensed data has developed quickly over the past decade Researchers have noted that NNs do better than standard statistical classifiers such as MLC (Tso and Mather 2009). NNs have been increasingly used since the 1990 s (Franklin 1995; Sugumaran 2001) in field of pattern recognition in general, and in the field of remote sensing analysis and classification in particular. It covers: supervised classification (Foody and Arora 1997); and unsupervised classification (Tso 1997). A broad-spectrum introduction to neural networks was given by Bishop (1995), while a very good presentation of applying neural network in classification and its relationship to conventional statistical classification was provided by Schurmann (1996). An overview in the context of remote sensing has been described by Benediktsson et al. (1990), and Kavzoglu (2001).

The user-selected factors affecting the NN-classifier are, according to Kavzoglu (2001): (1) learning factors: the back-propagation learning algorithm needs from the analyst to offer values of the learning rate and momentum; (2) initial weights: these random settings to the pre-trained network affect the network implementation; (3) number of training iterations: this defines the level of generalization as contrasting to specialization of the solution. If a network is trained using very large number of iterations, it might not work well on the test data. Equally, if it is not trained well enough, it will not be able to separate the classes; (4) number of hidden layers and units: this controls the ability of the network to learn and generalize; and (5) number of input patterns: some researchers have suggested that accuracy is influenced by the number of training patterns.

NNs are based poorly on the data distribution assumptions of examples and on the character of the relationship between inputs and outputs (Paola and Schowengerdt 1995). This is an advantage that makes these algorithms smarter than statistical classifiers, mainly in the case when the size of training data is incomplete and sufficient assessment of statistical parameters is hard to achieve (Tso and Mather 2009). Also, different sources of data can be applied as inputs which are then scaled to a general range (typically values between 0 and 1 like the node output values) before training and classification. According to Paola and Schowengerdt (1995), and Qiu and Jensen (2004), ANN-classifiers are strong to noise in the training data and has the ability to generalize. They are error-tolerant and relatively insensitive to background noise. The drawback of neural networks lies in that they work as a "*black box*" (Qiu and Jensen 2004), whilst lacking the ability to give details to further the understanding of the relationship between input and output. Because of their indicative structure and the element of random variations in the results (due to the randomization of the weights of the connection links before training), functioning prediction and the interpretation of results are not easy. Another drawback is that iterative training needs much more computation time than parametric methods (Paola and Schowengerdt 1995; Landgrebe 2003).

However, when the network is trained, the classification process in this way is rapid (Pal and Pal 1993). Despite the high cost of training expenses (Lillesand et al. 2008), neural networks have no stable rules for the network design and their functionality is influenced by some issues (e.g., the network architecture) (Foody and Arora 1997), which is dependent on the analyst.

Classification is improved by using hierarchical NN-classifiers and combining the classification results of multiple classifiers by a compromise rule (Lee and Ersoy 2007). It is established that the use of a collection of neural networks for LULC-classification of multispectral remotely sensed data can give a significant increase in classification accuracy (Canty 2009).

A successful method of classifying remotely sensed data based on different approaches in choosing the networks of ANNs has been referred in many studies (Bagan et al. 2008). E.g., *Multi-Layer Perception MLP* (Benediktsson et al. 1990; Arora and Mathur 2001); *ARTMAP* (Carpenter et al. 1997; Alilat et al. 2006); *radial basis function* (Bruzzone and Fernandez-Prieto 1999); and the *SOM-algorithm with Learning Vector Quantization* (*LVQ*) (Ito and Omatu 1999; Ji 2000). ARTMAP-systems, particularly ART2 and fuzzy-ART, can be practical in executing unsupervised classification on remotely sensed imagery (Tso and Mather 2009). An example of applying fuzzy-ARTMAP was presented by Carpenter et al. (1997), where the results are compared to those created by the MLC, nearest neighbor and multilayer perceptron approaches. It confirms that it is faster and more constant. The same conclusion is also confirmed by Mannan et al. (1998). Liu et al. (2004) presented an ARTMAP-based model called ART Mixture MAP (ART-MMAP) for approximation LULC-fractions within a pixel. Finally, in order to obtain fine results, one might have to try a variety of ART model-based parameters (Tso and Mather 2009). The most common NN-classifier in remote sensing is the MLP (the multi-layered feed-forward network) (Tso and Mather 2009). Excellent reviews about experiments using MLP are presented by Paola and Schowengerdt (1995), Atkinson and Tatnall (1997), and Kanellopoulos and Wilkinson (1997). MLP employs the *"generalized delta rule"*. "At the first stage of training a back-propagation network, the training sample vectors (with known classes/target outputs) are used as input for the network and propagated forward to calculate the output values for each output node. The error between the real and preferred output is calculated. In the case where each output node represents one class, the preferred output is a high value (e.g., 0.9) for the node of the correct class, and a low value (e.g., 0.1) for the other nodes. The second training stage features a backward pass from the output nodes through the network, during which the weights are changed according to the learning rate and the error signal passed backwards to each node" (Benediktsson et al. 1990). This process of inputting the training data (Fig. 5.38), estimating the output error and modifying the weights of the connection links is repeated many times (Foody 2004), until some condition is satisfied, and if possible until the network has stabilized in order that the changes in error and weight per cycle have become very small (iterative training). When the network is trained, i.e. suitable weights are found and, all the pixel vectors are fed into the network and classified.

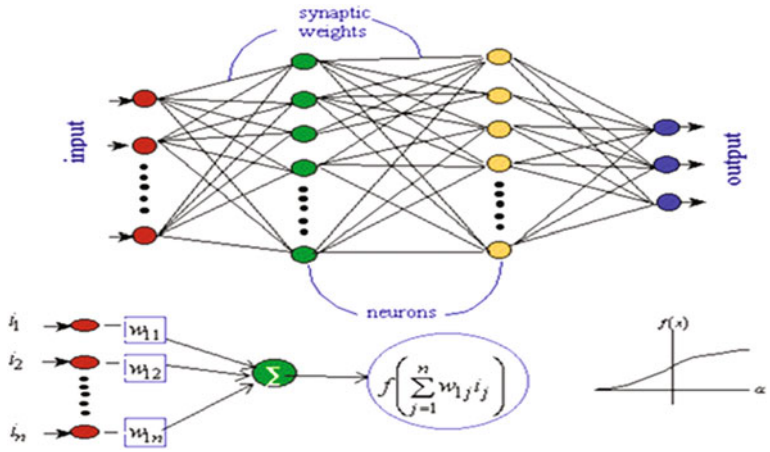

Fig. 5.38 The neural network classification model (*Source* adapted from www.ndt.net/article/v05n07/spanner2/spanner2.htm)

A review and analysis of papers published about ANNs before 1994 can be found in Paola and Schowengerdt (1995). Example applications of ANNs in remote sensing image classification for the period between 1994 and 2007 are given in Schowengerdt (2007).

The produced back-propagation neural network utilizes the "*generalized delta rule*" during the learning stage. The network was trained using the same class training samples which were also used in MLC and SVM. The activation type was Logistic; the training threshold contribution was 0.90; the training rate was set to 0.10; the momentum rate to 0.90; the training RMS-exit-criteria was 0.10; the number of hidden layers was 1; and the training cycle (adjustment of weights after forward and backward propagation of values through the network) was repeated for a maximum of 1,000 iterations, or until the maximum normalized total error was less than 0.01, or the maximum individual error was less than 0.001. The last two situations did not occur, so the training was always performed for 1,000 iterations. ("the individual error is the sum of errors in the output values for one sample, meaning the difference between target value and output value of each output node. The normalized total error is calculated as half the sum of the squares of the individual errors, divided by the number of samples") (PCI 2001). The error plot was then observed to see whether the value for the normalized total error had stabilized before the 1,000th iteration. This was the case for all classifications performed here, although the total error was still between 0.45 and 0.52. In a second step, the training and momentum rates were lowered to 0.05 and 0.20 respectively, for a slower, more stable training with smaller step increases for an enhancement of the network weights (PCI 2001). 1,000 additional iterations were improved with these parameters, resulting in final maximum total errors between 0.39 and 0.46.

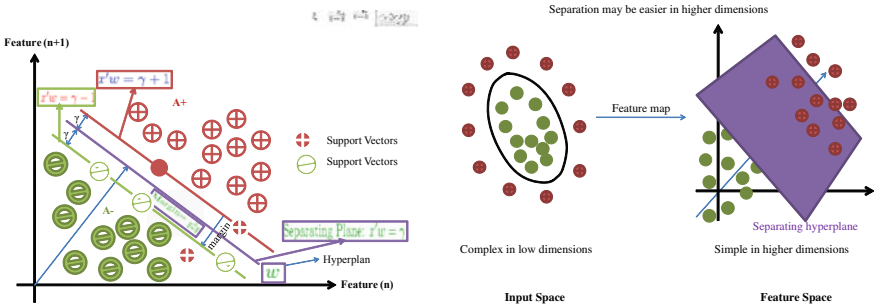

Fig. 5.39 Geometric explanation for the linear classification of SVM (*Source* modified from Vapnik 1998)

SVM

The *Support Vector Machine* (SVM) classification algorithm is based on statistical learning theory as proposed by Vapnik and Chervonenkis (1971). It is discussed in detail by Vapnik (1995) and Schölkopf and Smola (2002). The SVM is a newly developed method to train polynomial, radial basis function, or multilayer perceptron classifiers. Bennet and Campbell (2000) gave a geometric clarification of how the support vector machines functioned (Fig. 5.39). An overview on the application in remote sensing is given by Gualtieri and Cromp (1998), Huang et al. (2002), Melgani and Bruzzone (2004), Pal and Mather (2005, 2006), and Watanachaturaporn et al. (2006).

SVMs were at first presented as a binary classifier (Vapnik 1998). The idea is based on fixing an *Optimal Separating Hyper-plane* (OSH) to the training samples of two classes, so the pixels from each tested class are at last on the right side of the hyper-plane. The optimization problem that has to be removed is based on the minimization of structural risk. Its goal is to maximize the borders between the OSH and the nearest neighboring training samples, the so-called support vectors (Vapnik 1998). So, the model just considers samples nearly from the class boundary and operates well with small training samples, even when high dimensional data sets are used in classification (Pal and Mather 2006). Foody and Mathur (2004b) indicated that a complete description of each class is not necessary for an accurate classification. While only samples close to the hyper-plane are measured, other training data has no influence on the interpretation. However, a larger number of training samples guarantees the employment of sufficient samples (Foody and Mathur 2004b).

In contrast to other classification algorithms (e.g., decision tree), the initial output of a SVM does not have the final class label. The outputs include the distances of each pixel to the OSH-plane (rule images). These rule images can then be utilized to verify the final class membership that is based on the *multiclass strategy*. This principle is furthermore known as "*winner takes all*", where only one value (the maximum) is used for choosing the membership. Contrary to these

two multi-case-methods, other approaches directly identify the SVM as one multiclass problem (Sebald Hsu and Lin 2002). A simultaneous separation of more than two classes presents a more complex optimization problem (Sebald and Bucklew 2001). Thus, such approaches may be less professional in comparison to conventional multiclass approaches. In Melgani and Bruzzone (2004) a computationally promising hierarchical tree-based SVM was presented as an alternative concept.

SVMs work very well with high dimensional data. Their computational cost does not depend on data dimensionality and they need no feature selection. So, classification results for multisource data classification from a non-parametric classifier in particular, is maybe better than that received from a parametric classifier, since a non-parametric classifier can solve some of the problems of a stacked vector approach (Watanachaturaporn et al. 2008). SVM learning generally requires large memory, a great deal of computation time and small training sets (Su 2009). Some of the issues that influence the classification accuracy of SVM-classifiers (Huang et al. 2002) are: choice of kernel used (linear, polynomial, radial basis function, and sigmoid); and choice of the parameters related to a particular kernel (degree of kernel polynomial, bias in kernel function, gamma in kernel function, penalty parameter, pyramid levels, and classification probability threshold).

Recent studies have shown that the use of SVMs in remotely sensed data classification might present results with higher accuracy than other classifiers (Tso and Mather 2009). SVMs have been used for classification of RADAR-data (Shimoni et al. 2009), ASTER-data (Zhu and Blumberg 2002; Marcal et al. 2005), LANDSAT-TM-data (Keuchel et al. 2003) and hyper-spectral-data (Melgani and Bruzzone 2004). Only a few studies are known which have used SVMs for classifying multisource or multi-temporal data (Camps-Valls et al. 2006). Foody and Mathur (2004a, b, 2006) have examined both the characteristics and the size of training samples in SVMs. The paper from Hernandez et al. (2007) confirmed that applying a classification approach based on SVMs such as the SVDD could be used to provide more accuracy (97.5 %) than a MLC (90.0 %). Other significant papers on this topic include: Bruzzone and Marconcini (2009), and Su (2009).

The SVM-options that were used in the study were: Kernel type (polynomial); degree of kernel polynomial (2); bias in kernel function (1,000); gamma in kernel function (0.111); penalty parameter (100,000); pyramid levels (0); and classification probability threshold (0).

5.7.2 Results and Evaluation

This section present the results (thematic maps) of the comparison study which used the remotely sensed data obtained from LANDSAT: MSS-June-1975 with 60 m spatial resolution and four spectral bands (Fig. 5.41); TM-May-2007/30 m and six bands (Fig. 5.42); and TERRA: ASTER-May-2005/15 m and three bands

Land Cover Classification Legend 01.02.2011

List of Land Cover Classifiers Used

#	Classifier	Classifier Label
Dichotomous Phase		
1	A	Primarily Vegetated Area(s)
2	A1	Primarily Vegetated Terrestrial Area(s)
3	A11	Cultivated and Managed Terrestrial Area(s)
4	A12	Natural And Semi-Natural Primarily Terrestrial Vegetation
5	B	Primarily Non-Vegetated Area(s)
6	B1	Primarily Non-Vegetated Terrestrial Area(s)
7	B15	Artificial Surfaces and Associated Area(s)
8	B16	Bare Area(s)
9	B2	Primarily Non-Vegetated Aquatic or Regularly Flooded Area(s)
10	B28	Natural Waterbodies, Snow and Ice
Cultivated and Managed Terrestrial Area(s)		
11	A1	Tree Crops
12	A3	Herbaceous Crops
13	D1	Rainfed Cultivation
14	D3	Irrigated (General)
15	D8	Fallow System
16	S0302	Barley (Hordeum vulgare L.)
17	S0311	Wheat (Triticum spp.)
18	S0702	Fodder pulses
19	S1	Food Crops
Natural And Semi-Natural Primarily Terrestrial Vegetation		
20	A1	Woody Vegetation (Main Layer)
21	A14	Sparse (20-10) - 1% (Main Layer)
22	A2	Herbaceous Vegetation (Main Layer)
Natural Waterbodies, Snow and Ice		
23	A1	Inland Water
24	A4	(Flowing)
25	A5	(Standing)
26	V1	Fresh
27	V4	Very Saline

Fig. 5.40 LULC-classes that generated from the LCCS-software (version-2) for the four regions study area

(Fig. 5.43) fused with additional three spectral bands of LANDSAT: ETM+/SLC-Off-corrected/-May-2005/15 m (Fig. 5.44). Two supervised classification approaches (Multi Stage Classification Approach and One Stage Classification Approach) were adopted, using the three supervised classification algorithms MLC, ANN and SVM. This comparison study was carried out for the selected sub-study-area of the four administrative regions. The LULC-classes generated in relation to the selected testing area based on the LCCS-classification scheme, are described in Fig. 5.40.

An evaluation of the presented results was performed to define and confirm which classification approach and/or classification algorithm was optimized for the sub-study area and for the greater study area of the ERB. Two methods were used in the evaluation. The first (Fig. 5.45) was qualitative rather than quantitative, more manual, and used non-remotely sensed data (human-based data) as truth-reference for measurement of the accuracy of the produced thematic maps results.

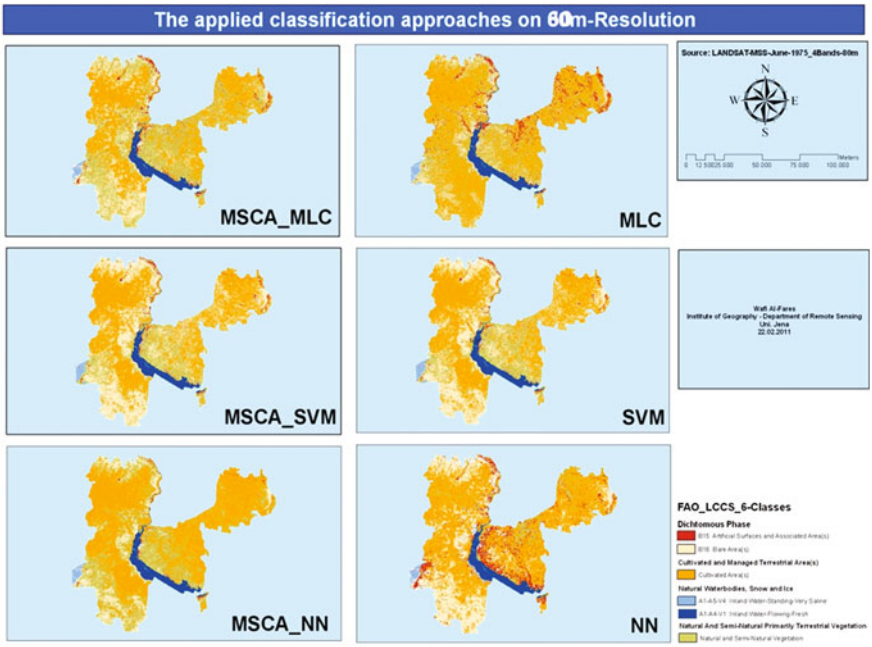

Fig. 5.41 The produced thematic maps from LANDSAT-MSS-data using various supervised classification approaches and algorithms for the testing area

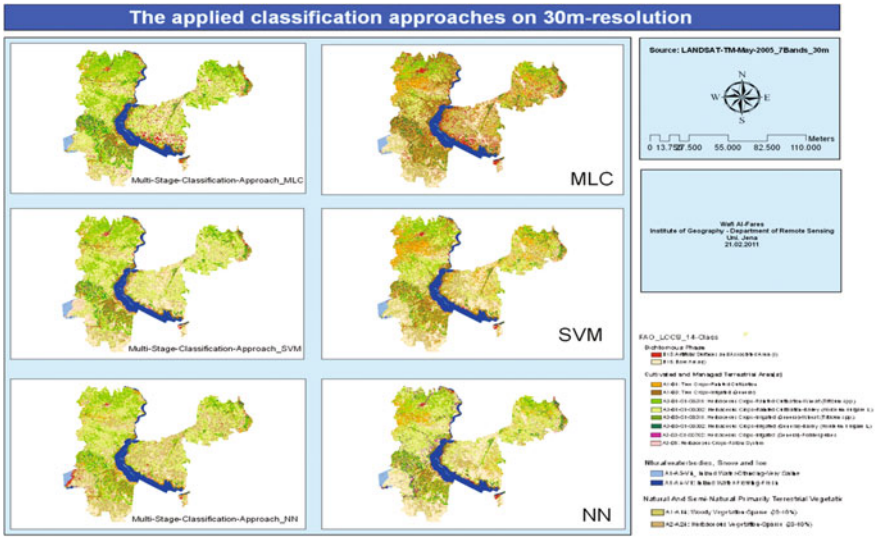

Fig. 5.42 The produced thematic maps from LANDSAT-TM-data using various supervised classification approaches and algorithms for the testing area

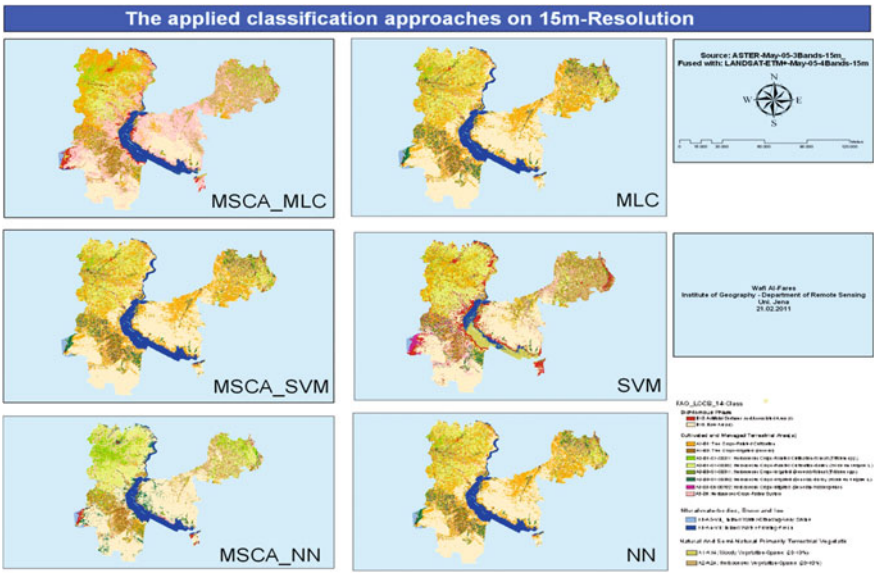

Fig. 5.43 The produced thematic maps from ASTER-data and LANDSAT-ETM+-data using various supervised classification approaches and algorithms for the testing area

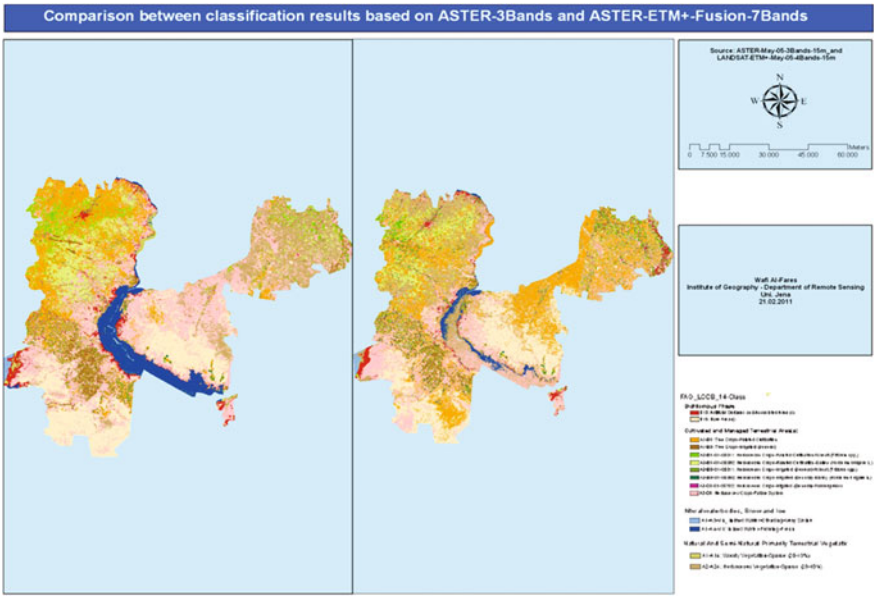

Fig. 5.44 The produced thematic map from ASTER-data with only the first three spectral bands (*right*), and the resulted map after fusing the previous three bands with the 4, 5, and 7 spectral bands of LANDSAT-ETM+-data (*left*) using various supervised classification approaches (here, one stage classification approach) and algorithms (here, MLC) for the testing area

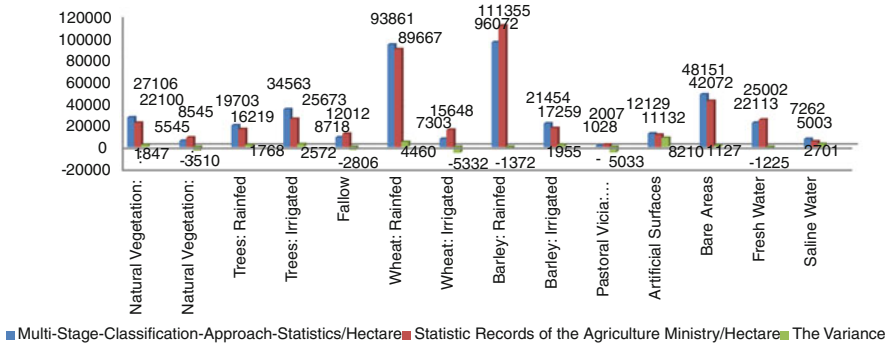

Fig. 5.45 The comparison between the areas of various LULC-classes that generated from the supervised classification of remotely sensed data with the statistical records in the Menbij Region in 2007

The second method (Table 5.6, Fig. 5.46) is quantitative, more automated, and used either non-remotely sensed data (e.g., GPS-measurements) or remotely sensed data as truth-reference/s, based on suitable founded mathematical equations (see Sect. 5.13).

This evaluation showed that: (1) the accuracy values range from 49.56 to 99.02 %; (2) after comparison of each of the three used algorithms (MLC, NN, and SVM) with the three different spatial resolutions of remotely sensed data (ASTER-15 m, LANDSAT-TM-30 m, and LANDSAT-MSS-60 m) and various spectral resolution (ASTER-3-bands, TM-6-bands, and MSS-4-bands), for the 12 individual classification levels, it can be concluded that the MLC-algorithm had the highest accuracies in general, followed by SVM and finally, NN. Generally, the accuracy decreased horizontally with the reduction of the spatial resolution at almost each classification level, with the exception of ASTER-data at the more detailed levels. Although these data had the best spatial resolution, there was no corresponding increase in accuracy. Therefore, the higher spectral resolution by LANDSAT-data with coarser spatial resolution was more important than the higher spatial resolution by ASTER-data with coarser spectral resolution. In addition, accuracy decreased vertically with the increase in the information extracted at individual level; (3) after comparison of the final overall accuracy of classification using the multi stage classification approach and the MLC, NN and SVM algorithms (with accuracy values resulting from using one classification approach and the same three algorithms), it was evident that the first approach always showed a higher accuracy among the three classification algorithms. Also here, MLC harvested the higher accuracy in both approaches. The higher accuracy was found by using LANDSAT-MSS-data, while the offered classified classes were too little and wide than those generated from other used remote sensing data; and (4) therefore, the optimized results for the used remote sensing data, the classification approach and classification algorithm were found to be LANDSAT-TM-data (ASTER-data had insufficient spectral resolution, while LANDSAT-

Table 5.6 The final resulted overall accuracy values of applying various classification approaches and algorithms on various remotely sensed data

	MLC ASTER-15 m-May-05	MLC Landsat-TM-30 m-May-07	MLC Landsat-MSS-60 m-June-75	NN ASTER-15 m-May-05	NN Landsat-TM-30 m-May-07	NN Landsat-MSS-60 m-June-75	SVM ASTER-15 m-May-05	SVM Landsat-TM-30 m-May-07	SVM Landsat-MSS-60 m-June-75	Average/level-based
A/B	99.02	98.73	92.85	98.58	97.73	91.25	98.92	97.41	93.52	96.44
A1/A2	97.69	96.31	88.54	96.56	95.58	85.59	96.92	95.89	86.55	93.29
A11/A12	95.56	94.08	80.21	92.56	90.98	79.55	90.69	87.36	77.56	87.61
A111/A112	80.56	90.31	–	80.00	90.17	–	81.57	89.41	–	85.33
A1111/A1112	78.21	89.81	–	76.54	88.44	–	77.66	89.96	–	83.37
A1121/A1122	57.21	60.88	–	56.58	60.52	–	58.58	61.68	–	59.18
A11211/A11212/A11213	58.25	65.22	–	59.85	65.13	–	56.55	66.36	–	61.92
A11221/A11222/A11223	65.54	75.02	–	64.59	72.12	–	66.99	75.36	–	69.93
A121/A122	50.59	57.32	–	49.56	50.36	–	54.55	55.52	–	52.98
B/A	99.02	98.73	92.85	98.58	98.73	91.25	98.92	99.41	93.52	96.77
B1/B2	96.69	95.32	89.54	95.56	94.58	85.96	95.92	95.62	87.55	92.92
B11/B12/B211/B212	92.69	95.72	90.51	90.31	94.45	88.24	91.54	96.86	92.28	92.45
										73.27
Average/algorithm-based/multi stage classification approach	80.91	84.81	89.08	79.96	83.21	86.97	76.18	84.17	88.49	83.75
One stage classification approach	77.32	83.23	88.14	73.25	82.59	84.87	70.24	83.15	86.59	81.04

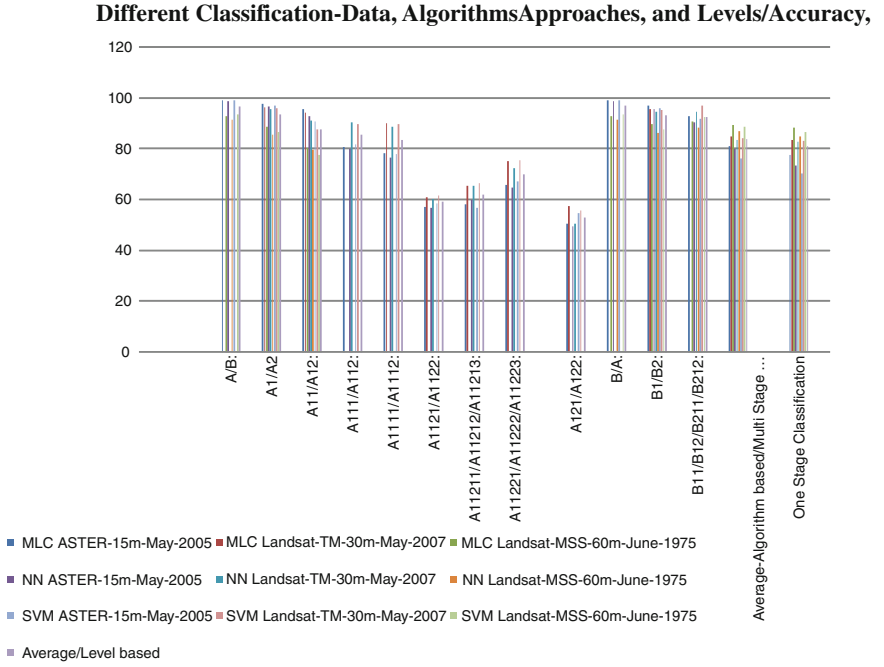

Fig. 5.46 Illustrate the accuracy assessment values presented in Table 5.6 visually

MSS-data had insufficient spatial resolution), the multi stage classification approach and the MLC-classification algorithm.

5.8 General Classes Classification

Drought is one of the main characteristics of large areas of the ERB, since variation in lands and natural coverage is partially measured by average precipitation. Geological and geomorphologic characteristics and soil types change depending on the availability of water or the climatic risks affecting the area. One of the more satisfying results of setting general classification controls representing the natural coverage and land uses of basin areas falling outside the borders of water agrarian projects, is the appearance of planted lands with trees in bare, uncultivated lands as shown in satellite images, particularly, in relatively dry areas with dominated light color soils. This may occur because of the ratio between dimensions of pixel in TM-30 m data, and the distance between planted trees within one field. In the region of Aleppo, pertaining to the widely spread Aleppo-pistachio and olive trees, the distance between every two trees is estimated with 8–10 m (Fig. 5.47), i.e., there will be an approximately 16 trees in each pixel of the TM-data. Because the

Fig. 5.47 The distances between the rain-fed olive trees in the study area (photo)

greater portion of this plantation lies on light soil, and since remotely sensed data are insufficient and unqualified in spatial resolution, it is difficult to detect the distribution of these plantations. It is also complex to represent them through automated classification.

However, where there is water availability (prevalence of irrigation projects), all types of cultivations and even gardens appear clearly on the satellite images used in current study. Time differentiation of termination of the agricultural crop rotation of rain-fed crops existed away from irrigation projects, compared to their counterparts included in irrigation projects. Consequently, it was necessary to have satellite image coverage to be compatible with the precise dates of the agrarian crop rotation of rain-fed crops in April.

The satellite images did not allow discrimination between barley and wheat fields, which were similar in relation to their spatial discrimination (the field areas of each crop) and spectral discrimination (there were no clear differences in spectral reflectance). These two major and strategic crops were planted widely in rain-fed areas based outside the borders of irrigation projects. Yet, the situation was different within the irrigation projects, as barley occupied few of the limited irrigated areas, but was commonly planted. This led to change in the agrarian crop rotation and its spectral behaviour, differentiating it from rain-fed wheat. This in turn led to the possibility of spectral separation between irrigated wheat and barley at the beginning of May, regarding the radiometric field measurements that proved the possibility of separation (see Sect. 5.5.1).

The study area was divided into two almost equal sectors corresponding in the western part with the second, third and fourth agricultural stabilization zones. The eastern part matched the fifth agricultural stabilization zone, which included the pasture Al-Badiaand the Syrian Desert. Each of these two general sectors corresponded with distinct areas concerning land use and natural coverage. Applied agrarian legislation was a factor, especially the total prevention of cultivation in the fifth agricultural stabilization zone. These two sectors were almost homogeneous in relation to spectral reflectance on this scale.

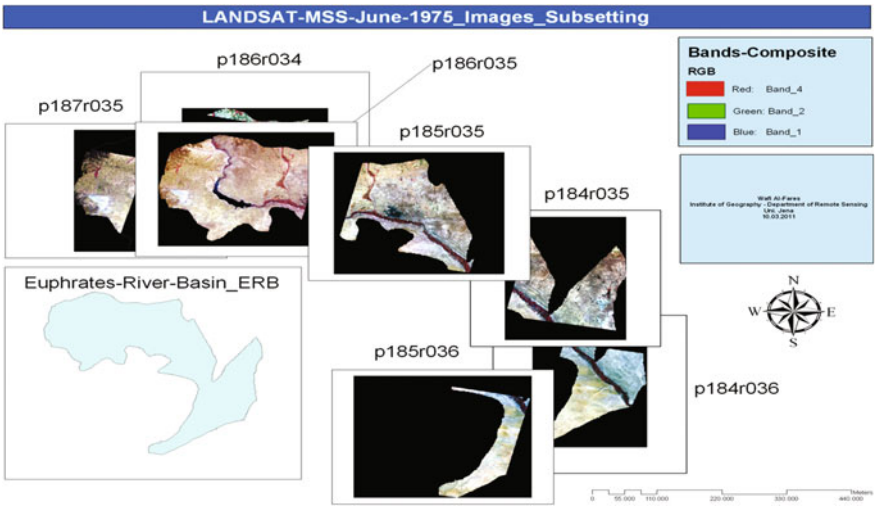

Fig. 5.48 LANDSAT-MSS-June-1975 imagery subsetting based on the spatial extent of the ERB in Syria

The general extracted and classified LULC-classes based on LCCS-scheme (see Sect. 5.3) were: Cultivated and managed terrestrial area(s); Natural and semi-natural terrestrial vegetation; Artificial surfaces and associated area(s); Bare area(s); and Natural water-bodies, snow, and ice.

The three period LANDSAT-imageries (MSS-June-1975, TM-May-1987 and TM-May-2007) and the one period ASTER-imagery (ASTER-May-2005 fused with the LANDSAT-ETM+/SLC-Off corrected/-May-2005-data) (see Chap. 4.1) were classified using the supervised classification technique MLC to generate the general LULC-classes of the first LCCS-classification scheme.

The concept used to produce the thematic maps of the general classes was divided into two ways: preprocessing steps and the mosaic-process (see Sect. 5.2). The classification process was carried out for all defined classes on the one mosaic-image that covered the whole spatial distribution of the study area. This mosaic-image was generated from more than one remote sensing image, in which the temporal, spatial, spectral and radio-metrical characteristics of each image were deemed to be compatible with each other, or when it was possible to enhance and/or correct the distortion in these characteristics. The second method was performed when it was impossible to generate a correct and suitable mosaic-image with no, or an acceptable level of, distortion in the above referred characteristics, or when it was possible to generate a more suitable mosaic-image which gave more accuracy in classification. For example, the second method was performed on the LANDSAT-MSS-June-1975 data, where subsetting of each of the seven images using the ERB-borders-vector-file extracted from the SRTM-data was conducted (see Sect. 5.1) (Fig. 5.48). The classification procedures were performed for each subsetted image after which mosaicing was carried out on all the individual

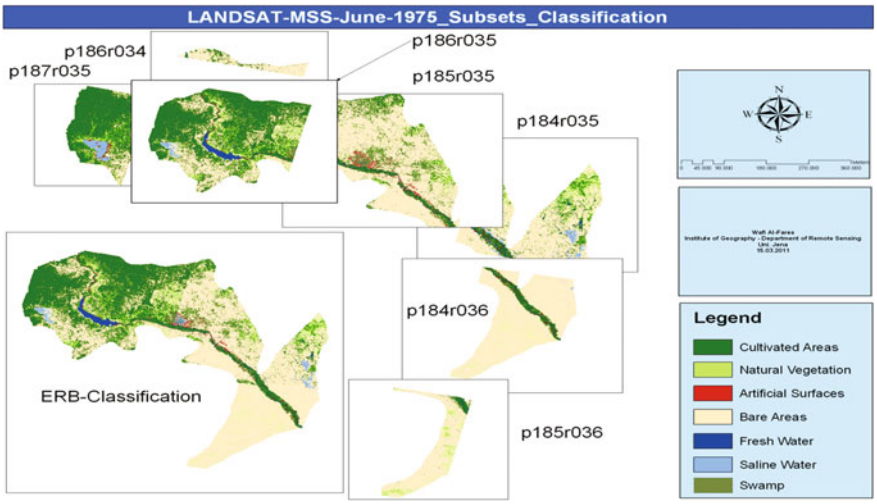

Fig. 5.49 LANDSAT-MSS-data-June-1975 classification results for each subsetted image and the mosaicing of all results in one thematic map

classification results to produce one final thematic map (Fig. 5.49). The procedures that were performed in the classification were: (1) Creation of the legend including the LULC-classes to be classified based on LCCS-scheme (see Sect. 5.3); (2) Selection of the training samples visually from the MSS-data itself; (3) Calculation of the separability values for the selected training samples (see Sect. 5.6); (4) Application of the MLC-algorithm that offered the best accuracies (see Sect. 5.7.2); and (5) Validation of the classification accuracy using the accuracy assessment methods (see Sect. 5.13).

5.9 Irrigated Areas Mapping

As shown in the information obtained from the Syrian Irrigation Ministry, the total reclaimed lands in the Euphrates River Basin in the period 1970–2007 comprised some 201,372 ha, distributed in the governorates of Aleppo(72,492 ha), Arraqqa (102,512 ha) and Deir Azzour (26,367 ha). However, the variation in the radiometric characteristics over the various imagery that were used to construct the final mosaic-images and the variation in the spectral, spatial and radiometric characteristics over the various multi-sensor datasets, added their own uncertainties to irrigated area estimates.

This section describes the methodology used to locate irrigated areas within the national administrative units in the Euphrates River Basin. Irrigation maps were derived from remotely sensed data (LANDSAT-MSS-June-1975, LANDSAT-TM-May-1987 and 2007, and TERRA-ASTER-May-2005), and from the very detailed

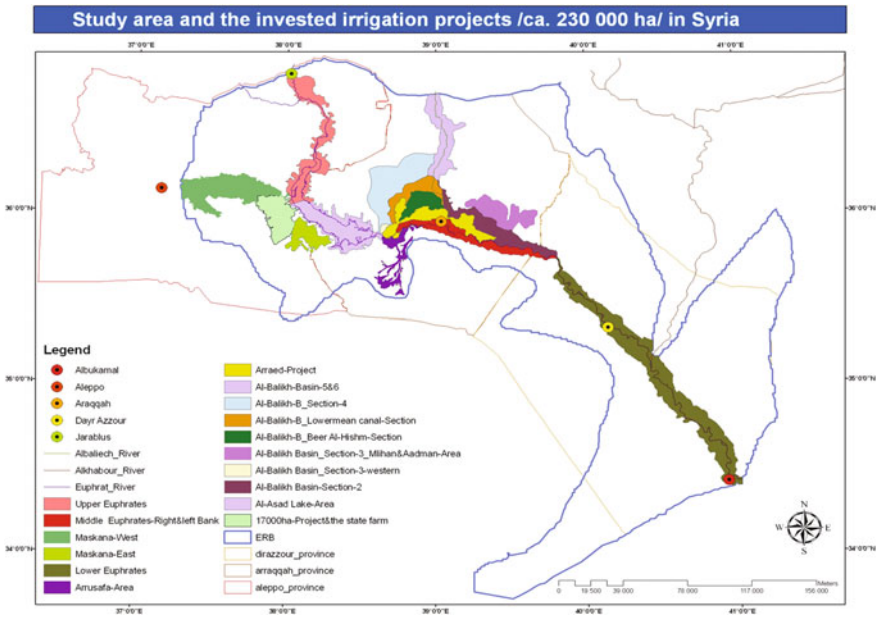

Fig. 5.50 The spatial distribution of the 16-projects in ERB (about 230,000 ha) that generated from the detailed irrigation projects-schemes and the remotely sensed data (as vector-file)

schemes of each irrigation project that were obtained from the Syrian Ministry of Irrigation and IGDEP. These schemes represent clearly each project's formative spatial distribution, but with no geographical reference. These schemes were linked with the remotely sensed data available using a hard visual interpretation. The information was also digitized to locate the detailed schemes on the various existed remote sensing data in order to extract the boundaries of the irrigation projects. After the maps were on-screen digitized, the borders of the irrigated areas were evaluated using satellite imagery in many areas. The both shape and size of the digitized areas were followed by an adjusting process where necessary. Finally, it was helpful to use publications such as project reports and the frequently published statistics about the development in the irrigation areas and the agricultural plan over the time.

In general, the following steps were adopted: (1) generation of a vector-file that defined the spatial distribution of the ERB-borders; (2) the register of national irrigation statistics for the ERB in Syria; (3) geospatial information (detailed schemes and various remotely sensed data) used to locate irrigated project areas within the ERB; (4) the production of a detailed vector-based digital map of irrigated project areas in the ERB (Fig. 5.50), to be used as a spatial indicator in combination with the remote sensing data during the agricultural classification within these projects; and (5) fusion of the digital maps of the irrigated areas in the ERB for the years 1975, 1987, 2005 and 2007.

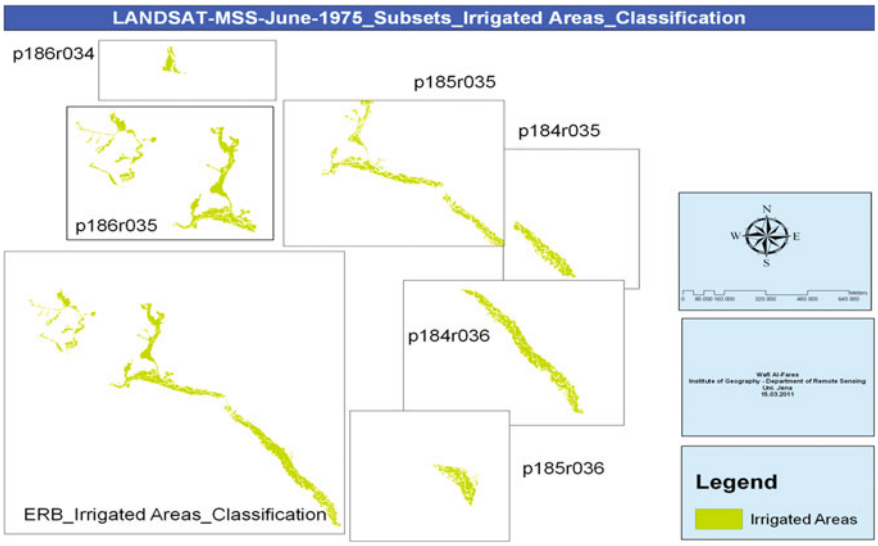

Fig. 5.51 Irrigation mapping in the ERB based on the traditional supervised classification approach (the first method)

Three methods in mapping the irrigated areas were followed. The first (Fig. 5.51) was based on the previous general classes classification results (see Sect. 5.8), where the class (cultivated areas) represented the irrigated areas, which were actually the agricultural areas (planted and fallow). Then, the irrigated areas vector-file was used to subset and extracts the actual irrigated agriculture within the projects from the ERB-borders. Here, the classification accuracy was equal to the gaining general classes accuracy, which was generally high for wide categories classification. The second method combined the transformed NDVI-values to vector-file (as mask). The drawback here was that NDVI can only detect the planted areas and not the fallow-fields. To overcome this problem, the two major agricultural seasons of winter and summer needed to be classified, where, as, the non-planted fields during winter would be almost completed planted in summer, especially in areas with an abundance of water. Then, the two winter and summer classification results were added into one thematic map that represented the actual irrigated areas over an individual year. The third method involved the analysis of each of the 16-projects alone. This was more major for crop classification within the irrigated areas, mainly when scarce truth-references existed. To this end, the use of statistical information was helpful. This method is presented in the next section.

The next task was to define the spatial distribution areas of irrigated agricultural projects within the natural borders of the ERB in the study's reference time period of 1975, 1987, 2005 and 2007 by calculating the values of NDVI and making a mask that covered the spatial prevalence of the projects' areas. This mask was the

study area for classification of the irrigated winter and summer crops during the previously mentioned time durations except for in 1975. The remotely sensed data (LANDSAT-MSS) available in that year had a low spatial resolution of 60 m, and for this reason, it was impossible to produce detailed maps of land uses, specifically in those areas included under wide classes (e.g., both wheat and barley are detailed classes that lie under the heading "wide general class", namely, the agrarian lands).

The total cultivated area of the Arraed project was c. 21,000 ha. However, due to bad land reclamation procedures, salinization had resulted in large areas of the project lands. In 2005, the arable land mass was only 2,433 ha.

5.10 Crops Classification

Classification of agricultural crops using remote sensing data requires in general, knowledge about crop phenology, climate of the exacting growing season and ground reference information about specific agricultural practices in the drainage basin. "The development of a regional-scale crop mapping methodology is challenging because it requires remotely sensed data that have large geographic coverage, high temporal resolution, adequate spatial resolution relative to the typical field size, and minimal cost". Remotely sensed data from customary sources such as the LANDSAT (TM and ETM+) and (AVHRR) proved the usefulness for the classification of LULC-features. Supervised classification is the most frequently used classification method in agricultural areas (Van Niel and McVicar 2000).

MSS data are used to set maps concerning the expansion of the agricultural lands and to distinguish them from constructional lands, for example. However, one drawback is that these data are unable to set thematic maps which view the more detailed crops' expansion. Of course, there are always exceptions; for instance, the agricultural cultivated fields planted with different crops are to some extent considered wide spaces, which enables the MSS-data to distinguish them. Yet, this condition was not verified in the ERB, which was characterized by having small agricultural fields, especially those located outside of the borders of the governmental irrigated agrarian projects. These areas were also organized following the agricultural crop rotation policy.

In the third part of this study, carefully timed remotely sensed data were used to map the location and extent of irrigated winter and summer crops for the years 1987, 2005 and 2007.

The commonly implemented crop classification approaches included: unsupervised classification; supervised classification; and decision tree classifier. In the cases where there was less information for a study area, only the characteristics of the image (also, statistical records and the detailed schemes, especially for 1987) were used.

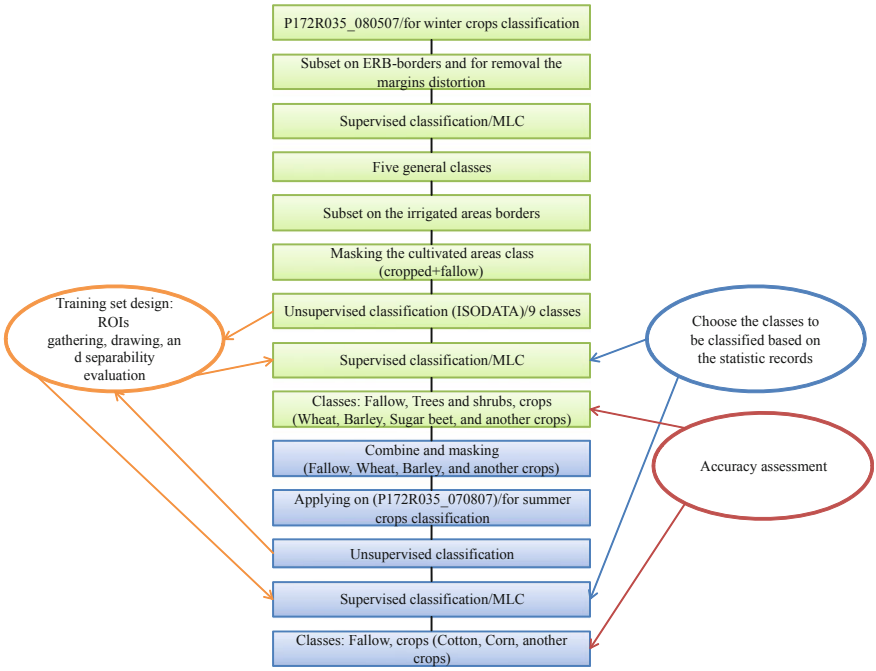

Fig. 5.52 The general concept-steps adapted to classify the various agricultural classes, especially the major strategic winter and summer crops

The adopted concept (Fig. 5.52) in agriculture classification was based on the results of the previous two sections (Sects. 5.8 and 5.9). The first step was to define the classes to be classified, based on the statistical records for the study year/s with no/or insufficient truth-data (e.g., 1987-data). This was followed by selection of the winter related data (Fig. 5.53), and subsetting to remove margin distortions, and to extract only the ERB spatial related areas. The time series of remotely sensed data were first used to generate a LULC-map of the whole ERB-area based on the LCCS-scheme (see Sect. 5.8). This process involved the use of one mosaic-image or each individual image, which was then mosaicked into one thematic-mosaic-map. The classification method was based on a MLC algorithm. The resulting classification had five general classes. The important general class which was used as the basis in irrigated agriculture classification was: cultivated areas: cropped and fallow. Using the derived vector-file which located the detailed spatial distribution of each project, sub-setting was conducted and the cultivated areas which existed only within the irrigation-projects and not within the whole ERB were extracted. Finally, using the unsupervised approach as an indicator for additional information about the spectral characteristics of the area, training samples were collected for some general classes (e.g., water), followed with the tested MLC approach (see Sect. 5.7) to generate the final thematic map of the major winter

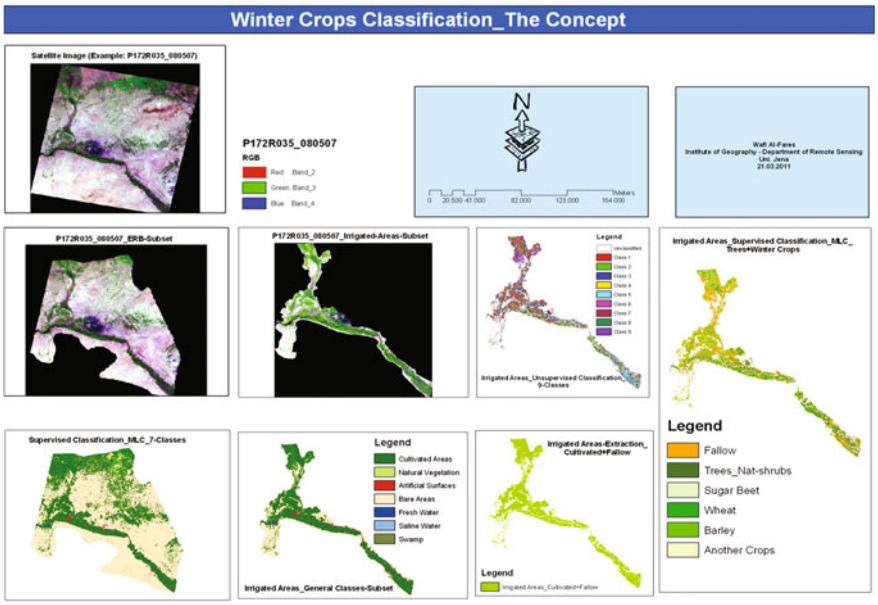

Fig. 5.53 The followed concept to classify the major winter crops based on both the previous general classes classification and the generated spatial distribution of the irrigated areas

crops of interest (wheat, barley, and sugar beet), in addition to fallow, which is classified in both seasons.

Trees and shrubs could be classified from either winter remotely sensed data or from data acquired in summer. This information was then combined and a mask constructed that included all the winter-data-based classified LULC-areas which could be planted during the summer (fallow, wheat, barley, and other crops). The other classified areas which were almost impossible to be changed during the summer of the same year (e.g., trees, permanent crops, etc.) were excluded. Finally, the before built mask was applied to the summer-related remote sensing data (Fig. 5.54) for classification of the summer crops of interest (cotton, and corn), plus fallow. Before the completion of this task, it was necessary to perform an accuracy assessment for all the produced classification results.

The other method that was adopted to classify the irrigation areas (especially the state projects) and the various permanent, winter, and summer agriculture-categories, was to integrate the remotely sensed data with the non-remotely sensed data (e.g., statistical records and detailed schemes), especially for the TM-May and August-1987 data. This is explained in the next section.

The most important point involved in these projects was the engineering organization and division of each project into several farms with names and known geographical sites. The cultivated fields were large enough to be easily distinguished by available remotely sensed data. In addition, the geographical distribution of those fields had well known coordinates and detailed charts, and

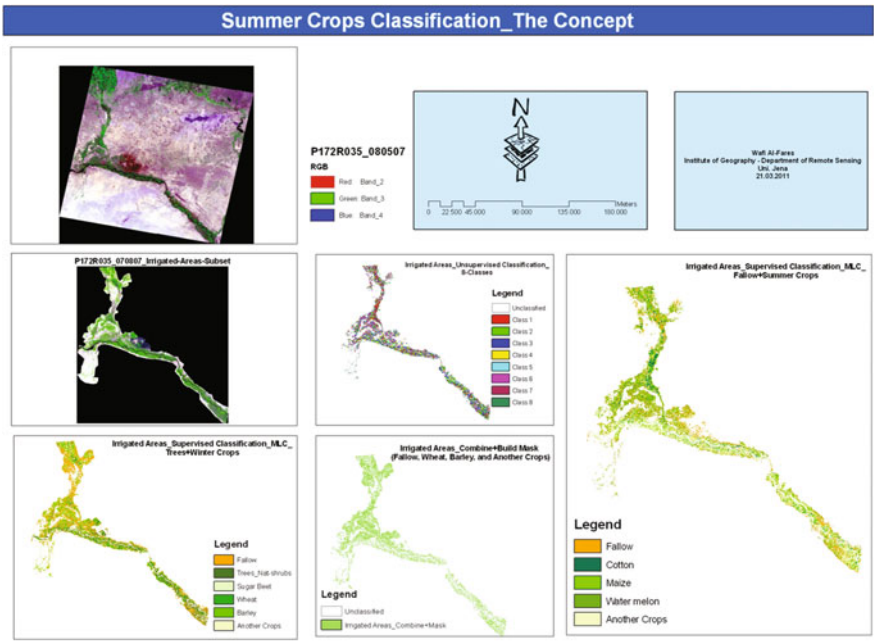

Fig. 5.54 The followed concept to classify the major summer crops based on both the previous winter crops classification and the generated spatial distribution of the irrigated areas

schematics were available for each project with large drawing scales. Because of this, I was able to become familiar with every irrigation project included in the basin and its spatial prevalence on the satellite images. So, I was able to integrate the spatial distribution with the available statistic numbers of each project in several time-durations. This was also compatible with the remotely sensed data about the study area in my possession. These links enabled me to select the training samples used in the supervised classification and to use them in assessment of the accuracy of the classification. This was, of course, in addition to the remaining referential data previously mentioned.

As for the other basin areas located outside the borders of the irrigation projects, since the required classification level is general and not detailed, it was decided it would be sufficient to count on the remotely sensed data in addition to the thematic, topographic and Google Earth maps and during the selecting process of the training-samples.

Here the problem is that full statistics concerning agrarian activities and types/classes of plantations were available, but only at a governmental and governorates level. This meant that the data did not provide information about what had been previously cultivated. The other problem was that many fields were not planted every year with the same crop. Detailed information about which specific crops had been planted in the training-samples was required. This level of detail was

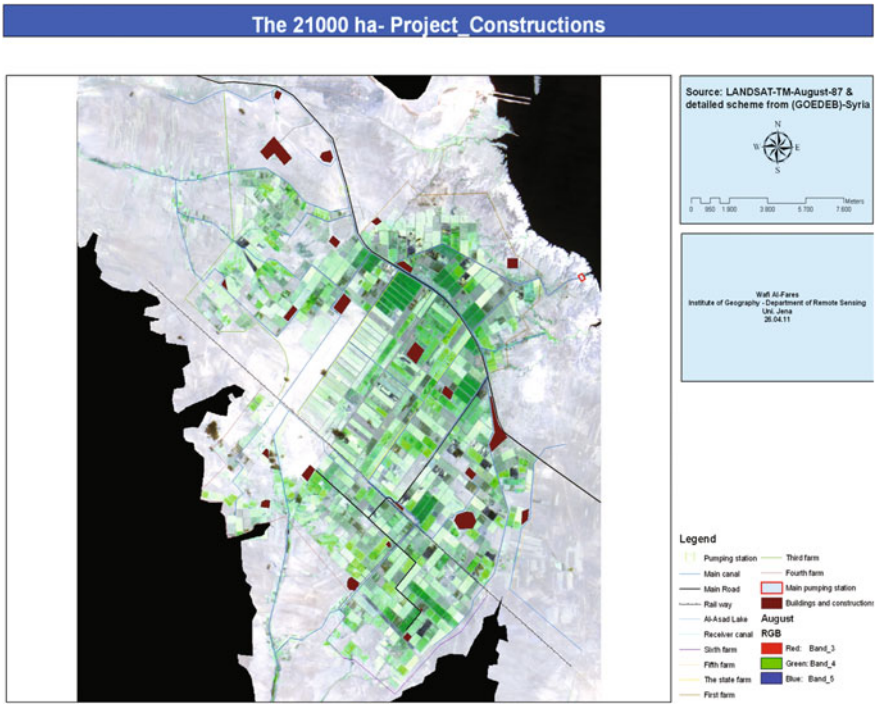

Fig. 5.55 The integration of the remotely sensed data with the construction scheme of the 21,000 ha project

possible for the State-run irrigation projects in the "Organization of Development of the Euphrates Basin", which has three branches—the Upper-Euphrates in A-leppo, the Mid-Euphrates in Arraqqah and the Lower-Euphrates in Deir Azzour. These areas were well managed, and a detailed agricultural statistics procedure was developed for every project.

One example of a training sample is a 17,000 ha project, which is integrated with a state farm (4,000 ha). Thus, the total area is 21,000 ha located within the Upper-Euphrates Basin in Aleppo, the reclamation began in 1979. The land is irrigated by pumping water from Lake Al-Asad. The temporal developments in the extension of this project were as followed: In 1979 (3,031 ha), 1980 (4,762 ha), 1981 (9,634 ha), 1982 (15,103 ha), 1990 (16,703 ha), 1991 (17,513 ha), 1992 (19,703 ha), 1993 (20,903 ha), and in 2005 (21,325 ha) with 100 % of the irrigation plan.

The first step was to integrate the construction scheme with the remotely sensed data to extract the spatial distribution of the project of interest (Fig. 5.55). This was complicated by the fact the area had no ground truth reference.

The second step was to define what ratio of agricultural crops existed. This was generated from non-remotely sensed/human-based collected data (Table 5.7).

Table 5.7 The statistical information about each farm of the 21,000 ha project for 1987

The Farms / The Crops	State farm 2937 ha	First farm 2040 ha	Third farm 3557 ha	Fourth farm 2753 ha	Fifth farm 3293 ha	Sixth farm 2320 ha	Total/ha / 1987
Winter							10,146
Wheat	707	562	943	782	974	1073	5,041
Sugar beet	300	130	174	234	231	150	1,219
Barley/irrigated				127			127
Barley/rain-fed	965	340	1061	496	463	302	3,618
Vicia beans	53			78	10		141
Fallow							5,359
Summer							3,052
Cotton	400	483	393	401	451	266	2,394
Maize	74	105	155	46	119	159	658
Fallow							12,453
Permanent crops							1,572
Fruit trees	109	53			112		274
Poplar	156	172			203		708
Alfalfa	189	98	42	73	95	93	590

Source adapted from GOEDEB, 1987

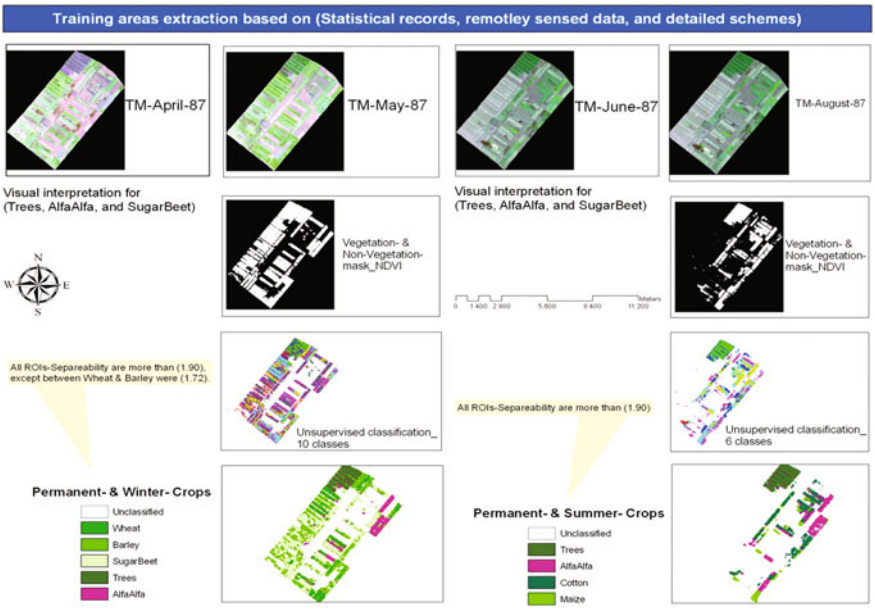

Fig. 5.56 The followed concept to collect training samples for the area/s with no truth-data or with insufficient reference data (the state farm)

The third step (Fig. 5.56) was to extract the smallest unit/farm in the 21,000 ha project to make the reorganization process of various agricultural features easier. Then, the various record-times/coverages were used in a visual interpretation to recognize various agricultural features and to define the training samples that represent these features in a supervised classification. For example, it was possible to recognize trees, alfalfa and sugar beet using multi-date remote sensing data and visual interpretation. Based on the agricultural calendar, trees fields appeared as planted areas over the three datasets (May, June and August); alfalfa appeared as green areas over the four datasets (April, May, June and August); and sugar beet fields appeared in April data as diverse planted areas in comparison to wheat and barley fields. The June data showed the area was still planted in comparison to other winter crops, especially those that had similar spectral response, such as wheat and barley. These three various appearances of the wheat at first degree and the barley in the June data, confirmed the selection for the training samples from the May data. The region also contained many dairy farms nestled among the irrigation projects with known geographical locations. These farms were planted only with barley, and provided a useful basis for training sites. Circular-irrigation fields also provided a useful source of reference, as the fields appear in a circle-shape. These fields were planted almost fully in wheat. To this end, the visual interpretation and unsupervised classification results were able to be compared with the statistical numbers, which provided a background about each farm's

planted crop. After all the representative training samples for each agriculture-category (permanent, winter, and summer) were collected, the supervised classification was conducted under the vegetation-mask generated from NDVI-values.

This resulted in the collection of several training samples within the irrigation agricultural land projects, which represented the majority of variations in the LULC-categories, especially the agriculture class. Some of training-samples were used in the automated classification process, whereas others were used to evaluate the accuracy of these classifications.

At this point, a query arose over what requirement was needed to link statistical records with spatial records concerning the irrigation projects. This was needed for the training-samples representing the LUs which would be used later in automated classification, despite the availability of other referential GPS-points. There were three reasons for this. Firstly, the GPS-points did not totally cover all the study sites. Points of ICARDA-1987 were all located within Aleppo governorate, but no points existed in the Arraqqa and Deir Azzour. The GORS-points for 2005 were all located within Deir Azzour. The only points distributed over the three governorates were those taken in 2007. Secondly, because of the relatively large extension of the study area which lies within various natural regions (climatic: rains, temperature, humidity and soil), there was too much variation in the cultivations and plants along the basin. As, points of ICARDA-1987 did not represent poplar tree farms which existed only within the irrigation agriculture projects area in the Arraqqa (Al-Asad institution project). Thirdly, the variation in the method of collecting the GPS-points and the training-samples proved of issue, as well as the potential error in measurements of the GPS, relating to technical reasons. It is hypothesized that if one of the points measured a wheat field which neighbored a field of barley, then if the GPS-device was inaccurate enough or the satellite image that received the point was not correctly referenced, then the point may be shown as lying within the closely bordered barley field. So, mistakes could occur in the classification process.

After the collection of enough training samples for the existing various LULC-features from the state farm, the whole 21,000 ha project was generalized via the supervised classification (Fig. 5.57). Here, the multi stage classification was followed with various created masks. Initially, both the unsupervised and supervised classification were used to classify the five general classes (see Sect. 5.8). Then, the approaches were combined into two more general classes, i.e., uncultivated and cultivated areas. The subset "cultivated areas" represented the actual planted fields and the fallow and/or drilled lands, and displayed the irrigated area in project-scale. A mask was then created to represent the spatial distribution of this cultivated areas class, and to eliminate the uncultivated areas and their negative spectral influence on the other features. It also reduced the computer processing-time of the data (though the user-data-interaction time was increased due to the greater number of processing-steps). After applying the masking-process and the supervised classification, the three classes were obtained (trees, herbaceous and fallow). The tree class was extracted from the next classification steps. Two masks were then built; the first for the herbaceous and the second for herbaceous and

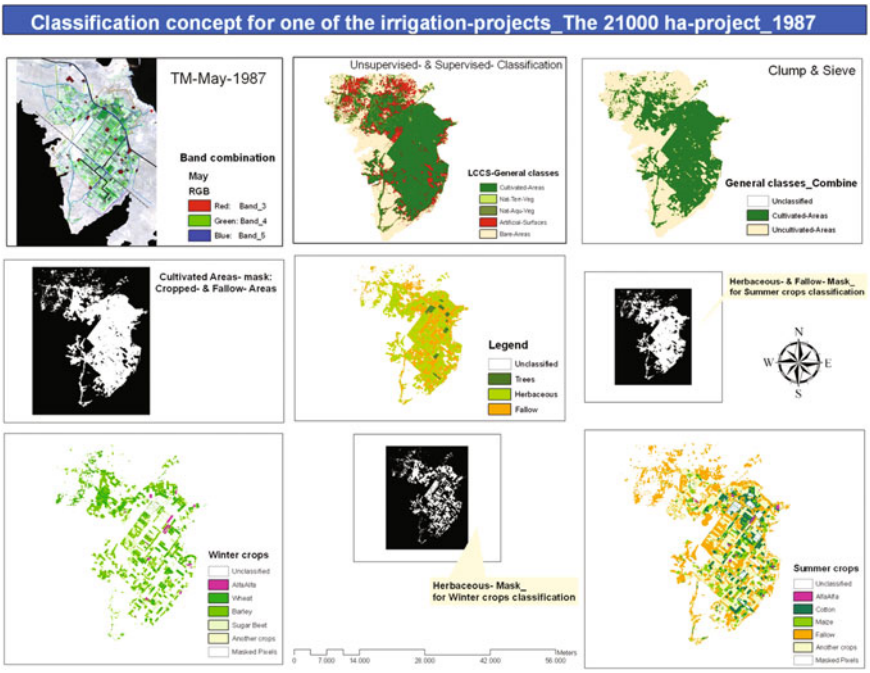

Fig. 5.57 The general classes classification, irrigation mapping, and agriculture classification methods that were performed based on the spatial extent of each irrigation project

fallow areas. Under the first mask, a supervised classification was carried out to obtain the permanent and winter crops classification results (alfalfa, wheat, barley, sugar beet and other crops). The second mask for herbaceous and fallow areas, where some of herbaceous areas would be replanted in summer (e.g., corn after barley), produced the thematic map of summer crops (cotton, corn and other crops) using summer remote sensing data for August.

The concept in classification adopted above was applied for other study years (Fig. 5.58) to obtain historical remote sensing based statistical numbers (Table 5.8).

Finally, all the previously adapted steps and methods were applied and data was added for the other 15 projects to the thematic map/s for the 21,000 ha project (Fig. 5.59).

5.11 Post-Classification Processing

Many researchers have argued that post-classification is a vital step to improve the results of classification (Lu and Weng 2004). Ancillary data are often used to enhance the classification result based on performed expert rules. As, dense forests

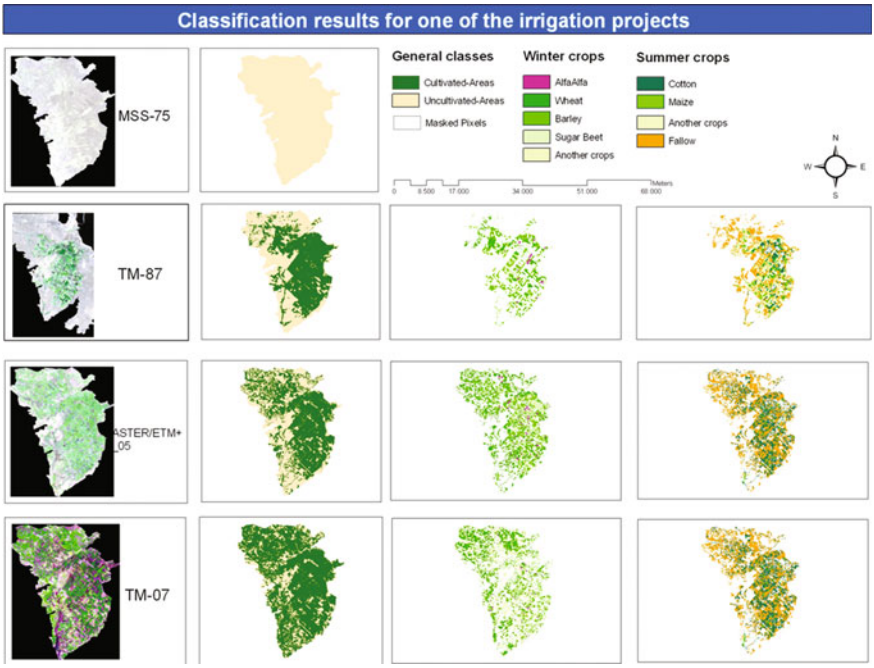

Fig. 5.58 The general classes classification, irrigation mapping, and agriculture classification results that were produced based on the spatial extent of each irrigation project

are often found in mountain areas in Syria, but food-trees (cultivated plantations) are essentially located in plain areas, with sparse houses and a low population density. So, expert knowledge can be performed based on the relationships between the high factor and the agricultural conditions to separate food trees from forested areas. Classical pixel-based classification methods often lead to "salt and pepper" effects in final classification results maps, caused by the isolated pixels of some classes within another dominant class. That is due to the complexity of biophysical environments, which potentially decrease the classification accuracy. It is more logical to join these isolated pixels to the dominant class that they are first assigned to. A suitable enhancing filter applied after the classification process on the produced thematic map will not only "clean up" the map and make it visually less noisy, but also increase the classification accuracy.

To improve the classification results, the majority/mode filter in ENVI, v. 4.6 was used as a post-classification procedure. This procedure is a low-pass filter that reduces the created effects and noises from the classification process, where it replaces the isolated pixels by whatever value constitutes the majority in their neighborhood. It could be regarded as a kind of post-classification spatial integration. This filter is simple, where it smoothes a thematic map without any numerical operations (Liu and Mason 2009). The classification results (the thematic maps) were filtered using a 3×3 majority filter window, followed by a

Table 5.8 The remotely sensed data classification based statistical results for the 21,000 ha irrigation project for 1975, 1987, 2005 and 2007

The 21,000 ha-project_all classes	1975	1987	2005	2007
Cultivated areas		23,834	25,806	34,792
Trees + shrubs		648	872	58
Herbaceous (winter crops)		12,561	22,377	23,366
Alfalfa		275	459	198
Wheat		3,669	11,693	10,560
Barley		5,305	4,150	1,211
Sugar beet		3,454	6,075	2,359
Other crops		62	200	9,038
Fallow		10,927	2,796	11,970
Herbaceous (summer crops)		50,499	24,272	13,303
Cotton		2,950	8,412	2,284
Corn		2,099	463	650
Other crops		8,143	127	10,369
Fallow		10,063	15,270	22,277
Water	0	0	0	0
Uncultivated areas	46,324	22,494	20,501	11,489

sieve filter. This caused a smoothing of the class boundaries. A small pixels-cluster of an individual class was added to the surrounding area of a larger class, and the boundaries of the LULC-classes were generalized and clearly identified. The sieve filter was used in addition to the majority filter to clean the classification result of further small pixel-clusters that were not eliminated from the majority filter. Clusters with less than 10 pixels were removed by merging them with their largest neighbor.

5.12 Automated Change Detection Mapping

5.12.1 Pre-Classification Approach

This approach was essential in mapping the increasing changes in the agricultural irrigated areas in the ERB. Data from the LANDSAT-program, MSS and TM spanning the period between 1975 and 2007 were chosen from a similar time of the year in order to allow each LULC-class of interest a similar spectral response and similar illumination conditions. The MSS-data set of six images (Fig. 5.60) were pre-processed (see Sect. 5.2) for radiometric normalization using iMAD. The master-scene was p185r035. It was impossible to correct the atmospheric effects because it was difficult to obtain weather parameters for such relatively old dates. However, it was possible to carry out radiometry and atmosphere corrections for the TM-data set of six images. The master-scene for this was p172r035. Each data

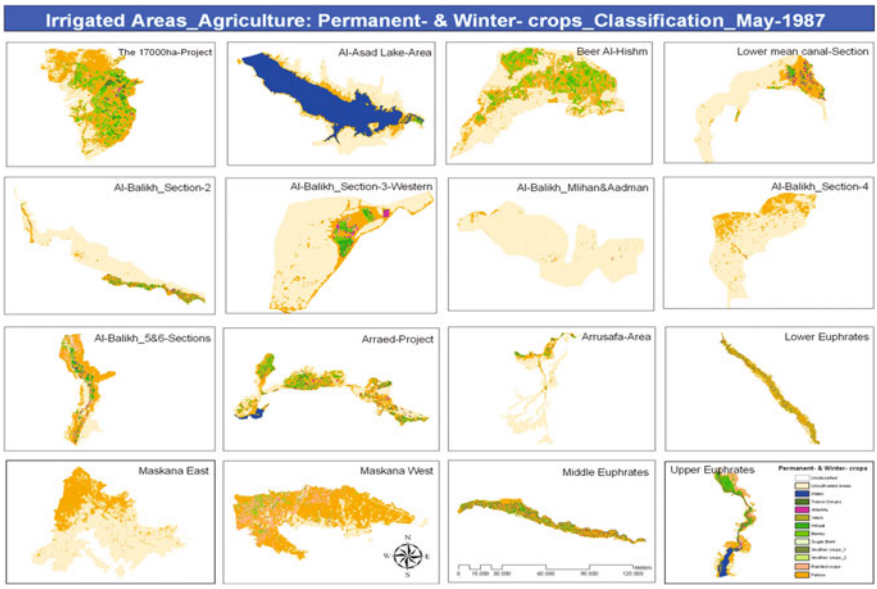

Fig. 5.59 Illustration of the individual 16-project-based classification results (permanent and winter crops classification results for 1987)

set was then mosaiced to produce only two mosaic-images, each representing one date. Again, iMAD was applied to the two resulting mosaic-images. The master-scene was chosen as the mosaic-scene produced from the TM-data in 2007, as it was possible to get weather data for the dates, and radiometric normalizations and atmospheric corrections were able to be performed. Finally, the two mosaic-scenes were geometrically registered using the *image to image method*. The MSS-scene was also resampled to the same spatial resolution of 30 m as TM-scene. Finally, the two remote sensing data-scenes were added to the change detection mapping process using the image differencing method. The three major mapped changes over the last 32 years were: natural areas to bare areas, bare areas to cultivated areas, and no change (see Chap. 6.3.1).

5.12.2 Post-Classification Approach

The post-classification change detection approach concerned the analysis of the differences between two more or less independently classified images. A comparison of the categorizations was performed using raster-based analysis (ENVI, v. 4.6). The major merit of this approach was that data normalization was not needed because the remote sensing data recorded at two dates were classified separately

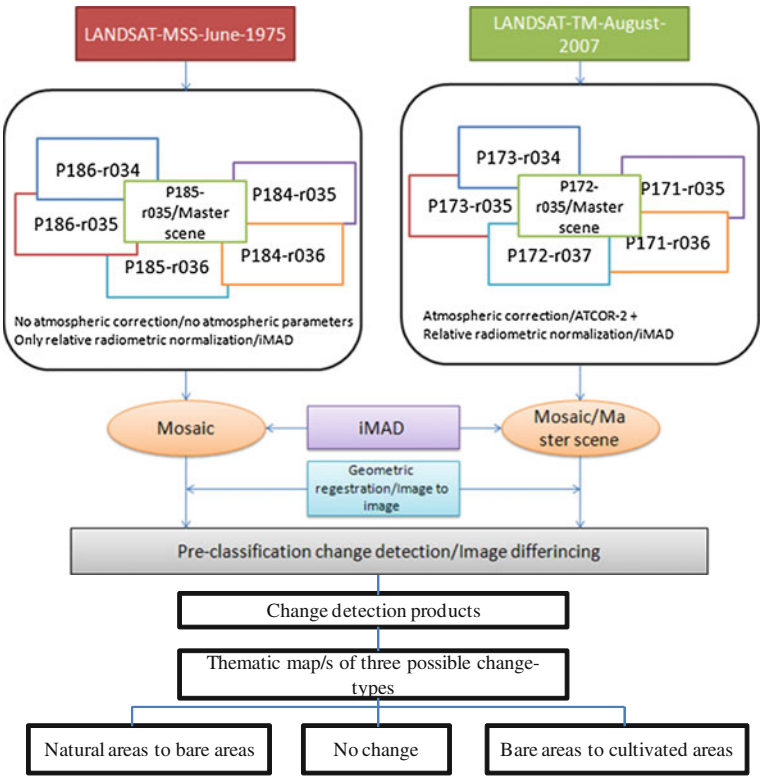

Fig. 5.60 The pre-classification change detection mapping concept that was performed for the two remotely sensed data sets (MSS-June-1975 and TM-August-2007)

(Singh 1989). Disadvantages that reduce the implementation of this approach are: cost; consistency; and error propagation (Lunetta 1999).

The post-classification change detection approach for the ERB (Fig. 5.61) was based on the two previously supervised classified remote sensing data sets (TM-May-1987 and TM-May-2007) using the MLC-algorithm (see Sect. 5.7.1.2). The resulted five general classes that provided input in the change detection were: cultivated and managed terrestrial areas; natural and semi-natural terrestrial vegetation; artificial surfaces and associated areas; bare areas; and natural water-bodies (see Sect. 5.8). The resulting 1987 and 2007 classification results were used as inputs for classification, then post classification, followed with change detection statistics under the ENVI-program with the version 4.6. This yielded a change image (change matrix), in which 20-types of change between the two dates were potentially possible (see Chap. 6.3.2).

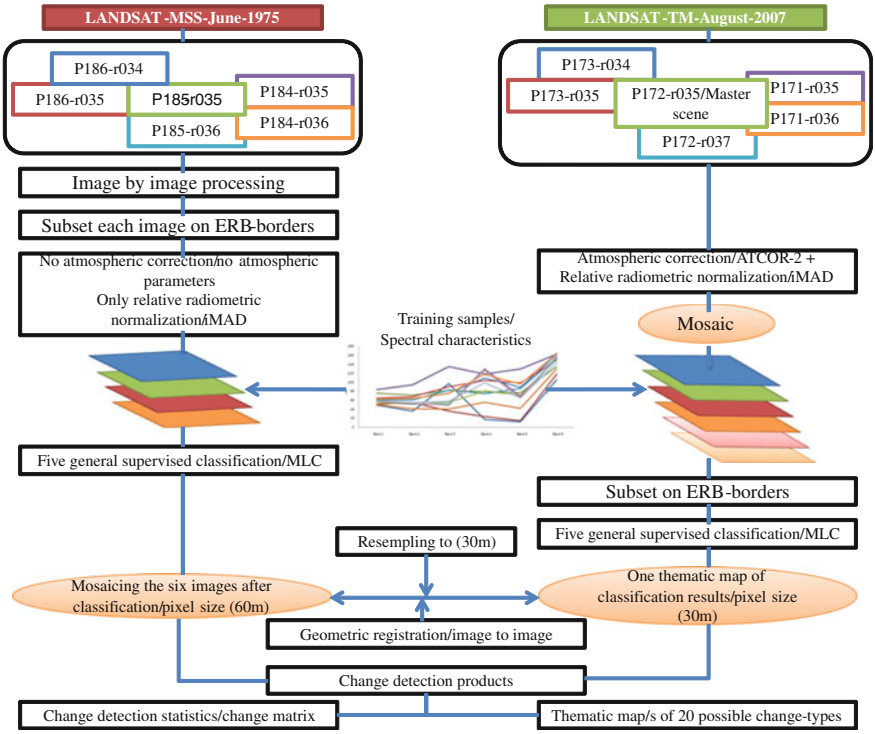

Fig. 5.61 Flow chart of the post-classification change detection mapping approach that was performed for the two remotely sensed datasets (TM-May-1987 and TM-May-2007)

5.13 Accuracy Assessment

The execution estimation of an applied classification approach is a complex process, involving various criteria. Cihlar et al. (1998) suggested six criteria. These are: "accuracy; reproducibility; robustness; ability to fully use the information content of the data; uniform applicability; and objectiveness". These requirements are difficult to satisfy using only one classification approach. The reason for this relates to the different environmental settings and datasets used. The acceptable accuracy values are relative, determined generally by the users themselves depending on the type of application. Accuracy values that are acceptable for specific application may be unacceptable for others.

Generally, there are no dependable rules for determining the testing samples that are required to evaluate the classification accuracy. However, there are some useful suggestions, including those made by Fitzpatrick-Lins (1981). Another idea, put forward by Congalton and Green (1999), is to use 50 testing samples as minimum for each classified LULC-category. If the study area is larger than 1,000,000 ha, or if there are more than 12 classified categories, then there should

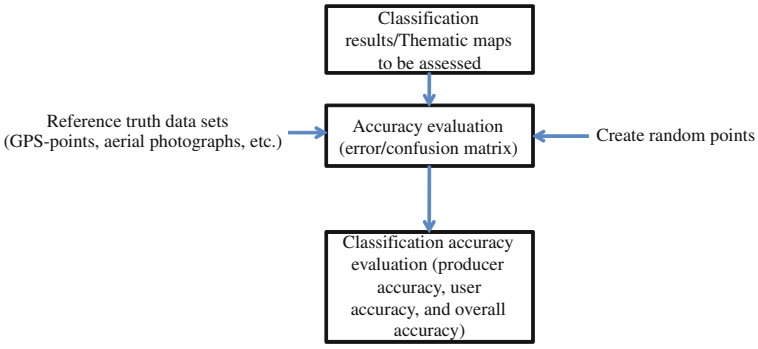

Fig. 5.62 The general accuracy assessment steps that were applied on the resulted thematic map/s from the classification process

be 75–100 samples for each LULC-category. This suggested approach samples small areas thoroughly, while large areas might be under-sampled. Thus, it is suggested that testing sample numbers could be set for variations in size and within-class variability.

Accuracy assessment is a post-classification step. It was accomplished for the purposes of this study using ENVI, v. 4.6, which was used to evaluate the correspondence of the classified LULC-maps to the *true and/or assumed true* geographical reference data (Congalton 1991). The reference data were: Part of the collected field-data for the years 1987, 2005 and 2007(see Sect. 5.4), where the first part was used as training samples; assumed truth data based on the integration of the remotely sensed data; irrigation projects statistical records and the detailed construction schemes of these projects, which were used locate the spatial distribution of the various agricultural features in the irrigation projects area for 1987 (see Sect. 5.10); thematic maps; visual interpretation based on the remote sensing data itself; and Google Earth. Figure 5.62 illustrate the major steps that were followed in assessing the various thematic maps that resulted from the classification process.

Results of classification were presented in form of thematic maps. Using the various truth reference data, accuracy assessments were carried out for all classification results. The reference data/classes were compared with the predicted classes by the adopted classifier/s (and probably enhanced using the post-classification processing). The final evaluation results were reported in the form of error matrices. The overall classification accuracy (percentage correct) was calculated for all classifications, as well as the accuracies of the class-specific user and producer.

Two accuracy assessment methods were performed in this thesis. The first method is ***based on the pixel scale*** to derive the accuracy of classification in the remotely sensed data, which resulted from the calculation of the error/confusion matrix.

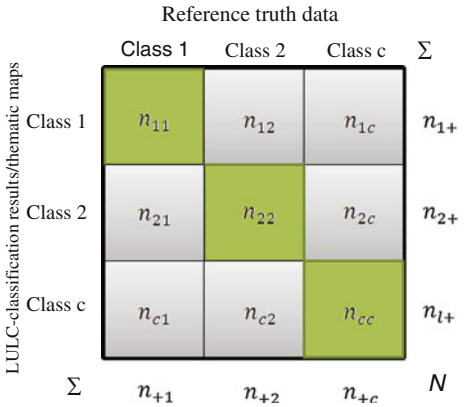

Fig. 5.63 Explanation of the error matrix approach (*Source* modified from Congalton and Green 1999)

Let, for a **(*l*-class)** classification problem, **(*N*)** be the total number of reference samples. The corresponding confusion matrix is illustrated in Fig. 5.63. The number of samples that are classified as class**/*ωi* (*i* = 1,2,…,*l*)/**and belong to land cover class**/*ωj* (*j* = 1,2, …,*l*)/**are described by **(** n_{ij}**)**, for example, (n_{11}) denotes the number of samples that belongs to class **(1)** and correctly assigned to class **(1)**, whereas (n_{21}) defines the samples belonging to class **(1)**, but incorrectly classified to class **(2)**. The diagonal cells (n_{cc}) (the highlighted elements in Fig. 5.63) of the error matrix contain the number of correctly classified samples (Congalton and Green 1999), while the off-diagonal cells represent the disagreement between the classified image and the ground truth data. The overall accuracy is calculated by their sum (the diagonal observations) divided by the total number of samples **(*N*)** (all observations included in the error matrix):

$$Overall\,accuracy = \frac{\sum_{c=1}^{L} n_{cc}}{N}$$

Generally, the individual LULC-class that accounts for a large rate of the study/testing area, might be classified with a high accuracy using an individual classification algorithm, which creates an alignment in overall accuracy. Therefore, it is necessary to consider the individual class accuracies to avoid the alignment. Class-specific accuracies can be created based on the confusion matrix (i.e., producer and user accuracy). It can be also used to create the corresponding error rates. "An error of omission is to exclude a sample from a class in which it originally belongs (a misclassification error is an omission from the correct class). A commission error on the other hand assigns a sample to a wrong class (a misclassification error is a commission into another class). Consequently, each error is an omission from the correct class and a commission to a wrong class. The producer accuracy, that is a measure of *error of omission*" (Story and Congalton 1986), for class **(*c*)** is

calculated by dividing the number of correct samples of **(*c*)** by the total number of reference samples of class **(*c*)**. The resulting percentage producer accuracy indicates the probability that a reference pixel will be correctly classified.

$$Producer\,accuracy = \frac{n_{cc}}{n_{+c}}$$

The user accuracy, that is a measure of *error of commission* (Story and Congalton 1986), describes how many samples that were classified as **(*c*)** in fact belong to class **(*c*)**. The measurement is resulted from:

$$User\,accuracy = \frac{n_{cc}}{n_{c+}}$$

Finally, multiplying the results of each the previous three accuracies by 100 forms the *percent correctly classified* (*PCC*) metric.

The second statistic used is the *kappa coefficient* (*kc*). It is generally known as a precision measure since it is considered as a measure of agreement in the absence of chance (Cohen 1960; Lillesand et al. 2008). Conceptually it can be defined as:

$$KC = \frac{Observed\,Accuracy - Chance\,Agreement}{1 - Chance\,Agreement}$$

The kappa statistic is calculated from the confusion matrix by using the following mathematical statement:

$$KC = \frac{n\sum_{i=1}^{p} x_{ii} - \sum_{i=1}^{p} x_{io}x_{oi}}{n^2 - \sum_{i=1}^{p} x_{io}x_{oi}}$$

where:

n	total number of pixels used for testing the accuracy of a classifier,
p	number of classes,
$\sum x_{ii}$	sum of diagonal elements of confusion matrix,
$\sum x_{io}$	sum of row i,
$\sum x_{oi}$	sum of column i

An example is presented to explain the derived classification accuracies for the 21,000 ha project for the year 2007 (Table 5.9).

The second method is ***based on the state administrative divisions*** (e.g., Menbij see Sects. 5.4 and 5.7.2) and/or ***on the state irrigation projects divisions*** (e.g., the 21,000 ha project see Sect. 5.10), to derive the accuracy of the correspondence between the derived statistical numbers from the automated classification of remote sensing data and those human-based statistical records.

The correspondence degree for a specific season at an administrative-scale was measured by calculating the *Percent Error* (*PE*):

$$PE = \frac{Observed_i - Predicted_i}{Observed_i} \times 100.$$

Table 5.9 The classification accuracy assessment for the resulted thematic map that represents the spatial distribution of the permanent and the winter agricultural classes in the 21,000 ha project

Reference classes (image/ground)	Resulted classified classes from LANDSAT-TM-images							Total/possible	Omissions (%)	Commissions (%)	Mapping accuracy (%)
	1	2	3	4	5	6	7				
Trees and shrubs (1)	9	1	0	0	0	1	0	11	2/11 = 0.18 × 100 = 18	3/11 = 27	9/9 + 2+3 = 64
Alfalfa (2)	1	7	0	0	1	0	0	9	2/9 = 22	2/9 = 22	7/7 + 2+2 = 63
Wheat (3)	1	1	17	4	1	0	0	24	7/24 = 29	5/24 = 20	17/17 + 1+5 = 73
Barley (4)	0	0	4	13	0	0	2	19	6/19 = 31	6/19 = 31	13/13 + 6+6 = 52
Sugar beet (5)	0	0	1	1	10	0	0	12	2/12 = 16	2/12 = 16	10/10 + 2+2 = 71
Fallow (6)	1	0	0	0	0	17	0	18	1/18 = 5	1/18 = 5	17/17 + 1+1 = 89
Other (7)	0	0	0	1	0	0	14	15	1/15 = 6	2/15 = 13	14/14 + 1+2 = 82
Total	12	9	22	19	12	18	16	108			

Overall LANDSAT-TM classification accuracy = 9 + 7 + 17 + 13 + 10 + 17 + 14/108 = 80 %

Mapping Accuracy for any Class (X) = $\frac{Pixels\ of\ X_{Correct}}{Pixels\ of\ X_{Correct} + Pixels\ of\ X_{Omission} + Pixels\ of\ X_{Commission}}$

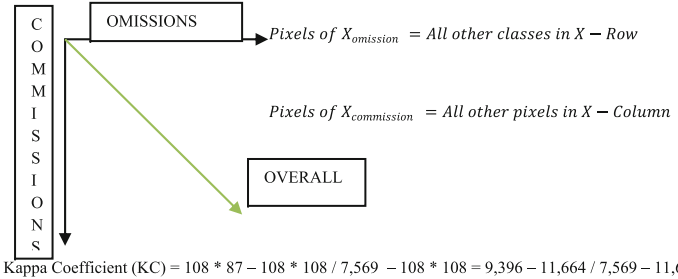

Kappa Coefficient (KC) = 108 * 87 – 108 * 108 / 7,569 – 108 * 108 = 9,396 – 11,664 / 7,569 – 11,664 = - 2,268 / - 4,095 = 0.55

PE is calculated as: the percent proportion of the variation between the remotely sensed area estimate (predicted) and the surveyed area estimate (observed) to that of the surveyed area estimate (observed) for each method for each year within a state administration's boundaries.

After finishing the automated classification process, and obtaining the results and evaluations, results were compared with statistical records on the level of the three governorates (Aleppo, Arraqqa, and Deir Azzour), on the administrative region level (e.g., Al-Bab) in each governorate, and on the level of the natural borders of agricultural stabilization zones within the borders of the three governorates and their administrative regions. Finally, these statistical records were reported on the level of the irrigation agricultural projects' borders.

References

Albertz, J. (2009). *Einführung in die Fernerkundung: Grundlagen der Interpretation von Luft- und Satellitenbildern* (3. Aufl.). Darmstadt: Wiss. Buchges.

Alilat, F., Loumi, S., & Sansal, B. (2006). Modified fuzzy ARTMAP and supervised fuzzy ART: Comparative study with multispectral classification. *International Journal of Computer Science, 1*(3), 232–238.

Arora, M. K., & Mathur, S. (2001). Multi-source classification using artificial neural network in a rugged terrain. *Geocarto International, 16*(3), 37–44.

Atkinson, P. M., & Tatnall, A. R. L. (1997). Introduction: Neural networks in remote sensing. *International Journal of Remote Sensing, 18*(4), 699–709.

Bagan, H., Qinxue, W., Masataka, W., Satoshi, K., & Yuhai, B. (2008). Land-cover classification using ASTER multi-band combinations based on wavelet fusion and SOM neural network. *Photogrammetric Engineering & Remote Sensing, 74*(3), 333–342.

Ball, G. H., & Hall, D. J. (1965). *A novel method of data analysis and pattern classification* (Technical Report). Menlo Park, CA: Stanford Research Institute.

Bastin, L. (1997). Comparison of fuzzy c-means classification, linear mixture modelling and MLC probabilities as tools for unmixing coarse pixels. *International Journal of Remote Sensing, 18*(17), 3629–3648.

Benediktsson, J. A., Swain, P. H., & Ersoy, O. K. (1990). Neural network approaches versus statistical-methods in classification of multisource remote-sensing data. *IEEE Transactions on Geoscience and Remote Sensing, 28*(4), 540–552.

Bennet, K. P., & Campbell, C. (2000). Support vector machines: Hype or hallelujah? *Special Interest Group on Knowledge Discovery and Data Mining, 2*(2), 1–13.

Berk, A., Bernstein, L. S., Anderson, G. P., Acharya, P. K., Robertson, D. C., Chetwynd, J. H., et al. (1998). MODTRAN Cloud and Multiple Scattering Upgrades with Application to AVIRIS. *Remote Sensing of Environment, 65*, 367–375.

Bernstein, R. (1983). Image geometry and rectification. In R. N. Colwell (Ed.), *Manual of remote sensing*. Falls Church: American Society of Photogrammetry.

Bishop, C. M. (1995). *Neural networks for pattern recognition*. Oxford: Oxford University Press.

Brisco, B., & Brown, R. J. (1995). Multidate SAR/TM Synergism for crop classification in western Canada. *Photogrammetric Engineering & Remote Sensing, 61*(8), 1009–1014.

Bruzzone, L., & Fernandez-Prieto, D. (1999). A technique for the selection of kernel-function parameters in RBF neural networks for classification of remote-sensing images. *IEEE Transactions on Geoscience and Remote Sensing, 37*(2), 1179–1184.

Bruzzone, L., & Marconcini, M. (2009). Toward the automatic updating of land cover maps by a domain-adaptation SVM classifier and a circular validation strategy. *IEEE Transactions on Geoscience and Remote Sensing, 47*(4), 1108–1122.

Campbell, J. B. (1981). Spatial correlation effects upon accuracy of supervised classification of land cover. *Photogrammetric Engineering and Remote Sensing, 47*(3), 355–363.

Camps-Valls, G., Gomez-Chova, L., Munoz-Mari, J., Vila-Frances, J., & Calpe-Maravilla, J. (2006). Composite kernels for hyperspectral image classification. *IEEE Geoscience and Remote Sensing Letters, 3*(1), 93–97.

Canty, M. J. (2009). Boosting: A fast neural network for supervised land cover classification. *Computers & Geosciences, 35*(6), 1280–1295.

Canty, M. J. (2010). *Image analysis, classification and change detection in remote sensing, with algorithms for ENVI/IDL* (2nd revised edition). Taylor & Francis, CRC Press.

Canty, M. J., Nielsen, A. A., & Schmidt, M. (2004). Automatic radiometric normalization of multitemporal satellite imagery. *Remote Sensing of Environment, 91*(3–4), 441–451.

Canty, M. J., & Nielsen, A. A. (2008). Automatic radiometric normalization of multitemporal satellite imagery with the iteratively re-weighted MAD transformation. *Remote Sensing of Environment, 112*(3), 1025–1036.

Carpenter, G. A., Gjaja, M. N., Gopal, S., & Woodcock, C. E. (1997). ART neural networks for remote sensing: Vegetation classification from Landsat TM and terrain data. *IEEE Transactions on Geoscience and Remote Sensing, 33*(2), 308–325.

Chavez, P. S. (1988). An improved dark-object subtraction technique for atmospheric scattering correction of multispectral data. *Remote Sensing of Environment, 24*(3), 459–479.

Chavez, P. S. (1996). Image-based atmospheric corrections-revisited and improved. *Photogrammetric Engineering & Remote Sensing, 62*(9), 1025–1036.

Chavez, P. S., & Mackinnon, D. J. (1994). Automatic detection of vegetation changes in the southwestern United States using remotely sensed images. *Photogrammetric Engineering & Remote Sensing, 60*(5), 571–583.

Chen, Z., Li, S., Ren, J., Gong, P., Zhang, M., Wang, L., et al. (2008). Monitoring and management of agriculture with remote sensing. In S. Liang (Ed.), *Advances in land remote sensing—system, modelling, inversion and adaptation* (pp. 397–421). University of Maryland, USA: Springer.

Chen, D. M., & Stow, D. A. (2002). The effect of training strategies on supervised classification at different spatial resolution. *Photogrammetric Engineering & Remote Sensing, 68*(11), 1155–1162.

Chen, Z., Zhou, Q., & Tang, H. (2004). The future agricultural applications' demanding on space-born remote sensing in China. In H. Tang (Ed.), *Research on the agricultural resource utilization and regional sustainable development* (pp. 236–250). Beijing: China Outlook Press.

Cihlar, J., Xiao, Q., Chen, J., Beaubien, J., Fung, K., & Latifovic, R. (1998). Classification by progressive generalization: A new automated methodology for remote sensing multispectral data. *International Journal of Remote Sensing, 19*(14), 2685–2704.

Cohen, J. (1960). A coefficient of agreement for nominal scales. *Educational and Psychological Measurement, 20*(1), 37–46.

Congalton, R. G. (1991). A review of assessing the accuracy of classifications of remotely sensed data. *Remote Sensing of Environment, 37*(1), 35–46.

Congalton, R. G., & Green, K. (1999). *Assessing the accuracy of remote sensed data: Principles and practices* (1st ed.). London: Lewis Publisher.

Coppin, P., Jonckheere, I., Nackaerts, K., Muys, B., & Lambin, E. (2004). Digital change detection methods in ecosystem monitoring: A review. *International Journal of Remote Sensing, 25*(9), 1565–1596.

Di Gregorio, A. (2005). *Land cover classification system LCCS: Classification concepts and user manual LCCS* (8th ed., part 1). Rome: Food & Agriculture Organization.

Du, Y., Teillet, P. M., & Cihlar, J. (2002). Radiometric normalization of multitemporal high-resolution satellite images with quality control for land cover change detection. *Remote Sensing of Environment, 82*(1), 123–134.

ERDAS. (1999). *Field guide: Earth resources data analysis system.* Atlanta, Georgia: ERDAS Inc.

Fitzpatrick-Lins, K. (1981). Comparison of sampling procedures and data analysis for a land-use and land-cover map. *Photogrammetric Engineering & Remote Sensing, 47*(3), 343–351.

Foody, G. M. (2004). Supervised image classification by MLP and RBF neural networks with and without an exhaustively defined set of classes. *International Journal of Remote Sensing, 25*(15), 3091–3104.

Foody, G. M., & Arora, M. K. (1997). An evaluation of some factors affecting the accuracy of classification by an artificial neural network. *International Journal of Remote Sensing, 18*(4), 799–810.

Foody, G. M., & Mathur, A. (2004a). A relative evaluation of multiclass image classification by support vector machines. *IEEE Transactions on Geoscience and Remote Sensing, 42*(6), 1335–1343.

Foody, G. M., & Mathur, A. (2004b). Toward intelligent training of supervised image classifications: Directing training data acquisition for SVM classification. *Remote Sensing of Environment, 93*(1–2), 107–117.

Foody, G. M., & Mathur, A. (2006). The use of small training sets containing mixed pixels for accurate hard image classification: Training on mixed spectral responses for classification by a SVM. *Remote Sensing of Environment, 103*(2), 179–189.

Foody, G. M., Mathur, A., Sanchez-Hernandez, C., & Boyd, D. S. (2006). Training set size requirements for the classification of a specific class. *Remote Sensing of Environment, 104*(1), 1–14.

Franklin, J. (1995). Predictive vegetation mapping: Geographic modelling of biospatial patterns in relation to environmental gradients. *Progress in Physical Geography, 19*(4), 474–499.

Fukunaga, K. (1990). *Introduction to statistical pattern recognition* (2nd ed.). Boston: Academic Press.

Geneletti, D., & Gorte, B. G. H. (2003). A method for object-oriented land cover classification combining Landsat TM data and aerial photographs. *International Journal of Remote Sensing, 24*(6), 1273–1286.

Gualtieri, J. A., & Cromp, R. F. (1998). Support vector machines for hyperspectral remote sensing classification (pp. 221–232). In *Proceedings of the SPIE, 27th AIPR Workshop: Advances in Computer Assisted Recognition, October 14–16, 1998, Washington, DC, USA*.

Hoffer, R. M. (1980). Computer-aided analysis techniques for mapping earth surface features. In G. Fraysse (Ed.), *Remote sensing applications in agriculture and hydrology* (pp. 133–152). Netherlands: A A Balkema Piblishers.

Hsu, C. W., & Lin, C. J. (2002). A comparison of methods for multi-class support vector machines. *IEEE Transactions on Neural Networks, 13(*2), 415–425.

Huang, C., Davis, L. S., & Townshend, J. R. G. (2002). An assessment of support vector machines for land cover classification. *International Journal of Remote Sensing, 23*(4), 725–749.

Huang, H., Legarsky, J., & Othman, M. (2007). Land-cover classification using Radarsat and Landsat imagery for St. Louis, Missouri. *Photogrammetric Engineering & Remote Sensing, 73*(1), 037–043.

Ito, Y., & Omatu, S. (1999). Extended LVQ neural network approach to land cover mapping. *IEEE Transactions on Geoscience and Remote Sensing, 37*(1), 313–317.

Jensen, J. R. (2005). *Introductory digital image processing: A remote sensing perspective* (3rd ed.). New Jersey: Prentice Hall Series in Geographic Information Science.

Jensen, J. R. (2007). *Remote sensing of the environment: An earth resource perspective* (2nd ed.). New Jersey: Pearson Prentice Hall.

Ji, C. Y. (2000). Land-use classification of remotely sensed data using Kohonen self-organizing feature map neural networks. *Photogrammetric Engineering & Remote Sensing, 66*(12), 1451–1460.

Justice, C. O., Wharton, S. W., & Holben, B. N. (1981). Application of digital terrain data to quantify and reduce the topographic effect on Landsat data. *International Journal of Remote Sensing, 2*(3), 213–230.

Kanellopoulos, I., & Wilkinson, G. G. (1997). Strategies and best practice for neural network image classification. *International Journal of Remote Sensing, 18*(4), 711–725.

Kaufman, Y. J. (1985). Atmospheric effect on the separability of field classes measured from satellites. *Remote Sensing of the Environment, 18*, 21–34.

Kaufman, Y. J., Karnieli, A., & Tanre, D. (2000). Detection of dust over deserts using satellite data in the solar wavelengths. *IEEE Transactions on Geoscience and Remote Sensing, 38*(1), 525–531.

Kavzoglu, T. (2001). *An Investigation of the design and use of feed-forward artificial neural networks in the classification of remotely sensed images*. Doctoral dissertation: The University of Nottingham, UK.

Keuchel, J., Naumann, S., Heiler, M., & Siegmund, A. (2003). Automatic land cover analysis for Tenerife by supervised classification using remotely sensed data. *Remote Sensing of Environment, 86*(4), 530–541.

Landgrebe, D. A. (2003). *Signal theory methods in multispectral remote sensing*. Hoboken, NJ: Wiley.

Lee, J., & Ersoy, O. K. (2007). Consensual and hierarchical classification of remotely sensed multispectral images. *IEEE Transactions on Geoscience and Remote Sensing, 45*(9), 2953–2963.

Leica Geosystems. (2005). *ERDAS IMAGINE 9.0.* Atlanta.

Liang, S. (2004). Estimation of land surface biophysical variables. In G. A. Kong (Ed.), *Qualitative remote sensing of land surfaces* (pp. 246–309). New York: Wiley Series in Remote Sensing, Wiley.

Liang, S., Fang, H., & Chen, M. (2001). Atmospheric correction of Landsat ETM+ land surface imagery, part 1: Methods. *IEEE Transactions on Geoscience and Remote Sensing, 39*(11), 2490–2498.

Lillesand, M. T., Kiefer, R. W., & Chipman, J. W. (2008). *Remote sensing and image interpretation* (6th ed.). Hoboken, NJ: Wiley.

Liu, J. G., & Mason, P. J. (2009). *Essential image processing and GIS for remote sensing*. London: Wiley.

Liu, X.-H., Skiedmore, A. K., & Van Oosten, H. (2002). Integration of classification methods for improvement of landcover map accuracy. *ISPRS Journal of Photogrammetry & Remote Sensing, 56*(4), 257–268.

Liu, W., Seto, K. C., Wu, E. Y., Gopal, S., & Woodcock, C. E. (2004). ART-MAP: A neural network approach to subpixel classification. *IEEE Transactions on Geoscience and Remote Sensing, 42*(9), 1976–1983.

Lo, C. P., & Yeung, A. K. W. (2002). *Concepts and techniques of geographic information systems*. Upper Saddle River, NJ: Prentice-Hall.

Lu, D., & Weng, Q. (2004). Spectral mixture analysis of the urban landscapes in Indianapolis with Landsat ETM+ imagery. *Photogrammetric Engineering and Remote Sensing, 70*(9), 1053–1062.

Lu, D., & Weng, Q. (2007). A survey of image classification methods and techniques for improving classification performance. *International Journal of Remote Sensing, 28*(5), 823–870.

Lunetta, R. S. (1999). Application, project, and analytical Approach. In Ross S. Lunetta & C. D. Elvidge (Eds.), *Remote sensing change detection environmental monitoring methods and applications* (pp. 1–19). London: Taylor and Francis.

Mannan, B., Rot, J., & Ray, A. K. (1998). Fuzzy ARTMAP supervised classification of multispectral remotely-sensed images. *International Journal of Remote Sensing, 19*(4), 767–774.

Marcal, A. R. S., Borges, J. S., Gomes, J. A., & Da Costa, J. F. P. (2005). Land cover update by supervised classification of segmented ASTER images. *International Journal of Remote Sensing, 26*(7), 1347–1362.

Markham, B. L., & Barker, J. L. (1987). Thematic mapper bandpass solar exoatmospheric irradiances. *International Journal of Remote Sensing, 8*(3), 517–523.

Mather, P. M. (2004). *Computer processing of remotely-sensed images: An introduction* (3rd ed.). Chichester: Wiley.

Mausel, P. W., Kramber, W. J., & Lee, J. K. (1990). Optimum band selection for supervised classification of multispectral data. *Photogrammetric Engineering and Remote Sensing, 56*, 55–60.

McCoy, R. M. (2005). *Field methods in remote sensing*. New York, NY: Guilford Press.

Medhavy, T. T., Sharma, T., Dubey, R. P., Hooda, R. S., Mothikumar, K. E., Yadav, M., et al. (1993). Crop classification accuracy as influenced by training strategy, data transformation and spatial resolution of data. *Journal of the Indian Society of Remote Sensing, 21*(1), 21–28.

Melgani, F., & Bruzzone, L. (2004). Classification of hyperspectral remote sensing images with support vector machines. *IEEE Transactions on Geoscience and Remote Sensing, 42*(8), 1778–1790.

McCloy, K. R. (1995). *Resource management system: Process and practice*. London: Taylor and Francis.

Moran, M. S., Jackson, R. D., Slater, P. N., & Teillet, P. M. (1992). Evaluation of simplified procedures for retrieval of land surface reflectance factors from satellite sensor output. *Remote Sensing of Environment, 41*(2–3), 169–184.

Nielsen, A. A. (2007). The regularized iteratively reweighted MAD method for change detection in multi- and hyperspectral data. *IEEE Transactions on Image Processing, 16*(2), 463–478.

Nilsson, N. J. (1965). *Learning machines*. New York: McGraw-Hill.

Olsson, K. (1985). *Remote sensing for fuelwood resources and land degradation studies in Kordofan, the Sudan*. Avhandlingar C: Meddelande från Lunds Universitets Geografiska Institution.

Pal, M., & Mather, P. M. (2005). Support vector machines for classification in remote sensing. *International Journal of Remote Sensing, 26*(5), 1007–1011.

Pal, M., & Mather, P. M. (2006). Some issues in the classification of DAIS hyperspectral data. *International Journal of Remote Sensing, 27*(14), 2895–2916.

Pal, N. R., & Pal, S. K. (1993). A review on image segmentation techniques. *Pattern Recognition, 26*(9), 1277–1294.

Paola, J. D., & Schowengerdt, R. A. (1995). A review and analysis of back propagation neural networks for classification of remotely sensed multispectral imagery. *International Journal of Remote Sensing, 16*(16), 3033–3058.

PCI. (2001). *Xpace help system* (softcopy, version 9.1). Ontario: Richmond Hill.

Price, J. C. (2003). Comparing MODIS and ETM+ data for regional and global land classification. *Remote Sensing of Environment, 86*(4), 491–499.

Qiu, F., & Jensen, J. R. (2004). Opening the black box of neural networks for remote sensing image classification. *International Journal of Remote Sensing, 25*(9), 1749–1768.

Richards, J. A., & Jia, X. (2003). *Remote sensing digital image analysis: An introduction* (3rd ed.). New York: Springer.

Richter, R. (1996a). A spatially adaptive fast atmospheric correction algorithm. *International Journal of Remote Sensing, 17*(6), 1202–1214.

Richter, R. (1996b). Atmospheric correction of satellite data with haze removal including a haze/clear transition region. *Computers & Geosciences, 22*(6), 675–681.

Richter, R. (2011). *Atmospheric/topographic correction for satellite imagery: ATCOR-2/3 User Guide*. DLR IB 565-01/11, Germany: Wessling.

Schölkopf, B., & Smola, A. (2002). *Learning with kernels*. Cambridge, MA: MIT Press.

Schott, J. R., Salvaggio, C., & Volchok, W. J. (1988). Radiometric scene normalization using pseudo-invariant features. *Remote Sensing of Environment, 26*, 1–16.

Schowengerdt, R. A. (1996). On the estimation of spatial-spectral mixing with classifier likelihood functions. *Pattern Recognition Letters, 17*(13), 1379–1387.

Schowengerdt, R. A. (2007). *Remote sensing models and methods for image processing*. New York: Academic Press.

Schroeder, T. A., Cohen, W. B., Song, C., Canty, M. J., & Zhiqiang, Y. (2006). Radiometric calibration of Landsat data for characterization of early successional forest patterns in western Oregon. *Remote Sensing of Environment, 103*(1), 16–26.

Schurmann, J. (1996). *Pattern classification: A unified view of statistical and neural approaches* (p. 373). New York, NY: Wiley.

Schultz, M. (2011). *Land cover change detection of the Vu Gia Thu Bon river basin central Vietnam*. Master Thesis, Institute of Geography, University of Jena.

Schott, J. R. (2007). *Remote sensing: The image chain approach*. USA: Oxford University Press.

Sebald, D. J., & Bucklew, J. A. (2001). Support vector machines and the multiple hypothesis test problem. *IEEE Transactions on Signal Processing, 49*(11), 2865–2872.

Smith, G. M., & Milton, E. G. (1999). The use of the empirical line method to calibrate remotely sensed data to reflectance. *International Journal of Remote Sensing, 20*(13), 2653–2662.

Shimoni, M., Borghys, D., Heremans, R., Perneel, C., & Acheroy, M. (2009). Fusion of PolSAR and PolInSAR data for land cover classification. *International Journal of Applied Earth Observation and Geoinformation, 11*, 169–180.

Singh, A. (1989). Review article: Digital change detection techniques using remotely-sensed data. *International Journal of Remote Sensing, 10*(6), 989–1003.

Song, C., Woodcock, C. E., Seto, K. C., Lenney, M. P., & MacOmber, S. A. (2001). Classification and change detection using Landsat TM data: When and how to correct atmospheric effect. *Remote Sensing of Environment, 75*(2), 230–244.

Story, M., & Congalton, R. G. (1986). Accuracy assessment: A user's perspective. *Photogrammetric Engineering and Remote Sensing, 52*(3), 397–399.

Strahler, A. H. (1980). The use of prior probabilities in maximum likelihood classification of remotely sensed data. *Remote Sensing of Environment, 10*(2), 135–163.

Su, L. (2009). Optimizing support vector machine learning for semi-arid vegetation mapping by using clustering analysis. *ISPRS Journal of Photogrammetry and Remote Sensing, 64*(4), 407–413.

Sugumaran, R. (2001). Forest land cover classification using statistical and artificial neural network approaches applied to IRS LISS-III sensor. *Geocarto International, 16*(2), 37–42.

Swain, P. H., & Hauska, H. (1977). The decision tree classifier: Design and potential. *IEEE Transactions on Geoscience and Remote Sensing, 15*(3), 142–147.

Tanre, D., Deschamps, P. Y., Devaux, C., & Herman, M. (1988). Estimation of Saharan aerosol optical thickness from blurring effects in thematic mapper data. *Journal of Geophysical Research, 93*(12), 15955–15964.

Teillet, P. M., & Fedosejevs, G. (1995). On the dark target approach to atmospheric correction of remotely sensed data. *Canadian Journal of Remote Sensing, 21*(4), 374–387.

Townshend, J. R. G., Justice, C. O., & Gurney, C. (1992). The impact of misregistration on change detection. *IEEE Transactions on Geoscience and Remote Sensing, 30*(5), 1054–1060.

Tso, B. (1997). *An investigation of alternate strategies for incorporating spectral, textural, and contextual information in remote sensing image classification*. Doctoral dissertation, School of Geography, The University of Nottingham, UK.

Tso, B., & Mather, P. M. (2009). *Classification methods for remotely sensed data* (2nd ed.). Boca Raton: CRC Press.

Van Niel, T. G., & McVicar, T. R. (2000). *Assessing and improving positional accuracy and its effects on areal estimation at Coleambally irrigation area*. Technical Report 101/00, p. 101, Cooperative Research Centre for Sustainable Rice Production.

Vapnik, V. N. (1998). *Statistical learning theory*. Chichester, New York: Wiley.

Vapnik, V. N., & Chervonenkis, A. Y. (1971). On the uniform convergence of relative frequencies of events to their probabilities. *Theory of Probability and Its Applications, 16*(2), 264–280.

Vermote, E., Tanre, D., Deuze, J. L., Herman, M., & Morcrette, J. J. (1997). Second simulation of the satellite signal in the solar spectrum, 6S: An overview. *IEEE Transactions on Geoscience and Remote Sensing, 35*(3), 675–686.

Watanachaturaporn, P., Arora, M. K., & Varshney, P. K. (2006). Sub-pixel land cover classification using support vector machines. In *Proceedings of the ASPRS Annual Conference, May 1–5, 2006, Reno, Nevada, USA*.

Watanachaturaporn, P., Arora, M. K., & Varshney, P. K. (2008). Multisource classification using support vector machines: An empirical comparison with decision tree and neural network classifiers. *Photogrammetric Engineering & Remote Sensing, 74*(2), 239–246.

Wolberg, G. (1990). *Digital image warping* (p. 318). Los Alamitos, CA: IEEE Computer Society Press.

Wulder, M. A., & Franklin, S. E. (2003). *Remote sensing of forest environments: Concepts and case studies*. Norwell: Kluwer Academic Publishers.

Yang, X., & Lo, C. P. (2000). Relative radiometric normalization performance for change detection from multi-date satellite images. *Photogrammetric Engineering and Remote Sensing, 66*, 967–980.

Zhu, G., & Blumberg, D. G. (2002). Classification using ASTER data and SVM algorithms: The case study of Beer Sheva, Palestina. *Remote Sensing of Environment, 80*, 233–240.

Chapter 6
Results, Analysis and Discussion

This chapter deals essentially with the results of this thesis, that are then followed with analysis and discussions. This chapter presents the various LULC-features classification results (the wide major classes, the irrigated areas development mapping, and the small detailed agricultural classes), and their accuracies. Factors which influence the classification results are also discussed. This chapter illustrates the various LULC-change detection mapping results (pre-classification approach results and post-classification approach results), and discusses the successes and the limitations of applying the various remotely sensed data used in this study, to satisfy investigation into the objectives of the thesis. Statistical records do not contain all elements of the irrigation projects. The second step in this research involves employing remotely sensed data to obtain statistical numbers which represent the areas in over past periods. Here, again, emerges the integration between statistical data and remote sensing data in study land uses, distribution of natural coverage and its change across time. In the first step (see Chap. 5.10), statistical numbers have been useful in the spatial determination of the spread of the targeted needed classes, and are represented in the automated classification process in order to represent the spectral characteristics of all classes. Plus the use of the total statistical records in evaluation, the accuracy of the classification needs to be determined through comparison of the final results of the automated classification with the results of the traditional human-based survey. The second step, after obtaining the training-samples from the irrigation projects which have statistical records or by using the available GPS-points as training-samples, is to determine the statistics of the regions which have no governmental statistical data.

6.1 LULC-Classification

The spatial resolution of LANDSAT 30 m makes LULC-mapping in some situations difficult as compared to other platforms such as IKONOS (4 m), SPOT-5 (2.4 m), and QUICKBIRD (less than 2 m) (Jensen 2005). Some parts of the ERB

W. Al-Fares, *Historical Land Use/Land Cover Classification Using Remote Sensing*, SpringerBriefs in Geography,
DOI: 10.1007/978-3-319-00624-6_6, © The Author(s) 2013

have strips of cultivation areas (planted: various crops, non-planted: fallow or drilled), and natural vegetation, that are less than 30 m in width and/or length (see Fig. 5.29), which were not mapped explicitly using the LANDSAT-sensor. This highlights a need to adopt more high-resolution images for this purpose, but unlike other remote sensing platforms (e.g., IKONOS, and ASTER), the LANDSAT-sensor can allow long term monitoring using data from the 1970s up until to present day (Jensen 2005).

6.1.1 The Broad Major LULC-Features

An ERB-map has been created which represents the state of five major LULC-features for the years 1975, 1987, 2005 and 2007. Table 6.1 and Fig. 6.1 provide a statistical overview of the LULC-distributions. The majority is occupied by bare lands, followed by cultivated areas, natural vegetation areas, natural water-bodies, and finally, artificial surfaces. The total area of these major classes is 5,033,537 ha.

Irrigated Aleppo's eastern plains. These plains are irrigated from the Euphrates River by pumping water from Lake Al-Asad. They extend from the south of Aleppo (near the Tall Addaman town) to the township of Maskana. The southern and southeast borders of the plains are formed by Al-Badia. The marsh of Al-Jabboul that lies east of the city of Assafira separates those irrigated plains from the southern Al-Hass mountain plains which extend to the beginning of the Syrian Desert (Al-Badia). Agriculture in the Al-Hass mountain plains often relies on rain-fed cultivation such as wheat, barley, lentil and cumin, with the omission of cotton. The Al-Badia lands that lie on the borders of the projects of east and west Maskana are protected pastoral lands, and cultivation within them is restricted to secure pastures for animals. The irrigated lands are bordered from north by a large major irrigation canal that transports water from Lake Al-Asad. North of this canal are rain-fed plantations, and in some places, artisan wells upon which the cultivation of vegetables, summer, and winter crops rely in small rates. Here, only one winter crop is planted—either wheat or barley—as ground water is rare and does not cover the need for irrigation of both crops. Recently, cumin has begun to be grown in the area and many farmers have started to cultivate olive trees, which require little water. These rain-fed cultivations extend from the irrigation canal in the south to the Turkish borders in the north.

Table 6.1 Overview of the LULC-occupations rate in several years

	1975	1987	2005	2007
Cultivated areas	1,123,268	1,316,117	1,670,625	1,783,286
Natural vegetation	562,890	710,093	686,718	403,113
Artificial surfaces	413,204	255,140	18,312	89,772
Bare areas	2,843,452	2,635,830	2,497,157	2,641,953
Natural waterbodies	90,723	102,730	160,725	109,580
Total	5,033,537	5,033,537	5,033,537	5,033,537

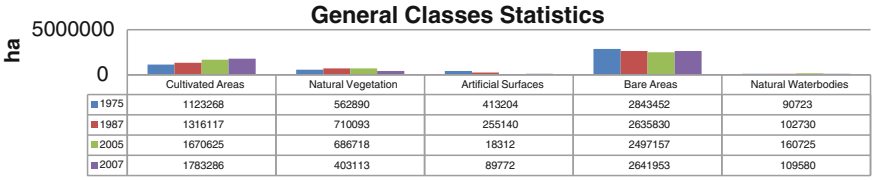

	Cultivated Areas	Natural Vegetation	Artificial Surfaces	Bare Areas	Natural Waterbodies
1975	1123268	562890	413204	2843452	90723
1987	1316117	710093	255140	2635830	102730
2005	1670625	686718	18312	2497157	160725
2007	1783286	403113	89772	2641953	109580

Fig. 6.1 Illustrated overview of the LULC-occupations rate in several years

A new project, begun in 2007 aims to redirect part of the Euphrates from the basic canal in Arbid Kabeer toward the north, to the Tadif and Al-Bab plains and ending at the village of Bershaia. This project will irrigate 5 km width of agricultural lands, using the modern technique of irrigation. In this area, wheat and cotton are largely cultivated, while peanuts and sugar beet are farmed in small spaces. Before the irrigation project, these areas featured bare land, void of planting coverage because of the scarcity of water in summer. The East Aleppo plains end at the city of Maskana and at the pumping station of Babiri. The plains of Maskana-west follow Aleppo administratively. In the winter, wheat, peanuts and sugar beet are cultivated and irrigated barley in low rates. The major cultivated summer crops are cotton, yellow corn, and low rates of vegetables and watermelon.

Therefore, these lands are all agricultural lands depending on rain-fed irrigation systems, with the exception of the recently irrigated plains of Tadif and Al-Bab, which amount to about 6,700 ha. Near Menbij City, there are individual dragging operations by pumps extending about one kilometre or more, which are detectable on the remote sensing data used.

Al-Badia/the pasture (the fifth agricultural stabilization zone) is largely classified under the general class of natural vegetation and a lesser part of bare areas. The Syrian Ministry of Agriculture defines this area as one in which precipitation is less than 200 mm per year. Al-Badia is characterized by natural plants, which are either seasonal or permanent, with different densities due to natural factors such as soil type, water recharge, and the local topography. Human factors, such as the density of the grazing, modern plantations and projects to improve pastures also have an impact.

Most of the wetlands and the water surfaces distributed in the study area were characterized by their short-term duration (except the Euphrates River). As, the large salty Al-Jabboul lake/marsh, and the marshes of Al-Haraik, Al-Adamy and Maraga are all exposed to seasonal or yearly floods, depending on precipitation amounts. The borders of these areas were represented on the thematic maps according to their expansion in spring season and in a rainy and wet year (TM-May-1987). This was done to show that the areas may sink underneath waters. As for temporal valley streams, they can be drawn digitally using topographic maps with 1/50,000 scale, for example.

In general, the detection, separation, classification and mapping of ***the roads*** (especially, the secondary roads) and the small villages, which underlie the general

class of artificial surfaces, were classified with low accuracy, using the available remote sensing data. If this is insufficient for other studies about the ERB, topographic maps offer the possibility of digitalization, from which the data can be extracted with very high accuracy. The use of other remotely sensed data with very high spatial resolution (e.g., IKONOS) is also recommended.

The problem in the separation and classification of the Earth features in the study area is the classification of the marginal land. The ability to classify these lands is linked to several factors.

The temporal factor: some lands were covered with temporary natural vegetation that grew during spring and at the beginning of summer (from March to early May). There were also very small areas covered with seasonal and permanent vegetation. Some of these areas could not be spectrally separated or classified from the surrounding bare areas because their spectral and spatial resolutions were insufficient. Another reason was the dispersion of vegetation that dominated the spectral reflectance of dry soils, particularly those that had light colours. Also, because of the presence of the natural vegetation during the synchronism season with cultivation of winter crops, there emerges the problem of spectral integration/mixing of these vegetation with one or more types of the agricultural crops classes. The presence of these marginal lands in the sensory data of August, led to the disappearance (or semi-disappearance) of the spectral correlation problem between the marginal lands that were covered with the temporarily natural coverage of vegetation during the spring months. Between the lands with agricultural crops this natural coverage almost vanished in August because of the absence of precipitation and domination of drought. But, in contrast, the remotely sensed data taken in August had the problem of spectral correlation of the marginal lands with the spectral characteristics of the fallow lands, especially if they were covered with light soil.

The spatial factor: the presence of these lands within the irrigated agricultural projects increased the problem size since more details were required concerning the credited classification system levels, where green areas were classified into several classes/agrarian crops. The presence of marginal land outside the borders of the irrigated areas was a secondary problem with only slight effects (here, a general degree of classification was required, i.e., 5 classes, where green areas were classified into two agricultural lands with all of their crops and classes, and natural vegetation).

The climatic factor: the rain-element determined prevalence, location and density of the natural vegetation, and as a result, it controlled the spectral behaviours which changed permanently according to time, place, kind of soil and amount of precipitation. Consequently, the spectral behaviour of these natural plants might look similar and correlate with a spectral behaviour of a crop (barley for example). This behaviour is likely to change across time from one year to another, and perhaps even in the same season and location/field, since, the natural plants may correlate with other spectral response of crops other than barley (e.g., wheat).

LANDSAT-MSS-June-1975 data. By classifying the study area using several scenes included in one mosaic-scene, it was possible to make classifications for only three classes (i.e., the cultivated areas, uncultivated areas and water areas).

There was a mixing between cultivated and uncultivated areas, particularly, in the inactive volcano cones area, which is found to the east of the city of Arraqqa, where dark colour soils are interrelated with fallow lands. Also, there were mixing and misclassification concerning water and cultivated areas, particularly in river areas with narrow width and shallow depth. It was possible to integrate the volcano area into the uncultivated areas by manually drawing the borders of the area in the form of vector-shapes. There was also significant mixing between fallow and bare areas, meaning the separation and classification between artificial surfaces and bare areas was impossible.

Each scene was classified separately after sub-setting based on the borders of study area. After that, classification results scenes were collected in one mosaic-scene (Fig. 6.2). Thus, the classification results were better rather than the above mentioned situation, as it was possible to obtain the five needed general classes. These results were improved for several reasons: technically, returning to the used remotely sensed data itself, where, whatever the quality of the present algorithms to correct satellite scenes that contain differences in their radiometric characteristics, they were not accurate 100 % of the time. Hence, using every scene separately ensured the spectral behaviour towards all Earth surfaces features (and the probable variations within each feature alone). The natural reasons for this included: The large size and extension of the study area and its relation with the geographical location that controlled the natural climatic characteristics (especially the precipitation-factor), led to variation in Earth surface features and consequently in their spectral behaviour on satellite images. This is turn provided

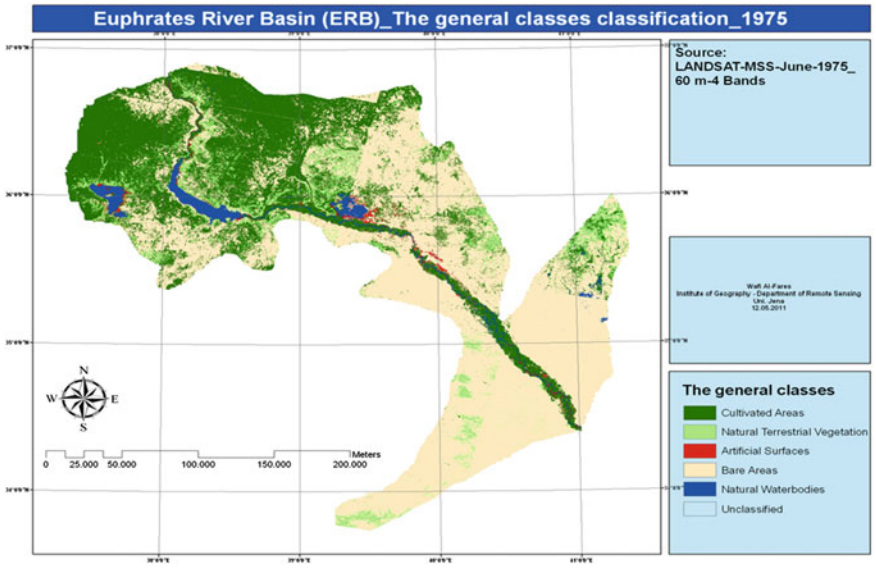

Fig. 6.2 The spatial distributions classification of the five major LULC-categories in the ERB for the data of LANDSAT-MSS acquired in June-1975

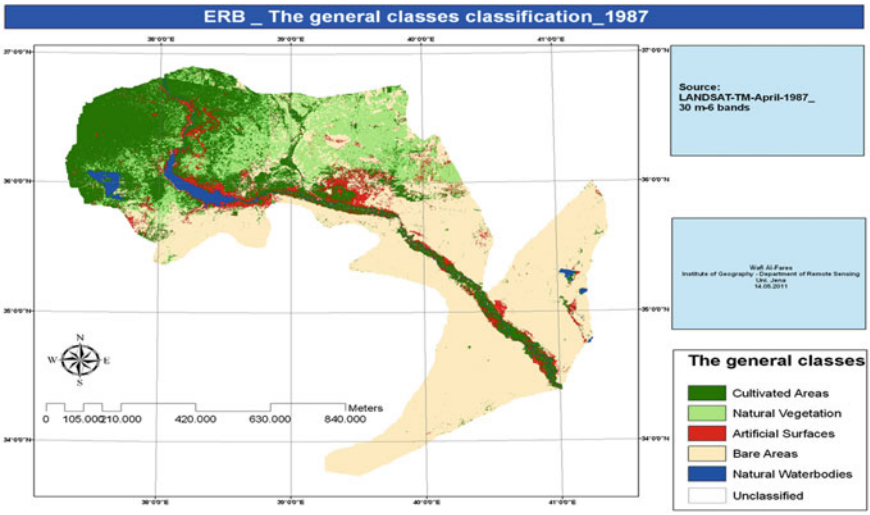

Fig. 6.3 The spatial distributions classification of the five major LULC-categories in the ERB for the data of LANDSAT-TM acquired in May-1987

more details and information within the image but with the decreased possibility of spectral separation between the features of interest (indicating that, spectral separation increases or decreases according to the used sensor and its techniques).

One of the negatives reflected by the classifying of each scene alone was the emergence of separating borders between two neighbouring scenes after the mosaicing-process, which meant there was no continuity in representing the prevalence of features and classes naturally and spatially. This problem was limited by use of a "majority-filter".

LANDSAT-TM-May-1987 data. This coverage was one of two coverages (in addition to the LANDSAT-TM-May-2007 coverage) which were used to produce a map of the change detection which has occurred in the past 20 years, through the application of the post-classification change detection approach. During the classification of both coverages into the five basic classes (Fig. 6.3), there was a mistake in classifying some areas of rain-fed cultivations as natural plant lands, because the most rain-fed plantations have a low density vegetal biomass, making them close to that which characterizes natural plants.

There was an increase in ratio of classification (over-classification) of the artificial surfaces specifically in volcano areas and Lake Al-Asad's banks, and also in some bare areas. The reason for this is that as is the case with the MSS, the negation or the lack of success ratio of radiometric correction imbued the radiometric properties of the same land features distributed in the several satellite scenes (i.e., those that construct the mosaic-scene), with similar or at least enough approximate compatible value/s. So, to overcome this problem, it was necessary to classify each image alone and then create mosaic-processes of scenes of the automated classification results.

The mixing between the natural vegetation class and the rain-fed based crops areas was lesser than it was in the LANDSAT-TM-May-2007 coverage. Also, the total water area was lesser than it was in the 2007-coverage, because of the recently constructed dams. There were areas located in the five agricultural stabilization zones, that classified in 1987-coverage as cultivated, but were reclassified in 2007-coverage as natural vegetation and/or bare areas. This was related to the prevention of agriculture after 1990 in the fifth agricultural stabilization zone.

There was also (using the all available remote sensing data for this study) a problem in separation and misclassification between fallow and bare areas with dark soils colours.

The ability to separate the inactive volcanoes area from the dark colored fallow fields and classify them, is better rather than with the MSS, because the higher spatial and spectral resolution of TM.

Another problem detected while using TM-data was correlation between the Euphrates River waters in the shallow and less wide areas because of the number of the training samples concentrating on cultivated lands at the expense of the water areas. However, this problem was overcome by increasing the number of the representative training samples of the water, which were distributed suitably over the whole borders of Euphrates River.

TERRA-ASTER-May-2005 data fused with LANDSAT-ETM+-May-2005 data. These data were found to be optimal in classifying the ERB to the 5 general LULC-classes (Fig. 6.4), especially for classifying the artificial surfaces which had been classified with poor accuracy using the 3 other data-coverages. So, their outcomes of classification can be considered as a base when more accurate statistical information is required about the distribution of the general classes within the ERB.

LANDSAT-TM-May-2007 data. There was a problem in spectral separation between the inactive volcanoes area with dark colour and the fallow lands. Yet, after drawing a large ROI in the volcano area, the spectral separability increased from 1.61 to 1.78. This accentuated the high significance of the process in selecting the training-samples and the bases it included (number of the experimental areas that represented each class, area or total areas of the samples for each class, the shape of the samples whether pixel or polygon, and the geographical spatial distribution of these training samples within the study area).

There was a limited spectral correlation between natural vegetation and the cultivated areas, particularly those lands of rain-fed plantations, because of their similarity in the green vegetation bio-mass (Fig. 6.5).

6.1.2 The Temporal Development Mapping of the Irrigated Areas

In Syria, the majority of irrigation projects were devised for two main crops, wheat in winter and cotton in summer. However, since the 1990s other crops have emerged, such as yellow corn, sunflower, peanuts and watermelon. These new

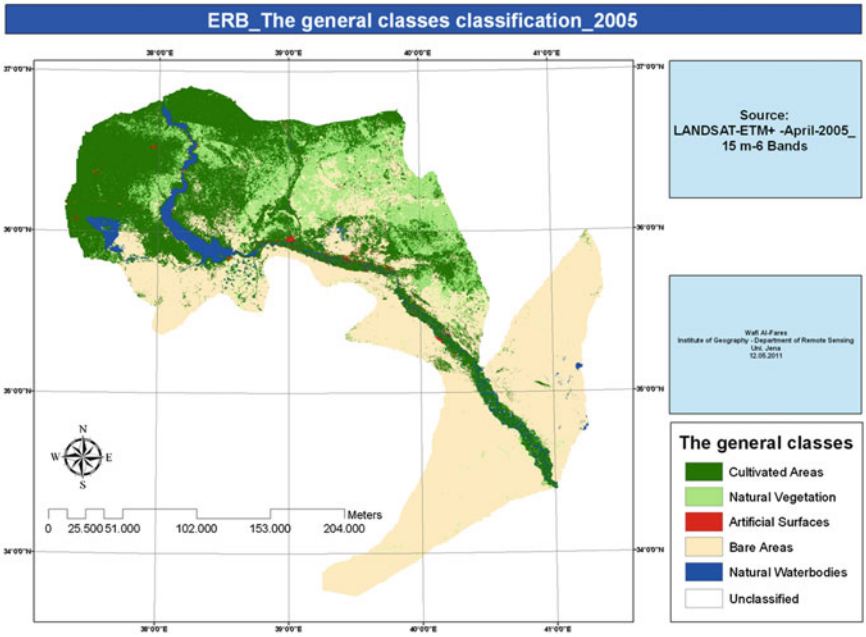

Fig. 6.4 The spatial distributions classification of the five major LULC-categories in the ERB for the data of TERRA-ASTER fused with LANDSAT-ETM+/SLC-Off/corrected acquired in May-2005

species have started to compete with the two main crops, because of their better financial outcomes and the possibility of farming fields for three seasons instead of two. Figure 6.6 presents the temporal development of the irrigated areas for the years 1975, 1987, 2005, and 2007 using different remotely sensed data. Table 6.2 presents the statistics of the extension of the irrigated areas over different times. It presents also the areas rates of the other two general classes, i.e., uncultivated areas and water.

Cultivation of sugar beet within the irrigation areas has clearly decreased (Table 6.3), because the high salinity of soil and irrigation water, which make the crop less sweet. At present, this crop is mainly used as animal feed.

The agrarian plains directly on the banks of the Euphrates River, specifically, those extending from Arraqqa to Deir Azzour, are relatively small extended plains in a north–south direction. They are mainly limited between high rocky cliffs (old river terrace) in the south and the Al-Badia/pasture in the north. After passing the pasture Al-Badia, the agrarian lands emerge again in the second, third and fourth agrarian settlement areas. The river plains are characterized by their very small fields and variation of crops even in the one field. Many farmers divide their fields into parts—a section for economic income, one for providing animals with food, and another for vegetables and fruit for domestic use. These plains are crossed by lots of trees and scattered houses. These factors decrease the ability of the used

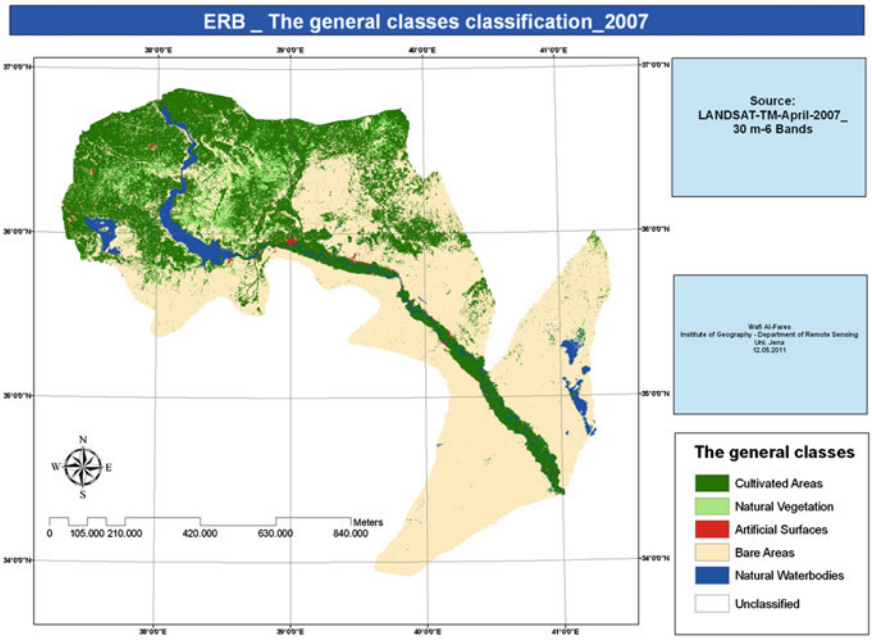

Fig. 6.5 The spatial distributions classification of the five major LULC-categories in the ERB for the data of LANDSAT-TM acquired in May-2007

satellite data to discriminate various interrelated land uses, to classify them and map their borders and spatial prevalence.

There are some small areas within the project of west Maskana which were classified as cultivated irrigated lands in 1987, although investment in this project began after this date. These irrigated areas are centred in valleys and seasonal small rivers (e.g., Quieck and Azzahab), while others depend on artisan wells for irrigation.

6.1.3 Distinguishing, Classification and Areas Measurement of the Strategic Crops

LANDSAT-TM-May-1987 data. The separability and classification of alfalfa during its presence with the winter crops is higher than when it is included with summer crops, since alfalfa mixes spectrally with corn. Hence, the cultivated lands with alfalfa are gathered to the created mask for trees (i.e., fruit, poplar trees, grapevines, and other trees and shrubs located in cities, residence areas, and on the Euphrates River banks).

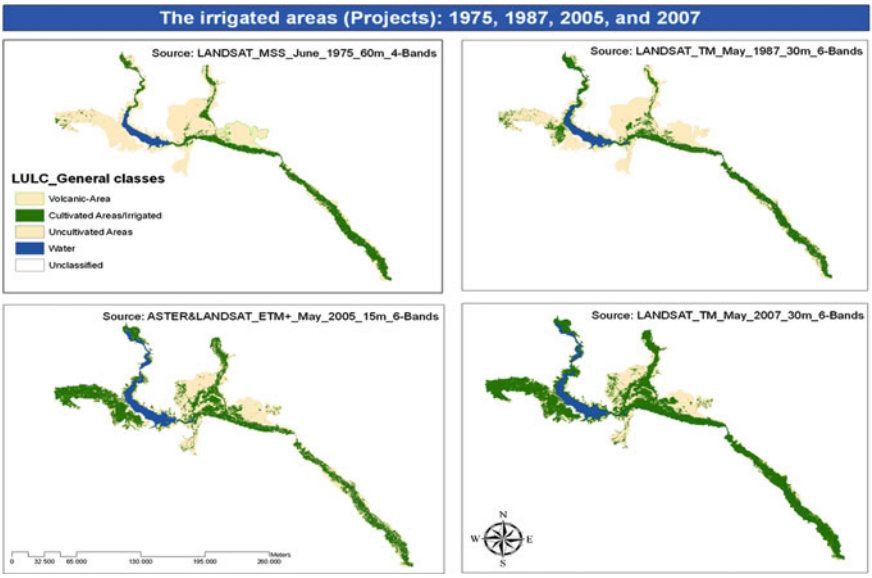

Fig. 6.6 The final irrigation mapping thematic maps, which explain the temporal development of the spatial distribution expansion of the irrigated areas during the last three decades using various remotely sensed data

Table 6.2 The areas rates of the three wide existing general classes based on the irrigated areas level

	1975	1987	2005	2007
Cultivated areas	249,681	301,517	458,288	596,612
Uncultivated areas	673,992	607,925	430,129	294,633
Water	52,030	65,980	87,284	84,347

Some areas which are considered as agriculturally uncultivated, such as the mask created from sensory data taken in May for uncultivated areas, were shown as cultivated lands on satellite images taken in August. Hence, an error in automated classification results due to the masking-process has been made.

The majority of winter and summer cultivation is centred in Deir Azzour governorate (Fig. 6.7); winter vegetable areas are remarkably rare in Arraqqa; instead while cultivation increases in summer. Sugar beet propagation is focused in Deir Azzour, while in Arraqqa there is comparatively little. Corn, cotton and sesame are equally distributed throughout the three governorates. Barley is the major crop among rain-fed crops, followed by wheat, lentils, cumin and chickpeas.

The spectral separability between vetch and barley is fair but not good (1.70) because of the interrelation of their planting in some areas, where vetch plant (Thamilip/charged) and barley are both considered forage crops. The separability

Table 6.3 The areas rates of the three wide existing general classes and the various agriculture features based on the irrigated areas level

			1975	1987	2005	2007
Cultivated areas			249,681	301,517	458,288	596,612
	Trees + shrubs			2,137	26,148	27,206
	Herbaceous (permanent- and winter-crops)			163,402	162,211	262,294
		Alfalfa		23,608		
		Vetch		2,328		
		Wheat		53,013	131,881	188,688
		Barley		4,902	19,423	16,299
		Sugar beet		2,349	7,683	1,803
		Rain-fed crops		37,707		
		Other crops		39,495	3,224	55,504
	Fallow			135,978	269,929	307,112
	Herbaceous (summer-crops)			111,968	183,334	126,207
		Cotton		67,881	136,392	37,475
		Corn		33,519	31,198	25,481
		Other crops		10,568	15,744	63,251
	Fallow			189,549	274,954	470,405
	Cropped_total			301,517	371,693	415,707
Uncultivated areas			673,992	607,925	430,129	294,633
Water			52,030	65,980	87,284	84,347

between irrigated barely and the rest of the rain-fed crops is good to some extent (1.83).

There was difficulty in the separation between the light fallow lands (as the training samples were selecting on purely fallow areas) and the uncultivated areas, including the artificial surfaces within the irrigation areas, to build the mask that represents the cultivated areas, under which the classification was carried out for agriculture features. To overcome this, the merging of training samples of both fallow and cropped areas offered better results in separation.

The differentiation in the spectral response of the winter crops (and the variation within each type) was limited by the early periods of vegetative germination of crops (March), which increased continuously until they reached their peak/s during April and early May, and then began to decline and disappear.

LANDSAT-TM-August-1987 data (Fig. 6.7). The problem of spectral correlation and separation between the uncultivated areas and the fallow was raised whether using remotely sensed data of May or August. It was, in general, less effective in August-data, where the separability reached 1.85, and where the most correlation was seen within the artificial surfaces. Here the question was raised

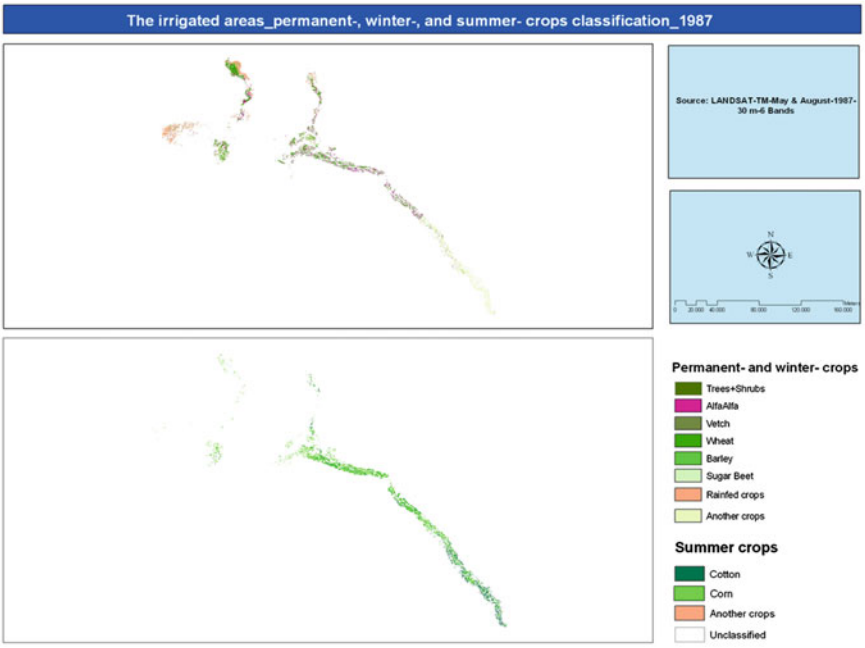

Fig. 6.7 The classification of the major permanent, winter and summer irrigated crops within the irrigation projects in the ERB for the data of LANDSAT-TM acquired in May and August 1987

"Why are the uncultivated areas again classified since the classification method relies on the hierarchical approach using the mask-process, which separated the uncultivated areas from the cultivated areas (including the fallow) in the previous classification level?"

The answer, previously mentioned (see Chap. 5.7.1.2.1), is that the hierarchical approach of classification has its drawbacks that lead to mistakes in the results just like any other approach. Accumulative errors result in those negatives brought by production/extraction of the mask's layer either counting on results of supervised or unsupervised classification, NDVI or others; or where, these credited approaches cannot reach a degree of perfection in spectral separating of the Earth surface features or the other classes of interest. This can also occur if these traditional approaches of classification have the ability to reach a suitable rate in spectral separation and classification. The hierarchical approach was not used in the classification process or in the creation of the masks at each classification level as it costs effort and time. As suggested in Fig. 5.35, the classification process was repeated on the classes which were not classified and completely extracted during the last classification process. The use of this approach was to increase the classification accuracy (the final product that resulted from collecting outcomes of each level and stage of the hierarchal classification), through a decreasing number of features and classes which exist in the study area, either by eliminating some

features out of classification process (i.e., insignificant classes in irrigated agricultural projects such as bare areas), or postponing classification to the next stage if spectrally possible. Here, the significance of the accredited methodological approach in building up the used classification system emerged, in the reduction of the number of classes in each stage of classification and the securing of some reduction in the spectral mixture.

One of the positives of the hierarchal principle is to reduce the effect of the geographical location and the natural and climatic properties that affect the spectral behaviour of the studied Earth surface features, specifically, if the study area is within a wide geographic distribution, peppered with large diversion in natural and climatic characteristics. For example, making a mask of the distribution of irrigated plantations gives a natural harmonious area, since all the cultivations here are irrigated and the majority of soils have close colours and close content of humidity, etc. The greater the study area with a geographic and spatial distribution featuring the same or similar natural and climatic characteristics, the more likely homogeneity will be achieved in the spectral response of the Earth surface features contained in the study area. This trait does not exist in the geographical and spatial distribution of the Euphrates River Basin, since, for example, the spectral behaviour of bare areas will be in the dozens.

One of the more significant positives of the masking process was the reduction in the problem of spatial correlation which produces classification errors, as well as separating borders areas and/or the mutual areas between two classes or more (the negative impact increases wherever the spatial resolution decreases and the spectral variation rises). This was most effective when the areas of the class (other crops) were over-classified. Taking into consideration that the mask layer resulted in application of the NDVI has meant a few of the agricultural areas were neglected.

Making automated classification on sensory data after applying the mask (through use of the option: apply mask in ENVI-program) and integrating the mask layer with/or on the satellite scene with spectral bands (layer stacked), will decrease the separability between the spectral signatures created from the training samples. Consequently, automated classification was conducted directly on sensory data through selecting the option of using mask in the ENVI-program.

The classification of water was more effective when using the remotely sensed data acquired during the summer season (e.g., August).

The reason that the corn was over-classified in some cases, was probably to do with the mixture between the lands that were cultivated previously with wheat during the winter season. This occurred when the wheat residues were not burnt or tilled, and the fields remained covered in yellowish dry residues (straw). In addition, some plants grew naturally after the harvesting of the wheat.

TERRA-ASTER-May-2005 data fused with LANDSAT-ETM+-May-2005 data. There was no negative or positive impact for using thermal spectral and panchromatic bands on the spectral discrimination and the separation between various crops, trees and other surface features in the study area. Therefore, they were dispensed in the automated classification, especially, the panchromatic

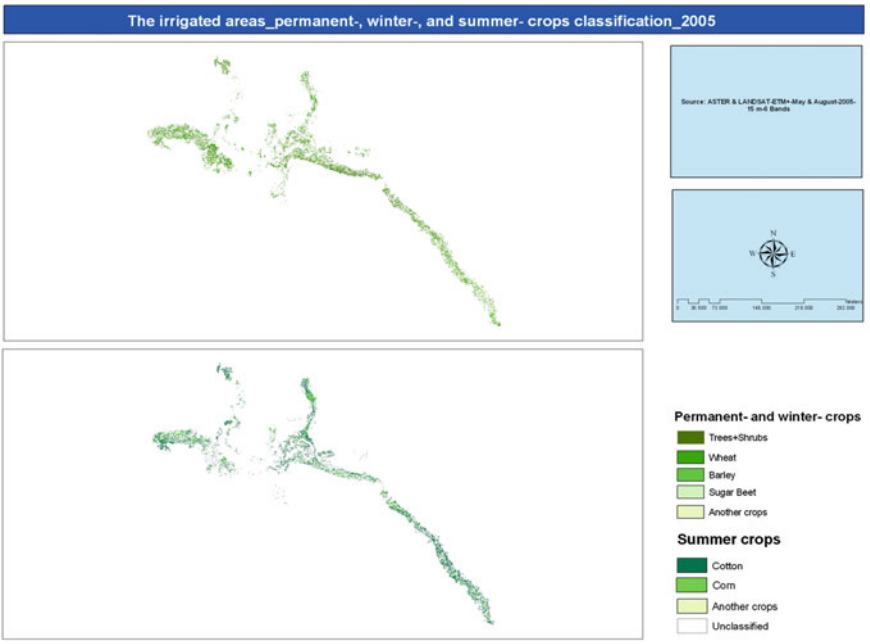

Fig. 6.8 The classification of the major permanent, winter and summer irrigated crops within the irrigation projects in the ERB for the data of TERRA-ASTER and LANDSAT-ETM+ acquired in May and August (2005)

bands, to decrease the time of classification. Hence, participation of these bands became a negative factor regarding to the time taken required for classification.

An error was also detected in classifying some constructional areas as well as some limited areas from the bare areas considered as fallow lands (Fig. 6.8).

Sugar beet was perfectly classified. Other crops classes were broken in form of lines among fields, either in the shape of trees, shrubs, bushes and fences, or as natural plants and crop residues.

The spectral mixture between wheat and barley was found mostly in the higher areas of the ERB (fortunately, the cultivation of irrigated barley is rare here), while further down the basin in the Deir Azzour governorate, the spectral separation ratio was reported as good because the majority of irrigated barley is a pastoral barley.

There was no large difference in the spectral separability and discrimination between the various agrarian crops in areas featuring irrigation projects and large, organized fields, either using the TM-data with spectral resolution of six bands and spatial resolution of 30 m, or the ASTER/ETM+-data with the same spectral resolution and a higher spatial resolution of 15 m. There was also no significance in obtaining or using sensory data of larger spatial resolution than 30 m; consequently, the negatives of this were the increases in time, cost and effort. The ASTER-data with the spectral resolution of three bands and a spatial resolution of

15 m were tried on large area fields, and the outcomes of spectral separability and classification were compared with data outcomes of the TM/6-bands/30 m. The result was that the high spatial resolution 15 m could be dispensed with, without lowering the spectral separability among crops.

But, a high spatial resolution data, such as ASTER/ETM+−15 m, was found to be useful when studying ancient and tiny agrarian areas, such as those centred along the banks of the Euphrates (from the Euphrates Dam to the border with Iraq). For this kind of research, it may even be preferable to use even higher spatial resolution while preserving the six spectral bands.

TERRA-ASTER-August-2005 data fused with LANDSAT-ETM+−August-2005 data. The appearance of fruit, poplar and other trees within dwelling areas and their margins were seen in a better and clearer way on satellite images acquired during summer (August) (Fig. 6.8) in contrast to those images acquired in April and May. There was a severe decline in the spectral properties of forest trees that previously existed in multiple places along the banks of Lake Al-Asad and the Euphrates River, in favour of the power and superiority of the spectral reflectance of light soil. This is due to the lowering of moisture and the dryness of the green mass of the forest trees (some are even crusty), in addition to an increase in sunshine levels.

The appearance of fields within the irrigated agriculture projects in very light colours made them look as if they were bare areas, while they were in fact wheat and barley fields seen after harvest (covered by the green mass of ex-crops that remains a very light yellow colour). These fields had been left for grazing purposes or the residue would be collected for use as hay during winter. In summer, these fields appeared after harvesting as a black colour as if they were water surfaces because of the residue left after burning. Here, the importance of the analyst's role in knowing his or her study area is important.

The third appearance the wheat and barley fields after harvesting was in a form in which the dry yellow remains of green mass (straw) of the 2 crops interacted with several kinds of natural plants that grew in these fields, benefitting from the remaining soil moisture. This occurred when the fields were not tilled. This field shape had a negative impact on summer crops classification, as the growing natural plants have a high vegetarian intensity, high vital mass and similar spectral behaviour as the some of the summer crops' spectral response. These fields were classified as fallow.

The cultivation of trees for agriculture purposes was centred in particular within the irrigation projects (especially poplar trees), in addition to their distribution along the main streets, between the agrarian fields (as separators between the fields or as wind barriers), and along some irrigation canals that were largely within the irrigation projects or reclaimed lands. This also related to the agriculture of forest trees (pine and cypress) in particular on Lake Al-Asad's banks.

Aquatic plants appeared clearly and were distributed more evidently within the August coverage in contrast to May, either in the Euphrates River waters (mosses were seen in shallower locations) or within prevailing swamps stretching out along the river, where the deserted river elbowed. These were seen along the river's bank

in an almost continuous linear way. Climatic factors played a basic role in this by providing moisture and temperature elements, with the ratio of aquatic plants rising in August due to the high number of sun accelerating the growth and density of the plants.

The increase of variation and differentiation in reflectance and in the spectral behaviour of plants (crops and trees) within the coverage of August was greater than that found in the May data.

Grapevine lands were classified under the orchard class. This was a new type of agriculture cultivation in the study area, which started at the beginning of this present decade in limited areas.

The appearance of some tree-lands (especially, the orchards) on satellite images is unclear, although these areas were irrigated and took on a regular and organized engineering shape. This was because of the disproportion among adapted distances in the cultivation of trees and their spacing from each other, and the available spatial resolution of the used remotely sensed data. They were in most cases classified as fallow or sometimes as a type of crop, although not to tree class.

The problem of classifying poplar trees was represented in that a land plot may be planted with trees of differing ages. Additionally, permanent cutting of part of these trees to be used in the paper, pulp and wood industry led to a mixture in classification from poplar trees to fallow. The problem lay not in how to separate these areas spectrally but in spatial separation resulted in continuous alternation between the two classes within small spatial areas, which allowed some errors to occur in evaluation and the calculation of distribution area. The spatial resolution of the available remotely sensed data did not have the ability to represent this alternation and introduce the spatial boundaries to separate the two classes. This coverage was found to be the best for separation between the uncultivated areas and the fallow areas.

LANDSAT-TM-August-2007 data. Sand storms emerged on the August data, which caused great changes in the spectral characteristics of the elements that needed to be classified. This impact was on p172r035 acquired in 07.08.07 along the extended area between Arraqqa and Deir Azzour.

It was noticed that in the past years within the irrigation projects (for instance, the previously referenced project of 21,000 ha), the cultivated areas with specific crops were significantly smaller (Fig. 6.9) in contrast to the beginning of these projects' establishment and for long periods, where regular agricultural policies were followed. The reason for this is likely to be that the governmental foundations who established the projects have since transferred management of the projects in favour of the farmers, who are not, in turn, committed to any agrarian policy and rotations accredited by the Ministry of Agriculture. This matter had a critically negative impact on the crops' classification using available data. The spatial resolution became less effective because of the limited area specified for the various crops' cultivation. This was the same negative impact in consideration to the spectral factor, because of the increase in the types of crops seen in this area (possibility of setting two comparative scenes of 1987 and 2007).

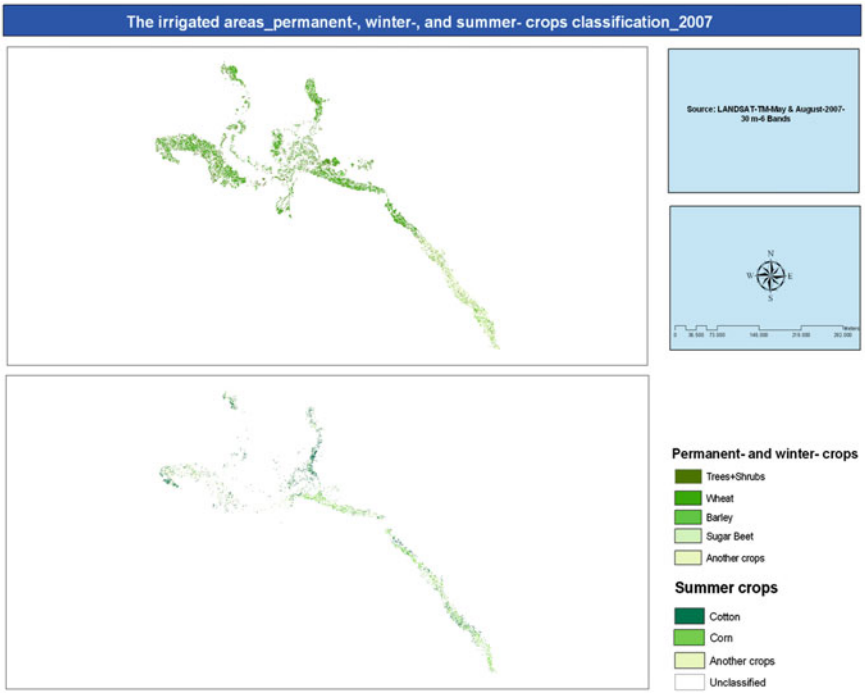

Fig. 6.9 The classification of the major permanent, winter, and summer irrigated crops within the irrigation projects in the ERB for the data of LANDSAT-TM acquired in May and August 2007

Table 6.4 presents the areas rates of the three broad existing classes (cultivated areas, uncultivated areas, and water) and the various agricultural features (permanent-, winter-, and summer-crops) within each adapted irrigation project borders for the time periods 1975, 1987, 2005, and 2007. Finally, this table presents the total area of each above mentioned class within the whole adapted borders of the different irrigation projects for the same four time periods (see too Tables 6.2 and 6.3).

6.2 Accuracy Assessment Comparisons

Table 6.5 shows the final comparison between the various accuracies of classification results. There was no classification achieved for the class/es with no accuracy value/s (e.g., alfalfa was included in the coverage of 1987 under broadly cultivated, but later the cultivated alfalfa areas were very small, thus it was included under the class of other crops). In general, the lower accuracies were made using MSS-data, while the higher were found by using ASTER-data fused

Table 6.4 The areas rates of the three wide existing general classes and the various agriculture features based on the individual 16-irrigated projects level

	Cultivated areas (ha)									
	Total	Permanent crops Trees + shrubs	Alfalfa	T	Winter crops Wheat	Barley	Sugar beet	Vetch	Rain-fed-crops	Other crops
17,000 ha-project and the state farm_75	5	n	n	n	n	n	n	n	n	n
1987	15,648	800	767	1,567	4,359	2,310	201	1,026	2,034	367
2005	23,479	2,565	0	2,565	12,904	673	8	0	0	2,321
2007	26,367	4,364	0	4364	12,877	1,033	116	0	0	2,172
Al-Asad lake area_75	3,175	n	n	n	n	n	n	n	n	n
1987	523	5	47	52	305	0	0	8	1	19
2005	4,544	462	0	462	2,412	193	25	0	0	3
2007	7,865	2,490	0	2,490	3,030	513	27	0	0	754
AL-Balikh basin_beer Al-Hishm section_75	164	n	n	n	n	n	n	n	n	n
1987	6,518	0	492	492	1,306	1,204	8	651	1,733	2
2005	10,015	313	0	313	4,633	207	124	0	0	82
2007	8,584	338	0	338	5,060	272	39	0	0	74
Al-Balikh basin_lower mean canal section_75	8,174	n	n	n	n	n	n	n	n	n
1987	2,759	0	1	1	1,000	35	14	29	163	92
2005	15,067	184	0	184	4,949	648	57	0	0	0
2007	11,124	643	0	643	4,408	132	28	0	0	71
Al-Balikh basin_section-2_75	8,924	n	n	n	n	n	n	n	n	n
1987	16,674	34	1,165	1,199	2,955	0	0	0	64	175
2005	14,146	1,152	0	1,152	3,927	543	271	0	0	0
2007	17,268	1,715	0	1,715	9,754	1,287	98	0	0	11

(continued)

Table 6.4 (continued)

	Cultivated areas (ha)									
		Permanent crops			Winter crops					
	Total	Trees + shrubs	Alfalfa	T	Wheat	Barley	Sugar beet	Vetch	Rain-fed-crops	Other crops
Al-Balikh basin_section-3-western_75	0	n	n	n	n	n	n	n	n	n
1987	252	0	57	57	60	2	0	12	17	0
2005	567	16	0	16	332	29	15	0	0	0
2007	924	32	0	32	532	66	2	0	0	37
Al-Balikh basin_section-3_Mlihan and Aadman area_75	0	n	n	n	n	n	n	n	n	n
1987	35	0	16	16	0	0	0	0	11	8
2005	2,159	17	0	17	1,651	197	7	0	0	0
2007	3,749	617	0	617	3,058	42	0	0	0	0
Al-Balikh basin_section-4_75	168	n	n	n	n	n	n	n	n	n
1987	144	0	28	28	5	0	0	0	78	1
2005	6,552	51	0	51	3,790	88	8	0	0	2
2007	13,997	800	0	800	10,637	1,173	121	0	0	117
Al-Balikh basin_sections-5 and 6_75	15,990	n	n	n	n	n	n	n	n	n
1987	13,040	23	1,810	1833	4,637	48	549	5	4,302	297
2005	25,488	290	0	290	8,732	733	139	0	0	10
2007	28,909	1,436	0	1,436	14,868	1,821	210	0	0	497
Arraed project_75	11,735	n	n	n	n	n	n	n	n	n
1987	20,243	186	2,808	2,994	6,156	480	113	278	1,397	113
2005	20,194	2,396	0	2,396	6,960	1,003	1,434	0	0	94
2007	20,505	3,355	0	3,355	10,226	394	107	0	0	614
Arrusafa area_75	2,914	n	n	n	n	n	n	n	n	n
1987	1,510	2	344	346	589	2	1	173	86	76
2005	7,262	455	0	455	4,836	167	70	0	0	0
2007	10,572	1,257	0	1,257	7,502	268	44	0	0	20

(continued)

Table 6.4 (continued)

	Cultivated areas (ha)									
	Total	Permanent crops Trees + shrubs	Alfalfa	T	Winter crops Wheat	Barley	Sugar beet	Vetch	Rain-fed-crops	Other crops
Lower Euphrates_75	124,523	n	n	n	n	n	n	n	n	n
1987	109,194	29	4,812	4841	6,599	0	2	0	3	37,218
2005	109,384	7,303	0	7303	23,125	12,162	3,791	0	0	1?
2007	119,115	3,577	0	3,577	20,016	6,347	461	0	0	49,234
Maskana east_75	0	n	n	n	n	n	n	n	n	n
1987	286	0	0	0	0	5	0	0	18	0
2005	12,836	654	0	654	7,509	169	0	0	0	59
2007	19,816	434	0	434	13,523	1,085	40	0	0	70
Maskana west_75	0	n	n	n	n	n	n	n	n	n
1987	18,885	15	666	681	476	468	814	6	16,077	147
2005	56,625	504	0	504	26,363	1,251	70	0	0	618
2007	62,205	2,500	0	2,500	35,866	440	335	0	0	510
Middle Euphrates_right and left Bank_75	41,514	n	n	n	n	n	n	n	n	n
1987	44,753	153	5,810	5,963	10,930	4	31	21	66	421
2005	40,035	7,796	0	7,796	12,008	731	1,630	0	0	0
2007	33,983	1,081	0	1,081	20,205	775	145	0	0	76
Upper Euphrates_75	25,180	n	n	n	n	n	n	n	n	n
1987	33,488	886	3,739	4,625	13,695	341	607	115	11,589	552
2005	23,107	2,004	0	2,004	7,619	617	26	0	0	32
2007	29,834	2,322	0	2,322	16,686	512	22	0	0	1,218
Sum_1975	249,681	n	n	n	n	n	n	n	n	n
Sum_1987	301,517	2,137	23,608	25,745	53,013	4,902	2,349	2,328	37,707	39,495
Sum_2005	458,288	26,148	0	26,148	131,881	19,423	7,683	0	0	3,224
Sum_2007	596,612	27,206	0	27,206	188,688	16,299	1,803	0	0	55,504

(continued)

Table 6.4 (continued)

								Unculti-vated areas (ha)	Water (ha)
	T	Fallow	Summer crops Cotton	Corn	Other crops	T	Fallow	T	T
17,000 ha-project and the state farm_75	n	n	n	n	n	n	n	46,325	0
1987	10,297	3,784	3,453	311	20	3,784	10,297		
2005	15,906	5,008	3,966	1,041	1	5,008	15,906		
2007	16,198	5,805	923	23	4,859	5,805	16,198		
Al-Asad lake area_75	n	n	n	n	n	n	n	37,845	38,124
1987	333	138	105	3	30	138	333		
2005	2,633	1,449	1,167	144	138	1,449	2,633		
2007	4,324	1,051	267	118	666	1,051	4,324		
AL-Balikh basin_beer Al-Hishm section_75	n	n	n	n	n	n	n	24,909	0
1987	4,904	1,122	1,010	62	50	1,122	4,904		
2005	5,046	4,656	3,748	905	3	4,656	5,046		
2007	5,445	2,801	1,365	22	1,414	2,801	5,445		
Al-Balikh basin_lower mean canal section_75	n	n	n	n	n	n	n	21,771	10
1987	1,333	1,425	783	567	75	1,425	1,333		
2005	5,654	9,229	7,561	1,654	14	9,229	5,654		
2007	4,639	5,842	3,331	447	2,064	5,842	4,639		

(continued)

Table 6.4 (continued)

								Unculti-vated areas (ha)	Water (ha)
	T	Fallow	Summer crops Cotton	Corn	Other crops	T	Fallow	T	T
Al-Balikh basin_section-2_75	n	n	n	n	n	n	n	45,373	197
1987	3,194	12,281	5,089	1,150	42	6,281	9,194		
2005	4,741	8,253	6,534	1,074	645	8,253	4,741		
2007	11,150	4,403	1,465	1,449	1,489	4,403	11,150		
0	n	n	n	n	n	n	n	2,174	0
1987	91	104	95	9	0	104	91		
2005	376	175	181	3	0	184	367		
2007	637	255	45	0	210	255	637		
Al-Balikh basin_section-3_Mlihan and Aadman area_75	n	n	n	n	n	n	n	46,599	0
1987	19	0	0	0	0	0	19		
2005	1,855	287	285	2	0	287	1,855		
2007	3,100	32	32	0	0	32	3,100		
Al-Balikh basin_section-4_75	n	n	n	n	n	n	n	86,564	0
1987	84	32	0	0	32	32	84		
2005	3,888	2,613	1,908	705	0	2,613	3,888		
2007	12,048	1,149	498	2	649	1,149	12,048		
Al-Balikh basin_sections-5 and 6_75	n	n	n	n	n	n	n	38,897	86
1987	9,838	1,369	594	742	33	1,369	9,838		
2005	9,614	15,584	10,918	4,654	12	15,584	9,605		
2007	17,396	10,077	6,135	334	3,608	10,077	17,396		

(continued)

Table 6.4 (continued)

								Unculti-vated areas (ha)	Water (ha)
			Summer crops						
	T	Fallow	Cotton	Corn	Other crops	T	Fallow	T	T
Arraed project_75	n	n	n	n	n	n	n	38,907	135
1987	8,537	8,712	7,484	1,105	123	8,712	8,537		
2005	9,491	8,307	7,113	888	306	8,307	9,491		
2007	11,341	5,809	1,553	837	3,419	5,809	11,341		
Arrusafa area_75	n	n	n	n	n	n	n	23,958	7
1987	927	237	212	2	23	237	927		
2005	5,073	1,734	1,543	80	111	1,734	5,073		
2007	7,834	1,481	371	111	999	1,481	7,834		
Lower Euphrates_75	n	n	n	n	n	n	n	63,237	3,460
1987	43,822	60,531	27,706	25,236	7,589	60,531	43,822		
2005	39,078	63,003	47,166	6,613	9,224	63,003	39,078		
2007	76,058	39,480	9,750	13,901	15,829	39,480	76,058		
Maskana east_75	n	n	n	n	n	n	n	28,836	0
1987	23	263	0	0	263	263	23		
2005	7,737	4,445	3,331	1,114	0	4,445	7,737		
2007	14,718	4,664	1,131	6	3,527	4,664	14,718		
Maskana west_75	n	n	n	n	n	n	n	84,258	0
1987	17,988	216	190	2	24	216	17,988		
2005	28,302	27,819	20,434	7,371	14	27,819	28,302		
2007	37,151	22,554	5,763	418	16,373	22,554	37,151		
Middle Euphrates_right and left Bank_75	n	n	n	n	n	n	n	6,680	2,457
1987	11,473	27,317	19,400	4,323	3,594	27,317	11,473		
2005	14,369	17,870	10,154	2,906	4,810	17,870	14,369		
2007	21,201	11,701	1,553	7,584	2,564	11,701	21,201		

(continued)

Table 6.4 (continued)

								Unculti-vated areas (ha)	Water (ha)
			Summer crops						
	T	Fallow	Cotton	Corn	Other crops	T	Fallow	T	T
Upper Euphrates_75	n	n	n	n	n	n	n	53,618	7,602
1987	26,899	1,964	1,758	6	200	1,964	26,899		
2005	8,294	12,809	10,308	2,032	469	12,809	8,294		
2007	18,438	9,074	3,279	232	5,563	9,074	18,438		
Sum_1975	n	n	n	n	n	n	n	673,992	52,030
Sum_1987	139,794	135,978	67,881	33,519	10,568	111,968	189,549	607,925	65,980
Sum_2005	162,211	269,929	136,392	31,198	15,744	183,334	274,954	430,129	87,284
Sum_2007	262,294	307,112	37,475	25,481	63,251	126,207	470,405	294,633	84,347

Table 6.5 The final overall accuracy of classification results of the general classes, the irrigated areas and the agricultural features (permanent, winter and summer), using various remote sensing data (LANDSAT: MSS and TM; and TERRA: ASTER fused with LANDSAT: ETM+) for the years 1975, 1987, 2005 and 2007)

			MSS-1975 (%)	TM-1987 (%)	ASTER and ETM+-2005 (%)	TM-2007 (%)
Irrigated areas			82	93	94	92
Cultivated areas			82	93	94	92
	Trees + shrubs		–	91	92	90
	Herbaceous (permanent- and winter-crops)		–	87	85	85
		Alfalfa	–	89	–	–
		Vetch	–	79	–	–
		Wheat	–	82	84	83
		Barley	–	71	74	73
		Sugar beet	–	89	88	91
		Rain-fed crops	–	93	–	–
		Other crops	–	88	86	84
	Fallow		–	96	97	95
	Herbaceous (summer-crops)		–	89	87	86
		Cotton	–	84	87	86
		Corn	–	74	78	76
		Other crops	–	82	85	78
	Fallow		–	87	86	83
Uncultivated areas			79	87	90	88
	Natural vegetation		60	67	73	63
	Artificial surfaces		40	81	77	65
	Bare areas		67	88	91	83
Water			79	92	89	77

with ETM+-data. Using TM-data, the accuracies were close. The greatest problems were found while classifying the artificial surfaces, especially by using MSS- and TM-2007-data. The classification accuracy of barley and corn was relatively slight. The details of these classification problems were discussed for each LULC-class and for each used remotely sensed data in Sects. 6.1.1, 6.1.2, and 6.1.3.

For evaluation of the change detection products, for instance, Macleod and Congalton (1998) proposed an adjusted change detection mapping products method for evaluating their accuracy. This process is based on Congalton (1991) and requires the regular confusion matrices to be applied on bi-temporal resulted change maps. These matrices can represent all combination classes of occurred change. A simplified no-change change matrix was also proposed.

The essential problem for assessing the accuracy of change detection products is the gathering of truth reference data, where the conditions of the initial time period (i.e., 1975) cannot be revisited as the land use has been significantly changed. Therefore, accuracy assessment depended on the remotely sensed data of the final time (i.e., 2007), in addition to ancillary data.

6.3 LULC-Change Detection Mapping

This section gives a historical view of the different LULC-features in the study area. It describes the rate of their changes over the last 32 years, in particular the irrigated agricultural lands. The results are essentially presented by maps, statistics/tables and graphs.

6.3.1 Pre-Classification Results

Each change detection process analysis/result, whether a pre-classification approach is used or a post-classification approach (see Sect. 6.3.2), consisted of four major components, which were: *Measure of changes/quantity*. This provided the quantity of the occurred change and measured the area/s of change/s to provide statistical numbers, i.e., how much was/were the change/s?

Pre-classification approach results (Fig. 6.10) were generalized but very effective in relation to estimating the occurred change on the cultivated areas, especially when these areas were vegetated and not fallow. The total change in the study area (5,062,082 ha, 100 %) between 1975 and 2007 was about 600,967 ha (11.93 %), in which 238,646 ha (4.74 %) was changed from natural vegetated areas to bare areas, and 362,321 ha (7.19 %) changed from bare areas to cultivated areas (especially to irrigated). Areas recording no change were about 4,461,115 ha, 88.62 %. In comparison, the results of the three previously-mentioned approaches generally changed classes with those that resulted from applying the post-classification approach (see Sect. 6.3.2), but for the duration

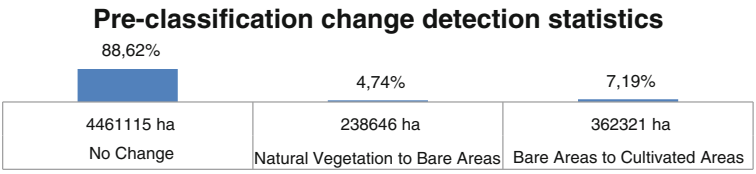

Fig. 6.10 Statistics of occurred changes in percentage and hectare, that resulted from applying the pre-classification approach using the data of LANDSAT-MSS from June-1975 and the data of LANDSAT-TM from August-2007

1987–2007 the total change in the whole study area was about 5,027,722 ha, 99.32 % in which 170,454 ha, 3.36 % changed from natural vegetated areas to bare areas; 263,863 ha, 5.21 % changed from bare areas to cultivated areas; and areas recording no change were about 34,360 ha (0.68 %).

Nature of changes/quality. This explained the quantity of the occurred change and whether it was positive/gain or negative/loss. In addition, the nature of change determined what LULC-feature/s was/were changing and to what (Braimoh 2004).

Based on the visual interpretation of the change map for the period 1975–2007, in addition to information obtained during field-work, secondary data and related previous literature, it can be shown that the land use which changed the most was agriculture, which increased largely because of the construction of irrigation projects among the Euphrates River and on account of a reduction in areas classified as bare. The most new agricultural lands were seen in the region near the Euphrates. This was obvious especially in the area of land which extends from the city of Arraqqa and the Euphrates Dam in the south toward the Turkish border (including the Al-Balikh tributary) in the north. In addition, the area located along the south bank of Lake Al-Asad and the lands located along the southern side of the major irrigation canal, which runs from Lake Al-Asad towards the city of Aleppo, also experienced significant agricultural growth.

There were also changes in vegetation cover within the lands of the five agricultural stabilization zone (the pastures). Figure 6.10 describes the nature of changes in LULC from 1975 to 2007. The result can be determined through three categories: LULC-no change, which remained unchanged, i.e., no loss and no gain (neutral/zero); LULC-Natural Vegetation to Bare Area change, where the natural vegetation class area decreased to bare area in 2007, i.e., loss and no gain; and the LULC-Bare Areas to Cultivated Areas category, where the cultivated class area increased in 2007 on account of changes to the bare area, i.e., gain and no loss.

Spatial distribution of changes/mapping. This provided the clear location and extension of occurred change by mapping and visualizing the area/s of change/s to produce the thematic map/s, i.e., where was/were the change/s?

By differencing the raw data mosaic-image/LANDSAT-MSS-June-1975 (pixel gray values) of the initial comparison date from those of mosaic-image/LANDSAT-TM-August-2007, the distribution of the three general levels of LULC-changes of interest could be detected, calculated and mapped. ArcGIS 9.3 and ENVI 4.6 packages were used for this purpose. Figure 6.11 visualizes the result of the changes.

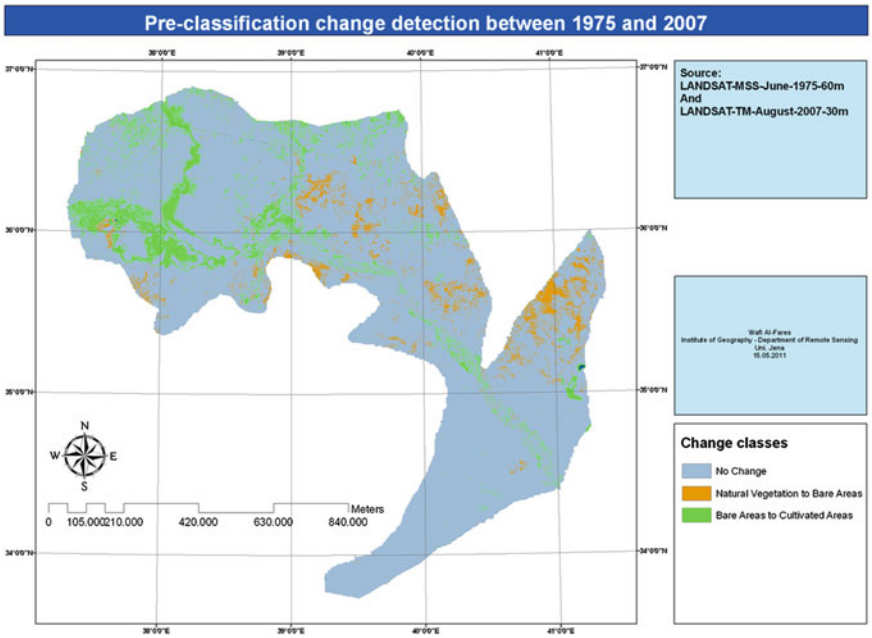

Fig. 6.11 The three wide major LULC-changes that resulted from applying the pre-classification change detection approach for the period (1975–2007)

Evaluation of changes/accuracy. This showed the accuracy of the produced change detection results by assessing the occurred errors which resulted from the adopted approach in change detection process and by using the general principle of the error matrix, i.e., How effective was the applied approach to detect the changes?

As the change classes are relatively general, it was possible to perform the accuracy visually using the remotely sensed data itself. Some 250, 200 and 150 testing points were automatically distributed (random-points) for the three resulted change classes respectively (i.e., no change, natural vegetation to bare areas, and bare areas to cultivated areas) over the resulted thematic map (Fig. 6.11). Then, the initial remotely sensed image, the final remotely sensed image and the resulted thematic map from the differencing process were geographically linked with each other. This was, of course, after the geographic registration (see Chap. 5.2.1). After that, came the manual step, where each point on the thematic map was compared to its land use/land cover in 1975 and again in 2007, using the visual interpretation of LANDSAT-MSS-June data and the LANDSAT-TM-August data. The point resulted change class (e.g., bare areas to cultivated) was found to be correct only when its use/s in both comparison dates (1975 and 2007) were compatible with the defined and resulted description of the change class. For example, it's the point resulted change class use in 1975 had to be as a bare area and then as a cultivated area in the year 2007. However, the thematic map that represented the change classes did not include all the possibilities of LULC-

Table 6.6 Accuracy assessment of pre-classification change detection approach results

Initial LANDSAT-MSS-data (1975)	Final LANDSAT-TM-data (2007)			Total/possible
	(1)	(2)	(3)	
No change (1)	230	21	7	258
Natural vegetation to bare areas (2)	13	155	4	172
Bare areas to cultivated areas (3)	3	8	132	143
Other (4)	4	16	7	27
Total	250	200	150	600
Overall pre-classification change detection accuracy = 230 + 155 + 132/600 = 86 %				

changes (e.g., cultivated areas to bare areas, etc.). Therefore, the class "other" was added for purposes of accuracy (i.e., the initial data), could be used to can represent the rest of the possibilities of the LULC-alternations between the two compared dates. The overall accuracy was 86 %.

This method would be useful for assessment of the accuracy of change detection mapping, where it is almost impossible to gather ground and/or reference data for the relatively old dates (Table 6.6).

6.3.2 Post-Classification Results

Measure of changes/quantity. Post-classification approach results (Figs. 6.12 and 6.13, Tables 6.7 and 6.8) were more obvious and detailed rather than those resulting from a pre-classification approach (see Sect. 6.3.1). The total change in the whole study area (5,062,082 ha, 100 %) between 1987 and 2007 was about 5,027,722 ha (99.32 %). Areas recording no changes were about 34,360 ha (0.68 %). The greatest changes (Table 6.7, Fig. 6.12) were in the artificial surfaces classification with a total change of 83.16 %, in which 38.77 % was changed to cultivated areas and 35.08 % transformed to the bare areas class; natural vegetation with 68.33 %, where 42.95 % changed to cultivated areas and 24.00 % to bare areas; natural water-bodies with 21.45 %, where 13.34 % changed to cultivated areas; followed by cultivated areas with 17.86 %, of which about 6 % was changed to each of the other two classes, i.e., natural vegetation and bare areas. The bare areas class showed the most stability over time with 13.89 % change. Three general trends in LULC-changes were found: negative values/loss, in which the represented classes were artificial surfaces (−64.81 %) and natural vegetation (−43.22 %); neutral value/stable, in which the represented class was bare areas (0.23 %); and positive values/gain, which included cultivated areas (+35.49 %) and natural water-bodies (+6.66).

Each LULC-class has three general trends (Table 6.8): (1) The stable trend, that represents the unchanged part of an individual class (e.g., cultivated areas: 1,080,987 ha) over the time period; (2) The positive trend (the horizontal direction

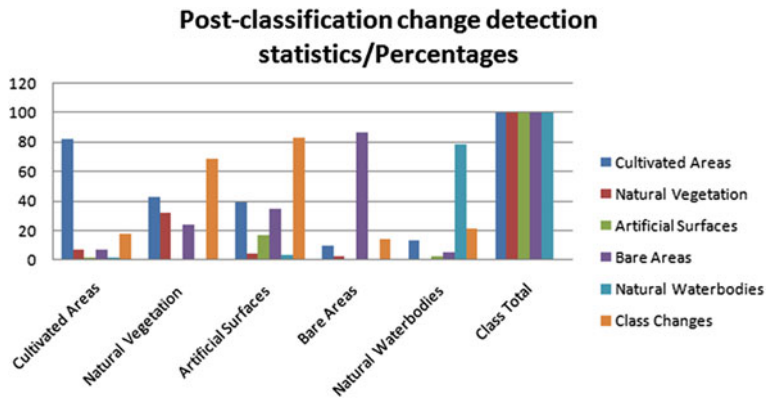

Fig. 6.12 Statistics of occurred changes in percentage which resulted from applying the post-classification approach using the data of LANDSAT-TM from May-1987 and the data of LANDSAT-TM from May-2007

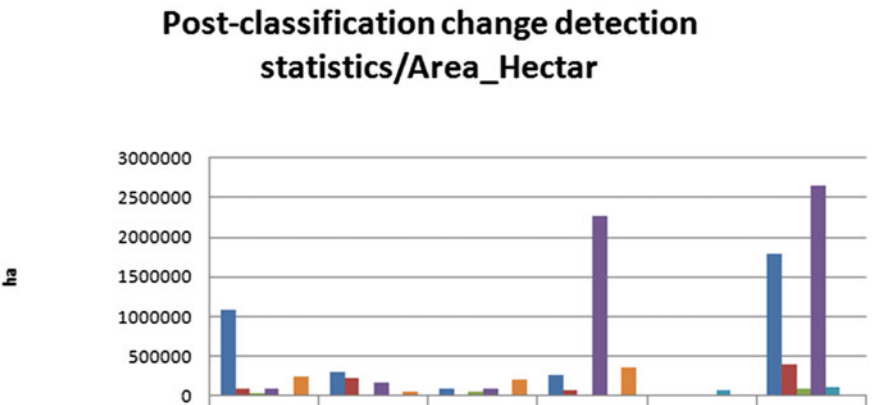

	Cultivated Areas	Natural Vegetation	Artificial Surfaces	Bare Areas	Natural Waterbodies	Class Total
Cultivated Areas	1080987	304983	98939	263863	13703	1783286
Natural Vegetation	86738	224868	11623	73150	41	403131
Artificial Surfaces	25600	1339	42943	16888	2938	89772
Bare Areas	90864	170454	89510	2269485	5112	2641953
Natural Waterbodies	19001	486	8493	503	80687	109580
Class Changes	235129	48522	212196	366344	22043	0

Fig. 6.13 Statistics of occurred changes in ha, that resulted from applying the post-classification approach using the data of LANDSAT-TM from May-1987 and the data of LANDSAT-TM from May-2007

Table 6.7 LULC-change matrix (%) in the study area for 1987 and 2007

	Cultivated areas	Natural vegetation	Artificial surfaces	Bare areas	Natural waterbodies	Class total
Cultivated areas	82.135	42.95	38.778	10.011	13.34	100
Natural vegetation	6.59	31.667	4.556	2.775	0.041	100
Artificial surfaces	1.945	0.019	16.831	0.641	2.86	100
Bare areas	6.904	24.005	35.083	86.101	4.977	100
Natural waterbodies	1.444	0.069	3.329	0.019	78.543	100
Class changes	17.865	68.333	83.169	13.899	21.457	0
Image difference	35.496	−43.228	−64.814	0.232	6.668	0

Table 6.8 LULC-change matrix (hectares) in the study area for 1987 and 2007

	Cultivated areas	Natural vegetation	Artificial surfaces	Bare areas	Natural waterbodies	Class total
Cultivated areas	1,080,987	304,983	98,939	263,863	13,703	1,783,286
Natural vegetation	86,738	224,868	11,623	73,150	41	403,131
Artificial surfaces	25,600	1,339	42,943	16,888	2,938	89,772
Bare areas	90,864	170,454	89,510	2,269,485	5,112	2,641,953
Natural waterbodies	19,001	486	8,493	503	80,687	109,580
Class changes	235,129	485,222	212,196	366,344	22,043	0

in the change matrix), which represents the transform or gain from the other four LULC-classes (i.e., natural vegetation: 304,983 ha, artificial surfaces: 98,939 ha, bare areas: 263,863 ha, and the natural water-bodies: 13,703 ha) into an individual class such as cultivated lands. Therefore, the total areas of cultivation were 1,783,286 ha in 2007; and (3) The negative trend (the vertical direction in the change matrix), that represents the transformation or loss from an individual class (e.g., cultivated areas) into one or more of the other four LULC-classes (i.e., natural vegetation: 86,738 ha, artificial surfaces: 25,600 ha, bare areas: 90,864 ha, and natural water-bodies: 19,001 ha). Therefore, the total area of cultivation was 1,303,190 ha. The greatest difference was for the class of cultivated areas—480,096 ha or +35.49 %.

The state of the land use/land cover in 2007 was expressed in the following areas: cultivated (1,783,286 ha), natural vegetation (403,131 ha), artificial surfaces (89,772 ha), bare lands (2,641,953 ha), and natural water-bodies (109,580 ha).

Nature of changes/quality. For this purpose, the change matrix was generated (Tables 6.7 and 6.8) based on classified images from 1987 and 2007. It presented the nature of changes of the LULC-categories for the period 1987–2007. The results were defined by twentieth detailed combinations of the five general classes. Figures 6.12, 6.13 show the statistics describing the nature of LULC-changes for the period 1987–2007.

Results from the land cover change analysis, carried out from the post-classification approach, show that cultivated land increased from 1,080,987 ha in 1987 to 1,783,286 ha in 2007 on account of the transformed areas from natural vegetation, bare areas, artificial surfaces and natural water-bodies lands into managed terrestrial areas. The greatest mistake was in accounting the change value in artificial surfaces, especially based on the remotely sensed data obtained in 1987 (TM), since this approach was based on the classification results. These results were not efficient in classifying the artificial surfaces because the low spectral separability within the bare areas. However, what is important is that the artificial surfaces (especially the built-up areas) had little spectral mixture with the cultivated areas (especially fallow), since the greatest interest of this study is related to it. Also, it was possible to estimate the real artificial surfaces areas from the other two remotely sensed data gathered in 2005/ASTER-images fused with ETM+-images and 2007 (TM).

The change from cultivated to natural water-bodies can be explained, in addition to the errors in classification process that exist almost in every classified class. This was due to the changes in the water capacity (flooding) of the Euphrates in relation to the water allowed to enter to Syria from Turkey, and the natural conditions, such as the actual planted areas and the impacts of the climatic elements. It distributes nearly from the river-bed, especially in the upper-Euphrates (Fig. 6.14). The change from natural vegetation to cultivated areas can be explained because of the construction of the irrigation projects (e.g., the lands of Maskana-east and the 21,000 ha-project). This change-class was also found in the marginal lands northeast from Lake Al-Asad to the Al-Balikh surrounded areas, where some of these lands had been cultivated or sometimes left as uncultivated

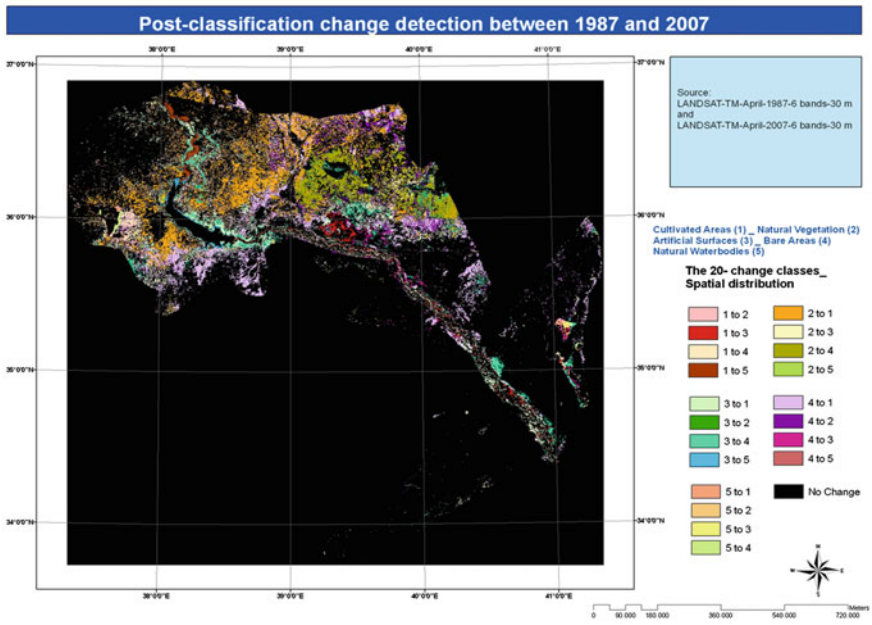

Fig. 6.14 The 21-detailed LULC-changes that resulted from applying the post-classification change detection approach for the period 1987–2007

according to the availability of rains. The change into bare areas can interpreted as being due to the climatic factors (precipitation in particular), as most of these lands exist in the five agricultural stabilization zones (Al-Badia), i.e., to the east of the Al-Balikh River. The change from artificial surfaces to cultivated areas can be seen almost as a misclassification between the artificial surfaces (especially the dark appeared civilization areas) and the cultivated areas (the fallow on dark soils).The change into bare areas can be analyzed because of the misclassification between the dark appeared civilization areas (e.g., the cities) and the dark colored bare areas (e.g., the inactive volcanoes area in the east of Arraqqa City), and the misclassification between the light appearing areas of artificial surfaces category (e.g., waste dumps and extraction sites) and the bare areas with light parent rocks or those that covered with shifting sands (e.g., dunes). The shift from bare areas to cultivated lands was because of the expansion in agriculture. Finally, the change of part of the water-bodies area into cultivated areas was because the misclassification of the TM-2007 final-data, where a dust-storm appeared over some river parts between the two cities of Arraqqa and Deir Azzour, in addition to the drying of the swamps, which has left the river without some of its elbows (the abandoned elbows).

Spatial distribution of changes/mapping. This is illustrated by the thematic change map (Fig. 6.14) for the period 1987–2007. This thematic map was produced by overlaying the two LULC-classification results of the two dates, to

Table 6.9 Accuracy assessment of post-classification change detection approach results

Initial LANDSAT-TM-data (1987)	Final LANDSAT-TM-data (2007)																					Total/possible
	12	13	14	15	21	23	24	25	31	32	34	35	41	42	43	45	51	52	53	54	N	
1 to 2	49	0	1	0	2	1	1	0	0	1	3	0	0	0	2	0	0	0	0	0	2	62
1 to 3	2	65	1	0	1	1	0	0	0	0	0	0	0	0	0	0	0	0	0	0	0	70
1 to 4	0	0	53	0	0	3	0	0	0	0	0	2	3	0	0	0	1	0	0	0	1	63
1 to 5	0	0	0	51	1	4	0	0	0	0	0	1	4	0	0	0	0	0	0	0	0	61
2 to 1	1	2	0	3	87	0	0	0	0	0	0	0	0	2	0	2	0	0	0	0	2	99
2 to 3	3	1	0	4	0	41	2	0	0	2	0	0	0	0	0	0	0	0	0	0	0	53
2 to 4	0	3	0	1	0	1	79	0	0	0	0	0	0	0	0	0	0	0	0	0	0	84
2 to 5	0	0	2	0	0	0	4	39	0	0	0	0	0	0	0	0	0	0	0	0	0	45
3 to 1	0	0	0	0	0	0	0	0	40	0	0	0	0	0	0	0	0	0	0	0	0	40
3 to 2	1	0	0	0	0	0	0	0	0	37	0	0	0	1	0	0	0	2	0	0	0	41
3 to 4	0	0	0	0	0	0	0	0	0	0	85	1	0	0	0	0	0	0	3	0	0	89
3 to 5	0	0	0	5	2	0	0	0	0	0	0	27	3	1	0	0	0	0	0	4	0	42
4 to 1	4	0	0	0	3	0	2	0	0	0	0	1	66	1	1	0	0	0	0	0	0	78
4 to 2	2	0	0	1	0	0	0	3	1	0	0	1	0	67	0	0	0	0	0	0	0	75
4 to 3	0	0	0	0	0	0	0	4	1	0	2	2	0	0	25	0	0	2	0	0	0	36
4 to 5	0	0	0	0	1	0	0	2	2	0	1	0	0	0	1	19	0	0	0	0	0	26
5 to 1	0	0	0	2	0	0	0	1	0	0	0	0	2	0	0	2	17	0	0	0	0	24
5 to 2	0	0	0	0	1	0	0	1	0	0	0	0	2	0	0	0	0	9	0	0	0	13
5 to 3	0	3	0	0	0	3	0	0	0	0	0	0	1	3	0	0	0	2	8	0	0	20
5 to 4	0	0	0	0	0	1	0	0	0	0	0	0	2	2	1	0	0	0	0	11	0	17
No change	3	0	1	0	1	0	0	0	0	0	2	0	0	2	0	1	0	0	1	0	91	102
Other	0	1	2	3	0	0	2	0	1	0	2	0	2	1	0	1	2	0	3	0	3	23
Total	65	75	60	70	99	55	90	50	45	40	95	35	85	80	30	25	20	15	15	15	99	1,163

Overall post-classification change detection accuracy = 49 + 65 + 53 + 51 + 87 + 41 + 79 + 39 + 40 + 37 + 85 + 27 + 66 + 67 + 25 + 19 +17 + 9 + 8 + 11 + 91/1,163 = 83 %

locate, compute and map the spatial distribution of each change-type. The results were defined by twentieth detailed combinations of the five classified general classes, in addition to the class of (no change), i.e., it presents 21-classes of changes. Figure 6.14 visualizes the results of the changes.

Evaluation of changes/accuracy. Some 15–99 testing points for each change combination were distributed, i.e., 1,163 in total (Table 6.9), automatically, for the twentieth resulted change combinations classes, over the resulted thematic map (Fig. 6.14). The overall accuracy was 83 %, i.e., lesser than those resulted using the pre-classification approach (86 %) (see Sect. 6.3.1). There were two major reasons. The first was because of the misclassification of the five general LULC-classes of interest, especially between the artificial surfaces and the bare areas, and the second was due to the pre-classification approach being limited to only three wide general change possibilities in contrast to the post-classification approach, that had twentieth one change possibilities to be tested.

References

Braimoh, A. K. (2004). *Modeling land-use change in the Volta Basin of Ghana*. Doctoral dissertation, Center for Research Development (ZEF), University of Bonn, Bonn, p. 159.

Congalton, R. G. (1991). A review of assessing the accuracy of classifications of remotely sensed data. *Remote Sensing of Environment, 37*(1), 35–46.

Jensen, J. R. (2005). *Introductory digital image processing: A remote sensing perspective* (3rd ed.). New Jersey: Prentice Hall Series in Geographic Information Science.

MacLeod, R. D., & Congalton, R. G. (1998). A quantitative comparison of change detection algorithms for monitoring eelgrass from remotely sensed data. *Photogrammetric Engineering & Remote Sensing, 64*(3), 207–216.

Chapter 7
Summary, Concluding Remarks and Recommendations

7.1 Summary

The overall and general objective of this thesis is as a contribution to the use of remotely sensed data of LANDSAT: MSS, TM, and ETM+; and ASTER for agricultural purposes in the arid and semi-arid areas of the Euphrates River Basin (ERB) in Syria. The study area is located in the northeast of Syria. The geographical coordinates of the ERB are 36°49′N, 38°02′E at the Turkish border, and 34°29′N, 40°56′E at the Iraqi border. Its total area is about 50,335 km^2. Starting in the 1970s, Syria began to utilize the water of Euphrates River in agriculture, reclaiming a large amount of uncultivated areas from the river. The main objective of this program was to increase the amount of cultivated areas in the basin, as Syria basically is an agricultural country. These irrigation projects during the past four decades produced a great deal of change in land use/land cover (LULC).

This thesis deals with four major emphases LULC-classification, LULC-change detection, irrigation mapping and irrigated agriculture classification of the Euphrates River Basin area in Syria. Four general LULC-classification products (see Chap. 6.1.1) have been generated for the years 1975, 1987, 2005 and 2007; also, two LULC-change detection maps (see Chap. 6.3) have been produced for the periods between 1975–2007 and 1987–2007. In addition, four thematic maps representing the development of the irrigation areas (see Chap. 5.1.2) in the last 37 years with the intervals 1975, 1987, 2005 and 2007 have also been produced. Finally, six detailed agricultural classes classification products (see Chap. 5.1.3) have been generated for the two major agricultural seasons in Syria, i.e., the winters (May data) and summers (August data) of 1987, 2005 and 2007.

To realize the objective of this study, eight scenes of LANDSAT-MSS obtained in June 1975 were chosen; 32 scenes of LANDSAT-TM obtained in May and August of the years 1987 and 2007; and 16 scenes of corrected LANDSAT-ETM+/SLC-OFF/obtained in May and August 2005 which were fused with scenes of TERRA-ASTER obtained in May and August of 2005 in a bid to increase spectral resolution from three to six spectral bands.

W. Al-Fares, *Historical Land Use/Land Cover Classification Using Remote Sensing*, SpringerBriefs in Geography,
DOI: 10.1007/978-3-319-00624-6_7, © The Author(s) 2013

Remote sensing techniques were approved and applied on the remotely sensed data (see Chap. 4.1) of 1975, 1987, 2005 and 2007 for the four major emphases (LULC-classification, LULC-change detection, irrigation mapping, and irrigated agriculture classification). There were no known determined adopted techniques that could be directly applied for the emphases. Therefore, it was necessary to set suitable methods that would be compatible with the used data, the thesis questions and the privacy of the study area environment. Most of the applied methods in this work were already recognized, some were modified and some were combined.

It is true that a lot of remotely sensed data and some processing programs are becoming more and more accessible to researchers at little or no cost, but remotely sensed data processing and interpretation techniques are still time consuming and not suitable for all regions of the Earth at the same level of accuracy. It has been shown in this study that the geometric, atmospheric and radiometric correction processes (see Chap. 5.2) are not always necessary for each image, each sensor data and each date. Geometric correction processes, especially for the geometric registration, were not difficult and were achieved at very high accuracies. However, atmospheric correction was impossible for the relatively old data (MSS-1975), where the weather parameters were difficult to obtain. Radiometric correction was applicable for all data, but this did not mean that it produced suitable results for the whole dataset. Therefore, when neither the raw data or the enhanced data after applying the atmospheric and/or the radiometric corrections gave good results (especially for use in mosaicing), then the data were processed and classified separately, i.e., each image alone. ATCOR-2 was used for atmospheric correction, while iMAD was used for radiometric correction. Both applications were relatively easy to use and required no additional external information. These programs were found to give better results than those methods that are time consuming and needed more external data such as MFF and 6S (Chavez 1996).

Where the results of the classifications were cartographic products, all spatial data were standardized, and were transformed and geometrically corrected to a general reference system: a UTM-projection of Zone 37 N with the international general ellipsoid/spheroid WGS84 and datum WGS84.

Geometric correction, geo-referencing and geometric registration formed the basis for mosaicing more than one image (see Chap. 5.2.5) for fusion of different remotely sensed data, i.e., the ASTER-data were fused with LANDSAT-ETM+-data (see Chap. 5.2.4) for detection of changes (see Chap. 5.12).

Precise mosaicing was very important for further remotely sensed data processing and interpretation (e.g., classification, change detection, etc.). The general algorithms of imagery mosaicing were not always able to produce a one mosaic-image with a consistent appearance in which the values of the histograms of each image were combined together in one mosaic-image. This gave an unsuitable presentation of the various LULC-features on the mosaic-image. In these situations, the MAD-technique was applied to satisfy a radiometric consistent mosaic. This was a comfortable relative radiometric calibration technique that built a data

calibration with linear values as gain and offset coefficients as unnecessary. This technique had the robust advantage of the ability to create a scene comparison even though values were not available or wrong.

The international hierarchical classification scheme (LCCS) of FAO was followed as guide in the classification processes. This approach defined and determined the LULC-classes to be included in the classification/s. These classes were defined before starting each automated supervised classification procedure.

The classification of the remotely sensed data was based on the traditional pixel-based classification method. The results of classifications were always presented as thematic maps. The results of the various tested approaches and algorithms of classification on the various obtained remote sensing data were interpreted based on the accuracy assessment method.

In this study, several automated classification approaches (i.e., one-step, and multi-stage classification) and several algorithms (i.e., MLC, NN, and SVM) were tested on several remote sensing data (LANDSAT: MSS, and TM; TERRA: ASTER fused with corrected LANDSAT-ETM+/SLC-OFF/), to find the optimized approach and algorithm. The multi stage classification approach and the MLC-algorithm harvested the best results (see Chap. 5.7).

The classification of coarse resolution (spatial and spectral) data like LANDSAT-MSS in relation to its geographical location of ERB, was suitable to produce thematic maps of the five wide general classes for the whole large area of the ERB and to represent the spatial distribution of the one irrigated areas class. These data had not the ability to classify any more detailed classification level (e.g., agriculture). LANDSAT-TM data were more suitable for classifying the general classes and the irrigated areas. However, it was less suitable for classifying the detailed agricultural classes. Finally, the low spectral resolution ASTER-data of only three bands was less suitable in comparison to TM-data, although they had a higher spatial resolution, i.e., 15 m. However, after fusing them with the LANDSAT-ETM+/SLC-OFF/corrected data to increase the spectral bands to six bands, these data harvested the best results. In general, the classification of the agricultural features using TM and ASTER- ETM+ data was very good over the State achieved irrigation projects (e.g., the 21,000 ha project, Maskana-East, etc.), where the individual planted fields were relatively large and thus classifiable in regard to the used remote sensing data, and the diversity in LULC-features was small. These were changed starting from the TM-data of 2007, where the fields became smaller and the diversity of planted agricultural types became more widespread. The diversity was acceptable over the State and farmer-cultivated irrigation areas (e.g., Maskana-West), where the private holdings were varied from small fields to very large fields. However, the classification results were unacceptable over the very old cultivated areas located on the Euphrates River banks, where the holdings were very small with great diversity in cultivated agricultural features. Therefore, this area requires remote sensing data with higher spatial and spectral resolution (e.g., IKONOS).

The classification of natural vegetation outside the irrigation areas in arid and semi-arid regions in Syria, especially in the fifth agricultural stabilization zone, was made difficult because of the dominant and variable soil signal (spectral response) (Huete et al. 1994). This was also true for the agricultural crops and trees (because of the relatively wide dimensions between the trees in relation to the spatial and spectral resolution of the used remotely sensed data), that were cultivated particularly in the third and fourth agricultural stabilization zones.

In this study, two approaches of change detection techniques were applied to almost all agricultural areas in the arid and semi-arid ERB-environment in Syria, to test the effectiveness of the two techniques in mapping the changes. The pre-classification change detection approach that was based on image differencing was very effective in mapping the change from bare areas to cultivated areas (the new irrigation projects) over the time period 1975–2007. The post-classification approach detected, mapped and defined 21 type of change. However, it offered a lower accuracy (83 %) rather than the first method (86 %), because it depended on the quality of already achieved classification and dealt with more types of change (21) rather than the first method (3). Therefore, it contradicted the assumption that this was the most accurate change detection approach (Mas 1999). The two approaches were easy to interpret.

Based on the pre-classification change detection approach (see Chap. 6.3.1), there were three major trends of activities of land use/land cover: The first trend (no change) was stable and the most dominant with about 88.62 %. The second was negative, where as in most arid and semi-arid regions, the major cause of natural vegetation change to bare areas (4.74 %) was related to the climatic factor of precipitation, which is unstable and changes from one year to another. In addition the human factor of overgrazing must be taken into consideration. The largest area of natural vegetation exists in the fifth Agricultural Stable Zone (ASZ) which is made up of natural pastures. The third major driving force was positive because it accounted to a decrease in bare areas (7.19 %), where as in most developed countries, it was related to the activities of cultivation agriculture. These results were confirmed by applying the post-classification change detection approach (see Chap. 6.3.2), where the change value of natural vegetation was 68.33 %, in which 42.95 % was transformed to cultivated areas and 24 % transformed to bare areas, and the loss was at 43.22 %; the change value of cultivated areas was 17.86 %, and the gain was at 35.49 %. This was on account of the natural vegetation with 304,983 ha and bare areas with 263,863 ha. The change in bare areas was about 13.89 %, where 10.01 % transformed into cultivated areas, and the gain was only 0.23 %.

The major limitations of this study were the MSS-data of 1975 that were characterized by low spatial resolution of 60 × 60 m and low spectral resolution of four bands. The corrected LANDSAT-ETM+/SLC-OFF/data of 2005 that were fused with ASTER-data to increase their spectral resolution from three bands to six bands, were obtained after the applying a correction method from USGS. The time period lag between the remotely sensed data of the years 1975 and 1987, and the field-work in 2007 and 2009 limited the full usefulness of using the remotely

sensed data, because it was very difficult to obtain the additional non-remotely sensed data (the ground reference data in particular), and the gathered ground reference data would only be partly suitable for some purposes. The study area was large with some locations inaccessible during field-work.

7.2 Concluding Remarks

The kernel of this study was whether, how and to what extent applying the various remotely sensed data that were used here, would be an effective approach to classify the historical and current land use/land cover, to monitor the dynamics of land use/land cover during the last four decades, to map the development of the irrigation areas, and to classify the major strategic winter- and summer-irrigated agricultural crops in the study area of the ERB.

It is true that the development of remote sensing techniques focuses greatly on construction of new sensors with higher spatial and spectral resolution, but it is not possible to ignore the data of the older sensors (especially, the LANDSAT-mission) when the historical mapping of land use/land cover and monitoring of their dynamics are needed, although their low spatial and spectral resolution in comparison to the new sensors launched in the last decade (e.g., IKONOS) needs to be taken into consideration. These older sensors are still precious. To maintain the advantages of these sensors, researchers during the last five decades have developed new and more effective digital image processing and interpretation methods, to harvest more accurate results. Therefore, it is important to focus on the development of new and enhanced techniques that can translate the relationship between the general characteristics of the old acquired data and the specific characteristics of each individual environment such as the arid and semi-arid lands.

Regarding to field-work, this remains very important as a basis in most remote sensing applications, offering the training samples for supervised classification. It provides for evaluation the results of classification using accuracy assessment techniques. It is also useful to understand the specific characteristics of the environment of the study area.

The application of the various remote sensing techniques, which were adopted in this study, was not only related to the location of the study area, but also to various types of remotely sensed data (see Chap. 4.1).

These techniques were: extraction of the borders of the study area using the SRTM-data and ArcGIS-extensions (see Chap. 5.1); geometric correction based on GCPs, and/or geometric registration based on image to image method (see Chap. 5.2.1); atmospheric correction using the ATCOR-2 program (see Chap. 5.2.2); relative radiometric normalization using the MAD-concept (see Chap. 5.2.3); enhancing the spatial resolution of LANDSAT-ETM+ data from 30 to 15 m using the Gram Schmidt Sharpening Technique to increase the spectral resolution of ASTER-data using the fusion-technique (see Chap. 5.2.4); mosaicing, subsetting and masking (see Chap. 5.2.5); training samples selection and

evaluation (see Chap. 5.6); unsupervised classification (see Chap. 5.7.1.1); supervised classification using the three algorithms of classification (i.e., MLC, NN and SVM) with the two approaches of classification, i.e., the one stage and the multi stage classification approaches (see Chap. 5.7.1.2.1); post-classification processing (see Chap. 5.11); automated change detection mapping using the pre-classification approach (see Chap. 5.12.1) and the post-classification approach (see Chap. 5.12.2); and finally, the accuracy assessment techniques (see Chap. 5.13).

The new relative radiometric normalization method that was used in this study, was, after Canty et al. (2003), favored, where it can be applied automatically. It is consistent, constant, rapid, parameter free and sensor independent, and is enhanced by an orthogonal regression.

The aforementioned and used techniques in this study have various alternatives of sub-technique (e.g., radiometric normalization can be performed using more than one method, such as 6S, dark object method, histogram matching, etc.) and/or various parameters (e.g., SVM-algorithm of supervised classification can be used with various of parameters combinations). Thus, some of these alternatives were mentioned, discussed and compared to justify the final choice of each alternative technique and/or parameters that were used in this study.

This study proved that the use of multi-sensor (MSS-1975 and TM-2007) and multi-scale 60 and 30 m data for change detection mapping is possible. Also, it is possible to use the multi-sensor ASTER-2005 and LANDSAT-ETM+ data for LULC-classification.

The available remotely sensed data of ASTER-sensor with low spectral resolution (three bands) and high spatial resolution (15 m) had given worse results with lower classification accuracy than those obtained after fusing with the data of LANDSAT-ETM+ to increase the spectral resolution.

New sensors (e.g., ASTER) offer higher accuracy rather than the old sensors (e.g., LANDSAT-MSS), but also bring new problems, such as the increasing time of processing because of the higher spatial resolution and the lower local coverage of each scene, and the increase of geometric errors because of the higher spatial resolution/pixel size.

Remotely sensed data spatial resolution/scale affects the level of useful information that can be extracted from the satellite imagery.

7.3 Recommendations/Outlook

Remote sensing techniques and data (LANDSAT and ASTER) were found to be very effective in the classification of land use/land cover and in the mapping of irrigation areas, and to detect and map changes that occurred over a number of years in the arid and semi-arid area of the Euphrates River Basin in Syria. However, these approaches were uneven for classification of agricultural crops, where their effectiveness were based on many factors, such as the used remotely sensed data type and its characteristics (e.g., spatial and spectral resolution, etc.), the agricultural

holdings area and construction (e.g., the classification accuracy is very good where the large fields exist), and the crop type to be classified (e.g., the existing of wheat and barley together would make the spectral separation difficult that will impact the accuracy of classification). Here, more positive results may be realized by obtaining images at more times during the annual agricultural growing cycle.

The use of remote sensing techniques and data periodically to monitor and evaluate above ground surface natural resources can save time, effort and capital which are needed for traditional human-based ground surveys.

It is important to integrate the gathered human-based statistical records (agricultural statistics in particular) with the remote sensing techniques to interpret the relative old data of remote sensing that have no or insufficient compatible reference data. It is useful too, when a part of the study area is inaccessible.

The adoption of remote sensing techniques is an essential cartographical tool to map the general wide land use/land cover classes.

Some demands include: The construction of user-friendly data archives with united data-formats as far as possible; the direction of more attention to the developed countries where there are many interesting topics to study using the remote sensing techniques. For instance, it is very difficult and time consuming to obtain remotely sensed data even if they are free of cost, and one requires a large amount of time to download one image because the slow Internet speed, in addition to a lack of digital image processing software.

For further research: This study, like all studies, is an unfinished work because of the limitations of time, resources and finance. Therefore, the results included in this study are the best they can be, considering these limitations.

It would be interesting if the results of this study which are based on medium- to high- resolution optical remotely sensed data, were compared with those from resulting from the application of a very high resolution optical data (e.g., IKONOS), especially for agricultural purposes; the use of remotely sensed hyperspectral data (e.g., Hyperion); and the application of remotely sensed RADAR-data (e.g., TerraSAR-X). In these cases, it would be necessary to apply new advanced digital analysis techniques, such as spectral un-mixing analysis.

Also, I am interested to link the results of this study and remote sensing techniques with GIS, for hydrologic study and regional water resources management of the Euphrates River Basin in Syria, and for agricultural water usage. I have collected a great deal of water data about the Euphrates, especially the water measurements at many measurement-stations along the river from the Syrian–Turkey borders to the Syrian–Iraqi borders over many decades.

This integration would be effective, because the classical applied approaches for estimating the hydraulic parameters are expensive and time consuming. Remote sensing can overcome these problems, by presenting a rapid and complete overview of the study area of interest. Here, weather satellites such as the NOAA-TIROS (National Oceanic and Atmospheric Administration-Television Infrared Observation Satellite), can provide us with some needed parameters (climatic parameters) which are essential for input in the hydraulic model. Evaporation or evapo-transpiration (ET) is the most important and difficult to estimate in the

hydraulic studies. Remote sensing techniques cannot measure it directly, but they suggest approaches based on LULC-features classification and climatic factors (e.g., solar radiation, temperature, humidity, surface albedo, etc.).

Also, for runoff measurement, techniques of remote sensing provide a source of input-data (watershed geometry, drainage networks, empirical flood peak, LULC-classes, etc.), and help to estimate equation coefficients and other model parameters.

References

Chavez, P. S. (1996). Image-based atmospheric corrections-revisited and improved. *Photogrammetric Engineering & Remote Sensing, 62*(9), 1025–1036.

Huete, A., Justice, C., & Liu, H. (1994). Development of vegetation and soil indices for MODIS-EOS. *Remote Sensing of Environment, 29*, 224–234.

Mas, J. F. (1999). Monitoring land-cover changes: A comparison of change detection techniques. *International Journal of Remote Sensing, 20*(1), 139–152.